Kunshan Gao
David A. Hutchins
John Beardall *Editors*

Research Methods of Environmental Physiology in Aquatic Sciences

Science Press
Beijing

Springer

Research Methods of Environmental Physiology in Aquatic Sciences

Kunshan Gao • David A. Hutchins • John Beardall
Editors

Research Methods of Environmental Physiology in Aquatic Sciences

Springer

Editors
Kunshan Gao
State Key Laboratory of Marine Environmental Science and College of Ocean and Earth Sciences
Xiamen University
Xiamen, China

John Beardall
School of Biological Sciences, Monash University
Clayton, VIC, Australia

David A. Hutchins
Marine and Environmental Biology, Department of Biological Sciences
University of Southern California
Los Angeles, CA, USA

ISBN 978-981-15-5353-0 ISBN 978-981-15-5354-7 (eBook)
https://doi.org/10.1007/978-981-15-5354-7

This Springer imprint is published by the registered company Springer Nature Singapore Pte Ltd.
The registered company address is: 152 Beach Road, #21-01/04 Gateway East, Singapore 189721, Singapore

Preface

Climate and other environmental changes, together with the physiology of the organisms involved, shape ecosystems, biogeochemistry and biogeography. Therefore, understanding both quantitative and qualitative changes in the physiology of aquatic organisms is essential for assessment and prediction of the consequences of environmental changes in marine and freshwater ecosystems. However, different methodologies or approaches have been employed to examine eco-physiological performance, in experiments run at different scales (for example using small flasks of <1 L or mesocosms with cubic metres of water). Most of the methods employed to date suffer from problems of inconsistency of approach such that different results could be due to different methodologies or genuine differences between species or treatments and struggle to provide reliable data at the organismal, population or community level that reflect their performance in situ. This is mainly due to the fact that physical and chemical conditions within experimental vessels often differ from those in natural waters as a consequence of issues such as the lack of mixing and advection, screening out of UV radiation, changing levels of nutrients and self-shading during rapid growth. However, there has to date been only limited documentation of appropriate research methods in aquatic environmental physiology. Some of these methods are now becoming dated, with new techniques being seen as more appropriate.

In this book, we provide detailed methods for a range of basic aquatic eco-physiological techniques for marine primary and secondary producers and viruses. One of the unique features of the book is that in each chapter the advantages and disadvantages of each method have been analysed, and recommendations or suggestions are provided. This book has 40 chapters, with contributions from scientists across different fields and from different regions of the world, including China, the European Union, Australia and the USA. This book was planned 4 years ago (2016) following a workshop on "Research Methods on Aquatic Environmental Physiology" held in Xiamen, China. The participating scientists all agreed that a book covering environmental physiological methods would provide useful information to

allow postgraduate students and young researchers to choose appropriate experimental approaches and design suitable experiments.

This book is suitable for research aquatic biological scientists, with detailed information to reflect the strengths and constraints of each method. However, each of the 47 authors, with their different expertise, has written their individual chapters in unique ways, with slightly different emphases; therefore, reference to the primary literature cited is strongly recommended. Nonetheless, we hope that the book will prove a useful guide to appropriate techniques for investigations of aquatic ecophysiology and will help to improve consistency of experimental approaches in future studies.

We are grateful for assistance from Xianglan Zeng and He Li, who helped to organize the book and redraw some figures.

Xiamen, China — Kunshan Gao
Los Angeles, CA, USA — David A. Hutchins
Clayton, VIC, Australia — John Beardall
Oct. 9, 2020

Contents

Part VIII Research Methods for Animals and Viruses

About the Editors

Kunshan Gao (PhD, 1989, Kyoto University) is chair professor at State Key Laboratory of Marine Environmental Science and College of Ocean and Earth Science, Xiamen University. His expertise focuses on marine environmental change ecophysiology, having published over 290 peer-reviewed papers and 10 book chapters and edited 3 books.

David A. Hutchins (PhD, 1994, University of California Santa Cruz) is a professor of marine and environmental biology at the University of Southern California. His research interests primarily revolve around understanding the consequences of anthropogenic global change processes for ocean biology and biogeochemistry. He has published 200 peer-reviewed papers. Prof. Hutchins is a fellow of the American Association for the Advancement of Science and a sustaining fellow of the Association for the Sciences of Limnology and Oceanography.

John Beardall (PhD, 1976, University of London) is an emeritus professor at Monash University, Australia. He has over 40 years' experience working in algal physiology and its regulation by environmental factors, having published over 240 peer-reviewed papers, 23 book chapters and 3 books. John is currently editor-in-chief of the journal *Applied Phycology*.

Part I
Measurement of Environmental Parameters Affecting Marine Plankton Physiology

Chapter 1
Characteristics of Marine Chemical Environment and the Measurements and Analyses of Seawater Carbonate Chemistry

Weidong Zhai

Abstract The changing marine chemical environment will affect all organisms living in it, to a considerable extent dominating the evolution and productivity of marine ecosystems. Moreover, the chemical environment is also highly influenced by biological activities. This section briefly introduces the chemical composition of seawater, the Marcet–Dittmar Law of marine major elements, and the distributions and controls of nutrients. This section will give much attention to the definition, analyses, and biogeochemical controls of seawater carbonate system parameters, including dissolved inorganic carbon, total alkalinity, pH, partial pressure of CO_2, and carbonate saturation states.

Keywords Seawater composition · Chemical environment · Ocean acidification · Carbonate system · Carbon dioxide

Natural seawater is a heterogeneous and dynamic system, with multiple media and multiple buffers, having an ionic strength of ~0.7 mol/L, and containing marine organisms. The major component of seawater is water, while the other components are mostly salts (Fig. 1.1). The salt components of seawater may be connected with the formation and evolution of the earth and the ocean. It is believed that most of the salt components come from the weathering products of the earth's crust and volcanic ejecta, as well as seafloor hydrothermal activity. Therefore, all elements on the earth should exist in the marine environment. Owing to concentration difference and/or technical limitations, however, some elements have not been found in seawater.

Different salt elements in the seawater salinity have different input fluxes and different geochemical behaviors in the ocean. Therefore, their contents are very

W. Zhai (✉)
Institute of Marine Science and Technology, Shandong University, Qingdao, China
e-mail: wdzhai@sdu.edu.cn

K. Gao et al. (eds.), *Research Methods of Environmental Physiology in Aquatic Sciences*, https://doi.org/10.1007/978-981-15-5354-7_1

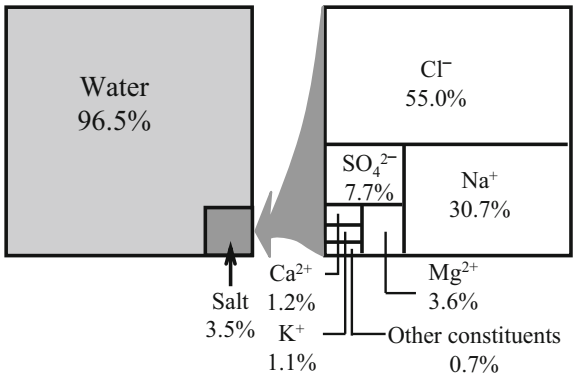

Fig. 1.1 Chemical composition of seawater in open oceans (with a salinity of 35)

Table 1.1 Different categories of dissolved and particulate components in seawater

Classification	Examples	Content magnitude
Macroelements	Cl^-, Na^+, Mg^{2+}, SO_4^{2-}, Ca^{2+}, K^+, HCO_3^-, CO_3^{2-}, Br^-, Sr^{2+}, F^-, H_3BO_3	mmol/L
Dissolved gases	N_2, O_2, Ar, CO_2, N_2O, $(CH_3)_2S$, CH_4	nmol/L–mmol/L
Nutrients	NO_3^-, NO_2^-, NH_4^+, $H_2PO_4^-$, HPO_4^{2-}, $Si(OH)_4$	nmol/L–μmol/L
Trace metals	Li, Ni, Fe, Mn, Zn, Pb, Cu, Co, U, Hg	pmol/L–μmol/L
Dissolved organic matters	Amino acid, humic acid	ng/L–mg/L
Colloids	Protein, polysaccharide	≤mg/L
Particles	Sand, clay, marine microbial organisms	μg/L–mg/L

different. The concentrations of abundant and rare elements may differ by 10^9 times or more (Table 1.1).

Various materials in seawater can be clustered into three categories according to their particle sizes: (1) truly dissolved matter with the particle size of less than 1 nm, including inorganic salts, inorganic molecules and small organic molecules in seawater, as well as dissolved gases such as inert gases (Ar, Xe, He, etc.), quasi-conservative gases (e.g., N_2), and biologically active gases (O_2, CO_2, N_2O, CH_4, $(CH_3)_2S$, H_2S, H_2, etc.); (2) particles usually larger than 0.7 μm, including marine microbial organisms and biogenic debris and other particulate organic matter, as well as mineral-composed particulate inorganic matters; (3) colloidal materials between 1 nm and 0.7 μm, composed of colloid organic matter such as polysaccharide and protein, as well as colloidal inorganic matters formed by Fe and Al.

Seawater ions and molecules are often classified as macroelements and trace elements according to their concentrations (Table 1.1). Macroelements in seawater are usually present at concentrations greater than 50 μmol/L, including five cations

(Na^+, Mg^{2+}, Ca^{2+}, K^+, Sr^{2+}) and five anions (Cl^-, SO_4^{2-}, HCO_3^- plus CO_3^{2-}, Br^-, F^-), and H_3BO_3 molecules. They account for more than 99% of the seawater salinity. The seawater trace elements, with the contents usually less than 50 μmol/L, include many metal elements such as Li, Ni, Mn, Zn, Pb, Cu, U, and Hg. Some trace elements (Fe, Co, Cd) have quite low concentrations of even pmol/L in the surface water of open oceans. In addition, some elements (including N, P, Si, Mn, Fe, Cu, Zn, and Mo) are required by organisms to perform their functions essential for life. They are regarded as nutrients in seawater. In accordance with their content levels, nutrient elements are divided into macro-nutrients (N, P, Si) and micronutrients (Mn, Fe, Cu, Mo, Zn, etc.).

Many investigations and analyses have shown that the relative proportions of macroelements are nearly constant in seawater, which is called as Marcet–Dittmar Principle. This principle indicates that the oceanic water circulation rate is faster than those geochemical processes controlling input and output of seawater macroelements. As the input and/or emigration of water do not change the total amount of salt in the ocean, the changes of macroelement concentrations are synchronous with the change of salinity, leading to constant ratios among them. This principle also shows that seawater macroelements behave conservatively in the sea. They are insensitive to biological processes and local geochemical processes, but dominated by physical dilution processes. Strictly speaking, the conservative behavior does not imply that these major components never undergo chemical change in seawater. For example, calcified organisms utilize seawater Ca^{2+} and Sr^{2+} for growth, and the freezing and thawing of sea ice affect Na^+ and SO_4^{2-}. The usual case is that the high concentrations of major elements mask the possible effects of most biological or geochemical processes. In sea areas near estuaries and hydrothermal vents on the seabed, and in the water bodies influenced by interstitial waters of the sediment, however, the proportions of major elements are expected to be inconstant.

Major nutrients in seawater vary very much. Vertically, the upper euphotic layer provides the place for phytoplankton growth and propagation in warm seasons, causing sea surface nutrient depletion. The sinking particles such as biological debris and excreta decompose below the euphotic zone. The regenerated nutrients are released into subsurface or deep waters. These regenerated nutrients can return to the upper euphotic zone through upwelling and/or convective water mixing in cold seasons, to be utilized by pelagic phytoplankton again. As for the horizontal distributions, deep-water nutrients are enriched from the Atlantic to the Pacific Ocean due to the coupled effect of deep ocean circulation and the remineralization of sinking particles. Coastal oceans are affected by river discharge and atmospheric deposition, usually having richer nutrient supplies than those in the adjacent open oceans. In some eutrophic coastal oceans, however, the molar ratio of dissolved inorganic nitrogen to phosphate has increased by tens times in the past few decades.

In practice, both pH and the carbonate system are essential for the health of aquatic environments. This is because pH affects chemical/biochemical properties of seawater, including chemical reactions, equilibrium conditions, and biological toxicity of many substances. Within the normal pH range of natural seawater, a series of

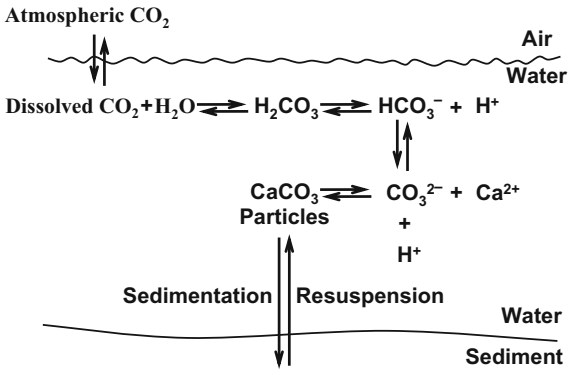

Fig. 1.2 Chemical equilibria in the seawater carbonate system

chemical equilibria of the carbonate system (Fig. 1.2) contribute 95% of the chemical buffer capacity of the seawater. The pH in open oceans is mainly controlled by the seawater carbonate system. Since short-term changes of total dissolved inorganic carbon (DIC) in sea water are mainly caused by photosynthesis and respiration, it is feasible to obtain information about metabolic status of the marine ecosystem by studying the changes of the seawater carbonate system. Moreover, our understanding of precipitation and dissolution of calcium carbonate in oceans is highly reliant on the study of the marine carbonate system. In addition, the seawater carbonate system plays an important role in regulating atmospheric CO_2 concentration. Since the oceanic inorganic carbon is a much larger reservoir than the atmospheric CO_2, any small changes in those processes affecting the marine inorganic carbon reservoir may have significant consequences for the atmospheric CO_2 concentration. Therefore, the seawater carbonate system is related to global change, and is an important component in the marine carbon cycle.

To study the seawater carbonate system, the commonly measured quantities are dissolved inorganic carbon (DIC), total alkalinity (TAlk), pH, and partial pressure of CO_2 (pCO_2). The DIC and TAlk have a dimension of concentration. Their units are μmol/kg (seawater). pH has no unit, while pCO_2 has the dimension of pressure, with a unit of either Pa or μatm (1 μatm ≈ 0.101 Pa). To better understand the response of calcified organisms to seawater acidification, carbonate mineral saturation states in seawater are also needed. However, this property must be calculated from the measurable parameters of the carbonate system. The definition, determination, and biogeochemical controls of these quantities are outlined below.

1.1 Dissolved Inorganic Carbon

DIC is the total of various dissolved inorganic carbon forms. Sometimes it is called total carbon dioxide (TCO_2). In some literature, it is abbreviated as ΣCO_2 or C_T. DIC includes two anions of HCO_3^- and CO_3^{2-}, and also includes two molecules of dissolved gas $CO_{2(aq)}$ and the hydrated CO_2, i.e., H_2CO_3. The two neutral molecules

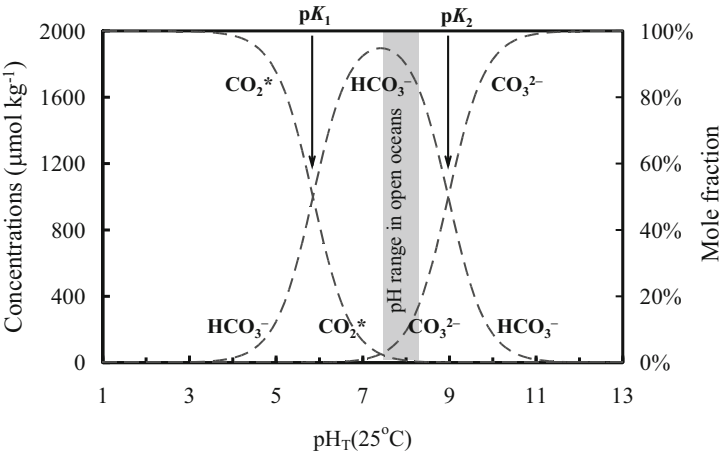

Fig. 1.3 Concentrations of CO_2*, HCO_3^-, and CO_3^{2-} as functions of pH. Note that the concentrations are plotted for a fixed DIC of 2000 μmol/kg and a salinity of 35. pK_1 and pK_2 are negative values of logarithmic dissociation constants to the base 10

of $CO_{2(aq)}$ and H_2CO_3 are often collectively denoted by free carbon dioxide CO_2*. Thus,

$$\mathrm{DIC} = [CO_2^*] + [HCO_3^-] + [CO_3^{2-}] \tag{1.1}$$

Within the normal pH range of sea water, most of the DIC is present as HCO_3^- ions, and the concentration of CO_3^{2-} ions is much higher than that of CO_2* (Fig. 1.3). For example, HCO_3^- and CO_3^{2-} ions usually account for 88.5% and 11% of surface DIC in open oceans, while CO_2* only amounts to approximately 0.5% of DIC.

The determination of DIC in seawater is usually conducted by infrared detection following acid extraction. The detector can be replaced by a gas chromatograph or a coulometric meter. Seawater DIC determination has been maintained as a routine measurement in many research laboratories. In a laboratory with good quality controls, the highest precision of seawater DIC determination is close to or even better than ±1 μmol/kg, while the accuracy can reach a satisfactory level of ±2 μmol/kg.

As a major element of seawater, DIC is affected by rainfall, evaporation, sea ice, water dilution and various physical processes, and thus shows correlations with salinity. DIC variations are also controlled by biological processes such as photosynthesis, organic matter decomposition, and $CaCO_3$ precipitation and dissolution. Marine photosynthetic organisms utilize solar energy, assimilating DIC to organic matter, and releasing oxygen into waters. The opposite organic matter decomposition is a dissimilation process, consuming dissolved oxygen and releasing CO_2 to the seawater. The positive process of formula (1.2) shows the traditional Redfield ratio

to represent the approximate stoichiometry of photosynthesis in seawater, and the inverse process exhibits a general stoichiometry of complete organic matter remineralization in aerobic environments.

$$124CO_2 + 16NO_3^- + HPO_4^{2-} + 140H_2O \leftrightarrow C_{106}H_{263}O_{110}N_{16}P + 18HCO_3^- + 138O_2 \quad (1.2)$$

In addition, marine calcifying organisms use seawater HCO_3^- or CO_3^{2-} to form their $CaCO_3$ shell and/or skeletons during the growth, leading to declines of DIC. When the $CaCO_3$ shell and skeletons dissolve, the seawater DIC will rise.

$$Ca^{2+} + CO_3^{2-} \rightarrow CaCO_3 \quad (1.3)$$

$$Ca^{2+} + HCO_3^- \rightarrow CaCO_3 + H^+ \quad (1.4)$$

$$CaCO_3 + CO_2 + H_2O \rightarrow Ca^{2+} + 2HCO_3^- \quad (1.5)$$

In open oceans, sea surface DIC usually ranges from 1840 to 2220 μmol/kg, with a global average of ~2000 μmol/kg. Usually high-latitude sea areas have relatively higher surface DIC than tropical sea areas around the equator. In deep waters, DIC is as high as 2200–2400 μmol/kg due to the combined effect of organic matter remineralization, $CaCO_3$ dissolution, and physical water mixing. In the last 50 years, the anthropogenic CO_2 intrusion via air-sea exchange has increased the global mean sea surface DIC by ~1 μmol/kg/year.

1.2 Total Alkalinity

Total alkalinity is defined as the amount of proton acceptor in seawater exceeding that of proton donor, i.e.,

$$TAlk = [HCO_3^-] + 2[CO_3^{2-}] + [B(OH)_4^-] + [OH^-] + [HPO_4^{2-}] + 2[PO_4^{3-}] + [SiO(OH)_3^-] + [NH_3] + [HS^-] - [H^+] - [HSO_4^-] - [HF] - [H_3PO_4] \quad (1.6)$$

Some researchers use A_T to indicate TAlk. Although TAlk has a unit of concentration, it is actually an equivalency rather than a concentration. In the natural seawater with the present-day normal pH, usually 99.5% of the TAlk is contributed by HCO_3^-, CO_3^{2-}, $B(OH)_4^-$, and OH^-. Therefore, for most seawater, TAlk can be roughly expressed as the sum of carbonate alkalinity ($[HCO_3^-] + 2[CO_3^{2-}]$), boric acid alkalinity $[B(OH)_4^-]$, and water alkalinity ($[OH^-] - [H^+]$). In estuarine, polluted and hypoxic/anoxic waters, however, contributions of sulfides, ammonia, and phosphate to TAlk are also significant. It is also worth noting that $[CO_2^*]$ does not affect seawater TAlk.

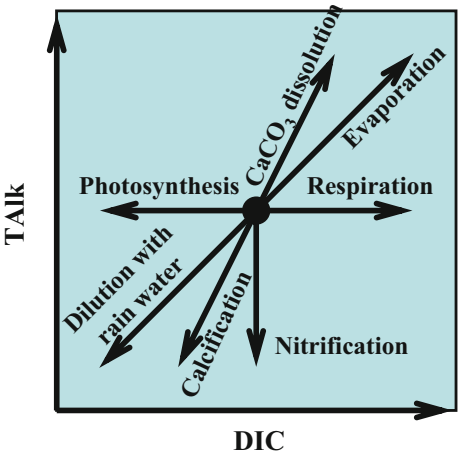

Fig. 1.4 Coupled effects of some marine biogeochemical processes on seawater DIC and TAlk. Contributions of ammonium, phosphate, and silicate on TAlk are ignored

In practice, seawater samples are accurately titrated using diluted and calibrated hydrochloric acid. This is to ensure all of HCO_3^- and CO_3^{2-} in the water sample is being converted to CO_2*, and then set the sudden jump of the conversion as the end point of titration. Finally calculate the seawater TAlk value based on the principle of acid–base titration.

In open oceans, surface TAlk ranges from 2110 to 2450 μmol/kg, behaving like a quasi-conservative parameter of seawater. Usually, ocean surface TAlk can be predicted using salinity and water temperature, with an error of $<1\%$. This suggests that the distribution of ocean surface TAlk is dominated by various physical mixing processes. Neither air–sea CO_2 exchange nor biological uptake/release of CO_2 affects the TAlk value. In the South China Sea and the East China Sea outer continental shelf waters affected by the Kuroshio, the salinity-normalized TAlk (corrected to the salinity 35) is almost constant at 2300 ± 10 μmol/kg.

The quasi-conservative nature of seawater TAlk can be explained from the geochemical point of view. In seawater, there is always a difference between total charges of the conservative cations and the conservative anions. This difference is just compensated by the TAlk defined via formula (1.6). Therefore, the quasi-conservative nature of seawater TAlk does not depend on the determining operation. It is fundamentally because both of the concentrations of the seawater conservative ions and the charge differences between conservative anions and cations are not changed during the air–sea CO_2 exchange and the metabolism-induced CO_2 uptake and release.

Seawater TAlk can be affected by environmental factors and some biogeochemical processes (Fig. 1.4). Firstly, TAlk is closely related to salinity. All processes affecting salinity (including rainfall, evaporation, river flushing, and sea ice) can cause changes in seawater TAlk. Secondly, the formation and dissolution of $CaCO_3$ minerals can result in changes in Ca^{2+} concentration in seawater, leading to changes of the charge differences between conservative cations and anions, and thereby changes in seawater TAlk. In some sea areas where marine calcifying organisms

form $CaCO_3$-involved shells and/or skeletons, seawater TAlk may decline to an unusually low level. After these organisms die and sink to the depths, the $CaCO_3$-rich shells and skeletons will dissolve, leading to much higher TAlk in deep seawater than that in surface waters of similar salinity. According to formulae (1.3–1.5), when one mole $CaCO_3$ is precipitated, seawater DIC will decrease by one mole, and TAlk will decrease by two moles. Conversely, the dissolution of one mole $CaCO_3$ will increase the seawater DIC by one mole, and TAlk will increase by two moles. It is worthwhile to note that these changes are irrelevant to the carbon sources (either HCO_3^- or CO_3^{2-} or CO_2) that marine organisms utilize for calcification. In addition, the utilization of various nitrogen sources by marine organisms, and the nitrification associated with organic matter remineralization, releases H^+ ion to seawater, also affecting TAlk.

1.3 pH

pH is one of the fundamental physical and chemical properties of aqueous solutions. All the natural phenomena and chemical variations involving aqueous solutions are related to pH. The original definition of pH is the negative logarithm of the activity of H^+ ions in the aqueous solution. For a highly diluted solution, the activity of H^+ ions is close to the concentration of H^+ ions. That is, $[H^+] = 10^{\{-pH\}}$. When the pH value decreases by 0.3, the aqueous solution exhibits doubled H^+ ion concentrations.

Aqueous pH values are usually measured via the colorimetric method (using the test paper or cuvettes), glass electrode method, and/or spectrophotometric method. All these pH measuring methods are relative measurements. The practical pH values are always defined based on the given operation. To make the pH values comparable, pH scales must be established. Therefore, all of the reported pH results should specify which scale is used. Practically, several standard buffers in the pH range of 0–14 are selected as reference points of the pH scale. Their $pH^{standard}$ values are determined using the most accurate method that modern technology can achieve. And then the standard buffer series and the well-determined $pH^{standard}$ values make up a pH scale.

As a commonly used precision determination of pH values, the glass electrode method actually determines the potential difference between the glass electrode and a reference electrode. Before the determination of water samples, the instrument needs to be calibrated, that is, a series of standard buffer solutions is determined first. The usual pH standards include a series of standard buffers being traced to the National Institute of Standards and Technology, USA. These standard buffer solutions, defining the NBS scale, are inexpensive and easy to use. However, their ionic strengths are very low and unsuitable for seawater pH measurements at the high ionic strength.

Ionic strength does not directly affect pH. It affects liquid junction potentials between reference electrode and the solution to be measured. Therefore, the pH measurement using the NBS scale contains liquid junction potential difference

induced by ionic strength changes. This liquid junction potential difference replicates poorly and cannot be calculated. This problem makes the NBS-based pH measurement unstable, with a real precision of worse than ±0.01. It is therefore difficult to use pH data on the NBS scale in high-quality quantification and calculation.

Moreover, the HSO_4^- ions and HF molecules dissociate incompletely in natural seawater. Therefore, pH on total-hydrogen-ion scale (pH_T) and pH on seawater scale (pH_{sw}) are used to characterize the acid–base property of seawater. They are,

$$pH_T = -\log_{10}\{[H^+] + [HSO_4^-]\}, \tag{1.7}$$

$$pH_{sw} = -\log_{10}\{[H^+] + [HSO_4^-] + [HF]\}. \tag{1.8}$$

In seawater with salinity 35, the HSO_4^- ions decrease the pH value by approximately 0.11 units at 25 °C, while the HF molecules further decrease the pH value by approximately 0.01 units. Therefore, the seawater pH scale is an issue to be seriously considered. To avoid confusion when comparing with others' data, clear and detailed records of pH scales must be kept during experiment, data report, and communication processes. When the dataset is published, the real information on the pH scale should be simultaneously reported along with the data. Nowadays marine chemists have defined two solutions of 2-amino-2-hydroxy-1,3-propanediol (tris) and 2-aminopyridine as standard buffers. Their pH_T values are 6.7866 and 8.0936 at 25 °C, respectively. Their formulations contain artificial sea water of appropriate salinity, so as to make the ionic strength of water samples similar to that of the standard buffer solutions, minimizing influences of the liquid junction potential. The detailed formulation refers to relevant manuals.

Seawater pH_T usually ranges from 7.5 to 8.5, and thus is weakly alkaline. In open oceans, surface pH_T is less variable (usually ranging from 8.0 to 8.2), while deep pH_T values can be as low as 7.5. In coastal oceans, algae blooms can induce very high surface pH_T values of 8.5 or even 9.0. These variations are related to the carbonate buffering system, and also controlled by metabolic activities of marine organisms. In some coastal aquaculture areas, pH varies tremendously, with a daily variation of more than 1.0 pH units.

1.4 Seawater Partial Pressure of CO_2

Seawater pCO_2 indicates the molecular tendency of CO_2* to escape from the water. It exhibits the driving force or dissipation capability when CO_2* transfers crossing the gas-liquid interface. In practice, seawater pCO_2 can be measured via pCO_2 determination of the gas phase in a confined space when it is in mandatory equilibrium with the seawater. For example, sea surface pCO_2 is usually determined using a continuous flow system equipped with a water-gas equilibrator with satisfactory accuracy and reliability. Because of operational difficulties, subsurface and deep-

water pCO_2 are usually calculated from the other measurable carbonate parameters using a CO2SYS software.

This property is very useful in discussing the source-sink issue of oceans against the atmospheric CO_2, since the air-sea CO_2 exchange is directly driven by the pCO_2 difference between sea surface and the overlying atmosphere. Chemically, seawater pCO_2 is in proportion with the concentration of CO_2*, i.e.,

$$pCO_2 = [CO_2^*]/K_H, \tag{1.9}$$

where K_H is the Henry coefficient of CO_2 in seawater, with a unit of mol/(kg·Pa) or μmol/(kg·μatm). The K_H is a function of temperature, salinity, and water pressure. Given the fact that the behaviors of CO_2 are actually different from that of ideal gases, the CO_2 fugacity (fCO_2) is sometimes recommended to be used in the same dimension and the same unit as pCO_2. In the usual temperature and pressure conditions of sea surface environments and shallow oceans, pCO_2 is only ~0.3% higher than fCO_2.

Spatial distributions of sea surface pCO_2 are complex, with field-measured data from 4 Pa in some coastal algae bloom areas to 80 Pa in equatorial eastern Pacific Ocean waters affected by upwelling such as off Peru. Some estuaries have an aqueous pCO_2 of higher than 800 Pa, which is 20 times the atmospheric equilibrium level. In general, very low seawater pCO_2 indicates significant phytoplankton photosynthesis, while the high estuarine pCO_2 is associated with either remarkable respiration or significant groundwater inputs. Deep seawater often has relatively high pCO_2 of 80–160 Pa, owing to a long-term accumulation of the organic matter decomposition product over the past several decades or even several centuries. If the CO_2-rich deep water rises to the sea surface, a CO_2-source area will take shape, releasing CO_2 to the atmosphere.

As suggested by formulae (1.3) and (1.4), the formation of $CaCO_3$ consumes a large amount of alkaline substance CO_3^{2-}, or produces a large amount of H^+, resulting in seawater pH decrease and pCO_2 increase. Therefore, the $CaCO_3$ formation (e.g., during a coccolithophore bloom) tends to release CO_2 to the atmosphere.

Seawater pCO_2 has a substantial temperature effect. A heating process leads to seawater pCO_2 increase by 4.23%/°C, while the cooling process makes the seawater pCO_2 decline. Therefore, the seasonal transition alone has the potential to change the CO_2 release-uptake behavior of a given water-mass.

In future scenarios where atmospheric CO_2 continues to rise, actual ocean acidification is characterized by a relatively stable TAlk of seawater. If seawater pCO_2 rises in proportion to the atmospheric CO_2 rise, the seawater carbonate components will change (Fig. 1.5). When seawater pCO_2 exceeds 200 Pa, the seawater concentration of CO_2* will exceed that of CO_3^{2-}. If pCO_2 is higher than 550 Pa, the seawater will change from weakly alkaline to weakly acidic.

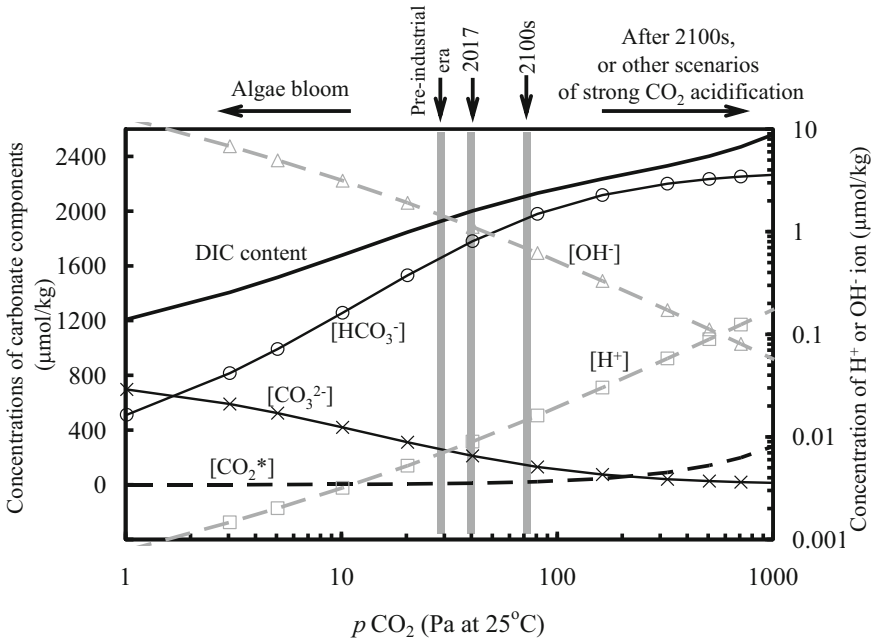

Fig. 1.5 Changes of seawater carbonate components along seawater pCO_2 rise. The salinity is set to 35, while TAlk = 2300 μmol/kg. Vertical gray lines indicate various atmospheric equilibrium scenarios in the given periods

1.5 Carbonate Mineral Saturation State

This property indicates the chemical potential of seawater carbonate system to form $CaCO_3$-involved skeletons or shells of marine organisms, usually expressed with the sign Ω. It is defined as the product of calcium and carbonate ion concentrations in seawater and divided by the apparent solubility product (K_{sp}*) for either aragonite or calcite, i.e.,

$$\Omega_{arag} = [Ca^{2+}] \times [{CO_3}^{2-}]/{K_{sp}}^*{}_{arag}, \tag{1.10}$$

$$\Omega_{cal} = [Ca^{2+}] \times [{CO_3}^{2-}]/{K_{sp}}^*{}_{cal}, \tag{1.11}$$

where subscripts arag and cal represent aragonite and calcite, respectively. Chemically, $\Omega_{arag} > 1$ or $\Omega_{cal} > 1$ indicates that the $CaCO_3$ mineral is stable in the seawater, while $\Omega_{arag} < 1$ or $\Omega_{cal} < 1$ indicates that aragonite or calcite is unstable. Without protective mechanisms, calcifying organisms such as corals and shellfish are vulnerable to $CaCO_3$ undersaturated seawater with $\Omega_{arag} < 1$ or $\Omega_{cal} < 1$ (Eq. 1.5).

The real situation in the marine environment is much more complex than the chemical definition above. $CaCO_3$ occurs in marine environments as three polymorphs, i.e., calcite, aragonite and magnesian calcite. Pure calcite (>99 mol% $CaCO_3$) is more stable than aragonite, while high-Mg calcite (>12 mol% $MgCO_3$) is more soluble than aragonite. Usually, marine calcifying organisms need a Ω_{arag} value of >1.5 to conduct normal calcification activities. In middle to lower latitudes, some coral calcite skeletons may undergo dissolution even at relatively high Ω_{arag} levels of 2–3.5. This is partially because, in present oceans with seawater Ca:Mg molar ratios of about 1:5, many carbonate biominerals are composed of unstable high-Mg calcite. Likely due to this reason, calcium contents of marine organisms decrease when the seawater Ω_{arag} declines.

Seawater Ω data is calculated using the CO2SYS software. In a qualified laboratory, Ω values calculated from DIC and TAlk versus those from pH and TAlk are comparable with each other at a deviation level of ±0.1. In the Pacific Ocean, the current surface Ω_{arag} values are 1–2 in high-latitude regions and 3–4.5 in low-latitude regions. In high-latitude regions, cold surface waters absorb a considerable amount of CO_2 from the atmosphere, resulting in low Ω_{arag} values. It is worthwhile to note that, the commonly used CO2SYS software does not require Ca^{2+} concentration data to be input. The Ca^{2+} concentrations are automatically calculated from salinity data and the proportion between ocean surface Ca^{2+} concentrations versus salinity, based on the law of constant ratio of major elements. This simplification will cause significant errors in some estuaries and coastal zones, where the Ca^{2+} ion concentrations deviate from the open ocean constant ratio of major elements. In these cases, the real relationship between Ca^{2+} ion concentration and salinity should be determined in accordance with the characteristics of local waters. Then, accurate Ω_{arag} data can be calculated via Eqs. (1.10) and (1.11).

1.6 Determination of Seawater Carbonate System Parameters

For sampling, both DIC and pH are gas-type parameters. Their sampling should follow a procedure similar to the dissolved oxygen sampling, i.e., using a narrow mouth bottle, sampling through the bottom of bottle with a tube, and overflowing the water sample. The operator should minimize air bubbles during sampling and transport. Filtering is not recommended. Otherwise, water–gas exchanges will bias DIC and pH data. TAlk is not a gas-type element. Its sampling is the same as other major elements. Besides avoiding contamination, the only requirement of TAlk sampling is to avoid evaporation and dilution.

Both determinations of DIC and TAlk involve chemical reactions between water samples and strong acids. Thus all acid-soluble particulate matter can make the determination fail. To ensure all those particles are settled, the sample quality assurance should include adding 0.05–0.10% volume of saturated mercuric chloride

solution immediately after sampling, fully mixing shortly after tightening the cap or stopper, and ensuring that all microorganisms have been killed. The water samples should be stored in the shade at relatively low temperature (but strictly away from freezing). Before determination, the water samples should be allowed to settle completely. Only supernatant can be used for determination. Once an acid-soluble particle is accidentally introduced into the testing system, the result will be strangely high. The determination should be repeated so as to confirm or exclude the unusual data.

Both the determination and application of seawater DIC and TAlk involve the issue of unit conversion. The usual determination is associated with the volume injection. However, both DIC and TAlk values of reference materials are certified with μmol/kg. To find out the real amounts of DIC and TAlk that the instrument detects, the operators must calculate the density before testing the certified reference material, using the salinity and local temperature, and then convert the concentration value from μmol/kg to μmol/L. After testing the water sample, the immediate results of DIC and TAlk (μmol/L) should be further corrected against the dilution effect caused by the previous addition of mercuric chloride dissolution. The concentration value of the water sample should then be converted from μmol/L (at the testing water temperature) to μmol/kg. The reportable and applicable data of DIC and TAlk are usually expressed in μmol/kg. Especially for the CO2SYS calculation through DIC and TAlk, the correct results can be obtained only by inputting DIC and TAlk contents expressed in μmol/kg, rather than those in μmol/L.

The pH value of seawater is greatly affected by temperature. Therefore, the qualified pH measurement should be carried out under temperature-controlled condition. Its application involves the temperature correction procedure, i.e., adjusting the pH data from the measurement temperature to the temperature condition under which the pH data are used. Many high-precision pH meters equipped with glass electrodes have a nominal precision of ± 0.002, corresponding to the electrode potential response of ± 0.1 mV. However, the determination is subject to many factors, such as the liquid junction potential and electrode efficiency. The actual analytical error is usually as high as ± 0.01 or even ± 0.05 pH units. The electrode efficiency indicates the real electrode potential response at a given temperature against the theoretical value calculated through the Nernst equation. If the electrode efficiency is lower than 98%, the electrode should be discarded or reactivated. Usually a precision pH electrode can be used for half a year or 1 year. The glass electrode method is also subject to instrument drift. To control the effect of instrument drift on pH data, it is necessary to repeat detection of the electrode potential response against the standard buffer series before, during, and after the measurement of each batch of water samples.

If the turbidity of water samples does not affect light transmission, it is recommended to determine seawater pH through spectrophotometry, with m-cresol purple as the chromogenic reagent. The absorbance is measured at two wavelengths of 578 and 434 nm. The absorbance quotient is then used to calculate the pH value. Spectrophotometry is usually applied for pH measurement in a pH_T range between 7.2 and 8.2, while its detectability could be extended to a high pH_T value of ~9

according to the discoloration range of the reagent. The spectrophotometric determination of seawater pH has a good precision of ±0.0004. However, most commercially available cresol purple reagents have an unsatisfactory purity of only 90%. Some colored impurities interfere with the pH determination. Researchers have found that reagents from different sources may result in a data inconsistency of up to ±0.02. It is recommended to purify the commercial reagent before use.

Chapter 2
Photosynthetically Active Radiation and Ultraviolet Radiation Measurements

Gang Li and Kunshan Gao

Abstract Solar radiation that drives the photosynthetic progress of phytoplankton is one of the key environmental factors. Therefore, the accurate measurement of light intensity and dose is vital for the researches of marine ecology and phytoplankton physiology. This section thus describes in detail the methods for measurements and conversions of visible and ultraviolet radiation in outdoor and indoor conditions.

Keywords Measurement · Photosynthetically active radiation · Ultraviolet radiation · Conversion · Instrument

2.1 Introduction

Light drives the photosynthesis of marine phytoplankton while light quality and quantity influence their photosynthetic activity and carbon fixation. The light spectra emitted from different types of light sources like fluorescent light or sunlight often differs greatly, which would affect the algal photosynthetic processes and primary productivity in aquatic ecosystems. Therefore, the actuate measurement of light quality and quantity is one of the important parts for algae researches.

G. Li
Key Laboratory of Tropical Marine Bio-resources and Ecology, South China Sea Institute of Oceanology, Chinese Academy of Sciences, Guangzhou, China

K. Gao (✉)
State Key Laboratory of Marine Environmental Science and College of Ocean and Earth Sciences, Xiamen University, Xiamen, China
e-mail: ksgao@xmu.edu.cn

K. Gao et al. (eds.), *Research Methods of Environmental Physiology in Aquatic Sciences*, https://doi.org/10.1007/978-981-15-5354-7_2

2.1.1 Light Intensity Measurement

Most indoor light sources like fluorescent tube and tungsten lamp etc., emit photosynthetically active radiation (PAR, 400–700 nm) and infrared radiation (IR, >700 nm) that is often measured using light meter with units of μE m^{-2} s^{-1}, μmol photons m^{-2} s^{-1} or Lux. For solar radiation, its spectra not only include longer wavebands of PAR and IR, but also include shorter wavebands of ultraviolet radiation A (UV-A, 315–400 nm) and B (UV-B, 280–315 nm). Such intensity of UV radiation is usually measured with broadband filter radiometers (e.g., Real Time Computer, Mohrendorf, Germany) or spectro-radiometers (e.g., OceanOptics, StellarNet Inc.) with the units of W m^{-2} or μW cm^{-2}. The different units mentioned above can be conversed with the following correlations: 1 E = mol photons; 1 μmol photons m^{-2} s^{-1} = 51.2 Lux = 0.217 W m^{-2}, with some changes among different light sources.

At present, a lot of devices for light intensity measurement are commercially available (Fig. 2.1). According to different light sources like solar radiation or indoor artificial light, a more suitable photometer can be selected: the terrestrial photo-radiometer (Fig. 2.1a, e) can be used to measure solar PAR radiation; and the broadband filter radiometers can be used to measure the solar PAR, UV-A, and UV-B radiation in atmosphere (Fig. 2.1b) or underwater (Fig. 2.1f). Moreover, the spectra of solar radiation can be measured with the spectro-radiometer (Fig. 2.1d), while the light level of the indoor light sources can be measured with illumination photometer (Fig. 2.1c, g, h). In particular in the incubator, the light intensities from different directions should be considered and the averaged levels should be used when measuring the light level at a certain position, because the light distributed at different sides differs. To accurately measure the culture-received light level within flasks, the spherical photometer should be dipped into the culture (Fig. 2.1h).

Fig. 2.1 Different types of light meters: the spherical photometers (**a**–**c**, **h**), planar lightmeter (**e**–**g**), and optical spectrum analyzer (**d**)

2.1.2 Light Absorption and Extinction Coefficient

Due to the effects of absorbing and scattering of seawater, dissolved matters and suspended particles etc., the underwater light intensity decays exponentially with water depth, following the Beer's law. Therefore, the light level at different depths can be calculated with the following equation:

$$I_z = I_o \times e^{-kz},$$

where I_Z and I_o indicate the light intensities at z m depth and surface layers of water column, respectively; k indicates the extinction coefficient, and z indicates the water depth. The extinction coefficient (k) is wavelength-specific and is influenced by the suspended matter's concentrations and species; therefore, the k differs greatly among different waters (Fig. 2.2) (Li 2009; Gao et al. 2007; Wu et al. 2010; Li et al. 2011).

In aquatic ecosystems, light intensity decreases with increasing water depth (Fig. 2.2). The profiles of light in water column can be measured with underwater PAR radiometer (Fig. 2.1a) or broad band radiometer (Fig. 2.1f). The diving broad band radiometer can record irradiance in three wavebands of UV-B, UV-A, and PAR, and also measure temperature and depth at the same time. The underwater light intensity can also be measured with Spectro-Radiometers (e.g., Stellar Net Inc. or Ocean Optics Inc.) that records the energy of each wavelength and integrate to obtain the intensities of different wavebands.

Naturally, phytoplankton stop growing when the synthesis of organic matters by photosynthesis is equal to consumption by respiration, which occurs at compensation point of light intensity. The depth of this compensation point is defined as the compensation depth of light for phytoplankton. In marine ecosystems, the depth of light compensation is generally considered to be the depth at which light intensity decays to 1% of the surface; and the water layer above the light compensation point is defined as euphotic zone (Z_{EU}). Furthermore, the optical depth can be obtained with the euphotic zone depth multiplying by extinction coefficient ($Z_{EU} \times K_{PAR}$). The decay of light intensity varies greatly among different waters due to the differences in concentrations and species of dissolved matters and suspended particles, which results in great differences in the depth of euphotic zone. Moreover, shorter wavelengths of ultraviolet radiation are easier to be absorbed and scattered by seawater itself and suspended maters therein, and decays quickly (Fig. 2.2), as compared with the longer wavelengths of PAR radiation (Li 2009; Gao et al. 2007; Wu et al. 2010; Li et al. 2011).

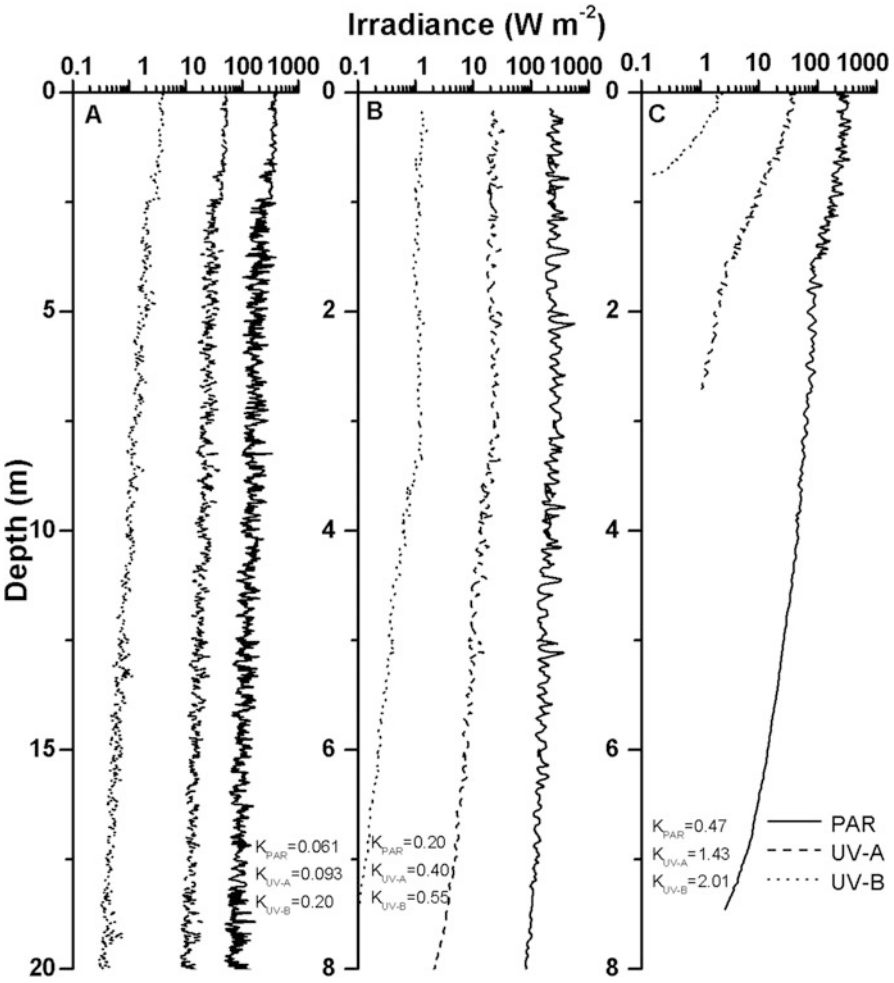

Fig. 2.2 Profiles of solar photosynthetically active radiation (PAR, 400–700 nm) and ultraviolet radiation A (UV-A, 315–400 nm) and B (UV-B, 280–315 nm) among the pelagic water (A, 14° 15′ N, 111° 45′ E), coral reefs (B, 16° 51′ N, 112° 20′ E) and coastal water (C, 23° 24′ N, 117° 07′ E) of the South China Sea

2.1.3 Planer and Spherical Radiometer Calibration

There are two kinds of light sensor commercially available, i.e., planar and spherical surface. Both of these two kinds of radiometers can give almost same value of light intensity when measuring the direct light levels, such as from a parallel light source or midday sun. However, if the light diffuses like from spherical light sources or sunlight in early morning and dusk, the radiometer with planar sensor surface will give a lower value due to the light energy loss caused by reflection. In this case, it

would be better to choose the radiometer with spherical sensor surface that can eliminate the effect of the reflection-caused energy loss. Therefore, the radiometer with planar sensor surface (Fig. 2.1e–g) is suitable to measure the light intensity of indoor parallel light sources, whereas that with spherical sensor surface is suitable to measure the light intensity of solar radiation or point light sources. In seawater, the energy losses due to reflection can be ignored, because the medium refractivity is similar between water and instrument probe cover; the radiometer with planner sensor surface is thus often used to measure the underwater profiles of solar radiation (Li 2009; Gao et al. 2007; Wu et al. 2010; Li et al. 2011).

Photosensitive unit is a part of perceiving light signaling of the light measuring devices, the most important part of an instrument, which will be aging after a certain time usage, and lead to the measured errors. So the instruments need to be calibrated after using for a certain time, under the help of standard light sources. To do this, the light intensity of standard light sources (e.g., DH-2000-CAL, Ocean Optics Inc.) can be measured with the radiometer; then, the measured values be compared with the standard intensities to get a correction factor. The measured data can thus be calibrated by manual or through revising the correction factor in software.

References

Gao K, Li G, Helbling EW, Villafañe VE (2007) Variability of UVR-induced photoinhibition in summer phytoplankton assemblages from a tropical coastal area of the South China Sea. Photochem Photobiol 83:802–809

Li G (2009) Studies on the relationships of solar ultraviolet radiation and photosynthetic carbon fixation by phytoplankton assemblages from the South China Sea. Doctoral dissertation, Shantou University Library, pp 1–171

Li G, Gao K, Yuan D, Zheng Y, Yang G (2011) Relationship of photosynthetic carbon fixation with environmental changes in the Jiulong River estuary of the South China Sea, with special reference to the effects of solar UV radiation. Mar Pollut Bull 62:1852–1858

Wu Y, Gao K, Li G, Helbling EW (2010) Seasonal impacts of solar UV radiation on the photosynthesis of phytoplankton assemblages in the coastal water of the South China Sea. Photochem Photobiol 86:586–592

Part II
Plankton Culture Techniques

Chapter 3
Manipulation of Seawater Carbonate Chemistry

Kunshan Gao

Abstract Different culture methods to grow microalgae could lead to different physical (light) and chemical environments in culture vessels. Photosynthetic carbon sequestration by the algae in light and their respiratory CO_2 release in darkness, can affect stability of carbonate systems (pH, various forms of inorganic carbon, total alkalinity) in culture systems. Usually, pH could increase during light period with active photosynthesis, and decrease during dark period. Such changes in pH and associated carbonate chemistry depend on culture methods and cell biomass or densities of microalgae in water body. The greater the amount of carbon fixation in the water, the greater the changes of the carbonate system. In experiments on the influence of other environmental factors on algae, controlling pH and other carbonate system parameters within known stable ranges is one of the keys to obtain reliable data. This section introduces the seawater carbonate system, compares the existing several kinds of carbonate system control methods, and provides basic suggestions for ocean acidification simulation experiments on marine organisms.

Keywords Algae · Carbonate chemistry · pH

The carbonate system in seawater includes CO_2 (water) (the sum of CO_2 and H_2CO^3), HCO_3^-, CO_3^{2-}, H^+, OH^- and several other weak acid-base system (mainly the boric acid and boric acid salts). At any given temperature, salinity, and pressure, knowing two elements of the carbonate system and the macronutrient concentrations, the values of other carbonate system parameters of seawater can be calculated. Dissolved inorganic carbon (DIC) is the sum of inorganic carbon species in a solution. And total alkalinity (TA) formally defined as the equivalent sum of the bases that are titratable with strong acid (TA = $[HCO_3^-]$ + $[CO_3^{2-}]$ + 2 (OH) 4 − [B] + [OH−] − [H+] + trace components), reflecting protons as the

K. Gao (✉)
State Key Laboratory of Marine Environmental Science and College of Ocean and Earth Sciences, Xiamen University, Xiamen, China
e-mail: ksgao@xmu.edu.cn

K. Gao et al. (eds.), *Research Methods of Environmental Physiology in Aquatic Sciences*, https://doi.org/10.1007/978-981-15-5354-7_3

receptor over the donor. TA value, by using strong acid titration to determine, can be regarded as index of solution buffering capacity. Any change of one composition in the carbonate system could cause changes of several other components. That is, any efforts to alter only one parameter of the carbonate chemistry and keep the other components the same, is impossible. The interdependence of carbonate chemistry parameters, has to be considered, when conducting CO_2 perturbation experiments.

When CO_2 dissolves in the seawater, it combines with water to form carbonic acid, and carbonic acid dissociates to release [H^+] and form bicarbonate ions (HCO_3^-). Then further dissociation to carbonate ions [(CO_3^{2-}) and [H^+] could happen. However, the second step dissociation may not happen, since excessive [H^+] may reverse it. Ocean acidification, for example, caused by increasing atmospheric CO_2 concentration and its dissolution into seawater, is known to change seawater carbonate system, increasing [CO_2], [HCO_3^-], and [H^+], decreasing [CO_3^{2-}], and $CaCO_3$ saturation state. With doubling of atmospheric CO_2 concentration (400–800 ppmv), pCO_2 of the surface water HCO_3^-, DIC (total inorganic carbon) will increase nearly 200%, 11%, and 9%, respectively. CO_3^{2-} concentration will decrease by about 45%. The reason for CO_3^{2-} concentration decline is that higher [H^+] levels promote the dissociation reaction to the left in the third reaction ($CO_2 + H_2O \rightarrow H_2CO_3$; $H_2CO_3 \rightarrow H^+ + HCO_3^-$; $HCO_3^- \leftarrow H^+ + CO_3^{2-}$).

3.1 Changes in the Carbonate Chemistry in Algal Cultures

During algal cultures, changes in pH are usually measurable, depending on levels of biomass density. Even under aeration with air or air of high CO_2 concentrations, pH changes can be detected, increasing in the light period, and decreasing in the dark period (Gao et al. 1991). This is because the rate of photosynthetic carbon sequestration (i.e., photosynthetic removal of "CO_2") in the water is faster than the rate of CO_2 dissolution in into it. If the former is equal to the latter, pH stabilizes, with the seawater carbonate system being stabilized. In the dark or night, respiratory CO_2 release, leads to decrease in pH. In addition, the assimilation of nitrate and phosphate, may lead to changes in [H^+] as well:

$$106CO_2 + 16NO_3^- + HPO_4^= + 122H_2O + 18H^+ = [C_{106}H_{263}O_{110}N_{16}P_1] + 138O_2.$$
$$106CO_2 + 16NH_4^+ + HPO_4^= + 108H_2O = [C_{106}H_{263}O_{110}N_{16}P_1] + 107O_2 + 14H^+.$$

As viewed from the phytoplankton element ratios (Redfield ratio), pH changes caused by N and P assimilation should be much smaller compared to CO_2 fixation. The diurnal pH changes during algal cultures process depend on their biomass densities in the culturing vessels. If the biomass density is low enough, the pH will be relatively stable (e.g., pelagic ocean of low photosynthesis biomass). Therefore, culture method and cell concentration or biomass/water mass ratio, is the key for the stability of carbonate system or pH in the process of algal cultures. In many physiological experiments or CO_2 perturbation (acidification) experiments, it is very

important to control the carbonate system stable and make the cells in a stable logarithmic phase to obtain reliable data. It is worthy noting that no matter unicellular or multicellular algae, there would be a carbon or oxygen or nutrient concentration gradient (diffusion boundary layer) surrounding the cells when cells perform photosynthesis or absorb nutrient. And the concentration gradients could affect the micro-environments surrounding the cells. In other words, maintaining stable carbonate chemistry in culture is not enough, carbonate system stability surrounding the cells should be considered. Aerating and oscillating the cultures can reduce or eliminate the diffusion boundary layer near the cell surface and stabilize the carbonate chemistry surrounding the cells.

3.2 Perturbation and Controlling of Seawater Carbonate Chemistry Parameters

There are several ways to change seawater [CO_2], [HCO^{3-}], and [H^+] concentrations. Firstly, maintain stable TA by altering the levels of dissolved inorganic carbon (DIC), such as aerating air that contains known higher CO_2 concentrations, injecting CO_2 saturated water, or adding $NaHCO_3$ or Na_2CO_3 before adding HCl. Secondly, keeping the DIC unchanged, change the TA, for example, adding NaOH or HCl directly into seawater. Since different experimental designs require different manipulations, choosing a way for carbonate system control depends on the experimental duration, cultivation method, volume or sampling intervals. Usually, it is widely accepted to aerate air of targeted CO_2 level to the water directly to adjust the CO_2 concentration (O_2, N_2 concentration constant) or continuously flow through the air of specific CO_2 concentration through the upper part of the culture (some species, such as dinoflagellates, are susceptible to bubbling disturbance).

3.2.1 Altering Concentration of Dissolved Inorganic Carbon

3.2.1.1 Controlling CO_2 Partial Pressures

Traditionally, during some physiological experiments or large-scale algae farming (such as *spirulina*) processes, aerating high concentration of CO_2 (1–100%) to the medium could alleviate the carbon limitation of water and lower pH.

It is usually difficult to maintain pH or other carbonate chemistry parameters stable during algal cultures. And O_2 concentration is also unstable due to photosynthesis and respiration. To explore the physiological response to changes of CO_2 concentrations, it is necessary to control the pH and maintain stable carbonate chemistry. At the same time, stabilizing concentration of dissolved oxygen is also necessary. In the automatic pH regulation system, when the pH is higher or lower than the set value, the control valve will be opened or closed, aerate or stop aerating.

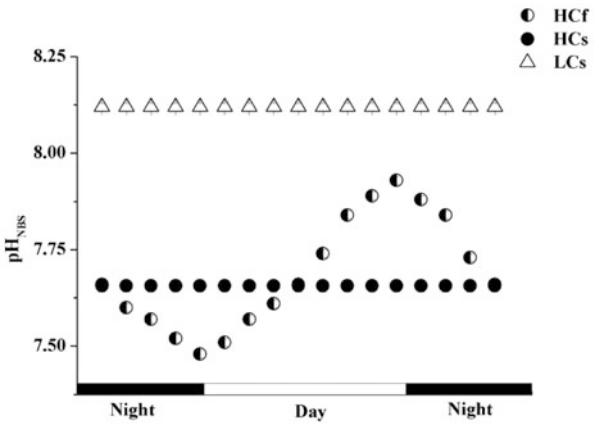

Fig. 3.1 Diel seawater pH variations under constant low (LCs) and high (HCs) CO_2 levels as well as under fluctuating levels of CO_2 (HCf)

Because there is a time lag for the water to reach a new balance of carbonate system, such automatic system can only maintain the pH within a certain range, and pH often fluctuates in a zigzag pattern. Because of this shortcoming, automatic controlling of pH cannot be practically applied to studies on effects of ocean acidification.

On the other hand, seawater pH in coastal oceans often exhibits diel fluctuation, rising with increasing sunlight due to photosynthetic CO_2 removal and declining with respiratory CO_2 release during night. To mimic such diel pH fluctuation under ambient and elevated CO_2 levels can help us to examine future ocean acidification effects in coastal waters. Typical pH diel patterns can be expected as Fig. 3.1 using CO_2 enriching devices (CO_2 enrichlors, Wuhan Ruihua instrument and equipment Ltd., Wuhan, China).

Aerating air of constant CO_2 concentrations can control the pH with negligible changes less than 0.05 units if the cell concentrations are maintained low and the culture medium is frequently renewed or diluted with the medium of target CO_2 level (see below). To obtain the air of certain levels of CO_2, following methods can be recommended: (1) mixing usual air with certain amount of pure CO_2 in a bag; (2) mixing CO_2-free air with pure CO_2 to achieve desirable CO_2 levels. Note, because indoor CO_2 concentration in the air is usually higher than the atmospheric CO_2 level, being influenced by people's respiration and instruments, the air to be considered as ambient one should be taken outside far away from human disturbances. Mixing air and pure CO_2 can be done manually or be achieved by using commercially available CO_2 enrichment instrument (Wuhan Ruihua instrument and equipment Ltd., Wuhan, China). The CO_2 enriching device can be used for both lab, outdoor and ship-board experiments (Gao et al. 2012).

When preparing CO_2-free air (ensure that there is no change of oxygen concentration in the air), one needs to use molecular sieve or soda-lime absorption column or NaOH and Ca $(OH)_2$ liquid to remove CO_2. It is better to use a mass flowmeter to mix CO_2-free air and pure CO_2, so that target CO_2 concentration can be achieved. In general, in culture systems, maintaining stable carbonate chemistry is desirable to reduce confounding factorial influences. Two factors should be considered when

conducting aeration for CO_2 partial pressure control. Aeration might increase released organic matters from the algal cells (Gattuso et al. 2010), most likely due to enhanced photorespiration (Gao et al. 2012), therefore, influencing air–water surface exchanges of gases, then drawback can be solved by the following ways, (1) keep low cell concentration and increase the frequency of dilution; (2) growing the cells in a dialysis bag, then put it in water, which can be aerated with air of targeted CO_2 levels. Gas and small molecules can pass through the dialysis bag. We need to inspect whether the membrane is chemically neutral when we use dialysis bags to avoid any confounding chemical influences. On the other hand, mixing dynamics induced by aeration can affect phytoplankton cells adversely, such as dinoflagellates. Under these circumstances, we can maintain a stable seawater carbonate system for some time without aeration. We can also aerate above the liquid to make gas phase CO_2 stable, so, the exchange of CO_2 between water and gas phases will maintain stable of carbonate chemistry if the CO_2 removal is low enough with low cell concentrations.

3.2.1.2 Adding CO_2 Saturated Sea Water

When two water masses are mixed, the amount of solute of the mixture is equal to the sum of two initial water masses' solutes. For example: in a closed system, we can gain designed partial pressure of CO_2 through adding certain amount of CO_2 saturated sea water to low pCO_2 seawater with the same total alkalinity, so we can obtain our designed levels of pCO_2 (Gattuso et al. 2010). Marine scientists from GEOMAR institute in Kiel, Germany, made partial pressure of CO_2 up to 1300 μatm through adding 200 L CO_2 saturated sea water to a mesocosm of 60 m^3. During the application of this method, one needs to prevent or minimize gas leakage, since the partial pressure of CO_2 is much higher than that of ambient air.

3.2.1.3 Adding Strong Acid and CO_3^{2-} or/and HCO_3^-

Adding CO_3^{2-} or/and HCO_3^- will make dissolved inorganic carbon (DIC) up to a target level. Then, we can accurately add acid to offset the changes of total alkalinity caused by added CO_3^{2-} or/and HCO_3^-. Adding HCl will restore total alkalinity to target level without affecting DIC (the operation should be carried out in a sealed circumstance to get rid of gas exchange). All parameters of the carbonate system can be obtained consequently. It should be noted that this method cannot be applied directly to cultures with cells.

3.2.2 Changing Total Alkalinity

3.2.2.1 Adding Strong Acid and Alkali

Reinforcing acids in a closed system, such as hydrochloric acid, or strong base, such as NaOH, will not change the concentration of DIC, but will change the total alkalinity of solution and partial pressure of CO_2. Total alkalinity decreases when acid is added, but increases when base is added. Changes of total alkalinity are the same regardless of open or closed system when use acid or base. Alteration of salinity due to addition of acid or base is very small, which can be ignored. While this method can help one to obtain desired pCO_2 levels, changes of TA make it not suitable for simulating ocean acidification conditions.

3.2.2.2 Adding CO_3^{2-} or/and HCO_3^-

Both DIC and total alkalinity will increase due to adding Na_2CO_3 or (and) $NaHCO_3$. This method made ratio of increase of DIC to changes of concentration of CO_3^{2-} and HCO_3^- proportionate (1:1) in a closed system. The contribution of these negative ions to total alkalinity is proportional to their charge and concentration, therefore, adding 1 mol CO_3^{2-} can lead to 2 mol increase, and adding 1 mol HCO_3^- can make 1 mol increase in total alkalinity. The change in carbonate system caused by the change in total alkalinity depends on the amount of CO_3^{2-} and HCO_3^- added. This method can be used to maintain a constant pH or maintain a constant total alkalinity with adding acid.

3.2.2.3 Controlling Concentration of Ca^{2+}

We can change concentration of Ca^{2+} to alter parameters of carbonate system, such as calcite saturation level. Calcification of coral, seashell and calcifying algae are related to seawater calcite saturation state (Ω) (Ruan and Gao 2007). $\Omega = [Ca^{2+}][CO_3^{2-}]/K_c$, where $[Ca^{2+}]$ and $[CO_3^{2-}]$ are the concentrations of Ca^{2+} and CO_3^{2-} in seawater, respectively. K_c is product of concentration of Ca^{2+} and CO_3^{2-} when $CaCO_3$ solution is saturated, with the crystal types of $CaCO_3$ (such as calcite, aragonite, etc.). It can be seen that the reduction of CO_3^{2-} caused by ocean acidification leads to a decrease in Ω, which can alternatively be achieved by changing $[Ca^{2+}]$ (Xu et al. 2011; Xu and Gao 2012).

3.3 Control of Microalgal Cell Density or Biomass

In the case of culture, depending on the culture methods and/or cell concentration, dissolved inorganic carbon (DIC) in the medium can be decreased and the pH be increased due to photosynthesis assimilation of CO_2 as organic matter. This phenomenon occurs even if the air is inflated or even under elevated concentration of CO_2 (Gao et al. 1991). Let's assume that the amount of inorganic carbon fixed by photosynthesis in the culture system is $X1$, the amount of carbon dissolved into the medium is $X2$. When $X1 > X2$, the pH increases and the DIC decreases; when $X1 = X2$, the carbonate system is stable, with constant pH and DIC. So, we need to accelerate balance of carbonate system or decrease the biomass density to achieve $X1 = X2$ or CO_2 equilibrated condition. The method of accelerating the balance of the carbonate system is to use a buffer or add carbonic anhydrase. The buffer solution has effects on algae physiology, and the cost of using it is high and will have an additional effect. Therefore, the optimal method is to control the concentration of cells to make the amount of cells per volume of water is sufficiently low to minimize $X1$ in and make it balanced with $X2$. In the case of bubbling air of constant CO_2 concentration, if $X1$ is less than $X2$, removal of CO_2 in the culture solution by algae will be small enough, so that partial pressure of CO_2, pH, and other carbonate system parameters can be maintained stable.

In order to control the carbonate system of the culture medium to maintain stable pH (the daily variation less than 0.05), semicontinuous or continuous cultures are recommended. For cultures of phytoplankton, if the initial inoculated cell concentration is low, such as less than 100 cells per milliliter, a short-term batch culture can be performed without dilution, since the cells can mostly maintained in the logarithmic growth phase for relatively longer periods. The stability of carbonate system can be affected by aeration rate and levels of light and temperature. Therefore, to control cell concentration ranges in cultures and maintain stable pH, dilution frequency and biomass density are the key. For example, under 5–50% solar radiation conditions and with an aeration at a rate of about 300 ml/min, cultures of the diatoms, *Phaeodactylum tricornutum*, *Skeletonema costatum,* and *Thalassiosira pseudonana*, can be maintained with the cell concentrations less than 300,000 cells/ml by diluting every 24 h with the cell concentration of about 50,000 cells/ml after the dilution. In this way, the carbonate system parameters can be controlled within the range shown in Table 3.1 (Gao et al. 2012). If the concentration of cells in the logarithmic growth period are very low (such as 100 cells/ml), the carbonate system can be relatively stable even without renewing the medium for 3–5 days (specific time length depends on cell growth rate). For calcifying microalgae, coccolithophores, usually aeration is not recommended. The pH can be maintained stable in a certain period of time (stable time depends on light intensity) if we dilute before the cell concentration reaches to 40,000 cells/ml. Since the algal calcification can release CO_2 and decrease

Table 3.1 Parameters of carbonate system in algae solution at different CO_2 concentrations

	pCO_2 (μatm)	pH_T	DIC (μmol kg^{-1})	HCO_3^- (μmol kg^{-1})	CO_3^{2-} (μmol kg^{-1})	TA (μmol kg^{-1})
Lab	390	8.02 ± 0.01^a	1913.6 ± 57.4^a	1739.7 ± 48.5^a	161.2 ± 8.9^a	2155.3 ± 68.3^a
	1000	7.68 ± 0.01^b	2116.3 ± 72.8^b	2000.5 ± 67.2^b	83.1 ± 5.5^b	2217.9 ± 79.6^a
Field	385	8.04 ± 0.01^a	1889.7 ± 38.6^a	1700.8 ± 32.0^a	176.3 ± 6.6^a	2134.0 ± 46.5^a
	800	7.76 ± 0.01^b	1981.8 ± 34.7^b	1854.7 ± 34.7^b	101.0 ± 3.8^b	2102.8 ± 43.2^a
	1000	7.69 ± 0.01^b	2097.2 ± 40.5^b	$1973.3 \pm 37.^b$	91.5 ± 3.4^b	2196.1 ± 44.7^a

Different superscript alphabets indicate significant differences ($p < 0.05$)

TA, therefore, it can offset to some extent increased pH due to photosynthetic carbon fixation.

Carbonate system parameters were measured in diatoms with semicontinuous cultures outdoor (Lab) or phytoplankton with field experiment in situ (Field). Both of them aerated with outdoor air or air enriched with CO_2. The aeration rate was 310 mL/min, and the cell concentration was diluted to about 50,000 cells/mL every 24 h (Lab case) (Table 3.1).

3.4 Analyses of Advantages and Disadvantages

1. Aerating to seawater with air enriched with CO_2 and adding acid in combination with adjustment with carbonates or bicarbonates are the two main approaches to alter carbonate chemistry for studies on ocean acidification effects. These methods all can increase DIC and lower pH. Addition of acid changes total alkalinity (TA). Aeration can be used to maintain long-term constant conditions without altering seawater TA. Nevertheless, it should be noted that the biological processes (e.g., photosynthesis, respiration, calcification, nutrient uptake etc.) can change the total alkalinity and DIC, alter the parameters of the carbonate system (Gao et al. 1991; Rost et al. 2008) if the cell concentrations or biomass densities are too high. We assume that if CO_2 dissolution exceeds photosynthetic carbon fixation, aeration can maintain a constant DIC concentration and pH, but cannot compensate for drift of total alkalinity (TA), unless the culture medium is frequently renewed. In addition to the total alkalinity, calcification (limited to calcifying algae) consumes large amount of Ca^{2+}, leading to changes in TA when the biomass density of algae is high or the intervals of renewing medium is long. Moreover, the consumption of nutrients will change TA. Therefore, continuous or semicontinuous cultures with low biomass are the ideal approach.
2. The methods of adding carbonate or/and bicarbonate are impractical. Due to the gas exchanges at the air–water interface, only aeration can successfully regulate the stability of the carbonate system in the open system. However, the force from aeration tends to affect the growth of certain algae (such as dinoflagellates). Without inflation, the stability of carbonate system can also be maintained with low cell concentration via semicontinuous culture. But it is difficult to eliminate the diffusion boundary layer surrounding the cells or thalli due to lack of mixing. Certainly, you can reduce or eliminate the diffusion boundary layer by shaking.
3. In a closed system, the method of adding acid can control pCO_2 precisely, but this way will change the total alkalinity of seawater.

3.5 Recommendations and Suggestions

For detained information toward ocean acidification studies, one can refer to "Guide to best practices for ocean acidification research and data reporting"(http://www.epoca-project.eu/index.php/guide-to-best-practices-for-ocean-acidification-research-and-data-reporting). Here, I only provide some basics for how to control the carbonate chemistry of algal cultures.

3.5.1 Filtration and Sterilization

As filtration would change the carbonate system, we should adjust it after filtration. If it's not permitted under certain conditions, the parameters of the carbonate system should be measured after filtration and the filtration should be carried out in darkness with low pressure levels, since vacuum and high pressure would change the pCO_2 and DIC and let cells break, which would then change the total alkalinity (TA).

The sterilization (autoclaving) should also be done before the adjustment of the carbonate system. As boiled water would disperse dissolved gases, the carbonate system would be totally changed with most of DIC lost as well as changed TA. In a word, the pCO_2 of sterilized seawater would be relatively low with fairly high pH. When seawater cools down, a few CO_2 would dissolve into water again, thus increasing the DIC. If natural sweater is used, we should measure parameters of the carbonate system before and after the sterilization to determine whether this process has an effect. If it is the artificial seawater, then adding acid or $NaHCO_3$ or Na_2CO_3 after sterilization to the target pH level wouldn't change the TA.

3.5.2 Maintain Carbonate Chemistry

To achieve designed pH for experiment, we can aerate with air of a certain concentration of CO_2 to adjust the system. Stable pH under the aeration means that the CO_2 partial pressure of the air and water is equilibrated. There are many factors that determines how long it will take to reach the equilibrium, such as biomass density, pCO_2, the size of bubbles, the flow amount of gas, and the volume and shape of flasks and temperature. Considering that the mixed air doesn't contain vapor (or little), it wouldn't influence the salinity if the gas goes through a bottle fulfilled with distilled water and becomes wet before inlet of the air flow. After the carbonate system reaches the target value, the seawater should be stored in a sealed container to prevent any exchange between the water and air, except that the culture is aerated in an open system.

Some processes such as calcification or photosynthesis would change the parameters of the carbonate system if the density of cells is high especially in a closed

culture system. This issue should also be considered in an aerated open system. To avoid or alleviate this situation, it is suggested to reduce the biomass or cell density.

3.5.3 *Effects of Dissolved Organic Matters, Inorganic Nutrients, and Buffers on TA*

When algae photosynthesize, they release dissolved organic matters which contain some groups that are easy to react with hydrogen ions H^+, thus influencing TA. And the extent of such effect depends on their types and how long the cultures last. This condition should be avoided in pH perturbation experiments. However, if using semicontinuous culture (dilution once a day) or continuous culture, this problem could be ignored especially under the indoor low light environment.

The concentration of nutrient or buffers would have an effect on TA. Using buffers make the carbonate system deviate seriously from natural seawater and TA determination difficult. Under such conditions, we can't use the value of TA to calculate other parameters. Instead, we should use the value of DIC or pH or pCO_2. Both addition of nutrients and consumption by organisms would change TA. Usually, PO_4^{3-} is added in seawater in the form of $NaH_2PO_4{\cdot}H_2O$. It releases $Na^+$and $H_2PO_4^-$ in the moment of dissolution so it won't increase TA. In contrast, if phosphorus is added in the form of H_3PO_4, it will decrease 1 mol TA after each addition of 1 mol H_3PO_4. Therefore, when calculating parameters by using the value of TA, the effect of H_3PO_4 should be considered. If the concentration of H_3PO_4 is below 1 μmol kg^{-1}, this effect could be ignored.

Nitrate is usually added in the form of $NaNO_3$ while it doesn't change the TA so it doesn't need to consider when calculating parameters by using the value of TA. However, if adding HNO_3, it will decrease the TA. Also, NH_3 has an effect and it should be considered. In fact, we usually ignore it as the concentration is relatively low.

Silicon is usually added in the form of $Na_2SiO_3{\cdot}9H_2O$. It will change the TA as SiO_3^{2-} would react with water and generate $H_2SiO_4^{2-}$,which would rapidly costs one proton and generates $H_3SiO_4^-$.What's more, it would absorb another proton and generate H_4SiO_4.Therefore,TA would increase 2 mol after each addition of 1 mol $Na_2SiO_3{\cdot}9H_2O$. We should add HCL to offset such increase of TA because the addition amount of $Na_2SiO_3{\cdot}9H_2O$ is large either in artificial sweater or natural seawater. Also, we should take it into consideration while calculating carbonate parameters. However, the amount of $H_3SiO_4^-$ is relatively low in the natural seawater, which can be ignored (Zeebe and Wolf-Gladrow 2001).

3.5.4 The Treatment of Isotope Inorganic Carbon

The preparation and operation should be careful when using ^{13}C or ^{14}C to label DIC to prevent the leakage of labeled C (in the form of CO_2). As the exchange between the air–water interface could decrease the concentration of isotope carbon, there shouldn't exist any space in the containers. Even the pCO_2 of seawater is same as in atmosphere, ^{13}C or ^{14}C would discharge at all times, whose partial pressure are close to 0 in air with 4 μatm for ^{13}C and 10^{-13} μatm for ^{14}C.

3.5.5 Determination of Carbonate System Parameters

Measurement of TA samples isn't influenced by the exchange of gas. It is supposed that there is no evaporation of seawater and the salinity is constant, even pCO_2 changes as temperature changes, the value of TA still keeps constant. If we measure pH or DIC, we should prevent the gas leakage. Kill the cells before the measurement and store samples in low temperature. Make sure there is no space in the tubes of DIC or pH samples. Cells should be eliminated before the measurement of TA or DIC, because the carbon or other materials they release would influence the values.

3.5.6 Measurement of pH

From the formula $pH = -\log[H^+]$, we can see a little change of pH represents a big change of the concentration of hydrogen ions$[H^+]$. For example, the concentration of hydrogen ions $[H^+]$ would increase by 100% if the pH value drops from 8.1 to 7.8. Thus, it's critical to measure pH accurately. The pH values of the same solution under different temperatures are different. Besides, there are so many kinds of pH meters and the accuracy would drift over time. Therefore, multi-point calibration should be done frequently. Most pH meters show electric potential that is fairly stable. That's why most of chemical analysis labs measure the potential then transform it to the value of pH according to the standard curve of the potential vs. pH. It is suggested to pay attention to the values showed in the pH meter during the measurement. The pH can be displayed under the temperature you measure or the value of 25 °C. Generally, the pH should be measured under the temperature of your experiment or the temperature of cultures. Apart from that, there are three ways of expressions for pH values, which are pH_t, pH_{nbs}, pH_{sw}, each of which depends on the solution for the calibration.

References

Gao KS, Aruga Y, Asada K, Ishihara T, Akano T, Kiyohara M (1991) Enhanced growth of the red alga *Porphyrayezoensis* Ueda in high CO_2 concentrations. J Appl Phycol 3:355–362

Gao KS, Xu JT, Gao G, Li YH, Hutchins DA, Huang BQ, Wang L, Zheng Y, Jin P, Cai XN, Häder DP, Li W, Xu K, Liu NN, Riebesell U (2012) Rising CO_2 and increased light exposure synergistically reduce marine primary productivity. Nat Clim Chang 2:519–523

Gattuso JP, Gao K, Lee K, Rost B, Schulz KG (2010) Approaches and tools to manipulate the carbonate chemistry. In: Riebesell U, Fabry VJ, Hansson L, Gattuso JP (eds) Guide to best practices for ocean acidification research and data reporting. European Commission, Belgium

Rost B, Zondervan I, Wolf-Gladrow D (2008) Sensitivity of phytoplankton to future changes in ocean carbonate chemistry: current knowledge, contradictions and research directions. Mar Ecol Prog Ser 373:227–237

Ruan ZX, Gao KS (2007) Relationship between algal calcification and elevating atmospheric CO_2 centration. Plant Physiol Commun 43(4):773–778. (in Chinese)

Xu K, Gao KS (2012) Reduced calcification decreases photoprotective capability in the coccolithophorid Emiliania huxleyi. Plant Cell Physiol 53:1267–1274

Xu K, Gao KS, Villafañe VE, Helbling EW (2011) Photosynthetic responses of *Emiliania huxleyi* to UV radiation and elevated temperature: roles of calcified coccoliths. Biogeosciences 8:1441–1452

Zeebe RE, Wolf-Gladrow DA (2001) CO_2 in seawater: equilibrium, kinetics, isotopes. Elsevier, Amsterdam, p 346

Chapter 4
Microalgae Continuous and Semi-continuous Cultures

Shanwen Chen and Kunshan Gao

Abstract For many studies using microalgae as research subjects, culture methodology is a key part that influences results. There are many advantages to using continuous or semicontinuous cultures compared to batch cultures. Continuous cultures can maintain a stable physical and chemical environment where cells grow. Semicontinuous cultures are easier to carry out and can also keep cells in the exponential phase of growth for a long time, with stable ranges of environmental changes. Different culture methods have different ways to calculate growth rates, all of which have advantages and disadvantages. It depends on the aim of the study and logistics.

Keywords Microalgae · Continuous · Culture · Medium · Growth

4.1 Introduction

Methods of microalgae incubations are a key influence on experimental results, and have an effect on chemical (such as the concentration of gases and nutrients) and physical features (the light intensity to which cells are exposed) of systems. There are two frequently used techniques, known as batch culture and fed-batch culture. These culture methods are simple and easily manipulated, but physical and chemical conditions in the culturing bottles or vessels change drastically. For example, the amount of nutrient decreases with the growth of microalgae and the amount of light absorbed per cell decreases with the increasing density of cells; pH and the level of dissolved oxygen increase in the period of light with decrease of pCO_2, while this is

S. Chen
Marine Science Institute, Shantou University, Shantou, China

K. Gao (✉)
State Key Laboratory of Marine Environmental Science and College of Ocean and Earth Sciences, Xiamen University, Xiamen, China
e-mail: ksgao@xmu.edu.cn

K. Gao et al. (eds.), *Research Methods of Environmental Physiology in Aquatic Sciences*, https://doi.org/10.1007/978-981-15-5354-7_4

reversed in the dark period. Growth rates and physiological activities of the same species of microalgae under different physical and/or chemical conditions could show a big difference. Therefore, there exists much uncertainty whether the results actually reflect the aim of your study. In addition, because of significant differences in growth rates at different growth phase in batch cultures, physiological state of cells are different and the comparability of data at different growth phases is low. That is, you can obtain data with these methods, but they are hard to compare, even if the experimental conditions surrounding the cultures are similar. Also, batch culture and fed-batch culture methods hardly mimic the dilute chemical environment of oligotrophic regions (LaRoche et al. 2010). It is thus clear that there are many limitations for studies culturing microalgae when batch cultures are employed. Instead, the use of continuous or semicontinuous cultures could keep chemical and physical environment relatively stable and have many advantages.

4.2 Microalgal Continuous Culture

A continuous culture is one in which the culture medium is continuously renewed. That is, the rates of fresh medium inflow and culture medium outflow are regulated so culture medium turbidity or nutrient remains relatively constant in the premise of the constant culture volume, known as turbidostat and chemostat methods, respectively (LaRoche et al. 2010). The continuous culture device needs to be equipped with flow controller and detector, and monitors of turbidity, chlorophyll fluorescence, pH, and dissolved oxygen (DO) according to experimental requirements. Continuous culture systems have various forms but use the same principle, so they can be self-assembled and purchased according to the experimental needs. The purchased apparatus, used for algae research, are generally composed of high transparency incubator, turbidity or chemical detector, liquid flow controller, fresh medium supply device and sterile aeration system (Borchard et al. 2011). Some also have stirrer or upender systems to avoid microalgae sinking, such as a shipborne continuous culture system (Hutchins et al. 2003). In actual research, the continuous culture system can be self-assembled according to its principle such as that shown in Fig. 4.1 (Chen and Gao 2011; Chen 2012).

4.2.1 Turbidostat

Turbidostat is a continuous culture method that maintains a constant turbidity by adjusting the rates of fresh medium inflow and culture medium outflow (Lee and Ding 1994; LaRoche et al. 2010). In each culture system, the overflow control method is used and the inflow rates are adjusted so that the inflow and outflow rates are the same. For microalgae, the turbidity can be determined by measuring the cell concentration, chlorophyll fluorescence or absorbance (OD, such as OD730). In

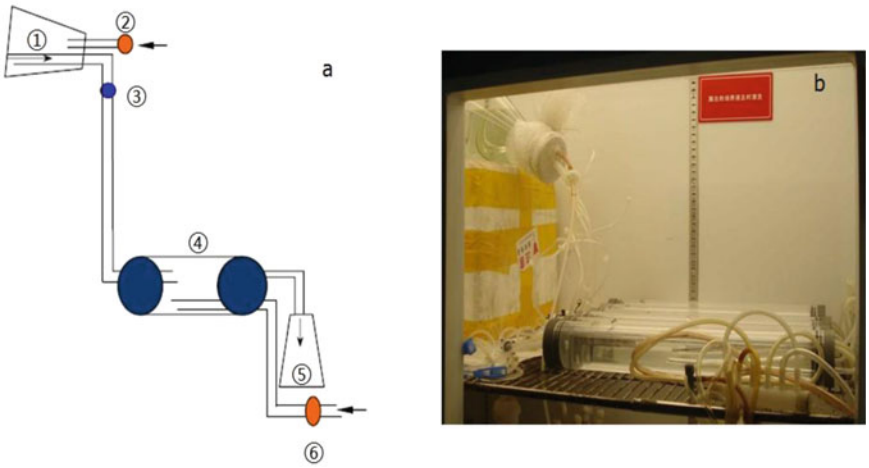

Fig. 4.1 Schematic diagram (**a**) and physical map (**b**) of continuous culture system in artificial climate chamber: ① culture medium container; ②, ⑥ 0.2 μm filter; ③ inflow regulating valve; ④ incubator; ⑤ overflow collection bottle

many experiments, it's pivotal that cell concentration is constant, so it is necessary to adjust the fresh medium inflow rates to make sure the cell is constant within and between treatments because of different cell growth rates under different conditions. In a fast-growing culture system, the nutrient consumption is fast and the accumulation of metabolites is also increased. Meanwhile the medium inflows are large, and the effluent is also large, so that there are not significant differences in the composition of the culture medium under different conditions.

Figure 4.1 shows a simple turbidostat system designed according to the principle of continuous culture and on the basis of existing facilities, which was used for research in the responses of *Phaeocystis globosa* Scherffel to light intensity and quality, and seawater acidification (Chen and Gao 2011; Chen 2012). The system consisted of three parts: the first was an incubator that was made of quartz; the second was medium supply and control device in which disposable medical infusion tubing was applied to controlling fresh medium supply rates; the last was aeration and overflow collection device period, Air intake was equipped with 0.2 μm filter to ensure axenic culture. For a turbidostat, chlorophyll fluorescence measurement is more convenient than cell counting at regular intervals to adjust fresh medium inflow rates. However, these factors affected photosynthetic pigment significantly but cell size insignificantly in this experiment, so cell concentration was determined every other hour and used as the basis of a adjusting inflow rates so that cell concentration was maintained in a certain range such as 0.9–1.1 $\times$ 10^5 cells/L (Chen and Gao 2011; Chen 2012). In addition, the reference basis of a practical turbidostat is determined by specific conditions.

4.2.2 Chemostat

Chemostat is a continuous culture method that adjusts the rates of fresh medium inflow and culture medium outflow to maintain constant chemical characteristics such as pH, nutrients, and so on (Novick and Szilard 1950). In the classical chemostat system, chemical factor (e.g., pH, N, P and so on) sensors connected to the flow rate regulator are equipped for adjusting automatically the inflow or outflow rates to ensure that the chemical characteristics of the culture medium are relatively constant.

Figure 4.2 shows a shipboard chemostat system for in situ research on the cruise (Hutchins et al. 2003). In order to accommodate the complex changes during the cruise, all of the containers were made of non-fragile polycarbonate bottles, flexible Teflon material tubes were used as connecting pipes, and culture bottles were fixed in the transparent plexiglass tank. In addition, the culture medium was kept axenic by filtration with a 0.2 μm filter. The sophisticated chemostat system has excellent automation, but it is often too expensive for the general researcher. In fact, the simple turbidostat system shown in Fig.4.1 can also be used for a chemostat (Chen and Gao 2011; Chen 2012), which was used for studying the responses of *Phaeocystis globosa* Scherffel to environmental factors such as seawater acidification, nitrogen limitation and phosphate limitation (Chen et al. 2014, 2015). According to the values of pH, N, and P measured at regular intervals (such as every other hour), fresh medium inflow rates were adjusted to ensure target factors changed within an appropriate range (such as pH fluctuated within 0.03). It is interesting to note that cell concentration kept relatively constant at the same time. The flow control kit used in a hospital can be applied to this simple continuous culture system. And the culture medium can be kept axenic by filtration with 0.2 μm filter connected at the air inlet of the system.

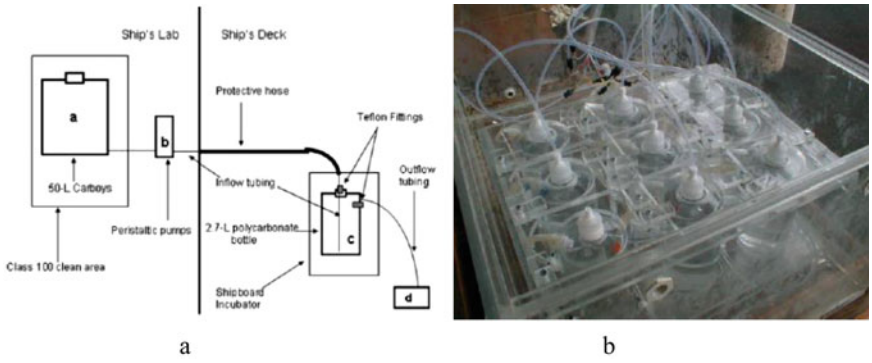

Fig. 4.2 Schematic diagram (**a**) and physical map (**b**) of continuous culture system on the cruise (From Hutchins et al. 2003)

4.3 Microalgal Semicontinuous Culture

Semicontinuous culture is a culture method between batch and continuous culture, which is diluted periodically by fresh medium to provide sufficient nutrients to maintain an exponential growth state for a long time (Hutchins et al. 2003). The dilution frequency is determined by the growth rate, and in general, less than half of the culture medium is replaced every 24 h. In order to make sure that cell concentrations in each culture container are the same after dilution, cell concentration should be measured and dilution ratios are calculated before dilution. To ensure the cell concentrations are kept within a certain range (such as 1×10^5–0.5×10^5 cells/L) before and after dilution, first the culture medium was shaken, then the calculated volume of culture medium was taken, and the remaining culture medium was removed; finally the calculated volume of culture medium was poured back to the culturing container, and the same volume of fresh culture medium as that of removed medium was poured into the container. The best dilution time is early in the dark period, and additionally two sets of the same culture containers are prepared to prevent too much bacteria adhesion on the wall leading to experiment failure.

4.4 The Specific Growth Rates Calculation

4.4.1 Batch Culture

The cell concentration (or other corresponding parameters) is measured at two points in the exponential phase when the biomass is linearly changed, and the specific growth rate was calculated as follows: $\mu = (\ln D_n - \ln D_{n-1})/(t_n - t_{n-1})$ where D_n and D_{n-1} represent the biomass at t_n and t_{n-1} respectively (usually expressed as cell density, dry weight or other representative of biomass) (Guillard 1973).

4.4.2 Semicontinuous Culture

The cell concentration measured before and after each dilution was substituted into the following formula to calculate the specific growth rate: $\mu = (\ln B_n - \ln A_{n-1})/\Delta t$, where B_n and A_{n-1} represent the cell concentrations before the nth dilution and after the n-1th dilution, respectively and Δt represents the interval between two adjacent dilutions (Guillard 1973; Gotelli 1995).

4.4.3 Continuous Culture

As the cell concentration is always constant during the whole culture process, the specific growth rate (μ) according to the following formula: $\mu = F/V$, where F and V represent the amount of the culture medium outflow per unit time and the amount of culture volume in the container, respectively (Monod 1950; Burmaster 1979).

4.5 Relative Merits and Optimization Recommendations

4.5.1 Relative Merits of Continuous Culture

The continuous culture of microalgae has obvious advantages, since it resembles natural survival states. Firstly, microalgae can maintain a stable physiological state in the whole culture process; secondly, repeatability is strong; and thirdly, the growth is stable. Additionally, it is particularly useful for studying metabolites during the growth process (Novick and Szilard 1950; LaRoche et al. 2010). The main drawback is that the equipment is complex, the medium needs are large, and the microbial contamination control is more difficult than with batch culture (LaRoche et al. 2010). The shortcomings of the simple continuous culture system shown in Fig. 4.1 are that the degree of automation is low and the regulation of day and night timing is required. What's more, the cell cycle of the microalgae and the cell's primary division time must be known in order to regulate the continuous culture system precisely.

4.5.2 The Advantages and Disadvantages of Microalgae Semicontinuous Cultures

Advantages: (1) Algal cells can maintain a relatively physiological stable state. (2) Cells always grow in exponential phase, and it's easy to find the maximum growth rate after several replicates. (3) It's easy to operate compared to continuous culture. (4) It's useful in nutrient-limitation studies.

Disadvantages: (1) It's more complex than batch culture. (2) A short lag in growth happens after dilution which could affect synchronization between treatments if the dilution rate differed. (3) This method is not applicable for cultivation of some delicate species.

4.5.3 Details in Culture Optimizing

More attention should be paid to culturing methodology in microalgae cultivation. It's the precondition to getting reliable results and achieving a successful experiment.

1. *Medium selection*. Different medium recipes are required in the cultivation of different species. Some universal media were used in previous studies, such as BG11 for fresh water cyanobacteria, HB4 for fresh water eukaryotic algae, and f/2 for marine microalgae. Specific medium suggested in the cultivation of different algae can be found at: http://algae.ihb.ac.cn/MeSearch.asp.
2. *Medium preparation and sterilization*. In medium preparation, if natural seawater is used, the sea water should be taken from the same site at the same time for the whole experiment. Considering that the seawater chemistry can change after sterilization (such as precipitation, DIC, and pH) (LaRoche et al. 2010), the medium should be aerated with axenic air to balance air-water oxygen and carbon dioxide, and used as soon as possible after preparation.
3. *Pre-cultivation*. Pre-cultivation is quite important before experiment. All physical conditions (such as light, temperature, and nutrient concentrations) should be the same as experiment conditions. What's more, the cells density of pre-cultivation should be controlled at a relatively low level (such as no more than 50,000 cells/L when the cell's diameter is below 10 μm), and the experiment can begin when the cells are in their physiological stable condition (generally 8–10 generations).
4. *Cultivating processes.* After medium is prepared and the algal species is adapted to the experimental conditions, culturing seems to be easy, but some details that can affect the experimental quality are required to be taken seriously: (a) the medium in the culture bottles should be moderate (between half and two thirds of the volume of culture bottles). (b) it's best to use sterile air if the cultivation is aerated (air goes through a 0.2 μm filter). The rate of the airflow should be moderate to avoid damage to cells (especially for some delicate species), and the cell density should be maintained at a low level. (c) It's best to start the experiment with algae from a stock culture in long-term experiments. Cells in exponential phase should not be used directly for an experiment to avoid the recession of algae due to rapid division. (d) The sampling time should be fixed during the whole experiment, because the physiological state of algae has daily rhythm with light and dark period alternation (Van Bleijswijk et al. 1994; Zondervan et al. 2002).

References

Borchard C, Borges AV, Händel N, Engel A (2011) Biogeochemical response of *Emilianiahuxleyi* (PML B92/11) to elevated CO_2 and temperature under phosphorous limitation: a chemostat study. J Exp Mar Biol Ecol 410:61–71

Burmaster DE (1979) The continuous culture of phytoplankton: mathematical equivalence among three steady state models. Am Nat 113:123–134

Chen SW (2012) Ecophysiological study on a red-tide alga *phaeocystis globosa*. Doctoral thesis. Shantou University Library, Shantou

Chen SW, Gao KS (2011) Solar ultraviolet radiation and CO_2-induced ocean acidification interacts to influence the photosynthetic performance of the red tide alga *Phaeocystisglobosa* (Prymnesiophyceae). Hydrobiologia 1:105–117

Chen SW, Gao KS, Beardall J (2014) A red tide alga grown under ocean acidification upregulates its tolerance to lower pH by increasing its photophysiological functions. Biogeosciences 11:4829–4838

Chen SW, Gao KS, Beardall J (2015) Viral attack exacerbates the susceptibility of a bloom-forming alga to ocean acidification. Glob Chang Biol 21:629–636

Gotelli NJ (1995) A primer of ecology. Sinauer, Sunderland, MA, p 206

Guillard RRL (1973) Division rates. In: Stein JR (ed) Handbook of phycological methods: culture methods and growth measurements. Cambridge University Press, Cambridge, pp 289–312

Hutchins DA, Pustizzi F, Hare CE, DiTullio GR (2003) A shipboard natural community continuous culture system for ecologically relevant low-level nutrient enrichment experiments. Limnol Oceanogr Meth 1:82–91

LaRoche J, Rost B, Engel A (2010) Bioassays, batch culture and chemostat experimentation. In: Riebesell U, Fabry VJ, Hansson L, Gattuso J (eds) Guide to best practices in ocean acidification research and data reporting. Luxembourg Press, Belgium, pp 81–94

Lee YK, Ding SY (1994) Cell cycle and accumulation of astaxanthin in *Haematoccoccuslacustris* (Chorophyta). J Phycol 30:445–449

Monod J (1950) La technique de culture continue théorieet applications. Ann Inst Pasteur 79:390–410

Novick A, Szilard L (1950) Description of the chemostat. Science 112:715–716

Van Bleijswijk JDL, Kempers RS, Veldhuis MJ, Westbroek P (1994) Cell and growth characteristics of types A and B of *Emilianiahuxleyi* (Prymnesiophyceae) as determined by flowcytometry and chemical analyses. J Phycol 30:230–241

Zondervan I, Rost B, Riebesell U (2002) Effect of CO_2 concentration on the PIC/POC ratio in the coccolithophore *Emilianiahuxleyi* grown under light-limiting conditions and different daylengths. J Exp Mar Biol Ecol 272:55–57

Chapter 5
Culturing Techniques for Planktonic Copepods

Wei Li, Xin Liu, and Zengling Ma

Abstract As the main contributors to aquatic secondary primary production, copepods play a key role in energy exchange and elemental cycling through food chains. The number of species of copepods and their abundance is large, and they are widespread from freshwater to saltwater environments across the world. The continuous harvest of copepods in significant quantities is important in both the scientific context such as physiological, ecological and taxonomic fields, and in fisheries production where copepods are used as the first feeds for larval rearing of fish, shrimps or molluscs. Therefore, it is necessary to know how to culture and produce copepods at the larger scale. In this chapter, we introduce some methods that are used in copepod culture.

Keywords Copepod · Culture method · Semi-extensive culture · Semi-intensive culture · Intensive culture · Tissue plate culture

5.1 Introduction

Copepods are found widely, across freshwater, saltwater and seawater ecosystems, and play a key role in energy exchange and elemental cycling. Whether it is an ecophysiological study or an application in the aquaculture industry, it is essential to have the target copepod species growing in multiple generation culture and capable of harvest in considerable quantity (Zillioux 1969; Di et al. 2015). However,

W. Li (✉)
College of Life and Environmental Sciences, Huangshan College, Huangshan, China
e-mail: livilike@hsu.edu.cn

X. Liu
State Key Laboratory of Marine Environmental Science, Xiamen University, Xiamen, China

Z. Ma (✉)
Zhejiang Provincial Key Laboratory for Subtropical Water Environment and Marine Biological Resources Protection, Wenzhou University, Wenzhou, China
e-mail: mazengling@wzu.edu.cn

K. Gao et al. (eds.), *Research Methods of Environmental Physiology in Aquatic Sciences*, https://doi.org/10.1007/978-981-15-5354-7_5

copepod culture technology for now is not yet mature, with species rarely successful in long term artificial culture, as copepod culturing needs people with knowledge in copepod classification, isolation and culture condition settings (Zheng 1980; Di et al. 2015). Also, species-specific characteristics make it more difficult to obtain a uniform culture method. Studies in relation to culture of copepods such as *Acartia tonsa* and *Tigriopus japonicus* began to rise from the 1960s (Heinle 1969; Kline and Laidley 2015), but until now, only a few species have been successfully cultured (Table 5.1, reviewed by Perumal et al. (2015)). We will briefly introduce the copepod culturing methods and operational procedures in this chapter.

5.2 Copepod Culturing Methods

According to the expectations of daily copepod production and the size scale and position (indoor and outdoor) of cultivation system, copepod culture techniques could be classified into three types which are semi-extensive culture, semi-intensive culture and intensive culture (Imelda et al. 2015) (Table 5.2).

Intensive copepod culture regimes have been reported since the 1960s. For example the continuous recirculating culture system for calanoid copepods was used in *Acartia claus* and *Acartia tonsa* culture (Zillioux 1969; Zillioux and Lackie 1970) (Fig. 5.1); except for calanoid species, harpacticoid and cyclopoid species are also successfully cultured in this system (reviewed by Kline and Laidley 2015) (Table 5.3). For the intensive culture, recirculation of seawater is used during the culture and copepods are fed with algae as food. Debris waste (e.g. algae debris, faecal pellets) produced during the culture process is filtered out through a filtration system associated with a foam tower which maintains the chemical condition of culture medium stable. Antibiotics are used for sterilization.

In comparison with the intensive copepod culture, semi-intensive and semi-extensive culture is normally implemented in outdoor conditions with larger volumes of culture system. The culture conditions (physical and chemical) cannot be accurately controlled as in the intensive culture system.

In addition to the larger volume of culture system introduced above, copepod culture can be achieved in even smaller volumes, for example in tissue culture plates (Fig. 5.2). Single healthy nauplli or adult individuals can be chosen and placed into each well of the 6-, 12- or 24-well plates, with 5, 2 or 1 mL culture medium, respectively. A male and a female individual can be loaded in the same well if reproduction is required. It is easy and convenient to monitor the whole life cycle of cultured copepods during the developmental process, and physiological and biochemical responses of copepod to environmental changes can be studied by using this culture method. For example, the calanoid *Acartia pacifica* was successfully cultured in 12-well tissue plates (Fig. 5.2). The advantage of using tissue culture plate for copepod culture is the small culture volume which means less medium will be used and the medium exchange is convenient. Also, the culture conditions such as

Table 5.1 Available reports on copepod culture in the world

Genus/species	Identification type: morphological or genetic	Geographical origin	Cultivation condition, temperature, salinity, light regime, food
Acartia grani	Morphological	Barcelona harbour, Spain (NW Mediterranean)	19 °C/38 ppt/12L:12D/ *Rhodomonas salina*
Acartia sinjiensis	Morphological	Townsville channel QLD (Australia)	27–30 °C/30–35 ppt/18 L:6D/ *Tetraselmis chuii* and *T-iso*
Acartia southwelli	Morphological	Pingtung-Taiwan, China	25–30 °C/15–20‰/12L:12D/ *Isochrysis galbana*
Acartia tonsa	Morphological	Origin Unknown	?
Acartia tonsa	Morphological and genetics	Oresund (Denmark)	17 °C/30 ppt/0L:24D/ *Rhodomonas salina*
Acartia tonsa	Morphological	Punta del Este, Uruguay	25–30 °C/17 ppt/indirect natural light/*T-Iso-Tetraselmis*
Ameira parvula	Morphological	Kiel Bight, Germany	18 °C, 17 ppt, 12L:12D, different algae
Amonardia normani	Morphological	Kiel Bight, Germany	18 °C, 17 ppt, 12 L:12D, different algae
Amphiascoides atopus	Morphological	USA	25 °C, 12/12, cultured phytoplankton
Apocyclops royi	Morphological	Pingtung-Taiwan, China	25–30 °C/15–20‰/12L:12D/ *Isochrysis galbana*
Centropages typicus	Morphological	Gulf of Napoli Italy (W Mediterranean)	19–21 °C/38 ppt/12L:12D/ *Prorocentrum minimum*/ *Isochrysis galbana*/*Tetraselmis suecica*
Eurytemora affinis	Morphological	River Seine Estuary (France)	10–15 °C/15 ppt/12L:12D/fed *Rhodomonas marina*
Eurytemora affinis	Morphological	Gironde Estuary (France)	10–15 °C/15 ppt/12L:12D/fed *Rhodomonas marina*
Eurytemora affinis	Morphological	Loire Estuary (France)	10–15 °C/15 ppt/12L:12D/fed *Rhodomonas marina*
Eurytemora affinis	Morphological	Canada	10–15 °C/15 ppt/12L:12D/fed *Rhodomonas marina*
Euterpina acutifrons	Morphological	Mediterranean	19 °C/38 ppt/12L:12D/ *Rhodomonas salina*
Eurytemora affinis	Morphological	Gironde Estuary (France)	10–15 °C/15 ppt/12L:12D/fed *Rhodomonas marina*
Euterpina acutifrons	Morphological	Mediterranean	19 °C/38 ppt/12L:12D/ *Rhodomonas salina*
Eurytemora affinis	Morphological	Gironde Estuary (France)	10–15 °C/15 ppt/12L:12D/fed *Rhodomonas marina*
Eurytemora affinis	Morphological	Canada	10–15 °C/15 ppt/12L:12D/ *Rhodomonas marina*

(continued)

Table 5.1 (continued)

Genus/species	Identification type: morphological or genetic	Geographical origin	Cultivation condition, temperature, salinity, light regime, food
Euterpina acutifrons	Morphological	Mediterranean	19 °C/38 ppt/12L:12D/ *Rhodomonas salina*
Gladioferens imparipes	Morphological	Swan River, Perth Western Australia	23–27 °C, 18 ppt, continuous dark, *T-Iso* and *Chaetoceros muelleri*
Mesocyclops longisetus	Morphological	Florida/USA	http://edis.ifas.ufl.edu/IN490
Macrocyclops albidus	Morphological	Florida/USA	http://edis.ifas.ufl.edu/IN490
Oithona davisae	Morphological	Barcelona harbour, Spain (NW Mediterranean)	20 °C/30 ppt/natural light/ *Oxyrrhis*
Pseudodiaptomus annandalei	Morphological	Pingtung-Taiwan, China	25–30 °C/15–20‰/12L:12D/ *Isochrysis galbana*
Tachidius discipes	Morphological	Kiel Bight, Germany	18 °C, 17 ppt, 12L:12D, different algae
Temora longicornis	Morphological	North Sea	15 °C, 30 ppt, 0:24D/ *Thalassiosira weissflogii, Rhodomonas salina, Heterocapsa, Prorocentrum minimum*
Temora longicornis	Morphological	Plymouth, Devon, UK	Temp according to current sea temperatures, salinity 30–36 ppt, 12L:12D, fed mixture of *Isochrysis galbana* and *Rhodomonas* and *Oxyrrhis*
Temora stylifera	Morphological	Gulf of Napoli Italy (W Mediterranean)	19–21 °C/38 ppt/12L:12D/ *Prorocentrum minimum/ Isochrysis galbana/Rhodomonas baltica*

Cited from Perumal et al. (2015)

Table 5.2 The culture techniques for copepods

Culture techniques	Culture volume	Productivity (eggs/day) (L)
Semi-extensive	Large ponds/lagoons l200–10,000 m^3	<50
Semi-intensive	Tanks: 200–300 m^3	<100
Intensive	Flasks or tanks 5–110 L	500–6000

Cite from Imelda et al. (2015)

temperature, salinity, food type and concentration are easy to control during the culture.

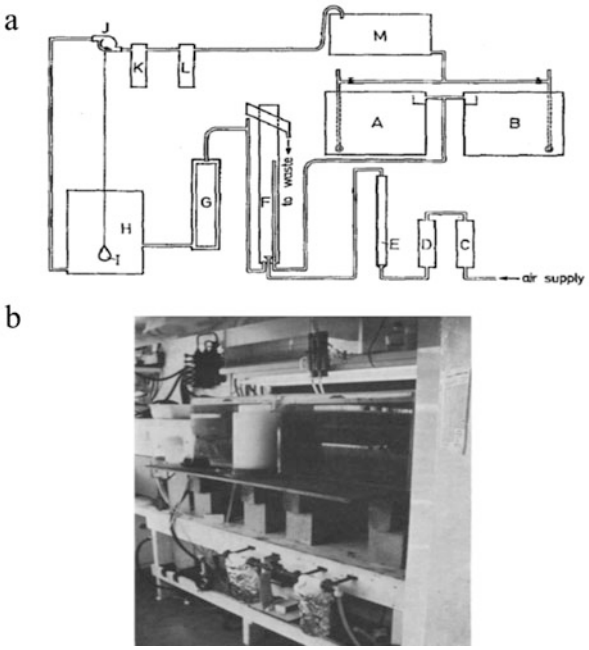

Fig. 5.1 Schematic diagram of (**a**) concept model and (**b**) the original recirculating culture system. (Cite from Zillioux 1969; Zillioux and Lackie 1970). (A) culture tank 1; (B) culture tank 2; (C) drying tube; (D) charcoal tube; (E) hydrator; (F) foam tower; (G) glass wool filter; (H) lower reservoir; (I) level switch; (J) jump; (K) 15 μm cartridge filter; (L) 0.45 μm cartridge filter; (M) upper reservoir

5.3 Procedures for Copepod Culture

5.3.1 Provenance Copepod Collection

Horizontal or vertical hauls with a plankton net are normally used in planktonic copepod collection. Plankton nets with different mesh sizes can be selected according to the target size of copepod, and customized mesh sizes from 6 to 1000 μm are available commercially according to requirements. Horizontal or vertical hauls for coastal copepods can be made at high tide during dawn or dusk, while for benthic copepods, for example *Tigriopus japonicas*, it is easy to collect these from low lying areas or rock cracks directly during low tide using a pipette.

5.3.2 Copepod Isolation, Purification and Culture

Field collected copepods need immediate transfer into the laboratory and screening out of the larger animals (larval fish, shrimp or crab) with a larger mesh (e.g. mesh size 500 μm), and then using 200 μm mesh to screen out the smaller animals and rotifers. As copepod community structure changes with season, therefore, it is necessary to learn the seasonal variations of copepod composition in the studied area, which will benefit the harvesting of target species.

Table 5.3 Production levels obtained from intensive production systems for calanoid, harpacticoid and cyclopoid copepod species

Copepod species	Tank size (L)	Production (10^6 m^{-3} day^{-1})	References
Calanoid species:			
Acartia tonsa	450	0.2	Støttrup (2000)
	1000	0.25	Schipp et al. (1999)
	70,000	0.12	Ogle et al. (2005)
Gladioferens imparipes	500	0.88	Payne and Rippingale (2001)
	1000	0.52	Payne and Rippingale (2001)
Parvocalanus crassirostris	400	4	Shields and Laidley (2003)
	400	3.75	Shields et al. (2005)
	1500	18	Kline and Laidley (2015)
Pseudodiaptomus pelagicus	1800	>1	Cassiano (2009)
Harpacticoid species:			
Amphiascoides atopus	1440	1.94	Sun and Fleeger (1995)
Tisbe holothuriae	10	7.14	Gaudy and Guerin (1982)
	150	1.53	Støttrup and Norksker (1997)
Tisbe biminiensis	4.5	28	Ribeiro and Souza-Santos (2011)
Cyclopoid species:			
Apocyclops panamensis	40	4.45	Phelps and Sumiarsa (2005)

Cite from Kline and Laidley 2015

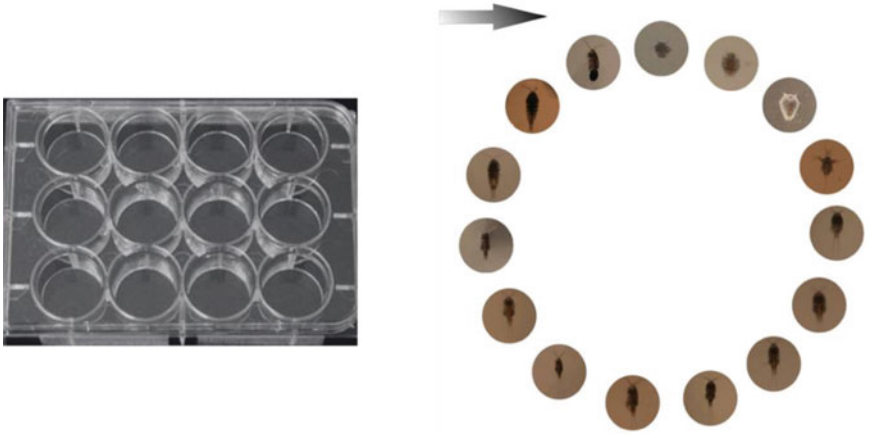

Fig. 5.2 Different developmental stages of *Acartia pacifica* grown in 12-well tissue culture plate

After screening with meshes, the target copepod will be selected out and transferred into different culture systems for culture at a larger scale (Table 5.2). During the culture, copepod density should be carefully monitored to avoid a high mortality rate and subsequent lower egg production due to crowding effects (Kline and Laidley 2015).

5.3.3 Feeding Food

Copepod feeding habits include herbivory, carnivory and omnivory. For the purpose of copepod culture, food types have to be chosen appropriately according to the feeding habits of the target copepod. For example, diatoms can be used as plant based food, and rotifers and *Artemia* normally used as animal based foods. Culture of the food organism may match the culture scale of copepod culture (semi-extensive, semi-intensive and intensive), with culture system volume ranging from indoor culture of small culture volume (1–10 L) to medium (10–100 L) and even larger volumes of outdoor culture (>100 L).

Food organisms are quite important for copepod culture. The often used food organisms include diatoms, dinoflagellate, rotifers, plankton nauplii and fungi (for example, yeast) (Fukusho 1980). The feed selection for different copepod species can be obtained from the literature. Species such as *Isochrysis sp.*, *Skeletonema costatum*, *Chaetoceros mulleri*, *Chlorella sp.* and *Platymonas sp.* are widely used as food for copepod culture (Zheng 1980; Perumal et al. 2015). Based on this, a preliminary experiment for determining the appropriate algae species selection and feeding concentration is required. Feeds can use either single species or a mixture of species as there is evidenced that a mixture of feed organisms is better for some copepod species (Zheng 1980).

5.3.4 Water Quality Control of Culture Medium

Accumulation of excrement from copepods (faecal pellets) and metabolites from feed algae will increase with increased copepod density during culture, which will change the medium conditions. For example, bacteria and NH_3-N concentration may increase, and dissolved O_2 concentration and medium pH may vary with culture time. Deterioration of water quality will significantly affect the growth and reproduction of copepods. Therefore, the physical and chemical parameters of the culture medium need to be monitored during the culture, as their stability may determine the success of the culture. Hypochloric acid can be used for disinfection of the culture water, followed by addition of sodium thiosulfate for antichloration. Using appropriate concentration of antibiotics, such as penicillin and streptomycin sulphate, will help in controlling bacterial proliferation. Regular exchange of the medium or

removal of debris with a syphon, screen or filtration will keep the water quality in good condition; continuous bubbling using an air stone at a suitable gas flow (high gas flow may damage copepods) can avoid the deleterious effects of low dissolved O_2 concentration (Perumal et al. 2015).

5.3.5 Harvesting

Continuous harvesting of copepods can be carried out when the optimal culture conditions are established. Depending on the volume of culture system, directly syphoning with a tube or hauling with a plankton net, or exposure of one side of the tank to light (exploiting their phototactic behaviour) can be used in copepod harvest. Fresh medium may be replenished if there is any decrease of culture volume during harvesting.

5.4 The Advantages and Disadvantages of Different Culture Methods and Points for Attention

Copepod community structure and reproduction are prone to be affected by changed culture conditions in extensive or semi-extensive culture systems, as the culture condition control is less than in the semi-intensive or intensive culture systems (Lemus et al. 2004; Lindley and Phelps 2009). Target copepod harvesting from an extensive culture system may be interrupted by the presence of copepod species, and copepod growth in this type of culture system is easy infected by pathogenic bacteria (Lahnsteiner et al. 2009).

In contrast, copepod composition, availability and biosecurity can be controlled well under an intensive culture system. Though the intensive culture system is still at a preliminary stage of development and with a lot of possibilities for improvements in the procedures, by controlling the culture system under optimized conditions, continuous and stable harvesting of target copepods can be achieved.

There are many factors that need to be considered during the process of artificial copepod culture. No matter which method is used, the original characteristics of the copepods (feeding habits and ecological habits) are critical as the culture condition setup of temperature, salinity, dissolved oxygen, pH, food type, concentration, quality, etc. are all have great importance for successful growth, development and reproduction of the copepods and subsequently determine the final harvesting stability. Before the larger-scale copepod culture is initiated experience and information from a thorough literature review and preliminary experimental tests are strongly recommended.

References

Cassiano EJ (2009) Evaluation of the calanoid copepod *Pseudodiaptomus pelagicus* as a first feed for Florida pompano, *Trachinotus carolinus*, Larvae, MS Thesis. University of Florida, Gainesville, USA, p 108

Di L, Marco C, Cecilia F, Paola GDM (2015) A protocol for a development, reproduction and population growth test with freshwater copepods. International conference on groundwater in Karst, Birmingham

Fukusho K (1980) Mass production of a copepod, *Tigriopus japonicus* in combination culture with a rotifer Brachionus plicatilis, fed omega-yeast as a food source. Nsugaf 46:625–629

Gaudy R, Guerin JP (1982) Population dynamics of *Tisbe holothuriae* (Copepoda; Harpacticoida) in exploited mass cultures. Neth J Aquat Ecol 16:208–216

Heinle DR (1969) Culture of calanoid copepods in synthetic sea water. J Fish Board Can 26:150–153

Imelda J, Sarimol CN, Bhaskaran B (2015) Copepod culture. CMfRI, Kochi

Kline MD, Laidley CW (2015) Development of intensive copepod culture technology for *Parvocalanus crassirostris*: optimizing adult density. Aquaculture 435:128–136

Lahnsteiner F, Kletzl M, Weismann T (2009) The risk of parasite transfer to juvenile fishes by live copepod food with the example *Triaenophorus crassus* and *Triaenophorus nodulosus*. Aquaculture 295:120–125

Lemus JT, Ogle JT, Lotz JM (2004) Increasing production of copepod nauplii in a brown-water zooplankton culture with supplemental feeding and increased harvest levels. N Am J Aquac 66:169–176

Lindley LC, Phelps RP (2009) Production and collection of copepod nauplii from brackish water ponds. J Appl Aquac 21:96–109

Ogle JT, Lemus JT, Nicholson LC, Barnes DN, Lotz JM (2005) Characterization of an extensive zooplankton culture system coupled with intensive larval rearing of red snapper *Lutjanus campechanus*. In: Lee C-S, O'Bryen PJ, Marcus NH (eds) Copepods in aquaculture. Blackwell Publishing Ltd., Iowa, USA, pp 225–244

Payne MF, Rippingale RJ (2001) Intensive cultivation of the calanoid copepod *Gladioferens imparipes*. Aquaculture 201:329–342

Perumal S, Ananth S, Nandakumar R, Jayalakshmi T, Kaviyarasan M, Pachiappan P (2015) Intensive indoor and outdoor pilot-scale culture of marine copepods. Springer, New York, NY

Phelps RP, Sumiarsa GS (2005) Intensive and extensive production techniques to provide copepod nauplii for feeding larval red snapper *Lutjanus campechanus*. In: Lee C-S, O'Bryen PJ, Marcus NH (eds) Copepods in aquaculture. Blackwell Publishing Ltd., Iowa, USA, pp 225–244

Ribeiro AC, Souza-Santos LP (2011) Mass culture and offspring production of marine harpacticoid copepod *Tisbe biminiensis*. Aquaculture 321:280–288

Schipp GR, Bosmans JM, Marshall AJ (1999) A method for hatchery culture of tropical calanoid copepods, *Acartia* spp. Aquaculture 174:81–88

Shields RJ, Laidley CW (2003) Intensively cultured paracalanid copepods—a high quality diet for small tropical marine fish larvae. Glob Aquac Advocate 6:80–81

Shields RJ, Kotani T, Molnar A, Marion K, Kobashigawa J, Tang L (2005) Intensive cultivation of a subtropical paracalanid copepod, Parvocalanus sp., as prey for small marine fish larvae. In: Lee CS, O'Bryen PJ, Marcus NH (eds) Copepods in aquaculture. Blackwell Publishing, Ames, IA, pp 209–223

Støttrup J (2000) The elusive copepods: their production and suitability in marine aquaculture. Aquac Res 31:703–711

Støttrup JG, Norksker NH (1997) Production and use of copepods in marine fish larviculture. Aquaculture 155:231–247

Sun B, Fleeger JW (1995) Sustained mass culture of *Amphiascoides atopus* a marine harpacticoid copepod in a recirculating system. Aquaculture 136:313–321

Zheng Z (1980) Study on the culture of marine zooplankton – new trends of marine planktology 5. Nature 3:134–138. (in Chinese)
Zillioux E (1969) A continuous recirculating culture system for planktonic copepods. Mar Biol 4:215–218
Zillioux EJ, Lackie NF (1970) Advances in the continuous culture of planktonic copepods. Helgoländer Meeresun 20:325–332

Part III
Determination of Key Enzymes in Primary Producers

Chapter 6
Carbonic Anhydrase

Jianrong Xia, Xiongwen Chen, and Mario Giordano

Abstract Carbonic anhydrase (CA) plays an important role in the inorganic carbon concentrating mechanism of algae, and can regulate intracellular and extracellular inorganic carbon concentration to promote the utilization efficiency of inorganic carbon in algal photosynthesis. This chapter describes the analysis techniques for the cellular concentration and activity of carbonic anhydrase in algae, and provides technical support for analysis of CA characteristics.

Keywords Carbonic anhydrase · Immunochemical quantitative analysis · *Chlamydomonas reinhardtii* · Protein · Electrophoresis

6.1 Introduction

Carbonic anhydrase contains a zinc ion, which catalyzes the interconversion of carbon dioxide and bicarbonate. In hydration, the CO_2 reacts with the Zn-OH at the enzyme active site, while in dehydration, HCO_3^- reacts with Zn-H_2O.

The enzyme was first discovered in mammalian red blood cells and subsequently found in fish, invertebrates, plants, and microbes. CA plays an important part of the inorganic carbon concentrating mechanism of algae by regulating the intracellular and extracellular CO_2 concentrations to maintain the stability of CO_2 supply to ribulose-1,5-bishosphate carboxylase/oxygenase (RubisCO), and thereby promotes photosynthetic efficiency under CO_2-limited conditions (Rawat and Moroney 1995;

J. Xia (✉)
School of Environmental Science and Engineering, Guangzhou University, Guangzhou, Guangdong, China
e-mail: jrxia@gzhu.edu.cn

X. Chen
College of Life Sciences, Hubei Normal University, Huangshi, Hubei, China

M. Giordano
Dipartimento di Scienze della Vita e dell'Ambiente, Università Politecnica delle Marche, Ancona, Italy

K. Gao et al. (eds.), *Research Methods of Environmental Physiology in Aquatic Sciences*, https://doi.org/10.1007/978-981-15-5354-7_6

Reinfelder 2011). Therefore, carbonic anhydrase plays a key role in carbon transport and metabolism in algae.

6.2 Immunochemical Quantitative Analysis of Carbonic Anhydrase

Experimental materials: *Chlamydomonas reinhardtii.*

Solutions and reagents:

1. Buffers for protein extraction: 20 mM Morpholine propanesulfonic acid buffers at pH 7.5 (Mops), 10 mM NaCl, 1 mM EDTA, 5 mM DTT, 1 mM Phenylmethylsulfonyl fluoride (PMSF) 1 mM Benzamidine (Fett and Coleman 1994).
2. 10% trichloroacetic acid (TCA).
3. Sodium dodecyl sulfate polyacrylamide gel.
4. 2 × SDS loading buffer: 125 mM Tris–HCl pH 6.8; 20% glycerinum; 4% SDS; 10% β-mercaptoethanol (BME); 0.005% Bromophenol Blue.
5. Protein molecular weight markers.
6. Purified CA standard sample.
7. Transfer buffer: 50 mM Tris, 200 mM Glycine, 20% ethanol.
8. Lichun Red Dye: 0.1% Lichun Red dissolved in 5% acetic acid.
9. Primary antibodies: CA antibody.
10. Secondary antibodies: Horseradish peroxidase (HRP) conjugated secondary antibody.
11. 10 × PBS solution: 26.8 mM KCl, 14.7 mM KH_2PO_4, 1.37 M NaCl, 100 mM Na_2HPO_4.
12. PBS-T solution: 0.1% Tween-20 dissolved in 1 × PBS buffer.
13. Blocking buffer: 5% of skim milk powder dissolved in PBS-T solution.
14. PVDF membrane.

Instrument: Protein electrophoresis system, Protein half dry transfer printer, Chemical fluorescence detector.

6.2.1 Preparation of a Protein Sample of Carbonic Anhydrase

Chlamydomonas reinhardtii with about 1×10^7 cells mL^{-1} at the exponential stage are collected by centrifugation at 15,000 × *g* for 5 min. An adequate amount of protein extraction buffer is added to fully suspend the cells which are then broken with ultrasonics in 4 °C ice bath, and then centrifuged at 20,000 × *g* for 30 min. TCA is added to the supernatant to a final concentration to 10%, and the sample

centrifuged to collect the protein. Protein can be stored in the refrigerator at −20 °C, or directly loaded onto a SDS-PAGE gel. Using BSA as a protein standard the total protein concentration is determined with a Bradford Elisa kit.

6.2.2 Separation of Proteins by Electrophoresis (Bailly and Coleman 1988; Zhao 2008)

6.2.2.1 Sample Treatment

A suitable amount of concentrated protein sample buffer is added to the protein samples, and the sample heated at 100 °C or a boiling water bath for 3–5 min.

6.2.2.2 Loading Sample and Electrophoresis

After cooling to room temperature, the protein sample is applied directly to the gel holder.

In order to observe the effect of electrophoresis and membrane transfer, and to determine the molecular weight of protein, it is better to use the pre-dye protein molecular weight markers. The voltage is usually set at 100 V for 90–120 min. When bromophenol blue reaches the bottom of the gel, electrophoresis can be stopped, or you can stop electrophoresis when the target protein is expected to have been properly separated based on the electrophoresis of pre-dye protein molecular weight markers.

6.2.3 Transfer Proteins to Membrane

We choose to use PVDF membrane, and dye it with Lichun Red Dye to observe the actual effect of membrane transfer.

6.2.4 Blocking

After the membrane transfer is finished, place the protein-loaded membrane in a prepared PBS-T solution and rinse for 1–2 min to remove the transfer buffer. The membrane is submerged in a blocking buffer, and slowly shaken in the shaker for 1 h.

6.2.5 Primary Antibody Incubation

Use a micro-pump or dropper to remove the blocking buffer, then immediately add the diluted primary antibody, and incubate for one hour at room temperature or 4 °C while placed in the shaker. Rinse the membrane twice with PBS-T solution, wash it for 15 min while shaking, and then replace the solution and wash it twice for 5 min each time.

6.2.6 Secondary Antibody Incubation

Use a micro-pump or dropper to remove the blocking solution, and immediately added the diluted secondary antibody, and incubate for one hour at room temperature or 4 °C while placed in the shaker. Rinse the membrane twice with PBS-T solution, wash it for 15 min while shaking, and then replace the solution to wash it twice for 5 min each time.

6.2.7 Protein Detection

The target protein signal on the membrane is directly detected by a chemical fluorescence imaging system. The amount of CA in the sample is calculated according to the intensity of signal based on the amount of a standard CA sample.

6.3 Determination of Activity of Carbonic Anhydrase (Willbur and Anderson 1948; Xia and Huang 2010)

Experimental materials: *Chlamydomonas reinhardtii.*

Solutions and reagents:

1. Barbital buffer (pH 8.3, 20 mM).
2. CO_2-saturated water (highly concentrated CO_2 is bubbled into doubled distilled water at 4 °C until the pH is less than 4.0).

Instruments: Thermostatic water bath, reaction vessel, pH meter, Ultrasonic processor.

6.3.1 Measurement of Extracellular CA

Chlamydomonas reinhardtii in exponential stage is collected by centrifugation at 5000 × g, and suspended in Barbital buffers at a concentration of 1×10^7 cells mL^{-1}. The suspension is placed in the reaction vessel at 4 °C, and 4 mL saturated CO_2 water is quickly injected to the bottom in order to avoid CO_2 leaks. The time needed for the pH drop from 8.3 to 7.3 is recorded by the pH meter. Extracellular carbonic anhydrase activity (EU) is calculated as follows:

$$\mathrm{EU} = 10 \times (T_0/T - 1),$$

In which T_0, T are the times needed for the pH to drop from 8.3 to 7.3 without or with algal cells in the reaction tank.

6.3.2 Measurement of Intracellular CA

The collected cells are broken using an ultrasonic processor in an ice bath. The total carbonic anhydrase activity of the cell is measured using the same method as for extracellular carbonic anhydrase activity. Intracellular carbonic anhydrase activity = total carbonic anhydrase activity − extracellular carbonic anhydrase activity. The unit of carbonic anhydrase activity is EU $cell^{-1}$ or EU mg chl^{-1}.

6.3.3 Advantage and Disadvantage

Advantage

1. The quantitative determination of carbonic anhydrase is conventional, simple, and sensitive.
2. The method for determination of carbonic anhydrase activity is easy to carry out and has low requirements for instruments and other equipment.

Disadvantage

1. The CA antibody involved in the quantitative method is not easy to obtain, and it is expensive.
2. More samples are needed in the determination of activity.

Attention

1. Loading quantities should be moderate for the quantitative determination of carbonic anhydrase. The collected protein samples should be used as soon as possible, and should not be stored for a long time.
2. The pH value of CO_2 saturated water must be less than 4, and it should be slowly injected into the bottom of the reaction vessel.

References

Bailly J, Coleman JR (1988) Effect of CO_2 concentration on protein biosynthesis and carbonic anhydrase expression in *Chlamydomonas reinhardtii*. Plant Physiol 87:833–840

Fett JP, Coleman JR (1994) Regulation of periplasmic carbonic anhydrase expression in *Chlamydomonas reinhardtii* by acetate and pH. Plant Physiol 106:103–108

Rawat M, Moroney JV (1995) The regulation of carbonic anhydrase and ribulose-1,5-bisphosphate carboxylase/oxygenaseactivase by light and CO_2 in *Chlamydomonas reinhardtii*. Plant Physiol 109:937–944

Reinfelder JR (2011) Carbon concentrating mechanisms in eukaryotic marine phytoplankton. Annu Rev Mar Sci 3:291–315

Willbur KM, Anderson NG (1948) Electronic and colorimetric determination of carbonic anhydrase. J Biol Chem 176:147–154

Xia J, Huang J (2010) Impacts of nitrogen and phosphorus on inorganic carbon utilization and carbonic anhydrase activity in *Nitzschia closterium f. minutissima*. Acta Ecol Sin 30 (15):4085–4092

Zhao Y (2008) Principles and applications of biochemical technology, 4th edn. Science Press, Beijing

Chapter 7
Rubisco

Cuimin Liu, Kaiyao Huang, and Jianrong Xia

Abstract The rate-limiting step for plant photosynthesis is the process of carbon assimilation catalyzed by Ribulose 1,5-diphosphate carboxylase oxygenase (Rubisco). Photosynthetic carbon fixation (CO_2 and Ribulose 1,5-diphosphate as the substrates) catalyzed by Rubisco is the first step in the production of carbohydrates in plants. It is a key hub for the conversion of inorganic carbon to organic compounds in photosynthesis, which is also the rate-limiting step of plant photosynthesis under current atmospheric conditions. Rubisco catalyzed carbon fixation is the main way to control greenhouse-gas CO_2 in the atmosphere and is the basis for the production of biomass and bioenergy in plants (including algae). Rubisco carbon fixation efficiency is very low, so to support adequate photosynthetic rates, very large amounts of Rubisco are needed and its synthesis consumes huge amounts of energy and nutrients. Altering the Rubisco carbon fixation efficiency to improve the photosynthesis of plants is an enduring research hotspot. In this chapter, the techniques of Rubisco quantification and catalytic activity analysis in algae are described and provide technical support for analyzing the properties of Rubisco enzymes.

Keywords Rubisco · Photosynthesis · Carboxylation · Algae · Carbon reaction · Catalytic activity

C. Liu (✉)
State Key Laboratory of Plant Cell and Chromosome Engineering, Institute of Genetics and Developmental Biology, The Innovative Academy of Seed Design, Chinese Academy of Sciences, University of Chinese Academy of Sciences, Beijing, China
e-mail: cmliu@genetics.ac.cn

K. Huang
Department of Algae Cell Biology, Institute of Hydrobiology, Chinese Academy of Sciences, Wuhan, Hubei, China
e-mail: huangky@ihb.ac.cn

J. Xia
College of Environmental Science and Engineering, Guangzhou University, Guangzhou, China
e-mail: jrxia@gzhu.edu.cn

K. Gao et al. (eds.), *Research Methods of Environmental Physiology in Aquatic Sciences*, https://doi.org/10.1007/978-981-15-5354-7_7

7.1 Introduction

Rubisco (Ribulose-1, 5-bisphosphate carboxylase oxygenase) is a key enzyme in photosynthetic carbon fixation in algae and higher plants. Rubisco catalyzes the use of CO_2 to carboxylate the substrate ribulose-1,5-diphosphate to produce two molecules of 3-phosphoglycerate, which is the critical and fundamental reaction to sequester inorganic the use of CO_2 into organic carbon compounds via photosynthesis. Rubisco is the most abundant enzyme in nature, and its production consumes large quantities of nitrogen and energy to make large amounts of the enzyme, which is generally believed to compensate for its inefficient catalytic capacity. Most enzymes catalyze thousands of reactions per molecule per second, but Rubisco fixes 3–9 CO_2 molecules per molecule per second. Furthermore, another opposing reaction catalyzed by Rubisco, photorespiration (O_2 as the substrate) can compete with photosynthetic carbon fixation (CO_2 as the substrate) using the same enzyme active site and substrate (ribulose-1,5-diphosphate), which decreases the efficiency of carbon fixation. Algae have evolved a CO_2 concentrating mechanism (CCM) that increases the concentration of CO_2 in chloroplasts, which in turn improves the carbon fixation efficiency of Rubisco, while Rubisco's carbon fixation capacity is still the rate-limiting step of algae photosynthesis under some conditions.

In this chapter, the quantification of Rubisco in algae, including the collection of algae cells, the extraction of denatured proteins and soluble proteins, activation of Rubisco and its catalytic activity detection are described. Methods of immunochemical and isotope assay can be used for quantification of Rubisco amount. Furthermore, two types of methods for determining Rubisco carboxylase activity are also described here, and high concentrations of CO_2 with an appropriate amount of ribulose-1,5-bisphosphate substrate are required in both. In one method, $H^{14}CO_3^-$ isotope is used, which can be detected by a liquid scintillation counter to calculate the Rubisco carboxylase activity. In the other method, a spectrophotometer is used to detect the yield of NADH in a linked-enzyme assay and thereby to determine the enzyme activity. Finally, we will compare the advantages and disadvantages of both methods and their applicability.

7.2 Experimental Materials and Methods

7.2.1 Protein Extraction

7.2.1.1 Extraction of Denatured Total Protein

Materials, Reagents, Instruments and Experimental Methods

Unless otherwise specified, all conventional chemical reagents are analytical grade reagents, available from SIGMA. Water used in all experiments is ultrapure water with high resistivity of 18 MΩ cm (25 °C).

Material

Chlamydomonas reinhardtii culture using TAP medium (Harris 1989), *cyanobacteria* culture using BG11 medium (Allen 1968). The following experimental method is described using *Chlamydomonas reinhardtii* as an example.

Reagents

- Denatured protein suspension buffer: 0.1 M Na_2CO_3, 0.1 M dithiothreitol.
- Denatured protein solution: 5% SDS, 30% sucrose.

Instrument

- Microscope.
- Centrifuge.
- Ultrasonicator.

Methods

1. Culture algae (*Chlamydomonas reinhardtii*) to about 6×10^6 cells per milliliter (cells are counted under a microscope) in 30 ml of TAP broth.
2. The cultured algae are collected in a 50 ml centrifuge tube and centrifuged at 16,000 *g* for 5 min, then the supernatant discarded.
3. Add 40 μl of denatured protein suspension buffer to fully suspend the precipitated cells.
4. Add 55 μl denatured protein solution, and mix the cells well.
5. Break the cells with the finest ultrasonic probe at low temperature.
6. Centrifuge at 10,000 *g* for 30 s to remove unbroken cells after sonication, take the supernatant, which contains denatured total protein.
7. Incubate the total protein extract at 95 °C for 2 min, then load on a SDS-PAGE gel for detection, or keep in a −20 °C refrigerator.

7.2.1.2 Extraction of Soluble Native Protein

Materials, Reagents, Instruments, and Experimental Methods

Unless otherwise specified, all conventional chemical reagents are analytical grade reagents, available from SIGMA. Water used in all experiments is ultrapure water with high resistivity of 18 MΩ cm (25 °C).

Material

Chlamydomonas reinhardtii culture using TAP medium (Harris 1989). The following experimental method is described using *Chlamydomonas reinhardtii* as an example.

Reagents

- Protein extraction buffer: 50 mM Tris–HCl, pH 7.6, 20 mM $MgCl_2$, 20 mM $NaHCO_3$, 0.2 mM EDTA.
- Protein extraction solution: Protein extraction buffer with 1 mM phenylmehtanesulphonylfluoride (PMSF), 5 mM dithiothreitol (DTT).

- Sucrose pad: 50 mM Tris–HCl, pH 7.6, 0.6 M sucrose.

Instrument

- Microscope.
- Centrifuge.
- Ultrasonicator.

Method

1. Culture algae (*Chlamydomonas reinhardtii*) to about 6×10^6 cells per milliliter (cells are counted under a microscope) in 1 L of TAP broth.
2. The cultured algae are collected by centrifuging at 10,000 *g* for 10 min and then discarding the supernatant.
3. Add 3 ml of pre-cooled protein extraction solution, and fully suspend the cells.
4. Sonicate the cells with a middle sized ultrasonic probe for 90 s at low temperature; pay attention to the sample temperature as it should not exceed 25 °C.
5. Add 8 ml of sucrose pad to the Beckman Ti50 centrifuge tube.
6. Carefully load the broken cell lysate onto the sucrose pad in the Beckman Ti50 centrifuge tube.
7. In a pre-cooled centrifuge, centrifuge at 152,000 *g*, 4 °C, 30 min.
8. Carefully take the supernatant on the sucrose pad, that contains the soluble native protein. The protein sample can be divided into aliquots, frozen quickly with liquid nitrogen and stored in a −80 °C refrigerator.

   Note: Depending on the purpose of the experiment, different preparation methods are required. The extracted denatured total protein is used for quantitative detection by immunochemical methods. Soluble native proteins ensure the native state of the protein for the next step in protein catalytic activity analysis.

7.2.2 Quantification of Rubisco

7.2.2.1 Rubisco Quantification Using Immunochemical Methods

Principle: In this method the target protein is monitored through immunochemical fluorescence. The target protein is recognized by a Rubisco specific primary antibody, which can be coupled to a horseradish peroxidase (HRP) secondary antibody and detected by catalyzing a luminescence reagent to generate fluorescence. Quantification of the target protein is accomplished according to the strength of the fluorescent signal. In general, the intensity of the immunochemical fluorescence signal is not always linear with the amount of target protein, and does not pass through the origin of the coordinates. Therefore, a standard curve made using a standard protein is usually needed for the target protein quantification.

Materials, Reagents, Instruments, and Experimental Methods

Unless otherwise specified, all conventional chemical reagents are analytical grade reagents, available from SIGMA; water used in all experiments is ultrapure water, with high resistivity of 18 MΩ cm (25 °C).

Material

The total denatured or native protein of *Chlamydomonas reinhardtii*, mixed with the same amount of 2 × SDS loading buffer.

Reagents and supplies

- The required denatured (SDS-PAGE) gel is typically prepared by our laboratory. Gels can also be purchased from companies such as Bio-Rad.
- 2 × SDS loading buffer: 125 mM Tris-HCl pH 6.8; 20% glycerol; 4% SDS; 10% β-mercaptoethanol; 0.005% Bromophenol blue.
- Protein molecular weight standard: purchased from Promega.
- Purified Rubisco Protein Standard: purchased from Agrisera.
- Western blot transfer buffer: 50 mM Tris, 200 mM glycine, 20% ethanol.
- Ponceau S Dye: 0.1% Ponceau S dissolved in 5% acetic acid.
- RbcL antibody: available from Agrisera.
- Secondary antibody: horseradish peroxidase (HRP) conjugated goat anti-rabbit antibody.
- 10 × PBS solution: 26.8 mM KCl, 14.7 mM KH_2PO_4, 1.37 M NaCl, 100 mM Na_2HPO_4.
- Protein Immunoblotting washing buffer (PBS-T): 0.1% Tween 20 dissolved in 1× PBS buffer.
- Protein immunoblot blocking solution: 5% skim milk powder dissolved in PBS-T solution.
- PVDF membrane or nitrocellulose membrane, cut into the same size as the gel.
- Whatman filter paper, cut into the same size as the gel.

Instrument

- Protein electrophoresis system: purchased from Beijing Six-One company.
- Protein semi-dry transfer instrument: Trans-Blot SD semi-dry transfer instrument purchased from Bio-Rad company.
- Chemical fluorescence detector: GE LAS 4000 chemical fluorescence detector.

Method

1. To detect the total protein concentration of the algae lysate, the standard curve is prepared with BSA (bovine serum albumin) as standard, and the protein concentration determined by a Bradford assay kit.
2. For sample preparation, adjust the protein sample concentration to between 0.01 and 0.1 μg/μl after addition of an equal volume of 2 × SDS loading buffer.
3. The sample is heated at 95 °C for 45 s, then put on ice and briefly centrifuged for a few seconds.

4. 10 μl of sample protein (about 0.1–1 μg total protein) is loaded onto a 12% SDS-PAGE gel. At the same time, the Rubisco standard protein (0.01–0.5 μg gradient) is loaded.
5. Run the SDS-PAGE gel at a constant voltage of 160 V for 80 min.
6. The protein samples separated on the SDS-PAGE gel are transferred to a nitrocellulose membrane using a semi-dry transfer instrument, using the membrane and transfer system according to the manuals.
7. The membrane is soaked in Ponceau S Dye for 1 min to check the transfer efficiency, and then washed with distilled water. The Ponceau S Dye solution can be reused.
8. The membrane is blocked in the protein immunoblot blocking solution with shaking for 1 h.
9. The blocking solution is discarded, and then the membrane incubated in a protein immunoblot blocking solution containing 10,000 times diluted Rubisco antibody for 1 h on a shaker.
10. The membrane is then washed twice with PBS-T solution briefly, washed further in PBS-T solution for 15 min on a shaker, then washed twice again for 5 min each time.
11. The membrane is then incubated in a protein immunoblotting solution containing a diluted 20,000-fold secondary antibody on the shaker for 1 h.
12. As in step 10.
13. The chemiluminescent agent (ECL) is usually used to detect the signal of target protein on the membrane. Chemical fluorescence imaging systems are used in many laboratories which can directly detect and quantify the signal on the membrane.

7.2.2.2 Quantitative Rubisco Using ^{14}C-CABP (2-Carboxy-D-arabinitol-1,5-bisphosphate)

Principle: CABP (2-Carboxy-3-keto-D-arabinol-1,5-diphosphate) is an analogue of a six carbon intermediate product (2-carboxy-3-keto-D-arabinol) of the Rubisco carbon fixation reaction. CABP tightly binds at the active site of Rubisco; each active site will bind a molecule of CABP. Rubisco content can then be calculated by the quantity of the radioisotope-labeled CABP bound.

Materials, Reagents, Instruments, and Experimental Methods

Unless otherwise specified, all conventional chemical reagents are analytical grade; reagents, available from SIGMA. Water used in all experiments is ultrapure water, with a high resistivity of 18 MΩ cm (25 °C).

Material
Extracted soluble native protein.

Reagents and supplies

- $Na^{14}CN$ or $K^{14}CN$, available from MP Biomedical.
- BME solution: 100 mM Bicine-NaOH, pH 8.2, 20 mM $MgCl_2$, 1 mM Na_2-EDTA.

Instruments

- Liquid scintillation counter.

Method

1. Synthesis of ^{14}C-CABP: 1 mCi ^{14}CN is dissolved in 10 mM Na_2CO_3 (pH 10.0) to get 100 mM ^{14}CN, then 3 ml of 10 mM Na_2CO_3 (pH 10.0), 150 µl of 100 mM RuBP are added and mixed for incubation overnight. Add 500 µl of 2 N HCl to stop the reaction. After drying the solution at 40 °C, add about 7 ml of the BME solution to dissolve the pellet. The concentration of ^{14}C-CABP produced now is about 2 mM. Prepare aliquots of 200 µl each and store at −20 °C.
2. Activation of Rubisco enzyme: The extracted soluble protein is mixed with BMEC solution at a ratio of 9: 1 and allowed to react to activate the extracted Rubisco protein at 25 °C for 10–20 min.
3. Take 2 µl of ^{14}C-CABP, 20 µl of the activated Rubisco protein extract, mix well and incubate at 25 °C for 20–30 min. Then place the sample on ice until the molecular sieve chromatography is ready.
4. Preparation of molecular sieve column: use a low pressure Sephadex G50 Fine column (Pharmacia) (30 × 0.7 cm). The chromatographic material is equilibrated with 20 mM EPPS-NaOH, 75 mM NaCl, pH 8.0 buffer, by adding the buffer until it reaches about 0.5 cm above the chromatographic material.
5. Gently add the sample from step 3, taking care not to stir the chromatographic material. Open the column valve and allow the sample to flow into the chromatographic material. The column is washed with 200 µl of 20 mM EPPS-NaOH, 75 mM NaCl, pH 8.0 solution.
6. Using the same solution to wash the molecular sieve column, collect and seven fractions of 750 µl samples are collected in scintillation vials.
7. Add 100 µl of liquid scintillation solution to each sample, mix and place the vials in the liquid scintillation counter. Typically, the first sample from the column provides is the background count, the second and third samples are the ^{14}C-CABP combined with Rubisco, and the counts in the remaining samples are from unbound ^{14}C-CABP.
8. Calculation of Rubisco activity binding sites: subtract the counts from the second and third samples by the specific activity of ^{14}C-CABP to obtain the number of Rubisco active binding sites. The specific activity of the 53.3 mCi/mmol $K^{14}CN$ used to prepare the ^{14}C-CABP results in 118,319 DPM/nmol binding site. Rubisco content is calculated assuming each Rubisco molecule has 8 binding sites.

   Note: Immunochemical methods can be applied in conventional laboratories without generating isotope waste, though the ^{14}C-CABP method is more accurate. ^{14}C is a beta-ray emitter and the radioactivity is very small. However, the ^{14}C half-life is 5730 years, so it is difficult to deal with the isotope waste.

7.2.3 Detection of Rubisco Activity

7.2.3.1 Detection of Rubisco Enzyme Activity Using $NaH^{14}CO_3$

Principle: This method is based on Rubisco's carbon fixation ability that involves $^{14}CO_2^-$ (from $^{14}CO_3^-$) fixed to the substrate RuBP, and the formation of acid-stable chemical products. The activity of the Rubisco enzyme is measured based on the isotopic content of the product.

Materials, Reagents, Instruments, and Experimental Methods

Unless otherwise specified, all conventional chemical reagents are analytical grade; reagents, available from SIGMA. Water used in all experiments is ultrapure water, with high resistivity of 18 MΩ cm (25 °C).

Material
Extracted soluble native protein and Rubisco standard sample.

Reagents and supplies
- $NaH^{14}CO_3$ purchased from Perkin.
- D-Ribulose 1,5- Bisphosphate (RuBP) purchased from Sigma.
- Acetic acid: purchased from Beijing Chemical Reagent Company.
- BME solution: 100 mM Bicine-NaOH, pH 8.2, 20 mM $MgCl_2$, 1 mM Na_2-EDTA.
- Pre-mix solution: 1 mM DTT, 300 mM $NaHCO_3$, 50 mM $MgCl_2$, 2 μCi $NaH^{14}CO_3$ in BME solution.

Instrument
- Liquid scintillation counter.

Method
1. Take 30 μl of the standard Rubisco (0.5 μM monomer) or 30 μl of the extracted soluble native protein in a 1.5 ml tube.
2. Add 10 μl of Pre-mix solution, mix and react at room temperature for 5 min to activate Rubisco.
3. 4.5 μl of 25 mM RuBP is added and the reaction run for 5 min.
4. Add 10 μl of acetic acid to stop the reaction.
5. Open the tube lid, place the tube in a 90 °C metal block and dry the sample in a ventilated hood.
6. Add 100 μl of water to dissolve the dried sample.
7. Add 1 ml of liquid scintillation solution, mix, put into liquid scintillation counter to monitor the signal.

7.2.3.2 Enzyme-Linked Method of Detection of Rubisco Enzyme Activity

Principle: Through the reactions catalysed by phosphoglycerate kinase (PGK) and glyceraldehyde-3-phosphate dehydrogenase, 3-phosphoglycerate, the carboxylation product of Rubisco can be converted to glyceraldehyde-3-phosphate. This process consumes the reductant NADH and ATP. The activity of Rubisco enzyme can be calculated by detecting the rate of oxidation of NADH. Each of the two molecules NADH oxidized to NAD^+ corresponds to a reaction of one molecule of CO_2 is fixed by one molecule of Rubisco.

Materials, Reagents, Instruments, and Experimental Methods

Unless otherwise specified, all conventional chemical reagents are analytical grade; reagents, available from SIGMA. Water used in all experiments is ultrapure water, with high resistivity of 18 MΩ cm (25 °C).

Material
Extracted soluble native protein and Rubisco standard protein.

Reagents and supplies
- D-Ribulose 1,5- Bisphosphate (RuBP) purchased from Sigma.
- ATP purchased from Sigma.
- Nicotinamide adenine dinucleotide, reduced (NADH-2Na) purchased from Merck.
- Phosphocreatine purchased from Sigma.
- Creatine phosphokinase purchased from Sigma.
- Glyceraldehyde-3-phosphate Dehydrogenase from rabbit muscle (GAPDH) purchased from Sigma.
- 3-Phosphoglyceric Phosphokinase from baker's yeast (PGK) purchased from Sigma.
- BME solution: 100 mM Bicine-NaOH, pH 8.2, 20 mM $MgCl_2$, 1 mM Na_2-EDTA.
- BMEC solution: 100 mM $NaHCO_3$ dissolved in BME solution.

Instrument
- Full spectrum spectrophotometer with temperature control.

Method
1. Take 30 μl of standard Rubisco (0.5 μM monomer) or 30 μl of Rubisco soluble native protein.
2. Add 10 μl BMEC solution, mix and react at room temperature for 5 min to activate Rubisco.
3. The following reagents are added and mixed thoroughly at a final concentration of 10 mM Phosphocreatine, 20 U/ml Creatine phosphokinase, 0.25 mM NADH, 20 U/ml GAPDH, 40 U/ml PGK, and 2 mM ATP, respectively.

4. Add 2.5 mM RuBP to start the reaction. Immediately after mixing, place the sample in the spectrophotometer and monitor the absorption value at 340 nm at 25 °C for 5 min.
5. To calculate the Rubisco enzyme activity: every two molecules of NADH oxidised to NAD^+ corresponds to a reaction of one Rubisco molecule reacting with CO_2 molecule. The absorption coefficient of NADH is 6220 M^{-1} cm^{-1}.

Note: The $NaH^{14}CO_3$ method is fast and sensitive. The enzyme-linked reaction method does not produce isotope waste, but the enzyme reaction involves many enzymes and catalytic steps which is also more likely to cause experimental error.

7.3 Advantages, Disadvantages, and Misunderstanding

In this chapter, we describe in detail methods of Rubisco quantification and detection of catalytic activity of the enzyme, a key component in photosynthetic carbon fixation in algae. For Rubisco quantification, one method used is the determination of the content of large subunits of Rubisco by Western Blot assays, in which the sample material used can be denatured protein. This method is simple, it can be accomplished in almost all biochemical and molecular laboratories, but the involved procedures are tedious. The second method is designed to quantify Rubisco by monitoring the binding of radioisotopically-labeled CABP which tightly integrates to the active site of Rubisco. This method requires synthesis of the labelled substrate and access to a liquid scintillation counter, and needs extraction of non-denatured samples which should be carefully manipulated to avoid degradation. However, the sensitivity of the second method is higher than the first. For detection of the catalytic activity of Rubisco, two kinds of methods are also provided here. The enzyme-linked method is easy to handle, but the isotope method is timesaving and sensitive. Researchers can choose which method to use according to the purpose of their study and the conditions.

Although the methods and procedures described here use algae cells as experimental material, they could be used for higher plant cell Rubisco quantification and activity determination providing the cellular breakage method is modified. By means of optimization, these methods can also be used to screening mutants of algae carbon fixation.

References

Allen MM (1968) Simple conditions for the growth of unicellular blue-green algae on plates. J Phycol 4:1–4

Harris E (1989) The *Chlamydomonas* sourcebook. A comprehensive guide to biology and laboratory use, 1st edn. Academic Press, San Diego, p 780. eBook ISBN: 9781483288604

Chapter 8
Phosphoenolpyruvate Carboxylase

Fan Hu and Hanhua Hu

Abstract This chapter describes the role of phosphoenolpyruvate carboxylase in C_4 photosynthesis and its activity assay protocols based on the measurement of oxaloacetate-dependent NADH oxidation.

Keywords Phosphoenolpyruvate carboxylase · C_4 photosynthesis · Diatom · CO_2 · Enzyme activity

Phosphoenolpyruvate carboxylase (PEP carboxylase, PEPCase, or PEPC; EC 4.1.1.31) catalyzes the irreversible β-carboxylation of phosphoenolpyruvate (PEP) in the presence of HCO_3^- and Mg^{2+} to yield oxaloacetate (OAA) and Pi:

$$\text{PEP} + \text{HCO}_3^- \rightarrow \text{oxaloacetate} + \text{Pi}$$

PEPC is widespread not only in all photosynthetic organisms such as plants, algae, cyanobacteria, and photosynthetic bacteria, but also in most nonphotosynthetic bacteria and protozoa. The enzyme is apparently absent in animals, fungi, and yeasts (Izui et al. 2004). Besides its cardinal roles in the initial fixation of atmospheric CO_2 during C_4 photosynthesis and Crassulacean acid metabolism (CAM), PEPC plays primarily an anaplerotic role by replenishing C_4-dicarboxylic acids utilized for both energy and biosynthetic metabolism. In addition, PEPC also plays specialized roles for the normal development of plants and for root responses to stress (Feria et al. 2016). Plants contain two types of PEPC, a plant-type and a bacteria-type PEPC. Plant-type PEPC has a phosphorylatable Ser residue and bacteria-type PEPC lacks the conserved residue. In general, PEPC is usually composed of four identical subunits of about 95–110 kDa, whereas

F. Hu
School of Foreign Languages, China University of Geosciences, Wuhan, China

H. Hu (✉)
Institute of Hydrobiology, Chinese Academy of Sciences, Wuhan, China
e-mail: hanhuahu@ihb.ac.cn

K. Gao et al. (eds.), *Research Methods of Environmental Physiology in Aquatic Sciences*, https://doi.org/10.1007/978-981-15-5354-7_8

bacterial-type PEPCs are composed of four each of the bacterial- and plant-type isozymes (O'Leary et al. 2009). Most PEPCs are allosteric enzymes whose activity is regulated by a variety of metabolic effectors. In addition, the activity of PEPCs is also regulated by light, temperature, pH value, salinity, and drought. PEPC is targeted to the cytoplasm and chloroplast, and the chloroplastic PEPC plays a crucial role in ammonium assimilation (Masumoto et al. 2010).

8.1 PEPC and C_4 Pathway

Although a PEPC gene has been identified in many sequenced microalgae genomes, the role of PEPC in carbon fixation is still not well documented (Parker et al. 2008). Except for *Thalassiosira weissflogii*, which has been shown to exhibit a plant-type biochemical C_4 metabolism (Reinfelder et al. 2000, 2004; Roberts et al. 2007), there is little direct evidence for a functional C_4 metabolic pathway occurring in other algae. The possible pathway of C_4 metabolism in microalgae cells can be summarized as follows: bicarbonate is added to the three-carbon acid PEP by the enzyme PEPC. The product of this reaction oxaloacetic acid (OAA) is subsequently transported to the plastid via specific transporters. Malate dehydrogenase (MDH) converts the OAA into malate, which is then decarboxylated by NADP-dependent malic-enzyme to generate the CO_2 fixed by RUBISCO. The by-product of the decarboxylation is pyruvate, which is phosphorylated by pyruvate-phosphate dikinase to regenerate PEP for export to the cytosol and completion of the cycle (Parker et al. 2008). In *Ostreococcus tauri*, all enzymes relating to C_4 organic acid metabolism have been identified, while their localization(s) are not known and the nature of its carbon concentration mechanism (CCM) is not clear. Evidence has been presented for a C_4-type CCM in at least one diatom, *T. weissflogii*, but there is little support for a C_4 mechanism in other diatoms. The extensive in silico analyses of gene sequences from two model diatoms, *Thalassiosira pseudonana* and *Phaeodactylum tricornutum*, showed that the decarboxylating enzymes phosphoenolpyruvate carboxykinase (PEPCK) and malic enzyme (ME) do not possess plastid targeting sequences (Kroth et al. 2008). GFP localization experiments provide evidence that the decarboxylation enzyme PEPCK (Yang et al. 2016) and ME are not located in the plastids (Tanaka et al. 2015; Ewe et al. 2018), which suggests that classical C_4 enzymes play little role in the CCMs in these two diatoms. Although the transcriptional level of *P. tricornutum* PEPC was not regulated by CO_2 concentration (McGinn and Morel 2008), metabolic flow analysis suggested that this diatom had C_4 photosynthesis (Huang et al. 2015). It is also controversial whether there is a C_4 metabolic pathway in *T. pseudonana* (Roberts et al. 2007). Kustka et al. (2014) suggested that the decarboxylation of oxaloacetic acid produced by PEPC may be accomplished by pyruvate carboxylase, which is usually considered to catalyze the irreversible carboxylation of pyruvate.

8.2 Preparation and Assay of PEPC

The most widely used method for the measurement of PEPC activity is the spectrophotometric coupled assay with MDH which reduces the OAA formed to malate and oxidizes NADH into NAD (Fig. 8.1). The simultaneous oxidation of NADH is followed at 340 nm in a spectrophotometer equipped with a recorder. NADH absorbs significantly at 340 nm, whereas NAD does not. An enzyme activity unit (U) is defined as a decrease of 0.01 in absorbance under standard assay conditions.

8.2.1 Preparation of Reagents

0.03 mol/L potassium phosphate buffer:

pH 6.9: 555 mL solution A + 445 mL solution B.
pH 8.0: 833 mL solution A + 167 mL solution B.
Solution A: 0.03 mol/L K_2HPO_4 (Add 5.23 g K_2HPO_4 to 1000 mL dH_2O).
Solution B: 0.03 mol/L KH_2PO_4 (Add 4.08 g KH_2PO_4 to 1000 mL dH_2O).

Buffer 1: 0.03 mol/L potassium phosphate—0.55 mol/L sorbitol, pH 6.9.

Add 99.0 g sorbitol to 0.03 mol/L pH 6.9 potassium phosphate buffer with a final volume of 1 L.

Buffer 2: 0.06% lysozyme (in 0.03 mol/L potassium phosphate—0.55 mol/L sorbitol buffer).

Add 0.06 g lysozyme to 100 mL buffer 1.

Buffer 3: 0.03 mol/L potassium phosphate—0.55 mol/L sorbitol, pH 8.0.

Add 99.0 g sorbitol to 0.03 mol/L pH 8.0 potassium phosphate buffer with a final volume of 1 L.

0.15 mol/L Tris–HCl buffer (adjust to a pH of 8.5 with 20% NaOH).
0.3 mol/L $MgCl_2$.

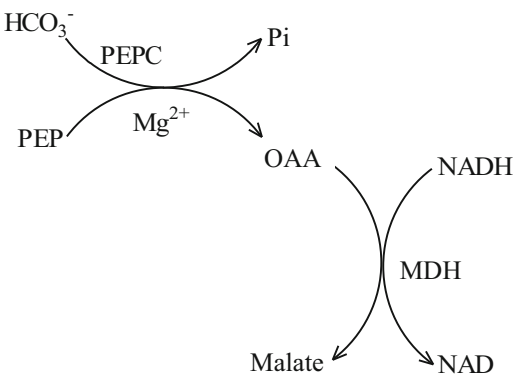

Fig. 8.1 The principle of measuring PEPC activity

0.6 mol/L $NaHCO_3$ (must be prepared fresh).
3.0 mmol/L NADH (must be prepared fresh).
0.1 mol/L phosphoenolpyruvate (must be prepared fresh).
15 mmol/L acetyl CoA (must be prepared fresh).
10,000 U/mL malate dehydrogenase (Sigma).

8.2.2 Preparation of Cell Extract

Cells (500–800 mg dry weight) at the exponential growth phase are harvested by centrifugation (5000 *g*, 20 min). Cell pellets are washed once in dH_2O, and then suspended in 100 mL of **buffer 2** and subjected to shaking (100 rpm) in the dark at 30 °C for 2 ~ 3 h. The samples are then centrifuged at 5000 *g* for 20 min at 4 °C, and the precipitate washed twice with **buffer 3**. 20 mL of potassium phosphate buffer (pH 8.0) is added to the precipitate and mixed gently. Samples are centrifuged at 12,000 *g* for 20 min at 4 °C and the supernatant used for the enzyme activity assay.

8.2.3 Procedure

For each assay, prepare the two cocktails shown in the following table into two separate UV-translucent cuvettes, and keep them on ice.

	Volume (μL) added to	
Solution	Blank	Test
H_2O	190	140
0.15 mol/L Tris–HCl buffer (pH = 8.5)	1000	1000
0.6 mol/L $NaHCO_3$	25	25
0.3 mol/L $MgCl_2$	25	25
3.0 mmol/L NADH	50	50
15 mmol/L acetyl CoA	50	50
10,000 U/mL Malate dehydrogenase	10	10
0.1 mol/L PEP	0	50

Taking them directly from the ice when ready to commence the assay, place the two cuvettes (each containing 1350 μL) into the spectrophotometer holder. Wait 10 min to allow the temperature of the solutions in the cuvettes to equilibrate. Simultaneously add 150 μL of diluted enzyme to the cuvettes. Record the decrease in A_{340} to establish the rate. The activity is calculated as follows:

$$\text{Units/mg} = [\Delta A_{340}/\text{min (Test)} - \Delta A_{340}/\text{min (Blank)}]/[6.22 \times \text{mg enzyme/mL reaction mixture}].$$

8.2.4 ^{14}C Isotope Assay Methods

For the assay using ^{14}C isotope, $NaHCO_3$ in the cocktail mentioned above is replaced by $NaH^{14}CO_3$, and neither NADH nor malate dehydrogenase is added. After 5–-10 minutes, the reaction is terminated by adding four times the volume of 0.5 mol/L HCl solution. Aeration is used to remove the remaining $H^{14}CO_3^-$, and radioactivity measured by liquid scintillation counting.

8.3 Note

For enzymatic extracts, the assay should be performed immediately. Usually, the reaction rate is constant within 5–8 min, and is proportional to the protein concentration. It is generally believed that the spectrophotometric method is more accurate and that the ^{14}C isotope method is susceptible to the influence of atmospheric CO_2.

References

Ewe D, Tachibana M, Kikutani S et al (2018) The intracellular distribution of inorganic carbon fixing enzymes does not support the presence of a C_4 pathway in the diatom *Phaeodactylum tricornutum*. Photosynth Res 137:263–280

Feria AB, Nadja B, Sánchez A et al (2016) Phosphoenolpyruvate carboxylase (PEPC) and PEPC-kinase (PEPC-k) isoenzymes in *Arabidopsis thaliana*: role in control and abiotic stress conditions. Planta 244:901–913

Huang A, Liu L, Zhao P et al (2015) Metabolic flux ratio analysis and cell staining suggest the existence of C_4 photosynthesis in *Phaeodactylum tricornutum*. J Appl Microbiol 120:705–713

Izui K, Matsumura H, Furumoto T et al (2004) Phospho*enol*pyruvate carboxylase: a new era of structural biology. Annu Rev Plant Biol 55:69–84

Kroth PG, Chiovitti A, Gruber A et al (2008) A model for carbohydrate metabolism in the diatom *Phaeodactylum tricornutum* deduced from comparative whole genome analysis. PLoS One 3: e1426

Kustka AB, Milligan AJ, Zheng H et al (2014) Low CO_2 results in a rearrangement of carbon metabolism to support C_4 photosynthetic carbon assimilation in *Thalassiosira pseudonana*. New Phytol 204:507–520

Masumoto C, Miyazawa S-I, Ohkawa H et al (2010) Phospho*enol*pyruvate carboxylase intrinsically located in the chloroplast of rice plays a crucial role in ammonium assimilation. Proc Natl Acad Sci U S A 107:5226–5231

McGinn PJ, Morel FMM (2008) Expression and inhibition of the carboxylating and decarboxylating enzymes in the photosynthetic C_4 pathway of marine diatoms. Plant Physiol 146:300–309

O'Leary B, Rao SK, Kim J et al (2009) Bacterial-type phospho*enol*pyruvate carboxylase (PEPC) functions as a catalytic and regulatory subunit of the novel Class-2 PEPC complex of vascular plants. J Biol Chem 284:24797–24805

Parker MS, Mock T, Armbrust EV (2008) Genomic insights into marine microalgae. Annu Rev Genet 42:619–645

Reinfelder JR, Kraepiel AML, Morel FMM (2000) Unicellular C_4 photosynthesis in a marine diatom. Nature 407:996–999

Reinfelder JR, Milligan AJ, Morel FMM (2004) The role of the C_4 pathway in carbon accumulation and fixation in a marine diatom. Plant Physiol 135:2106–2111

Roberts K, Granum E, Leegood RC et al (2007) C_3 and C_4 pathways of photosynthetic carbon assimilation in marine diatoms are under genetic, not environmental, control. Plant Physiol 145:230–235

Tanaka R, Kikutani S, Mahardika A et al (2015) Localization of enzymes relating to C_4 organic acid metabolisms in the marine diatom, *Thalassiosira pseudonana*. Photosynth Res 121:251–263

Yang J, Pan Y, Bowler C, Zhang L, Hu H (2016) Knockdown of phosphoenolpyruvate carboxykinase increases carbon flux to lipid synthesis in *Phaeodactylum tricornutum*. Algal Res 15:50–58

Chapter 9
Nitrate Reductase

Dinghui Zou

Abstract Nitrate reductase (NR) is an intracellular enzyme commonly occurring in the cytoplasm. This enzyme is the rate-limiting enzyme in nitrate assimilation, and its activity is strongly related to the bioavailability of nitrate. Here a method is described to determine the in vivo NR activity by using the marine macroalga *Gracilaria lemaneiformis* as the experimental organism.

Keywords Nitrate reductase · Enzyme activity · Nitrate assimilation · Nitrate · Marine macroalgae

9.1 Introduction

The inorganic nitrogen in natural waters mainly exists in the form of NO_3^-, and most of the nitrogen nutrients absorbed by algae is contributed as NO_3^- (Zou and Xia 2011). After NO_3^- enters the cell, it must be reduced to NH_4^+ to be utilized. The NO_3^- reduction process is divided into two steps. Firstly, the NO_3^- is reduced to NO_2^- under the action of nitrate reductase (NR, EC, 1.7.1.3). NR usually uses NAD(P)H as an electron donor, driving the catalytic reduction from nitrate to nitrite. Secondly, NO_2^- is further reduced to NH_4^+ catalyzed by nitrite reductase (NiR) and in this form N finally enters the assimilation processes leading to organic matter. The first step is the rate-limiting reaction of the whole nitrate reduction process, and thus NR is the rate-limiting enzyme for the whole sequence. It is generally located in the cytoplasm, and may also be connected to the plasma membrane. NR activity is regulated by many environmental and physiological factors (Lopes et al. 1997; Zou 2005), and therefore can be used as a key physiological index to evaluate the utilization ability of algae to NO_3^-. The method described here uses the marine macroalga *Gracilaria lemaneiformis* as the test material.

D. Zou (✉)
School of Environment and Energy, South China University of Technology, Guangzhou, China
e-mail: dhzou@scut.edu.cn

K. Gao et al. (eds.), *Research Methods of Environmental Physiology in Aquatic Sciences*, https://doi.org/10.1007/978-981-15-5354-7_9

9.2 Materials and Method

9.2.1 Materials

Thallus of the marine macroalga *Gracilaria lemaneiformis*.

9.2.2 Reagent Preparation

1. Reaction media preparation: 0.1871 g Na-EDTA, 0.0018 g glucose, 20.2200 g KNO_3, dissolved in 1 l 0.1 M potassium dihydrogen phosphate buffer (13.6090 g; pH 7.5).
2. 1% Sulfanilamide solution preparation: take 1.000 g sulfanilamide in 100 ml 3 mM HCl;
3. 0.1% α-ethylenediamine solution: 0.1000 g α-ethylenediamine dissolved in 100 ml pure water, and stored in a brown bottle.
4. 1 g/ml Potassium nitrite standard solution: 3.6999 g potassium nitrite dissolved in 1000 ml of pure water, and then dilute 5 ml to a volume of 1000 ml.

9.2.3 Methods

NR activity can be assayed by colorimetric methods through determining the production rate of nitrite according to the in situ procedure described by Corzo and Niell (1991). About 0.1 g FW of *Gracilaria lemaneiformis* algal samples cut into smaller pieces is added to the test tubes, which contains 10 ml reaction medium (incubation mixture 0.1 M KH_2PO_4, 0.5 mM Na-EDTA, 0.1% propanol (v/v), 0.01 mM glucose, and 50 mM KNO_3, with a pH value of 8.0). The reaction medium is flushed with N_2 gas for 2 min to obtain anaerobic conditions. The reaction systems are then closed with screw caps and incubated for 1 h in darkness.

After the incubation period, nitrite concentration is determined colorimetrically at 540 nM. The NR activity is expressed as μmol NO_2^- g^{-1} FW h^{-1}.

9.3 Discussion

Because NRA is strongly influenced by the nutrient supply state, illumination, and physiological state (such as circadian rhythm) and other factors, there is not a complete standard determination method or procedure for NRA determination. The procedure is usually modified according the differences existing in algal materials and the purpose of the experiment. For example, as the activity of NR usually exhibits a circadian rhythm, usually reaching a maximum during the light period and

a minimum in darkness, the algal samples are collected after they have experienced 6–8 h in the light period and the measurement is carried out immediately. Thus the measured activity is a potential estimate of the NR activity of the cells under the conditions prior to the assay. Additionally, in the determination process the reaction time is generally 30–60 min. Within such a duration range, the quantity of nitrite generated and the duration are linear; and the reaction medium pH value and temperature can also be adjusted to the desired levels according to the purpose of study.

References

Corzo A, Niell FX (1991) Determination of nitrate reductase activity in *Ulva rigida* C. Agardh by the *in situ* method. J Exp Mar Biol Ecol 146:181–191

Lopes PF, Oliveira MC, Colepicolo P (1997) Diurnal fluctuation of nitrate reductase activity in the marine red alga *Gracilaria tenuistipitata* (Rhodophyta). Phycologia 33:225–231

Zou DH (2005) Effects of elevated atmospheric CO_2 on growth, photosynthesis and nitrogen metabolism in the economic brown seaweed, *Hizikia fusiforme* (Sargassaceae, Phaeophyta). Aquaculture 250:726–735

Zou DH, Xia JR (2011) (2011). Nutrient metabolism of marine macroalgae and its relationship with coastal eutrophication: a review. Chin J Ecol 30(3):589–595

Chapter 10
Antioxidants and Reactive Oxygen Species (ROS) Scavenging Enzymes

Yahe Li and Zengling Ma

Abstract Photosynthetic alga, like higher plants, generate reactive oxygen species (ROS), such as superoxide anion radicals (O_2^-), hydroxyl radicals (·OH) and hydrogen peroxide (H_2O_2). Normally, the generation and detoxification of ROS in the cell are kept in equilibrium, but the production of ROS could be enhanced by biotic and abiotic stress, in which case algae need mechanisms to protective themselves from oxidative stress. The algal defence system against reactive oxygen involves reactive oxygen scavenging enzymes, including superoxide dismutase (SOD, EC1.15.1.1), catalase (CAT, EC1.11.1.6), peroxidase (POD, EC1.11.1.7), ascorbate peroxidase (APX, EC.1.11.1.11) and glutathione reductase (GR, EC1.6.4.2), and antioxidants such as ascorbate, glutathione, carotenoids, vitamin E, and proline. Here methods are described to determine the SOD, CAT, POD, APX, and GR activities using the marine macroalga *Ulva prolifera* as experimental material.

Keywords Activity measurement · Ascorbate peroxidase · Catalase · Peroxidase · Glutathione reductase · Reactive oxygen species scavenging enzymes · Superoxide dismutase

10.1 Introduction

Oxidative stress is an unavoidable side effect of aerobic metabolism. In order to repair the damage and scavenge excess reactive oxygen species (ROS), the algae have developed a number of efficient antioxidative systems including enzymic and

Y. Li
Key Laboratory of Marine Biotechnology of Zhejiang Province, School of Marine Sciences, Ningbo University, Ningbo, China
e-mail: liyahe@nbu.edu.cn

Z. Ma (✉)
Zhejiang Provincial Key Laboratory for Subtropical Water Environment and Marine Biological Resources Protection, Wenzhou University, Wenzhou, China
e-mail: mazengling@wzu.edu.cn

K. Gao et al. (eds.), *Research Methods of Environmental Physiology in Aquatic Sciences*, https://doi.org/10.1007/978-981-15-5354-7_10

nonenzymic antioxidants (Mallick and Mohn 2000; Noctor and Foyer 1998; Sharma et al. 2012). Superoxide dismutase (SOD, EC1.15.1.1) acts on superoxide anion radicals (O_2^-) to produce hydrogen peroxide (H_2O_2) and oxygen (O_2), thereby playing an important role in the defense mechanism (Bowler et al. 1992). Catalase (CAT, EC 1.11.1.6), a tetrameric heme-containing enzyme, converts H_2O_2 into water and O_2 (Mallick and Mohn 2000), while peroxidase (POD, EC1.11.1.7) with ferric porphyrin as the auxiliary group, decomposes H_2O_2 by oxidation of co-substrates such as phenolic compounds and/or antioxidants (Capma 1991; Gaspar et al. 1991; Rao et al. 1996), and ascorbate peroxidase (APX, EC.1.11.1.11) has been frequently observed (Mittler 2002). APX, a heme-containing protein, utilizes ascorbic acid (AsA) as electron donor to scavenge H_2O_2 with the generation of monodehydroascobate (MDA) and/or dehydroascorbate (DHA) (Asada 1992; Rao et al. 1996). Glutathione reductase (GR, EC1.6.4.2), a flavoprotein, catalyzes the NADPH-dependent reduction of glutathione disulfide (GSSG) to glutathione (GSH). GSH has a major role as a reductant in oxidation-reduction processes, and also serves in detoxication and several other cellular functions of great importance (Carlberg and Mannervik 1985). The assay methods for these enzymes are described in this chapter using the marine macroalga *Ulva prolifera* as the example experimental material.

10.2 Superoxide Dismutase (SOD) Activity

10.2.1 Materials

Marine macroalga *Ulva prolifera.*

10.2.2 Reagent Preparation

1. Phosphate buffer (50 mmol L^{-1}, pH 7.8, hereafter termed PBS): dissolve 35.814 g $Na_2HPO_4 \cdot 12H_2O$ (molecular weight 358.14) in 500 mL distilled water to prepare disodium phosphate solution (0.2 mol L^{-1}; Solution A), then 15.601 g $NaH_2PO_4 \cdot 2H_2O$ (molecular weight 156.01) was used to prepare dihydrogen phosphate solution (0.2 mol L^{-1}; 500 mL; Solution B). The PBS (1000 mL) is prepared by mixing 228.75 mL solution A, 21.25 mL solution B and distilled water (750 mL).
2. 130 mmol L^{-1} methionine solution (Met): 1.9399 g methionine dissolved in PBS with 100 mL as the final volume.
3. 2.25 mmol μmol L^{-1} nitrogen blue tetrazole solution (NBT): 0.1840 g nitrogen blue tetrazole methionine dissolved in PBS with 100 mL as the final volume, then kept in darkness until use.
4. 30 μmol L^{-1} EDTA-Na_2: 0.001 g EDTA-Na_2 dissolved in 100 mL PBS.

5. 60 μmol L^{-1} riboflavin solution: 0.0115 g dissolved in distilled water with 500 mL as the final volume, kept in darkness until use.
6. Reaction solution: a 3 mL reaction solution for each sample is needed; the total volume of reaction solution is calculated based on the number of samples, then the reaction mixes are prepared according to the proportions as follows, Met: EDTA-Na_2: PBS: NBT: riboflavin = 30:1:9:10:10.

10.2.3 Methods

Approximately 0.1 g fresh weight (FW) of *Ulva prolifera* samples are placed in a mortar (pre-cooled to under −20 °C) and are ground into a homogenate with 2 mL 50 mmol L^{-1} PBS (pH 7.8), then the homogenate is centrifuged (12,000 × *g*) for 20 min. Supernatants are removed and transferred to clean 2 mL centrifuge tubes, and stored at −4 °C until analyzed.

SOD (EC1.15.1.1) activity is determined by using nitroblue tetrazolium according to Giannopolitis and Ries (1977) with some modifications. Supernatant (50 μL) is transferred to test tubes which contain 3 mL reaction medium, the reaction mixture is allowed to incubate for 20 min at 20 °C and a light intensity of 100 μmol m^{-2} s^{-1}. Two controls with the corresponding PBS buffer instead of the enzyme solution are set up. One of them is exposed to the same light reaction as the sample tube and acts as the maximum light reduction tube, while the other one is placed in darkness and is used to provide a zero when the absorbance is measured. After the incubation period, the absorbance of the reaction mixture is measured at 560 nm. The SOD activity is calculated as: SOD activity (U (g FW)$^{-1}$) = $[(A_{CK} - A_E) \times V]/(0.5\ A_{CK} \times W \times V_t)$, where the A_{CK} and A_E represent the absorbance of control and samples, respectively; V and V_t represent the volume of phosphate buffer used for enzyme extract (2 mL) and supernatant (50 μL) used in reaction. W represents the FW.

10.3 Catalase (CAT) Activity

10.3.1 Materials

Marine macroalga *Ulva prolifera.*

10.3.2 Reagent Preparation

1. Phosphate buffer (50 mmol L^{-1}, pH 7.8, PBS) is prepared as described above for SOD measurements.

2. H_2O_2 (0.1 mol L^{-1}): is purchased commercially and calibrated with 0.1 mol^{-1} potassium permanganate.
3. Reaction solution: A 3 mL reaction mix for each sample is required; the total volume of reaction solution is calculated based on the number of samples, then they are prepared immediately, with five parts PBS and one part H_2O_2, before use.

10.3.3 Methods

Approximately 0.1 g FW of *Ulva prolifera* samples is placed in a mortar (pre-chilled to under −20 °C) and are ground into a homogenate with 2 mL 50 mmol L^{-1} PBS (pH 7.8) then the homogenate centrifuged (12,000 × *g*) for 20 min. The supernatant is removed and transferred to clean 2 mL centrifuge tubes, and stored at −4 °C until analyzed.

CAT (EC.1.11.1.6) activity is determined according to Rao et al. (1996). 3 mL reaction mixture and 0.1 mL enzyme extract are added at 25 °C, then the absorbance at 240 nm is measured at intervals of 1 min for a total of 4 min. The CAT activity is calculated as a consequence of H_2O_2 consumption. $\mathrm{CAT(U/g/min)} = \Delta A_{240} \times V / (0.1 \times V_t \times t \times W)$, where ΔA_{240} represents the change in absorbance during the measurement period; V and V_t represent the volume of phosphate buffer used for enzyme extract (2 mL) and supernatant (0.1 mL) respectively, used in the reaction. W represents the FW. The factor 0.1 means 1 unit of enzyme activity (U) for every 0.1 unit decrease in A_{240}.

10.4 Peroxidase (POD) Activity

10.4.1 Materials

Marine macroalga *Ulva prolifera.*

10.4.2 Reagent Preparation

1. Phosphate buffer is prepared as described above for the SOD activity measurement.
2. H_2O_2 solution (30%; V/V): is prepared immediately before use.
3. Guaiacol solution: This is purchased commercially with a purity of 99%.
4. Reaction solution: A 3 mL reaction mix for each sample is required. The total volume of reaction solution required is calculated based on the number of samples. Thus for 15 samples for example, 50 mL PBS and 28 μL guaiacol solutions are mixed, slowly heated and stirred until the guaiacol is completely

dissolved, then 19 μL H_2O_2 is added, mixed well and the solution stored in the refrigerator until use.

10.4.3 Methods

Approximately 0.1 g FW of *Ulva prolifera* sample are placed in a mortar (pre-cooled to under −20 °C) and are ground into a homogenate with 2 mL 50 mmol L^{-1} PBS (pH 7.8). Then the homogenate is centrifuged (12,000 × *g*) for 20 min. The supernatant is removed, transferred to clean 2 mL centrifuge tubes, and stored at −4 °C until analyzed.

POD (EC1.11.1.7) activity was determined according to Rao et al. (1996). 1 mL enzyme extract is added into a 3 mL reaction mixture and the absorbance at 470 nm is measured at intervals of 0.5 min for a total of 4 min. The POD activity was calculated as POD(U/g/min) = $\Delta A_{470} \times V/(0.01 \times V_t \times t \times W)$, where ΔA_{470} represents the change in absorbance during the measurement period; V and V_t represent the volumes of phosphate buffer used for enzyme extract (2 mL) and supernatant (1 mL) respectively used in the reaction. W represents the FW. The factor 0.01 means 1 unit of enzyme activity (U) for every 0.01 unit decrease in A_{470}.

10.5 Ascorbate Peroxidase (APX) Activity

10.5.1 Materials

Marine macroalga *Ulva prolifera.*

10.5.2 Reagent Preparation

1. Phosphate buffer is prepared as described above for the SOD assay.
2. 0.3 mmol L^{-1} ascorbic acid (AsA): 0.0264 g ascorbic acid dissolved in 50 mL PBS before use.
3. H_2O_2 solution (30%; V/V): prepared immediately before use.
4. Reaction solution: 1.9 mL reaction solution for each sample is needed, the total volume of reaction solution is calculated based on the number of samples, then they are prepared immediately in the proportions PBS: AsA: H_2O_2 = 1.7: 0.1:0.1.

10.5.3 Methods

Approximately 0.1 g FM of *Ulva prolifera* samples are placed in a mortar (pre-chilled to under −20 °C) and are ground into a homogenate with 2 mL 50 mmol L^{-1} PBS (pH 7.8), then the homogenate is centrifuged (12,000 × *g*) for 20 min. The supernatant is removed and transferred to clean 2 mL centrifuge tubes, and stored at −4 °C until analyzed.

The activity of APX (EC.1.11.1.11) is determined based on the method described by Nakano and Asada (1981) with some modification. Enzyme extract (0.1 mL) is added to 1.9 mL reaction mixture and the absorbance at 290 nm is measured at intervals of 10 s for a total of 1 min after 30 s of the reaction starting. One unit of APX activity determines the amount necessary to decompose 1 μmol of ascorbate per min. The APX activity was calculated as APX(U/g/min) = $\Delta A_{290} \times V/(V_t \times t \times W)$, where ΔA_{290} represents the change in absorbance during the measurement period; V and V_t represent the volume of phosphate buffer used for enzyme extract (2 mL) and supernatant (0.1 mL) used in reaction. W represents the FW.

10.6 Glutathione Reductase (GR) Activity

1. Phosphate buffer is prepared as described above for the SOD assay.
2. 2 mol L^{-1} reduced nicotinamide adenine dinucleotide phosphate (NADPH) solution: 1.5 mg NADPH dissolved in 0.9 mL distilled water, mixed well and stored at −70°.
3. Oxidized glutathione (GSSG): add 10 mL distilled water into a bottle containing 14.2 mg GSSG, and store at −20°.
4. Reaction solution: 1.8 mL reaction solution for each sample is needed, the total volume of reaction solution is calculated based on the number of samples, then they prepared immediately in the proportions of GSSG: PBS: NADPH = 10:7:1.

10.6.1 Methods

GR (EC1.6.4.2) activity was measured as described by Carlberg and Mannervik (1985), with some modification. Enzyme extract (0.2 mL) is added to 1.8 mL reaction mixture and the absorbance at 340 nm measured at intervals of 1 min for a total of 4 min. The GR activity is calculated as GR(U/g/min) = $\Delta A_{340} \times V/(0.1 \times V_t \times t \times W)$, where ΔA_{340} represents the changed in absorbance during the measurement period; V and V_t represent the volume of phosphate buffer used for enzyme extract (2 mL) and supernatant (0.2 mL) used in reaction. W represents the FW. The factor 0.1 means 1 unit of enzyme activity (U) for every 0.1 unit decrease in A_{340}.

10.7 Discussion

Methods for the determination of antioxidant activity abound (Alam et al. 2013). Here, only one method for each enzyme is listed, and these methods are most frequently used because of their lower requirements for instruments. However, the amount of samples and chemicals, as well as the incubation conditions, should be determined by preliminary experiments to take into account species-specific differences. Additionally, the measurement time required for a decrease in A_{240} from 0.45 to 0.40 was also used to calculate the CAT activity (Mishra et al. 1993). Finally, commercially available kits are now available to determine the activity of the enzymes described above.

References

Alam MN, Bristi NJ, Rafiquzzaman M (2013) Review on in vivo and in vitro methods evaluation of antioxidant activity. Saudi Pharm J 21:143–152

Asada K (1992) Ascorbate peroxidase – a hydrogen peroxide-scavenging enzyme in plants. Physiol Plant 85:235–241

Bowler C, Montagu M, Inze D (1992) Superoxide dismutase and stress tolerance. Annu Rev Plant Physiol Plant Mol Biol 43:83–116

Capma A (1991) Biological roles of plant peroxidases: known and potential function. In: Everse J, Everse K, Grisham MB (eds) Peroxidases in chemistry and biology, CRC Press, vol ii. Boca Raton, FL, FL, pp 25–50

Carlberg I, Mannervik B (1985) Glutathione reductase. Methods Enzymol 113:484–490

Gaspar TH, Penel C, Hagega D, Greppin H (1991) Peroxidases in plant growth, differentiation and development processes. In: Lobarzewski J, Greppin H, Penel C, Gaspar TH (eds) Biochemical, molecular and physiological aspects of plant peroxidases. University de Geneve, Geneve, pp 249–280

Giannopolitis CN, Ries SK (1977) Superoxide dismutases I. Occurrence in higher plants. Plant Physiol 59:309–314

Mallick N, Mohn FH (2000) Reactive oxygen species: response of algal cells. J Plant Physiol 157:183–193

Mishra NP, Mishra RK, Singhal GS (1993) Changes in the activities of anti-oxidant enzymes during exposure of intact wheat leaves to strong visable light at different temperatures in the presence of protein synthesis inhibitors. Plant Physiol 102:903–910

Mittler R (2002) Oxidative stress, antioxidants and stress tolerance. Trends Plant Sci 7:405–410

Nakano N, Asada K (1981) Hydrogen peroxide is scavenged by ascorbate-specific peroxidase in spinach chloroplasts. Plant Cell Physiol 22:867–880

Noctor G, Foyer C (1998) Ascorbate and glutathione: keeping active oxygen under control. Annu Rev Plant Physiol Plant Mol Biol 49:249–279

Rao MV, Paliyath G, Ormrod DP (1996) Ultraviolet-B- and ozone-induced biochemical changes in antioxidant enzymes of *Arabidopsis thaliana*. Plant Physiol 110:125–136

Sharma P, Jha BA, Dubey RS, Pessarakli M (2012) Reactive oxygen species, oxidative damage, and antioxidative defense mechanism in plants under stressful conditions. J Bot 2012:217037

Part IV
Measurements and Analyses of Pigments

Chapter 11
Chlorophylls

Wenting Ke, Yanchao Yin, Xiongwen Chen, and Baosheng Qiu

Abstract Chlorophyll participates in the absorption and transformation of light energy and the primary photochemical reaction. It is the most important photosynthetic pigment. So far, five kinds of chlorophylls have been identified, including chlorophylls *a*, *b*, *c*, *d,* and *f*, which were named according to the discovery order. In the fields of photosynthesis research and ecology, accurate quantification of chlorophyll is a very important task. In this section, the distribution, structure, spectral properties, and quantitative analysis of five kinds of chlorophylls in different algae are summarized. The advantages and disadvantages of chlorophyll quantification by spectrophotometry and high performance liquid chromatography are also discussed.

Keywords Algae · Chlorophyll · Cyanobacteria · HPLC · Quantitative analysis · Spectrophotometry

Chlorophylls are the most important group of photosynthetic pigments. To date, five types of chlorophylls have been found. According to the order of discovery, they were named chlorophyll *a* (Chl *a*), chlorophyll *b* (Chl *b*), chlorophyll *c* (Chl *c*), chlorophyll *d* (Chl *d*), and chlorophyll *f* (Chl *f*) (Chen 2014). Among them, Chl *a*, *b,*

W. Ke
School of Life Sciences, and Hubei Key Laboratory of Genetic Regulation and Integrative Biology, Central China Normal University, Wuhan, Hubei, People's Republic of China

College of Primary Education, Wuhan City Polytechnic, Wuhan, Hubei, People's Republic of China

Y. Yin · B. Qiu (✉)
School of Life Sciences, and Hubei Key Laboratory of Genetic Regulation and Integrative Biology, Central China Normal University, Wuhan, Hubei, People's Republic of China
e-mail: bsqiu@mail.ccnu.edu.cn

X. Chen
College of Life Sciences, and Hubei Key Laboratory of Edible Wild Plants Conservation and Utilization, Hubei Normal University, Huangshi, Hubei, People's Republic of China

K. Gao et al. (eds.), *Research Methods of Environmental Physiology in Aquatic Sciences*, https://doi.org/10.1007/978-981-15-5354-7_11

and *c* are more common and were identified in the nineteenth century (Govindjee and Krogmann 2004). Chl *d* was first reported in 1943 (Manning and Strain 1943), and Chl *f* was a newly discovered chlorophyll molecule in 2010 (Chen et al. 2010). More than 50 years ago, Chl *e* had been reported, but only a very vague description of this pigment was provided. There is no follow-up in-depth study, and so its characteristics are not clear. Since the maximal absorption peak of newly discovered chlorophyll molecules in 2010 is different from that reported for Chl *e*, it is named Chl *f* in order to avoid confusion and maintain the naming continuity (Chen et al. 2010). On the one hand, chlorophylls act as antenna pigments, being involved in the absorption and transformation of light energy. On the other hand, a small number of chlorophyll molecules (Chl *a* and Chl *d*) can also act as reaction center pigments, being involved in charge separation after excitation. The chlorophyll molecule can bind specifically to related polypeptides in a non-covalent manner to form a chlorophyll-protein complex, such as the photosystem II core complex and the photosystem I core complex.

11.1 Distribution, Structure, and Spectral Characteristics of Chlorophylls

Chl *a* or its 8-vinyl derivatives are present in almost all algae and serve as the primary photosynthetic pigments. Chl *b* is present in Chlorophyta (including Charophyceae), Euglenophyta, and *Prochloron*. Chl *c* is a large family, more than 11 compounds have been found so far, and Chl c_2 is the most common one (Zapata et al. 2006). They are distributed in the Dinophyta, Cryptophyta, Haptophyta, Phaeophyta, Raphidophyceae, Bacillariophyceae, Xanthophyceae, and Chrysophyceae (Table 11.1). Chl *b* or its 8-vinyl derivative and Chl *c* are antenna pigments, present only in the light-harvesting complex. Manning and Strain (1943) found Chl *d* in field-collected red algae samples, but it was not clear for a long time whether it was synthesized in red algae or by its epiphytic organisms. In 1996, Miyashita and his colleagues isolated the cyanobacterium *Acaryochloris marina* from *Diplosoma*. This species uses Chl *d* as the main photosynthetic pigment, which constituted 95–99% of total chlorophyll (Miyashita et al. 1996). In 2004, it was found that red algae did not synthesize Chl *d*, and the Chl *d* detected in red algae are derived from the epiphytic cyanobacterium *A. marina* (Murakami et al. 2004). In *A. marina*, Chl *d* not only replaces the function of Chl *a* in the light-harvesting complex (Chen et al. 2002; Tomo et al. 2011), but also replaces the function of Chl *a* in the reaction center (Hu et al. 1998; Chen et al. 2005; Tomo et al. 2007). Up to now, Chl *d* has been found in seven *A. marina* strains (MBIC11017, HICR111A, AWAJI-1, CRS, MPGRS1, CCMEE 5410, and CCNUM4) (Miyashita et al. 1996; Murakami et al. 2004; Miller et al. 2005; Mohr et al. 2010; Larkum et al. 2012; Behrendt et al. 2013; Zhang et al. 2019). Some studies show that Chl *d* is distributed in oceans and lakes with

Table 11.1 Distribution of chlorophylls in different algae groups

Group		Chlorophyll				
		a	*b*	*c*	*d*	*f*
Cyanobacteria	Most cyanobacteria	+				
	Prochlorococcus, *Prochlorothrix*, *Prochloron*	+	+			
	Acaryochloris marina	+			+	
	Halomicronema hongdechloris	+				+
	Leptolyngbya sp. JSC-1	+			+	+
Glaucophyta		+				
Rhodophyta		+				
Chlorophyta		+	+			
Euglenophyta		+	+			
Dinophyta		+		+		
Cryptophyta		+		+		
Heterokontophyta	Chrysophyceae	+		+		
	Synurophyceae	+		+		
	Eustigmatophyceae	+				
	Pinguiophyceae	+		+		
	Dictyophyceae	+		+		
	Pelagophyceae	+		+		
	Bolidophyceae	+		+		
	Bacillariophyceae	+		+		
	Raphidophyceae	+		+		
	Xanthophyceae	+		+		
	Phaeophyceae	+		+		
Haptophyta		+		+		

Note: "+" indicates the presence of such chlorophyll

different temperatures and salinity (Kashiyama et al. 2008; Behrendt et al. 2011). Chl *f* was first discovered in the cyanobacterium *Halomicronema hongdechloris* isolated from stromatolites in of Western Australia (Chen et al. 2012), and a plurality of cyanobacteria containing Chl *f* have been found in several places. Some strains such as *Leptolyngbya* sp. JSC-1, *Synechococcus* sp. PCC 7335, *Chroococcidiopsis thermalis* PCC 7203 also contain a small amount of Chl *d* (Gan et al. 2014, 2015). A recent study reveals widespread occurrence of red-shifted Chl *d* and Chl *f* producing cyanobacteria in humid subtropical forest ecosystems (Zhang et al. 2019).

Chlorophyll molecules are lipophilic pigments containing four pyrrole rings, which are linked to four methylenes to form porphyrin rings with a central magnesium atom attached to four nitrogen atoms on the porphyrin ring. The two carboxyl groups of E ring and D ring are esterified by methyl and phytol groups respectively, and the structural formulae of various chlorophylls are shown in Figs. 11.1 and 11.2. Among them, the structures of Chl *b*, Chl *d,* and Chl *f* are very similar to Chl *a*, and

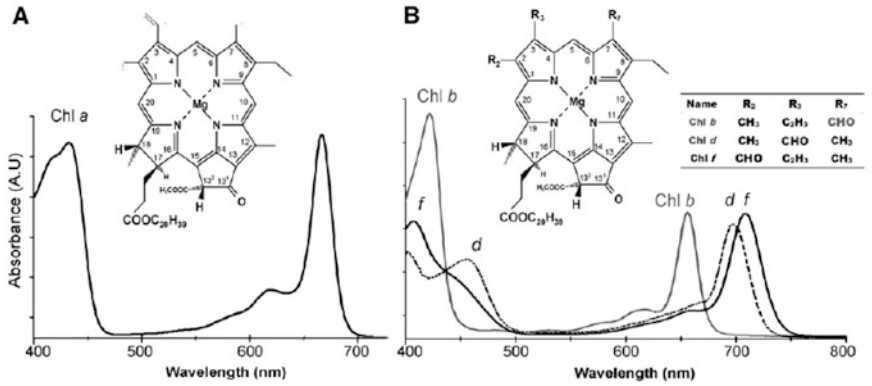

Fig. 11.1 Chemical structure of chlorophyll *a* (a), *b*, *d* and *f* (b) and their absorption spectra in methanol solution (Li et al. 2012)

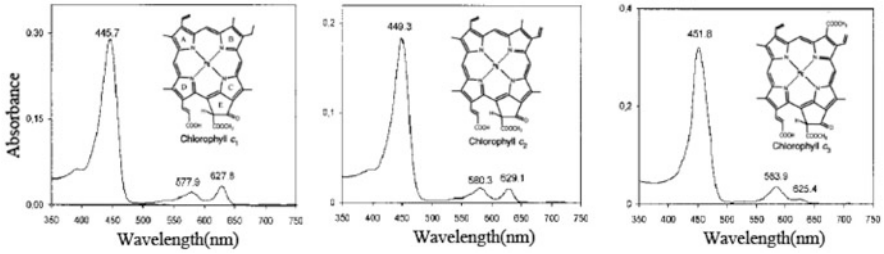

Fig. 11.2 Chemical structures of three common chlorophyll *c* forms and their absorption spectra in acetone solution (Zapata et al. 2006)

only the methyl, vinyl, or methyl side chains connected to C-7, C-3 or C-2 atoms respectively are changed into the aldehyde (Li et al. 2012). However, Chl *c* is a protochlorophyllide compound containing magnesium atoms, and the C-17 and C-18 of D ring are unsaturated double bonds (Zapata et al. 2006; Green 2011). The D-ring C-17 of all polar Chl *c* is linked to trans-acrylic acid, which is not esterified with phytol or other long-chain fatty alcohols, but the C-17 of a few Chl *c* forms (Chl $c_{CS\text{-}170}$ and [DV]-PChlide) is linked to propionic acid, and several C-17 acrylic of Chl *c* are esterified to large side chains (Zapata et al. 2006).

The solar radiation reaching the Earth's surface covers the range from ultraviolet light of 280 nm to infrared light of 2600 nm, while the wavelengths between 400–700 nm comprise the visible part of the spectrum. Chlorophylls *a*, *b*, *c*, *d,* and *f* have different absorption spectra (Figs. 11.1 and 11.2). Chl *a* and *b* have a maximum absorption area in the blue-violet zone of 430–450 nm and red zone of 640–660 nm, respectively. The maximum absorption peak of various Chl *c* forms is

at ~450 nm blue violet, and there are two absorption peaks at ~580 and ~630 nm (Chen and Blankenship 2011). Compared with Chl *a*, the absorption spectra of Chl *d* and *f* are shifted toward longer wavelengths, and the absorption peaks of Chl *d* in 100% methanol solution are at 400, 455.5, and 697 nm, and the absorption peaks of Chl *f* in 100% methanol solution are at 406.5 and 707 nm (Li et al. 2012).

11.2 Quantitative Analysis of Chlorophyll

Accurate quantification of chlorophyll is important for the study of algal photosynthesis. Spectrophotometry and high performance liquid chromatography (HPLC) are commonly used for chlorophyll quantitative analysis, and the former is more widely used.

11.2.1 Spectrophotometry

Due to the different solvents used in chlorophylls extraction, spectrophotometry can be based on various calculations. For example, when 100% methanol was used to extract chlorophylls, the specific operation is carried out as in Fig. 11.3.

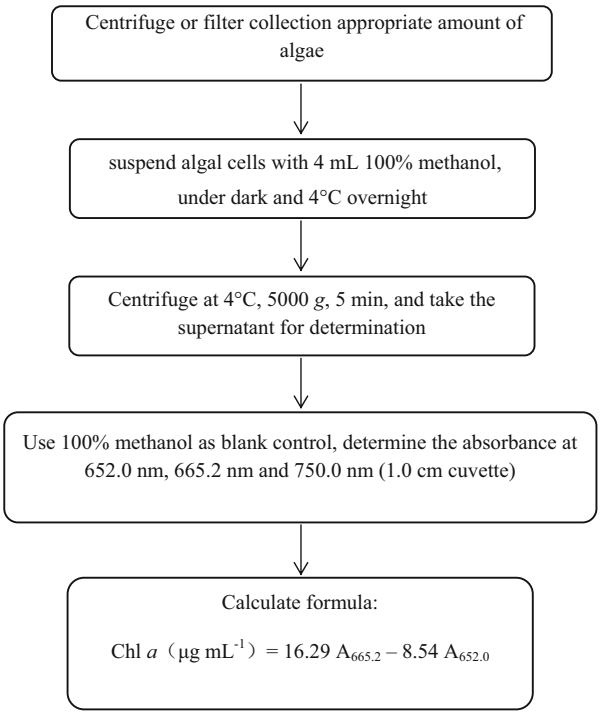

Fig. 11.3 The process of quantification of chlorophylls by the spectrophotometry method (the absorbance value used in the equation is the difference between the absorbance value of the measured band and A_{750})

Table 11.2 Recommended formulae with different solvents used for extraction of chlorophylls

Solvent	Calculation of chlorophyll content ($\mu g\ mL^{-1}$)	Reference
90% acetone	Chl $a = 11.93\ A_{664} - 1.93\ A_{647}$ Chl $b = -5.5\ A_{664} + 20.36\ A_{647}$ Chl $a = 11.43\ A_{664} - 0.40\ A_{630}$ Chl $c_2 = -3.80\ A_{664} + 24.88\ A_{630}$ Chl $a = 11.47\ A_{664} - 0.40\ A_{630}$ Chl $c_1 + c_2 = -3.73\ A_{664} + 24.36 A_{630}$	Humphrey and Jeffrey (1997)
100% methanol	Chl $a = 16.29\ A_{665.2} - 8.54\ A_{652.0}$ Chl $b = 30.66\ A_{652.0} - 13.58\ A_{665.2}$	Porra et al. (1989)
85% methanol + 1.5 mM sodium dithionite	Chl $a = 16.41\ A_{664.0} - 8.09\ A_{650.0}$ Chl $b = 30.82\ A_{650.0} - 12.57\ A_{664.0}$	Porra (1990a)
85% methanol + 2% KOH + 1.5 mM sodium dithionite	Chl $a = 21.87\ A_{640.0} - 8.88\ A_{623.0}$ Chl $b = 60.14\ A_{623.0} - 21.74\ A_{640.0}$	Porra (1990b)
95% ethanol	Chl $a = 13.36\ A_{664.1} - 5.19\ A_{648.6}$ Chl $b = 27.43\ A_{648.6} - 8.12\ A_{664.1}$	Lichtenthaler and Buschmann (2001)
100% ethanol	Chl $a = 13.70\ A_{665} - 5.76\ A_{649}$ Chl $b = -7.60\ A_{665} + 25.8\ A_{649}$	Rowan (1989)
100% ethyl ether	Chl $a = 9.92\ A_{663} - 1.15\ A_{688}$ Chl $d = -0.166\ A_{663} + 9.09\ A_{688}$	Ritchie (2006)

For the spectrophotometric determination of chlorophyll content, the formulae used to calculate the content of Chls *a*, *b*, *c* and *d* are summarized in Table 11.2 according to different extraction solvents. It is better to use the original extraction

solution for chlorophyll determination, and any dilution may enlarge the deviation between the measured value and the true value. The quantification of Chl *f* can be calculated using the extinction coefficient $\varepsilon_{707\ nm} = 71.11 \times 10^3$ L mol^{-1} cm^{-1} in 100% methanol solution (Li et al. 2012).

11.2.2 High Performance Liquid Chromatography (HPLC)

High performance liquid chromatograph can be used to isolate, identify, and quantitatively analyze the chlorophylls and carotenoids of algae. Through continuous improvement, the isolation and identification processes of chlorophylls and carotenoids can be simple and quick. A C_{18} reversed phase column is used as the stationary phase, and chromatographic grade methanol and deionized water are used as the mobile phase. After effective separation of photosynthetic pigments by HPLC, the pigments can be identified by UV-VIS spectrophotometer and other detectors. Chlorophyll and carotenoids in various algae are separated simultaneously, and each pigment is quantified by spectral results and HPLC peak area. According to the high selectivity of HPLC, Chl *a*, Chl *d*, and Chl *f* can be effectively distinguished. When the solvent is 100% methanol, the extinction coefficient of Chl *a* is $\varepsilon_{665.5\ nm} = 70.20 \times 10^3$ L mol^{-1} cm^{-1}, the extinction coefficient of Chl *d* is $\varepsilon_{697\ nm} = 63.68 \times 10^3$ L mol^{-1} cm^{-1} and the extinction coefficient of Chl *f* is $\varepsilon_{707\ nm} = 71.11 \times 10^3$ L mol^{-1} cm^{-1} (Li et al. 2012). Here, we will introduce the pigment analysis from a methanol extract by HPLC as an example (Chen et al. 2012).

Instrument: SHIMADZU LC-20 high performance liquid chromatograph, including Essentia HGE-UV, an ultraviolet and visible detector, and a fraction collector, reverse chromatographic column C_{18} (Inersil ODS-SP, 3.5μm, 4.6 × 150 mm).

Reagent: Chromatographic grade methanol, deionized water.

Mobile phase: Eluent A (methanol) and Eluent B (deionized water), the elution gradient can be adjusted according to the experimental conditions. The specific experimental procedures are as follows (Figs. 11.4 and 11.5).

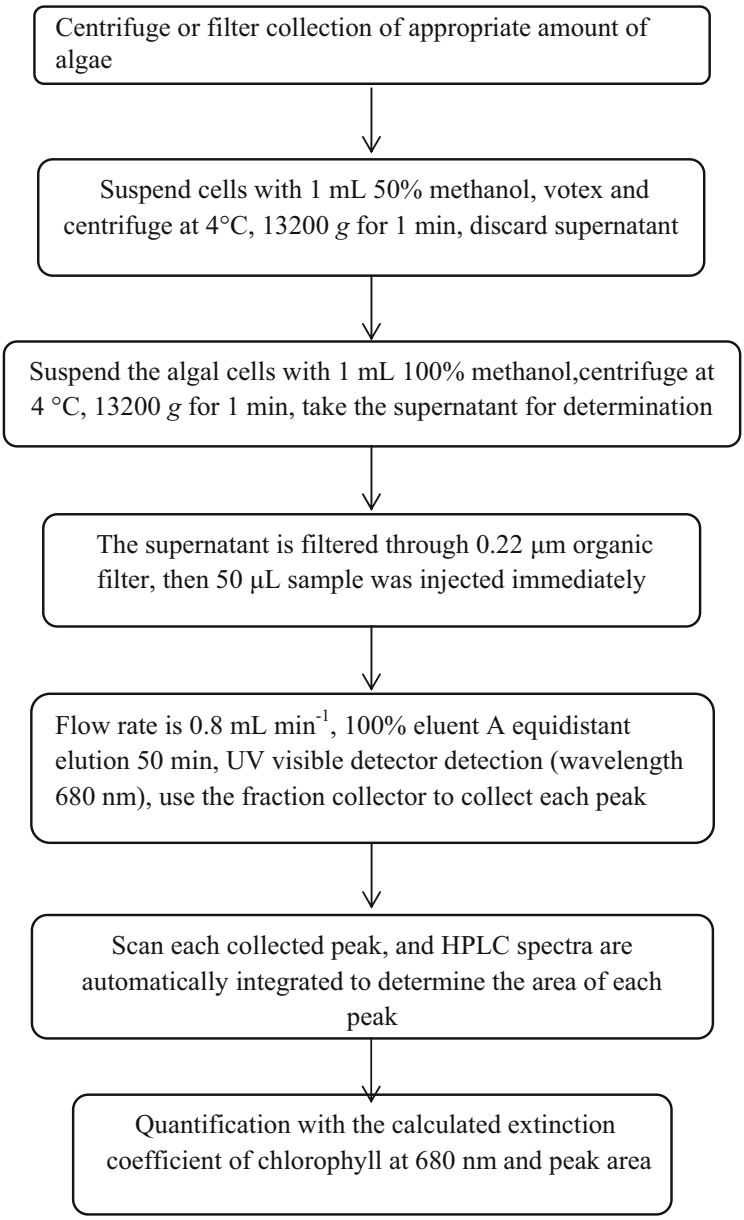

Fig. 11.4 Quantification of chlorophylls by HPLC

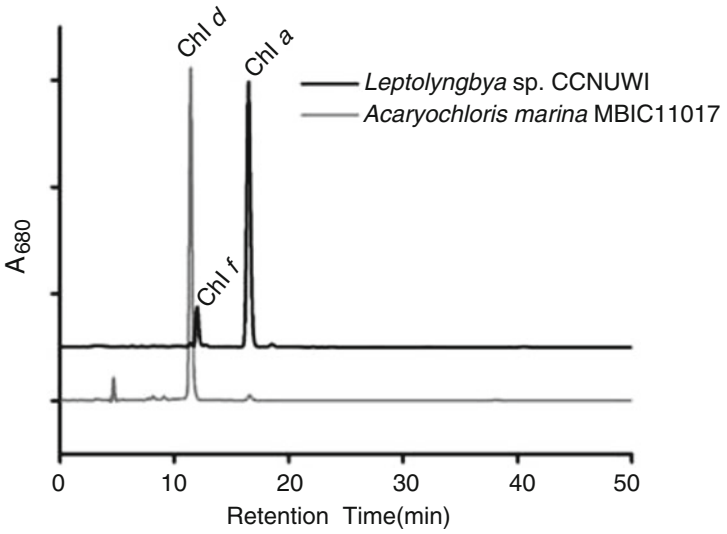

Fig. 11.5 HPLC analysis of pigments extracted from *A. marina* and *Leptolyngbya* sp. CCNUW1

11.3 The Advantages and Disadvantages of These Methods

For spectrophotometry, we can use a variety of solvents to extract chlorophyll. However, each reagent has its advantages and disadvantages.

1. Acetone. The chlorophyll absorption peak in acetone solution is very evident, so acetone is commonly used to extract chlorophyll. However, the extraction efficiency of acetone for chlorophyll is not very good, especially when it is used to extract the chlorophyll from algae (Wright et al. 1997). Acetone is also highly flammable and volatile. High concentrations of acetone have an anesthetic effect. It can bring on headaches and skin irritation. Therefore, acetone is not suitable for teaching experiments. In addition, acetone corrodes plastic products. It is not appropriate to use a plastic cuvette when extracting chlorophyll with acetone (Ritchie 2006). In general though, it is still a good choice to extract chlorophyll using 80% acetone solution (Porra 2006).
2. Methanol. Methanol is a good chlorophyll extractant, especially for algae whose chlorophylls are difficult to extract (for example, *Nannochloris atomus*). An 85% methanol solution containing 2% KOH and 1.5 mM hyposulphite or containing 1.5 mM hyposulphite solely can be used to extract chlorophyll. The corresponding calculation formula is shown in Table 11.2. On the other hand, methanol is often used as a solvent for extracting chlorophyll for HPLC analysis (Ritchie 2006). The volatility and flammability of methanol is lower than that of acetone, but methanol is also toxic. Thus the operator needs to avoid inhalation of methanol. Furthermore, methanol can slowly dissolve polystyrene colorimetric cuvettes, which can cause erroneous readings.

3. Ethanol. The safety performance of ethanol is higher than that of acetone and methanol. It also has some advantages in price. So it is especially suitable for teaching experiments (Ritchie 2006). In addition, ethanol does not corrode plastics so plastic cuvettes can be used when using ethanol as solvent to extract pigments.
4. Ether. Ether can be used as a solvent to prepare pure chlorophyll (Porra et al. 1989; Porra 1991; Scheer 1991). With the exception of freeze-dried experimental materials, ether cannot be directly used as an extractant for chlorophyll. Ether is insoluble in water, so this helps to separate chlorophyll from other aqueous solutions with ether (Li et al. 2012). Conventional laboratory teaching or scientific research do not use ether to extract chlorophyll because ether is very volatile. It is also inflammable, explosive, and anesthetic to humans. In addition, ether also corrodes plastic cuvettes and various plastic containers (Ritchie 2006).

Compared with the spectrophotometric determination of chlorophyll content, HPLC has a higher sensitivity. Moreover, the range of pigments that can be identified using HPLC is broader. However, the requirements for instruments, equipment, and reagents are higher when using HPLC to determine chlorophyll content. Usually, spectrophotometry is used for quantitative analysis of the algal samples with known pigment types. The HPLC method can be used to identify the pigments in natural samples and the pigment composition of different algae. On the other hand, HPLC can be combined with mass spectrometry or nuclear magnetic resonance to provide structural information about chlorophyll molecules. This provides the basis for the discovery of new pigments.

References

Behrendt L, Larkum AWD, Norman A, Qvortrup K, Chen M, Ralph P, Sørensen SJ, Trampe E, Kühl M (2011) Endolithic chlorophyll *d*-containing phototrophs. ISME J 5:1072–1076

Behrendt L, Staal M, Cristescu SM, Harren FJM, Schliep M, Larkum AWD, Kühl M (2013) Reactive oxygen production induced by near-infrared radiation in three strains of the Chl *d*-containing cyanobacterium *Acaryochloris marina*. F1000 Res 2:44

Chen M (2014) Chlorophyll modifications and their spectral extension in oxygenic photosynthesis. Annu Rev Biochem 83:317–340

Chen M, Blankenship RE (2011) Expanding the solar spectrum used by photosynthesis. Trends Plant Sci 16:427–431

Chen M, Quinnell RG, Larkum AWD (2002) The major light-harvesting pigment protein of *Acaryochloris marina*. FEBS Lett 514:149–152

Chen M, Telfer A, Lin S, Pascal A, Larkum AWD, Barber J, Blankenship RE (2005) The nature of the photosystem II reaction centre in the chlorophyll *d*-containing prokaryote, *Acaryochloris marina*. Photochem Photobiol Sci 4:1060–1064

Chen M, Schliep M, Willows RD, Cai ZL, Neilan BA, Scheer H (2010) A red-shifted chlorophyll. Science 329:1318–1319

Chen M, Li YQ, Birch D, Willows RD (2012) A cyanobacterium that contains chlorophyll *f*—a red-absorbing photopigment. FEBS Lett 586:3249–3254

Gan F, Zhang S, Rockwell NC, Martin SS, Lagarias JC, Bryant DA (2014) Extensive remodeling of a cyanobacterial photosynthetic apparatus in far-red light. Science 345:1312–1317

Gan F, Shen GZ, Bryant DA (2015) Occurrence of far-red light photoacclimation (FaRLiP) in diverse cyanobacteria. Life (Basel) 5:4–24

Govindjee, Krogmann D (2004) Discoveries in oxygenic photosynthesis (1727–2003): a perspective. Photosynth Res 80:15–57

Green BR (2011) After the primary endosymbiosis: an update on the chromalveolate hypothesis and the origins of algae with Chl*c*. Photosynth Res 107:103–115

Hu Q, Miyashita H, Iwasaki I, Kurano N, Miyachi S, Iwaki M, Itoh S (1998) A photosystem I reaction center driven by chlorophyll d in oxygenic photosynthesis. Proc Natl Acad Sci U S A 95:13319–13323

Humphrey GF, Jeffrey SW (1997) Test of accuracy of spectrophotometric equations for the simultaneous determination of chlorophylls *a*, *b*, c_1 and c_2. In: Jeffrey SW, Mantoura RFC, Wright SW (eds) Phytoplankton pigments in oceanography: guidelines to modern methods. UNESCO Publishing, Paris, pp 616–621

Kashiyama Y, Miyashita H, Ohkubo S, Ogawa NO, Chikaraishi Y, Takano Y, Suga H, Toyofuku T, Nomaki H, Kitazato H, Nagata T, Ohkouchi N (2008) Evidence of global chlorophyll *d*. Science 321:658–658

Larkum AWD, Chen M, Li YQ, Schliep M (2012) A novel epiphytic chlorophyll *d*-containing cyanobacterium isolated from a mangrove-associated red alga. J Phycol 48:1320–1327

Li YQ, Scales N, Blankenship RE, Willows RD, Chen M (2012) Extinction coefficient for red-shifted chlorophylls: chlorophyll *d* and chlorophyll *f*. Biochim Biophys Acta 1817:1292–1298

Lichtenthaler HK, Buschmann C (2001) Chlorophylls and carotenoids: measurement and characterization by UV-VIS spectroscopy. In: Current protocols in food analytical chemistry. John Wiley & Sons, Inc., New York, pp F4.3.1–F4.3.8

Manning WM, Strain HH (1943) Chlorophyll *d*, a green pigment of red algae. J Biol Chem 151:1–19

Miller SR, Augustine S, Olson TL, Blankenship RE, Selker J, Wood AM (2005) Discovery of a free-living chlorophyll *d*-producing cyanobacterium with a hybrid proteobacterial/cyanobacterial small-subunit rRNA gene. Proc Natl Acad Sci U S A 102:850–855

Miyashita H, Ikemoto H, Kurano N, Adachi K, Chihara M, Miyachi S (1996) Chlorophyll *d* as a major pigment. Nature 383:402–402

Mohr R, Voß B, Schliep M, Kurz T, Maldener I, Adams DG, Larkum ADW, Chen M, Hess WR (2010) A new chlorophyll *d*-containing cyanobacterium: evidence for niche adaptation in the genus *Acaryochloris*. ISME J 4:1456–1469

Murakami A, Miyashita H, Iseki M, Adachi K, Mimuro M (2004) Chlorophyll *d* in an epiphytic cyanobacterium of red algae. Science 303:1633–1633

Porra RJ (1990a) A simple method for extracting chlorophylls from the recalcitrant alga, *Nannochloris atomus*, without formation of spectroscopically-different magnesium-rhodochlorin derivatives. Biochim Biophys Acta 1019:137–141

Porra RJ (1990b) The assay of chlorophylls *a* and *b* converted to their respective magnesium-rhodochlorin derivatives by extraction from recalcitrant algal cells with aqueous alkaline methanol: prevention of allomerization with reductants. Biochim Biophys Acta 1015:493–502

Porra RJ (1991) 1.2 Recent advances and re-assessments in chlorophyll extraction and assay procedures for terrestrial, aquatic and marine organisms, including recalcitrant algae. In: Scheer H (ed) Chlorophylls. CRC Press, Boca Raton, Ann Arbor, Boston, Landon, pp 31–57

Porra RJ (2006) Spectrometric assays for plant, algal and bacterial chlorophylls. In: Grimm B, Porra RJ, Rüdiger W, Scheer H (eds) Chlorophylls and bacteriochlorophylls: biochemistry, biophysics, functions and applications. Springer, The Netherlands, pp 95–107

Porra RJ, Thompson WA, Kriedemann PE (1989) Determination of accurate extinction coefficients and simultaneous equations for assaying chlorophylls *a* and *b* extracted with four different solvents: verification of the concentration of chlorophyll standards by atomic absorption spectroscopy. Biochim Biophys Acta 975:384–394

Ritchie RJ (2006) Consistent sets of spectrophotometric chlorophyll equations for acetone, methanol and ethanol solvents. Photosynth Res 89:27–41

Rowan KS (1989) Photosynthetic pigments of algae. Cambridge University Press, Cambridge

Scheer H (ed) (1991) Chlorophylls. CRC Press, Boca Raton, Ann Arbor, Boston, Landon

Tomo T, Okubo T, Akimoto S, Yokono M, Miyashita H, Tsuchiya T, Noguchi T, Mimuro M (2007) Identification of the special pair of photosystem II in a chlorophyll *d*-dominated cyanobacterium. Proc Natl Acad Sci U S A 104:7283–7288

Tomo T, Allakhverdiev SI, Mimuro M (2011) Constitution and energetics of photosystem I and photosystem II in the chlorophyll *d*-dominated cyanobacterium *Acaryochloris marina*. J Photochem Photobiol B 104:333–340

Wright SW, Jeffrey SW, Montoura FRC (1997) Evaluation of methods and solvents for pigment analysis. In: Jeffrey SW, Montoura RFC, Wright SW (eds) Phytoplankton pigments in oceanography guidelines to modern methods. UNESCO Publishing, Paris, pp 261–282

Zapata M, Garrido JL, Jeffrey SW (2006) Chlorophyll *c* pigments: current status. In: Grimm B, Porra RJ, Rüdiger W, Scheer H (eds) Chlorophylls and bacteriochlorophylls: biochemistry, biophysics, functions and applications. Springer, The Netherlands, pp 39–53

Zhang ZC, Li ZK, Yin YC, Li YQ, Jia Y, Chen M, Qiu BS (2019) Widespread occurrence and unexpected diversity of red-shifted chlorophyll producing cyanobacteria in humid subtropical forest ecosystems. Environ Microbiol 21:1497–1510

Chapter 12
Phycobiliproteins

Yiwen Yang, Juntian Xu, and Baosheng Qiu

Abstract Phycobiliproteins are major light-harvesting antenna proteins for cyanobacteria, red algae, cryptomonads, and some dinoflagellates. They can be covalently associated with one of several phycobilins, and regularly aggregated into macromolecular complexes in the thylakoid membrane. The most commonly used way for extracting phycobiliproteins in the laboratory is the repeated freezing and thawing method. It has been shown that this method combined with ultrasonic extraction can give a suitable extraction of phycobiliprotein. In this section, the steps of purification of phycobiliprotein by ion exchange chromatography are also introduced, and the methods of extraction, separation, and purification are compared.

Keywords Allophycocyanin · Phycobiliprotein · Phycoerythrin · Phycocyanin · Purification · Extraction

Phycobiliproteins (PBPs) are water-soluble pigment-proteins which distributed in cyanobacteria, red algae, cryptomonads, and some dinoflagellates. The PBPs are covalently associated with several linear tetrapyrrole chromophore molecules called phycobilins (PBs) by a thioether linkage. Phycobilins can harvest and transfer light energy in the photosystem. To date, four phycobilins have been identified (Fig. 12.1), i.e., phycocyanobilin (PCB), phycoerythrobilin (PEB), phycourobilin (PUB), and phycobiliviolin (PVB) (Zhou and Zeng 1990; Colyer et al. 2005; Blot et al. 2009). Phycobilins are isomers to each other and the major difference among various PBs is the arrangement of conjugated double bonds.

Y. Yang · B. Qiu (✉)
School of Life Sciences, and Hubei Key Laboratory of Genetic Regulation and Integrative Biology, Central China Normal University, Wuhan, Hubei, People's Republic of China
e-mail: bsqiu@mail.ccnu.edu.cn

J. Xu
Jiangsu Key Laboratory of Marine Bioresources and Environment, Jiangsu Ocean University, Lianyungang, Jiangsu, People's Republic of China

K. Gao et al. (eds.), *Research Methods of Environmental Physiology in Aquatic Sciences*, https://doi.org/10.1007/978-981-15-5354-7_12

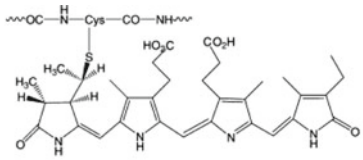

Peptide-linked phycocyanobilin

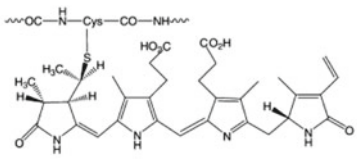

Peptide-linked phycoerythrobilin

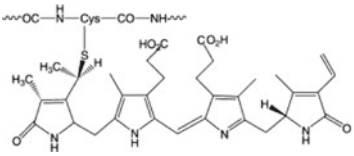

Peptide-linked phycourobilin

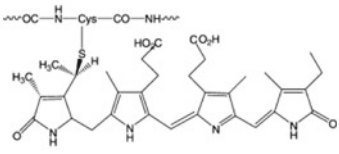

Peptide-linked phycobiliviolin

Fig. 12.1 Phycobilins linked with peptides

According to the maximal absorption, phycobiliproteins are divided into phycoerythrin (PE), phycoerythrocyanin (PEC), phycocyanin (PC), and allophycocyanin (APC) (Colyer et al. 2005). The PEC is distributed in algae with heterocysts but lacking phycoerythrin (Wang et al. 2008). Both the type and content of bilin are variable in different phycobiliproteins. The phycocyanobilin is found in PC, APC and PEC, phycoerythrobilin and phycourobilin are found in PE, while the phycobiliviolin is found only in PEC (Liang 1986; Glazer 1988). The purity of phycobiliproteins is usually indicated by the value of A_{max}/A_{280}. The PEs are pink and have maximal absorption at 540–570 nm; PECs are purple and have maximal absorption at 570–590 nm; PCs are blue and have maximal absorption at 610–620 nm; APCs are blue-green and have maximal absorption at 650–655 nm (Glazer 1988; Colyer et al. 2005). Absorption and fluorescence spectra of common phycobiliproteins are shown in Fig. 12.2. According to the type and content of phycobilin, each type of phycobiliproteins can be further divided as R-, C-, and B-subtypes, such as C-phycocyanin, R-phycocyanin, B-phycoerythrin, and R-phycoerythrin (Viskari and Colyer 2002; Colyer et al. 2005).

Phycobilisomes are complexes of phycobiliproteins which are regularly aggregated and arranged on the thylakoid membrane, and interact with one to several photosystem reaction centers as the light-harvesting complex. Phycobilisomes are usually divided into four types (hemidiscoidal, hemiellipsoidal, bundles, and lumps) according to their different shapes. The most studied phycobilisome is hemidiscoidal phycobilisome, which consists of an APC-core and several PC (with PE or PEC) rods (Fig. 12.3). Energy harvested by the phycobilisomes is transferred from PE (or PEC) → PC → APC and finally to the chlorophyll *a* of photosynthetic reaction center with a nearly 100% efficiency (Zhang et al. 1999a).

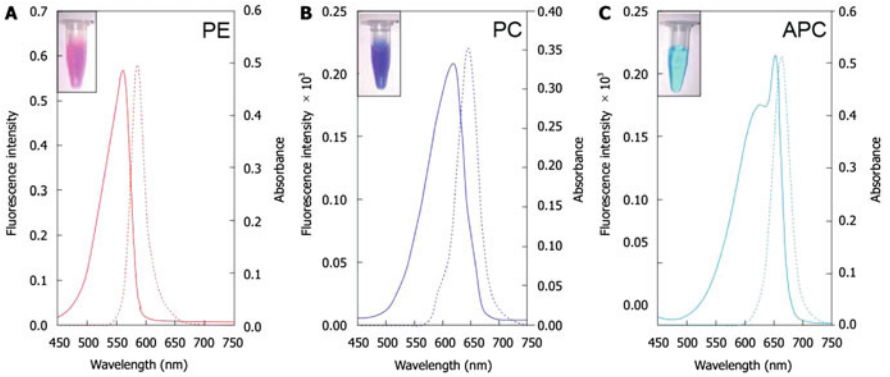

Fig. 12.2 Absorbance (solid line) and fluorescence emission (dotted line) spectra, and appearance (inset) of phycoerythrin (**a**), phycocyanin (**b**), and allophycocyanin (**c**) (Sonani et al. 2016)

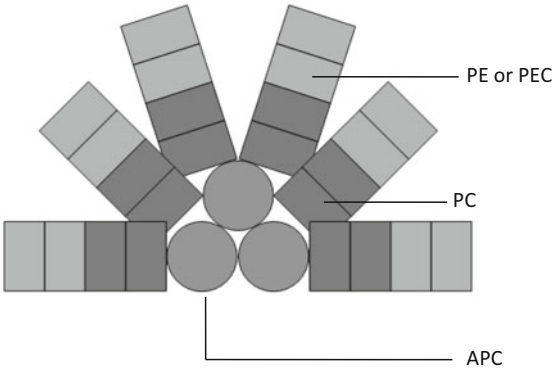

Fig. 12.3 Model structure of a phycobilisome

12.1 Quantitative Analysis of Phycobiliprotein

Phycobiliproteins are water-soluble photosynthetic pigment-protein complexes. The first step for extracting these proteins is to break the algal cells, to allow phycobiliproteins to be released in the dissolved state. The most common methods for breaking the cells are repeated freezing-thawing (Abalde et al. 1998; Qiu et al. 2004), chemical reagent treatment (Zhang et al. 1999b), ultrasonic methods (Patel et al. 2005), high-pressure homogenation (Patil and Raghavarao 2007) and grinding (Beer and Eshel 1985). The repeated freezing-thawing method and mechanical grinding method are most commonly used in the laboratory for breaking the microalgae and macroalgae, respectively. The principle of the repeated freezing-thawing method is that the majority of water within and out of the cell forms ice crystals and produces expansion pressure, which leads to mechanical damage to the

cells. At the same time, the precipitation of ice crystals causes the concentration of cytoplasm and the increasing electrolyte and osmotic pressure. Finally the cell will swell up and be broken when the ice crystals melt. The grinding method uses the mechanical strength of a rod and quartz sand to break algal cells, and then the water-soluble phycobiliprotein is dissolved in the buffer.

The repeated freezing-thawing method is used for isolating and quantifying phycobiliproteins (Soni et al. 2006). *Oscillatoria quadripuntulata* cells were cultured for 34 days and collected by centrifugation (3000 × *g*, 5 min). Cells were washed one time with 1 M Tris-Cl buffer (pH = 8.1) and suspended with 5 volumes of the same buffer. Repeated freezing-thawing was performed at −25 °C and 4 °C several times. The supernatant was obtained by centrifugation (4 °C, 17,000 × *g*, 20 min), and the absorption was measured at 562, 615, and 652 nm by spectrophotometer. Phycobiliprotein content (mg ml^{-1}) was calculated according to the following formula (Bennett and Bogorad 1973): $PE = [A_{562} - (2.41 \times PC) - (0.849 \times APC)]/9.62$, $PC = (A_{615} - 0.474 \times A_{652})/5.34$, $APC = (A_{652} - 0.208 \times A_{615})/5.09$.

The steps of the grinding method for phycobiliprotein extraction and quantification in large red algae are as follows: collect 0.05–0.50 g of algae, add a small amount of quartz sand and phosphate buffer (pH = 6.8) to grind algae in a mortar, add about 10 ml of phosphate buffer and homogenize. Then centrifuge at 5000 × *g* for 15 min, collect the supernatant and re-grind the sediment, repeat the above steps, combine the supernatant and finally dilute to 25 ml, and then determine the absorbance at 455, 564, 592, 618, and 645 nm using a spectrophotometer. The content of phycobiliproteins was calculated according to the following formula (Beer and Eshel 1985): $PE = [(A_{564} - A_{592}) - (A_{455} - A_{592}) \times 0.2] \times 0.12$, $PC = [(A_{564} - A_{592}) \times 0.51] \times 0.15$.

Previous studies have shown that compared to phosphate buffer, a 3-[(3-cholesterol aminopropyl)dimethylamino]-1-propanesulfonic acid (CHAPS) buffer supplemented with crude lipids (adding crude lipids into 3% (w/v) CHAPS buffer to a final concentration of 0.3% (w/v)) has a better effect on phycobiliproteins isolation (Zimba 2012).

12.2 Isolation and Purification of Phycobiliprotein

It has been shown that the phycobiliproteins have anti-cancer activity, can promote blood cell regeneration and can also be used as fluorescent reagents in molecular biological studies (Patel et al. 2005). Most of the harvested phycobiliproteins are isolated and purified from *Spirulina* (Minkova et al. 2003; Patil et al. 2006). According to the value of A_{620}/A_{280}, the purity of phycocyanin can be divided into food grade (purity 0.7), drug grade (purity 3.9), and reagent grade (purity >4.0) (Rito-Palomares et al. 2001).

Commonly used methods for phycocyanin purification are ammonia sulfate precipitation (Patel et al. 2005), column chromatography (Ramos et al. 2011), rivanol precipitation (Minkova et al. 2003), and aqueous two phase method (Patil

et al. 2006). Column chromatography is widely used, and can be divided into adsorption chromatography, gel chromatography, and ion exchange chromatography according to the purification principle.

For the ion exchange chromatography method, the ion exchange agent is used as a stationary phase. When the component ions in the mobile phase are reversibly exchanged with the counter ion on the exchanger, proteins are separated according to their different binding force. This method is often used in combination with dialysis, which is a classical method for the purification of proteins. The specific process is as follows (Soni et al. 2006; Sonani et al. 2014):

1. Wash the cell mass one time with 20 mM potassium phosphate buffer (pH = 7.2) and resuspend in the same buffer. Cells are broken by several rounds of freezing (−25 °C)–thawing (4 °C) treatment. Supernatant of the crude extract is collected after the cell debris is removed by centrifugation (17,000 × *g*, 4 °C, 20 min).
2. Add fine ammonium sulfate powder slowly into the crude extract to ammonium sulfate saturation of 20%, and stir continuously for 1 h at 4 °C. After centrifugation (4 °C, 17,000 × *g*, 20 min), collect the supernatant and continually add ammonium sulfate to a saturation of 40%.
3. Centrifuge at 4 °C, 17,000 × *g* for 20 min. Supernatant and red precipitate are collected respectively. The red precipitate is the crude extract of PE. Add Triton X-100 into the supernatant to a final concentration of 0.1% (w/v), stir for 15 min and allow to stand overnight at room temperature.
4. Centrifuge at 17,000 × *g* for 20 min at room temperature, and the resulting blue precipitate is the crude extract of PC. Ammonium sulfate powder is added to the supernatant to a saturation of 70%. Centrifuge at 17,000 × *g* for 20 min at room temperature, and the cyan precipitate is the crude extract of APC.
5. The phycobiliprotein pellets obtained in steps (3) and (4) are dissolved in 20 mM potassium phosphate buffer (pH = 7.2) and resolved through a Sephadex G-150 gel column in 20 mM potassium phosphate buffer (pH = 7.2) at a flow rate of 0.75 ml/min. Collect the PE (red), PC (blue), and APC (blue-green) components.
6. The phycobiliproteins purified by size exclusion chromatography can be further purified using a DEAE-cellulose column. The column is equilibrated with 20 mM potassium phosphate buffer (pH = 7.2) before the sample is injected. The column is washed with 10 column volumes of potassium phosphate buffer and finally eluted with a gradient of potassium phosphate buffer containing 0–0.5 M NaCl, and the phycobiliproteins are eluted at different concentrations of NaCl.

12.3 Advantages and Disadvantages of Extraction Methods

The repeated freezing and thawing method is simple and easy to operate, and does not require special equipment, but takes a long time and is only suitable for processing small amounts of materials in the laboratory (Table 12.1). However,

Table 12.1 Advantages and disadvantages of extraction methods

Methods		Advantages	Disadvantages
Cell breakage	Freezing-thawing	Mild conditions; simple and convenient; conducive to protein dissolution, easy to scale up to larger samples	Need refrigeration equipment, energy consumption, only suitable for small laboratory experiments
	Ultrasonic extraction	Large-scale extraction; auxiliary method to improve the protein dissolution rate	Heat production, can cause phycobiliprotein degeneration
	Osmotic crushing	Simple operation; the scale of production can be linearly expanded	Time-consuming; not suitable for large algae
	Liquid nitrogen grinding	Low-temperature operating environment to maintain the activity of natural phycobiliprotein, the cost is low, and less time-consuming	Loses more material during the operation, is not conducive to quantitative analysis
	Chemical reagent treatment	High extraction efficiency, suitable for large-scale preparation of samples	The introduction of chemical reagents, late purification is difficult
Purification	Dialysis	Simple and convenient, samples are concentrated during the purification, is conducive to follow-up treatment	The larger amount of drugs used, produces a lot of waste water
	Chromatography	High purification speed, large scale, and can quickly achieve purification for a large number of products	Cost is relatively high; need a variety of chromatography methods
	Aqueous two-phase extraction	Simple operation, high yield, can achieve the advantages of large scale, separation, and concentration at the same time	High cost and time-consuming
	Rivanol precipitation	High efficiency, high yield, low cost, and easy to expand.	Follow-up need to use column separation, limiting large-scale production

previous studies have shown that the repeated freezing and thawing method is better than sonication (Abalde et al. 1998). Advantages of sonication are its speed, less loss, and high protein-content, while its main drawback is that ultrasound intensity and uniformity need to be well controlled. Otherwise, it is easy to cause protein denaturation, and the cell debris and other protein components will increase the difficulties of late processing. At the same time, this method produces a lot of heat and needs an ice bath, which limits the amount of material. If laboratory conditions permit, there is a good way to perform the extraction by combining the repeated freezing-thawing method with sonication (Lawrenz et al. 2011; Zimba 2012). Grinding can also break algal cells, but more material is lost during sample processing and it is not as conducive to quantitative analysis as the repeated freezing and thawing method (Sarada et al. 1999). A chemical reagent treatment can be used for preparing large

amount of phycobiliproteins, but the main drawback is that the addition of chemical reagents increases the difficulty of post-purification treatment, and chemical reagents also easily cause protein denaturation.

The advantage of dialysis is that the target protein is concentrated during the process of purification. This is beneficial for subsequent treatment. But this method uses large amount of drugs and will produce a lot of waste water. The ion exchange chromatography method has the advantages of high adsorption capacity, easy elution, and good stability, but it is difficult to obtain high purity phycocyanin by a single chromatography method. It is usually necessary to use multi-step chromatography, and the chromatography operation is more cumbersome and time-consuming. The rivanol precipitation method is more efficient, but the subsequent operations need to use column separation, which limits large-scale production. Compared with the traditional column separation, aqueous two-phase extraction has the advantages of simple operation, rapidity, and easy scalability. All of the above methods have their advantages and disadvantages, and several are often used in combination to achieve the best results in actual operation.

References

Abalde J, Betancourt L, Torres E, Cid A, Barwell C (1998) Purification and characterization of phycocyanin from the marine cyanobacterium *Synechococcus* sp. IO9201. Plant Sci 136:109–120

Beer S, Eshel A (1985) Determining phycoerythrin and phycocyanin concentrations in aqueous crude extracts of red algae. Aust J Mar Freshw Res 36:785–792

Bennett A, Bogorad L (1973) Complementary chromatic adaptation in a filamentous blue-green alga. J Cell Biol 58:419–435

Blot N, Wu XJ, Thomas JC, Zhang J, Garczarek L, Böhm S, Tu JM, Zhou M, Plöscher M, Eichacker L, Partensky F, Scheer H, Zhao KH (2009) Phycourobilin in trichromatic phycocyanin from oceanic cyanobacteria is formed post-translationally by a phycoerythrobilin lyase-isomerase. J Biol Chem 284:9290–9298

Colyer CL, Kinkade CS, Viskari PJ, Landers JP (2005) Analysis of cyanobacterial pigments and proteins by electrophoretic and chromatographic methods. Anal Bioanal Chem 382:559–569

Glazer AN (1988) Phycobiliproteins. Methods Enzymol 167:291–303

Lawrenz E, Fedewa EJ, Richardson TL (2011) Extraction protocols for the quantification of phycobilins in aqueous phytoplankton extracts. J Appl Phycol 23:865–871

Liang L (1986) Study on crystal structure of phycobiliprotein. Prog Biochem Biophys 3:32–35. (in Chinese)

Minkova KM, Tchemov AA, Tchorbadjieva MI, Fournadjieva ST, Antova RE, Busheva MC (2003) Purification of C-phycocyanin from *Spirulina (Arthrospira) Fusiformis*. J Biotechnol 102:55–59

Patel A, Mishra S, Pawar R, Ghosh PK (2005) Purification and characterization of C-Phycocyanin from cyanobacterial species of marine and freshwater habitat. Protein Expr Purif 40:248–255

Patil G, Raghavarao KSMS (2007) Aqueous two phase extraction for purification of C-phycocyanin. Biochem Eng J 34:156–164

Patil G, Chethana S, Sridevi AS, Raghavarao KSMS (2006) Method to obtain C-phycocyanin of high purity. J Chromatogr A 1127:76–81

Qiu B, Zhang A, Zhou W, Wei J, Dong H, Liu Z (2004) Effects of potassium on the photosynthetic recovery of the terrestrial cyanobacterium, *Nostoc flagelliforme* (cyanophyceae) during rehydration. J Phycol 40:323–332

Ramos A, Acién FG, Fernández-Sevilla JM, González CV, Bermejo R (2011) Development of a process for large-scale purification of C-phycocyanin from *Synechocystis aquatilis* using expanded bed adsorption chromatography. J Chromatogr B 879:511–519

Rito-Palomares M, Nuñez L, Amador D (2001) Practical application of aqueous two-phase systems for the development of a prototype process for c-phycocyanin recovery from *Spirulina maxima*. J Chem Technol Biotechnol 76:1273–1280

Sarada R, Pillai MG, Ravishankar GA (1999) Phycocyanin from *Spirulina* sp.: influence of processing of biomass on phycocyanin yield, analysis of efficacy of extraction methods and stability studies on phycocyanin. Process Biochem 34:795–801

Sonani RR, Singh NK, Thakar D, Madamwar D (2014) Concurrent purification and antioxidant activity of phycobiliproteins from *Lyngbya* sp. A09DM: an antioxidant and anti-aging potential of phycoerythrin in *Caenorhabditis elegans*. Process Biochem 49:1757–1766

Sonani RR, Rastogi RP, Patel R, Madamwar D (2016) Recent advances in production, purification and applications of phycobiliproteins. World J Biol Chem 7:100–109

Soni B, Kalavadia B, Trivedi U, Madamwar D (2006) Extraction, purification and characterization of phycocyanin from *Oscillatoria quadripunctulata*-isolated from the rocky shores of Bet-Dwarka, Gujarat, India. Process Biochem 41:2017–2023

Viskari PJ, Colyer CL (2002) Separation and quantitation of phycobiliproteins using phytic acid in capillary electrophoresis with laser-induced fluorescence detection. J Chromatogr A 972:269–276

Wang F, Zhou M, Zhao JM, Zhao KH (2008) Chromatography analysis of peptides from the β-subunit of phycoerythrocyanin *in vivo* reconstitution. Acta Hydrobiol Sin 32:74–77. (in Chinese)

Zhang YZ, Chen XL, Zhou BC, Zeng CK, Liu J, Shi DX, Pang SJ (1999a) A new model of phycobilis in *Spirulina platensis*. Sci China (Series C) 29:145–150. (in Chinese)

Zhang YF, Liu XC, Li QH (1999b) Study on characteristic and purification of *Spirulina* phycocyanin. J Yunnan Univ (Natural Science Edition) 21:230–232. (in Chinese)

Zhou BC, Zeng CK (1990) A study on the translation of algae photosynthetic pigment. Plant Physiol Commun 3:57–60. (in Chinese)

Zimba PV (2012) An improved phycobilin extraction method. Harmful Algae 17:35–39

Chapter 13
Carotenoids

Fan Hu and Hanhua Hu

Abstract This chapter describes carotenoid distribution in algal class and methods of carotenoid analysis by high performance liquid chromatography (HPLC) and spectrophotometer.

Keywords Pigments · Carotenoids · HPLC · Absorption spectrum · Algae

Carotenoids are widely distributed in all living organisms including higher plants, algae, bacteria, and yeast. They are insoluble in water, but are fat-soluble and contain conjugated double bond systems. Carotenoids are classified into two major groups, the carotenes and the xanthophylls. Carotenes are hydrocarbons without oxygen and are few in number, such as α-, β-, γ-, δ-, ε-, ζ-carotene, and lycopene. Xanthophylls contain at least one atom of oxygen in the molecule and make up the vast majority of the carotenoids. Presently, over 700 carotenoids have been identified. Carotenoids act as accessory light-harvesting pigments, effectively extending the range of light absorbed by the photosynthetic apparatus, and perform an essential photoprotective role by quenching triplet state chlorophyll molecules and scavenging singlet oxygen and other toxic oxygen species formed within the chloroplast. Fucoxanthin, peridinin, and siphonaxanthin are class-specific carotenoids in light-harvesting complexes and work as efficient antenna pigments harvesting blue-to-green light (Rowan 1989).

F. Hu
School of Foreign Languages, China University of Geosciences, Wuhan, China

H. Hu (✉)
Institute of Hydrobiology, Chinese Academy of Sciences, Wuhan, China
e-mail: hanhuahu@ihb.ac.cn

K. Gao et al. (eds.), *Research Methods of Environmental Physiology in Aquatic Sciences*, https://doi.org/10.1007/978-981-15-5354-7_13

13.1 Distribution of Carotenoids in the Algal Class

Over 40 kinds of xanthophylls and five carotenes have been found in the various algal species, as summarized in Table 13.1. Different algal phyla have distinct carotenoid profiles. Some carotenoids are found only in some algal divisions or classes; therefore, these carotenoids can be used as chemotaxonomic markers (Goodwin 1974; Rowan 1989; van den Hoek et al. 1995; Takaichi 2011; Huang et al. 2017).

13.2 Carotenoid Analysis by HPLC

There are many methods for the analysis of photosynthetic pigments, including classical paper chromatography and thin layer chromatography (TLC). The simple TLC method has been used for the rapid separation of pigments of algae. The separation is carried out on plates coated with adsorbents, such as silica gel, cellulose, Al_2O_3, or polyamide. Colored spots separated by TLC are scraped off the plates and extracted in a small funnel fitted with a sintered glass filter. The light absorption spectrum of the compound may thus be determined. As for more quantitative and accurate methods, high performance liquid chromatography (HPLC) has been applied to the analysis of algal pigments in recent decades (Wright et al. 1991; Wang et al. 1999; Hu 2003). HPLC has made it possible to simultaneously determine the concentration of a wide range of carotenoids and chlorophylls and their degradation products. Although numerous HPLC techniques have been published to date, pigment separations are typically conducted with a reverse-phase C18 column and a mobile phase of methanol, acetone, ammonium acetate, and ethyl acetate (Schmid and Stich 1995). HPLC-separated pigment peaks are routinely identified by comparison of retention time values with those of standards and on-line diode array UV/Vis spectroscopy at 440 nm.

In reversed-phase chromatography, substances eluting at the solvent front are considered to be polar, such as chlorophyllide *b*, chlorophyllide *a*, and chlorophyll *c* (peak 1 in Fig. 13.1). Peridinin is the most polar carotenoid (peak 2 of *Peridinium pusillum* in Fig. 13.1), then siphonaxanthin, fucoxanthin, violaxanthin (peak 3), diadinoxanthin (peak 4 of *P. pusillum*), diatoxanthin (peak 8) and lutein are eluted in order of decreasing polarity. At the non-polar end of the chromatogram, there are chlorophyll *b*, chlorophyll *a* (peak 9), pheophytin *b*, pheophytin *a*, and carotenes (Wright et al. 1991). The retention time values of peaks 4 in *P. pusillum* and *Nannochloropsis* sp. are the same (Fig. 13.1), but the latter carotenoids is violaxanthin-like based on its absorption spectrum. Therefore, to identify a pigment, both retention time and absorption spectrum should be considered. Pigment quantification is based on the linear relationship between the weight of standard injected and the resulting peak area.

Table 13.1 The distribution of carotenoids in the algal classes and absorption maxima of these carotenoids

	Cyanophyceae	Cryptophyte	Dinoflagellate	Prymnesiophyte	Chlorophyte	Euglenophyte	Prasinophyte	Rhodophyte	Bacillariophyte	Chrysophyte	Eustigmatophyceae	Phaeophyte	Raphidophyte	Xanthophyte	Absorption maxima in acetone (nm)[a]
α-Carotene		+						+							422, 445, 474
β-Carotene	+			+	+	+		+	+	+	+	+			452, 476
Peridinin			+												474
Siphonaxanthin								+							450
Diadinoxanthin			+	+					+					+	446, 476
Diatoxanthin				+					+						452, 480
Echinenone	+														466, 666
Heteroxanthin														+	445, 474
Dinoxanthin			+												418, 442, 470
Myxoxanthophyll	+														451, 476, 509
Vaucheriaxanthin											+			+	445, 473
Neoxanthin					+	+									418, 440, 468
Fucoxanthin				+					+	+		+	+		447, 469
Lutein					+		+	+							445, 473
Alloxanthin		+													453, 483
Zeaxanthin	+				+	+	+								442, 470
Violaxanthin					+						+	+	+		418, 440, 470

[a]From Rowan (1989) and Hu (2003)

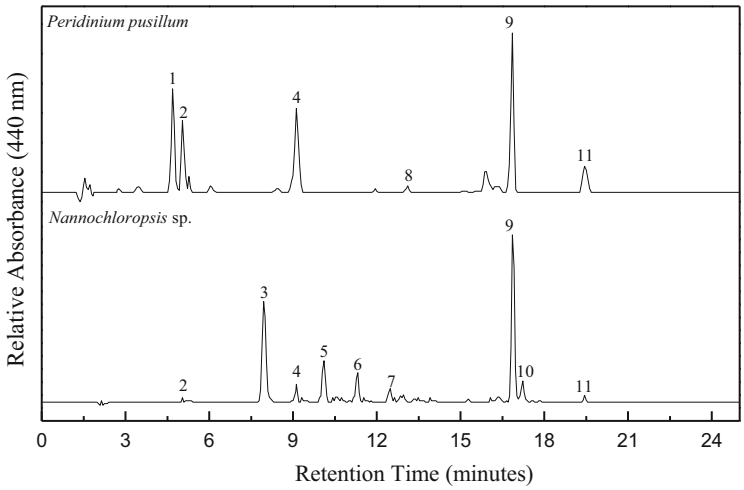

Fig. 13.1 The HPLC chromatogram (440 nm) of pigments in *Peridinium pusillum* and *Nannochloropsis* sp.

13.3 Quantification of Total Carotenoids

Since carotenoids are sensitive to oxygen, heat, light, and acids, all operations should be performed in dim light or in total darkness and at low temperature.

1. Extraction: Centrifuge the fresh culture, add acetone or methanol, ultrasonicate (for macroalgae, grind samples gently) and transfer the extract to a new tube, repeat extraction until no more colored material can be extracted.
2. Purification: Extracts might contain chlorophylls and can be removed by saponification. Saponification is performed in a small volume of ether and an equal volume of 10% methanolic KOH solution is added. The saponification takes place at room temperature for 1–2 h in the dark, then water is added (containing 5% NaCl) to a separatory funnel, and the ether layer is separated from the aqueous phase. The latter is extracted several times with more ether and the combined extracts washed three times with water to remove alkali and methanol. The content of carotenoids is estimated from the maximum absorbancy measured in the 450 nm region as follows (Jensen 1978):

$$C = (D \times V \times f \times 10)/2500$$

The total amount of carotenoids is then C (in milligrams), the absorbancy D in a 1.0 cm cell, the volume (milliliters) of the original extract is V, and the dilution factor is f. It is assumed that the pigments have an average extinction coefficient of 2500.

13.4 Note

HPLC can be used as a qualitative and quantitative analysis, while spectrophotometry can only be used for measuring the total carotenoid content. Relatively speaking, the former method is more accurate.

References

Goodwin TW (1974) Carotenoids and biliproteins. In: Stewart WDP (ed) Algal physiology and biochemistry. University of California Press, Berkeley, pp 176–192

van den Hoek C, Mann DG, Jahns HM (1995) Algae: an introduction to phycology. Cambridge University Press, New York

Hu H-H (2003) Method for determining phytoplankton pigments by high-performance liquid chromatography and diode array detector. Plant Physiol Commun 39(6):658–660. (in Chinese)

Huang JJ, Lin S, Xu W, Cheung PCK (2017) Occurrence and biosynthesis of carotenoids in phytoplankton. Biotechnol Adv 35:597–618

Jensen A (1978) Chlorophylls and carotenoids. In: Hellebust JA, Craigie JS (eds) Handbook of phycological methods: physiological and biochemical methods. Cambridge University Press, New York, pp 59–70

Rowan KS (1989) Photosynthetic pigments of algae. Cambridge University Press, New York

Schmid H, Stich HB (1995) HPLC-analysis of algal pigments: comparison of columns, column properties and eluents. J Appl Phycol 7(5):487–494

Takaichi S (2011) Carotenoids in algae: distributions, biosyntheses and functions. Mar Drugs 9:1101–1118

Wang H, Hong H, Xu L (1999) Separation and determination of chlorophylls and carotenoids from marine phytoplankton by RP-HPLC. Mar Sci 4:6–9. (in Chinese)

Wright SW, Jeffrey SW, Mantoura RFC et al (1991) Improved HPLC method for the analysis of chlorophylls and carotenoids from marine phytoplankton. Mar Ecol Prog Ser 77(2–3):183–196

Chapter 14
Phenolic Compounds and Other UV-Absorbing Compounds

Peng Jin and Kunshan Gao

Abstract Biochemical compounds such as phenolics and UV-absorbing compounds are an important group of natural products involved in responses to different kinds of biotic and abiotic stress in high plants, macroalgae, and microalgae. Here, we review the advances of the responses of these compounds in aquatic primary producers to environmental changes, and discuss various methods that are applied to determine them. Advantages and disadvantages of different methods are also discussed.

Keywords Phenolics · UV-absorbing compounds · MAAs · HPLC · Spectrophotometer

14.1 Introduction

Phenolic compounds are an important group of natural products involved in responses to different kinds of biotic and abiotic stresses in high plants, macroalgae, and microalgae (Treutter 2006). Rico et al. (2013) showed that total phenolic contents increased under increasing levels of copper and iron, which may reflect the involvement of these compounds in protection against metal toxicity. It has been also demonstrated that ocean acidification increases the production of phenolic compounds in phytoplankton under the elevated CO_2 concentrations projected for the end of this century, compared with the ambient CO_2 level (Jin et al. 2015). The resulting products of phenolic compounds' biodegradation are further metabolized via β-oxidation and Krebs cycle, which were enhanced under ocean acidification

P. Jin (✉)
School of Environmental Science and Engineering, Guangzhou University, Guangzhou, China
e-mail: pengjin@gzhu.edu.cn

K. Gao
State Key Laboratory of Marine Environmental Science and College of Ocean and Earth Sciences, Xiamen University, Xiamen, China

K. Gao et al. (eds.), *Research Methods of Environmental Physiology in Aquatic Sciences*, https://doi.org/10.1007/978-981-15-5354-7_14

condition and could thus meet any extra energetic demand to allow phytoplankton to tolerate acidic stress (Jin et al. 2015).

UV-absorbing compounds have long been suggested to protect cells from UV damage (Vernet et al. 1989; Helbling et al. 1996; Häder et al. 2015). Among all the UV-absorbing compounds, mycosporine-like amino acids (MAAs) and scytonemins are well-known UV-absorbing/UV-screening compounds for their pivotal role in photoprotection of phytoplankton cells (Rastogi and Incharoensakdi 2013). MAAs are small (<400 Da), colorless, water-soluble compounds composed of cyclohexanone or cyclohexenimine chromophores conjugated with the nitrogen substituent of an amino acid or its imino alcohol. More than 20 MAAs have been reported in bacterial, microalgae, macroalgae as well as several animals (Sinha et al. 2007). Contrary to MAAs, scytonemin is exclusively synthesized by cyanobacteria (Garcia-Pichel and Castenholz 1991). It is a yellow brown, lipid-soluble dimeric compound located in the extracellular polysaccharide sheath of some cyanobacteria and acts as a passive sunscreen in protection against UV radiation (Proteau et al. 1993).

In conclusion, phenolic compounds and UV-absorbing compounds play important role in responding to environmental stressors, and they can be determined by spectrophotometry and high performance liquid chromatography (HPLC).

14.2 Determination of Phenolic Compounds

14.2.1 Spectrophotometer

Total phenolic compounds contents can be estimated by the protocol by Shetty et al. (1995) with minor modifications. The cell pellets of microalgae harvested by centrifuging were placed in 2.5 mL of 95% ethanol for a period of 48 h at 47 °C. The cells are sonicated and the supernatant separated by centrifugation (4500 × *g*) for 10 min, 1.0 mL of which is transferred to glass test tubes along with 1.0 mL 95% ethanol, 5.0 mL distilled water and 0.5 mL of 50% Folin-Ciocalteu reagent (Sigma Chemical, USA). The solution is allowed to react for 5 min, then 1.0 mL of 5% Na_2CO_3 is added, and the mixture vortexed and placed in the dark for 1 h. Absorbance is determined with a scanning spectrophotometer (DU800, Beckman, Fullerton, California, USA) at 725 nm and plotted against a standard curve obtained from gallic acid.

14.2.2 HPLC

HPLC can be applied to determine the profile of phenolic compounds in microalgae.

14.2.2.1 Preparation of Microalgae Extracts for Isolation and Quantification of Phenolic Compounds

The algae are freeze-dried and 1 g of the dry material is extracted by stirring with methanol (25 mL) for 1 h. After centrifugation at 3500 revolutions per minute (rpm) for 30 min, the supernatant is collected and evaporated. The dry residue (100 mg) and 4 mL of acetone: hexane (1:4) are mixed and stirred for 10 min. The supernatant is discarded and the residue is mixed and homogenized with 5 mL of methanol using a vortex (10 min). After centrifugation at 3000 rpm, the supernatant is separated and the residue is extracted twice with 5 mL of methanol. All the methanolic fractions are collected and evaporated in a rotary vacuum evaporator at 30 °C (6800 rpm). The residues are resolved in 5 mL of HCl (1 mol L^{-1}) and the samples are hydrolyzed at room temperature, 3800 rpm for 30 min. The hydrolysates are purified using solid-phase extraction (SPE).

14.2.2.2 Solid-Phase Extraction

The cartridge Chromabon Easy is preconditioned by successive elution with 3 mL of methanol and 3 mL of deionized water. The hydrolysates (5 mL) are passed through the cartridges at a flow of 2.5 mL min^{-1}. The cartridge is then rinsed using 2% acetic acid in a 5% methanol solution. The retained analytes are subsequently eluted using aqueous methanol solutions (5%, 10%, and 20% methanol, 2 mL for each). Prior to the analyses, the fractions are evaporated to dryness in a rotary vacuum evaporator at 25 °C, 3500 rpm, resolved in 500 μL of methanol, filtered through a 45 μm nylon syringe filter, and injected directly into the HPLC system.

Seawater enriched with microalgae exudates (2.5 L) are passed through the conditioned cartridges (as described above) at a flow of 2.5 mL min^{-1} (800 mL per cartridge, using three cartridges), following the same elution procedure described above for each cartridge. The fractions from the three cartridges are collected, evaporated as above, and the residue resolved in 500 μL of methanol, and then filtered to be injected into the HPLC system.

14.2.2.3 Quantification of the Phenolic Compounds

Chromatographic analysis was performed on a system, equipped with a vacuum degasser, a binary pump, a thermostatted column compartment, and a diode array detector. A reverse-phase Pursuit XRs C18 (250 mm × 4.6 mm, 5 μm) column and a Pursuit XRs C18 (10 mm 3 4.6 mm, 5 μm) guard column with a gradient system involving two mobile phases were used. The flow rate was 1.0 mL min^{-1} and the injection volume was 60 μL of crude extracts. The system operated at 27 °C. The phenolic compounds gallic acid, protocatechuic acid, catechin, vanillic acid, epicatechin and syringic acid, chlorogenic acid, gentisic acid, caffeic acid,

p-coumaric acid and ferulic acid, rutin, myricetin, and quercetin are quantified as follows. In brief, the eluent A is Milli-Q water with 0.1%formic acid and eluent B is methanol. The elution conditions applied are 0–5 min, 20% B isocratic; 5–30 min, linear gradient from 20% to 60% B; 30–35 min, 60% B isocratic; 35–40 min, linear gradient from 60% to 20% B; and, finally, washing and reconditioning of the column. Each standard is individually tested to determine its retention times (RT) as follows: gallic acid (RT: 5.3 min), protocatechuic (RT: 10.0 min), catechin (RT: 12.7 min), chlorogenic acid (RT: 14.9 min), gentisic acid (RT: 17.1 min), vanillic acid (RT: 17.7 min), epicatechin (RT: 17.9 min), caffeic acid (17.9 min), syringic acid (RT: 18.9 min), coumaric acid (RT: 23.4 min), rutin (RT: 28.1 min), ferulic acid (RT: 24.3 min), myricetin (RT: 30.6 min), and quercetin (RT: 34.6 min) are well resolved. Simultaneous monitoring is set at 270 nm (gallic acid, protocatechuic acid, (+)-catechin, vanillic acid, (2)-epicatechin, and syringic acid), 324 nm (chlorogenic acid, gentisic acid, caffeic acid, *p*-coumaric acid, and ferulic acid), and 373 nm (rutin, myricetin, and quercetin) for quantification. Limits of detection (LODs) and limits of quantification (LOQs) are estimated from signal-to-noise ratio of the individual peaks, assuming a minimum detectable signal-to-noise level of 3 and 10, respectively. The LODs are found to be in the range of 1.59×10^{-3}–0.52 nmol mL^{-1} and the LOQs are observed in the range of 4.25×10^{-3}–0.17 nmol mL^{-1}.

14.2.3 Strengths and Limitations

HPLC can be applied to determine each profile of phenolic compounds, while only the total contents of phenolic compounds can be measured by spectrophotometry. However, HPLC is time and money consuming, and spectrophotometry is of low cost and straightforward.

14.3 Determination of UV-Absorbing Compounds

14.3.1 Extraction of Samples for HPLC Analysis of Mycosporine Amino Acids

Cultures are centrifuged in a refrigerated centrifuge at 5000 × *g* for 5 min. The cell pellets are extracted with 1–2 mL of cold (5 °C) tetrahydrofuran: methanol (20:80, v/v) in an ice bath, by using sonicator with a 4 mm needle probe (1 min), and left for 30 min at 5 °C to fully extract. MAAs are stable in wet methanol under the following conditions: 1–2 days at room temperature (e.g., 20 °C), 1 week at 5 °C, 2–3 weeks at −20 °C, and 2 months at −80 °C. Since stability rapidly decreases with storage temperatures greater than 30 °C care is taken to keep temperatures around 5 °C

during experimental treatments. When dry, samples are stable at room temperature for several months.

After centrifugation of the combined extracts (about 5–6 mL), a small aliquot (0.1–0.2 mL) is diluted for spectrophotometry, and equal volumes of the remaining extract are placed in four Eppendorf tubes and evaporated in evaporator for several hours at ambient temperature (0.9–1.5 mL). Samples could be left overnight at −20 °C if evaporation is not complete, and evaporations are then completed the following day. The quadruplicate tubes of the lyophilidized algal extracts of each species are then dispatched for HPLC analysis.

14.3.2 HPLC Analysis

Analyses of MAAs are performed according to published procedures (Dunlap et al. 1986, 1989; Stochaj et al. 1994; Carroll and Shick 1996; Helbling et al. 1996; Jeffrey et al. 1999). Lyophilized algal extracts are reconstituted in 80% aqueous methanol. Individual MAAs were separated and quantified by isocratic HPLC on a reverse-phase, Brownlee RP-8 column (Spheri-5, 4.6 i.d. × 250 mm) protected with a RP-8 guard column with a mobile phase consisting of aqueous 25% methanol containing 0.1% acetic acid which was delivered at a flow rate of 0.8 mL min^{-1}. MAAs are identified by comparison and CO-chromatography (where applicable) with authenticated standards and quantified by dual wavelength absorbance at 313 and 340 nm (Waters Model 440 dual wavelength detector) and peak area integration (Spectra-Physics 4400 dual channel integrator).

References

Carroll AK, Shick JM (1996) Dietary accumulation of UV absorbing mycosporine-like amino acids (MAAs) by the green sea urchin (*Stronglocentrotus droebachiensis*). Mar Biol 124:561–569

Dunlap WC, Chalker BE, Oliver JK (1986) Bathymetric adaptations of reef-building corals at Davies Reef, Great Barrier Reef, Australia. 111. UV-B absorbing compounds. J Exp Mar Biol Ecol 104:239–248

Dunlap WC, Williams DMB, Chalker BE, Banaszak AT (1989) Biochemical photoadaptation in vision: UV-absorbing pigments in fish eye tissues. Comp Biochem Physiol 93B:601–607

Garcia-Pichel F, Castenholz RW (1991) Characterization and biological implications of scytonemin, a cyanobacterial sheath pigment. J Phycol 27:395–409

Häder D-P et al (2015) Effects of UV radiation on aquatic ecosystems and interactions with other environ- mental factors. Photochem Photobiol Sci 14:108–126

Helbling EW, Chalker BE, Dunlap WC, Holm-Hansen E, Villafaiie VE (1996) Photoacclimation of antarctic marine diatoms to solar ultraviolet radiation. J Exp Mar Biol Ecol 204:85–101

Jeffrey SW, MacTavish HS, Dunlap WC, Vesk M, Groenewoud K (1999) Occurrence of UVA and UVB-absorbing compounds in 152 species (206 strains) of marine microalgae. Mar Ecol Prog Ser 189:35–51

Jin P, Wang TF, Liu NN, Dupont S, Beardall J, Boyd P, Riebesell U, Gao KS (2015) Ocean acidification increases the accumulation of toxic phenolic compounds across trophic levels. Nat Commun 6:8714

Proteau PJ, Gerwick WH, Garcia-Pichel F, Castenholz R (1993) The structure of scytonemin, an ultraviolet sunscreen pigment from the sheaths of cyanobacteria. Experientia 49:825–829

Rastogi RP, Incharoensakdi A (2013) UV radiation-induced accumulation of photoprotective compounds in the green alga *Tetraspora* sp. CU2551. Plant Physiol Biochem 70:7–13

Rico M, López A, Santana-Casiano JM, González AG, González-Dávila M (2013) Variability of the phenolic profile in the diatom *Phaeodactylum tricornutum* growing under copper and iron stress. Limnol Oceanogr 58:144–152

Shetty K, Curtis OF, Levin RE, Witkowsky R, Ang V (1995) Prevention of vitrification associated with the *in vitro* shoot culture of oregano (*Origanum vulgare*) by *Psuedomonas* spp. J Plant Physiol 147:447–451

Sinha RP, Singh SP, Häder D-P (2007) Database on mycosporines and mycosporine-like amino acids (MAAs) in fungi, cyanobacteria, macroalgae, phytoplankton and animals. J Photochem Photobiol B 89:29–35

Stochaj WR, Dunlap WC, Shick JM (1994) Two new UV absorbing mycosporine-like amino acids from the sea anemone *Anthopleura elegantjssirna* and the effects of zooxanthellae and spectral irradiance on chemical composition and content. Mar Biol 118:149–156

Treutter D (2006) Significance of flavonoids in plant resistance: a review. Environ Chem Lett 4:147–157

Vernet M, Neon A, Haxo FT (1989) Spectral properties and photosynthetic action in red-tide populations of *Prorocentrum micans* and *Gonyaulax polyedra*. Mar Biol 103:365–371

Part V
Measurements and Analyses of Photosynthesis and Respiration

Chapter 15
Photosynthetic Oxygen Evolution

Guozheng Dai, Hualing Mi, and Baosheng Qiu

Abstract Photosynthetic oxygen evolution rate is an important physiological index, which can be used to evaluate the ability of oxygenic organisms to utilize light and inorganic carbon. By using different inhibitors of the photosynthetic electron transport chain and an artificial electron donor/acceptor, the activity of photosynthetic electron transport can also be measured. The oxygen electrode method is the most commonly used method for the measurement of photosynthetic rate. This section will introduce the working principle, operating procedures, matters needing attention, advantages, and disadvantages of the Clark oxygen electrode method for measuring the photosynthetic oxygen evolution rate, by taking several cyanobacterial species as examples.

Keywords Liquid oxygen electrode · Photosynthetic electron transport · Photosynthetic response to inorganic carbon · Photosynthetic response to irradiance · Oxygen evolution rate

A Clark oxygen electrode is usually used to measure the change of dissolved oxygen content in aqueous solution. It consists of silver electrode (anode) and platinum electrode (cathode) embedded in insulating material. The electrode surface is covered with a layer of polytetrafluoroethylene or polyhexene membrane about 20–25 μm in thickness. The silver electrode and the bottom of the membrane are filled with semi-saturated KCl solution as electrolyte, and the anode and cathode are connected with the bridge paper by absorbing KCl solution. When the applied polarization voltage between the two electrodes exceeds the decomposition voltage

G. Dai · B. Qiu (✉)
School of Life Sciences, and Hubei Key Laboratory of Genetic Regulation and Integrative Biology, Central China Normal University, Wuhan, Hubei, People's Republic of China
e-mail: bsqiu@mail.ccnu.edu.cn

H. Mi
National Key Laboratory of Plant Molecular Genetics, Institute of Plant Physiology and Ecology, Shanghai Institutes for Biological Sciences, Chinese Academy of Science, Shanghai, People's Republic of China

K. Gao et al. (eds.), *Research Methods of Environmental Physiology in Aquatic Sciences*, https://doi.org/10.1007/978-981-15-5354-7_15

of the oxygen molecule, the dissolved oxygen in the KCl solution is reduced on the platinum electrode ($O_2 + 2H_2O + 4e^- \rightarrow 4OH^-$) and the silver oxidation reaction ($4Ag + 4Cl^- \rightarrow 4AgCl + 4e^-$) occurs on the silver electrode. At this time, the electrolytic current is generated between the anode and cathode. The oxygen concentration on the cathode surface decreases rapidly due to the rapid reaction of the electrode. Oxygen in the solution diffuses and replenishes to the cathode, and the reduction process continues. Because of the relatively slow diffusion of oxygen in water, the electrode current is limited by the diffusion rate of oxygen, which is also called the diffusion current. Under constant temperature, the diffusion current is controlled by the oxygen concentration difference between the solution and electrode surface. With the increase of applied voltage, the concentration of oxygen on the electrode surface will inevitably decrease, the oxygen concentration difference between the solution and electrode surface will increase, and the diffusion current will also increase. When the applied polarization voltage reaches a certain value where the oxygen concentration on the cathode surface approaches zero, the diffusion current depends entirely on the oxygen concentration in the reaction solution. At this point, even if the polarization voltage is increased the diffusion current will not increase further, so that the polarographic wave (i.e., current–voltage curve) reaches a plateau. When the polarization voltage is selected in the middle of the plateau, the diffusion current is not affected small fluctuations of voltage. Therefore, under conditions of constant polarization voltage and temperature, the magnitude of the diffusion current can be used as the basis for the quantitative determination of dissolved oxygen. The diffusion current signal between electrodes can be converted into voltage output by the circuit of the electrode controller and recorded by an automatic recorder or computer.

15.1 Instruments and Equipment

1. Liquid oxygen electrode.
   In this section, the Clark liquid phase oxygen electrode (Chlorolab 2, Hansatech Instruments Ltd., King's Lynn, Norfolk, UK) of the Hansatech Company is taken as an example to illustrate the oxygen electrode configuration, as shown in Fig. 15.1. The reaction chamber is usually made of transparent plexiglass with a volume of about 2 mL and a waterproof jacket. The temperature is controlled by connecting a constant temperature circulating water bath. The electrode is placed at the bottom of the reaction chamber with a small hole in the plug, and various reagents can be added into the chamber by a microinjector during the process of determination. The electrode stirrer is located below the reaction chamber, which controls the rotational speed of the magnetic rod in the reaction chamber, so that the samples in the reaction chamber are uniformly distributed without sinking, thus the real oxygen evolution rate of samples can be measured. The electrode controller is used to provide polarization voltage and output the signal to the computer. The schematic diagram of the oxygen electrode configuration and the equipment needed for the experiment (except for the electrode) are as follows.

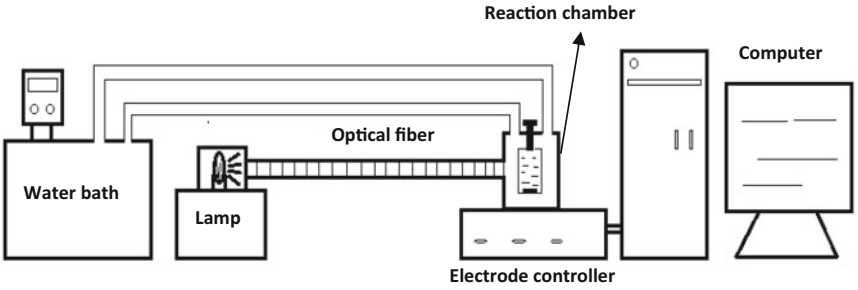

Fig. 15.1 Schematic diagram of oxygen electrode

2. Constant temperature circulating water bath (Cole-Parmer Instrument Co., Vernon Hills, IL, USA).
3. Light source, fiber-optic cable (A8, Hansatech) and neutral density filters with different transmittance.
4. Illuminance quantum sensor (QRT1, Hansatech).
5. Stirrer.

15.2 Solution Preparation

1. Reaction solution for the determination of oxygen evolution rate for intact cells of algae.
   Ten mmol L^{-1} $KHCO_3$ is added to the algal culture medium to ensure sufficient carbon supply in the closed measurement environment, and a certain concentration of pH buffer (such as 25 mmol L^{-1} Bis-Tris Propane, BTP) is added to adjust the pH to the required value for the experiment.
2. Carbon-free reaction solution.
   BG11 medium is a common medium for freshwater algae culture. Its carbon-free reaction medium is prepared as follows: Na_2CO_3 is deleted from the BG11 medium recipe, and $NaNO_3$ was replaced by the same concentration of KNO_3. The modified BG11 medium is used as the basic reaction medium. Add 25 mmol L^{-1} NaCl and 25 mmol L^{-1} BTP (Useful buffering pH range 6.0–9.5) powder to the basic reaction solution, adjust the pH to 1.0 with 1 mmol L^{-1} HCl, aerate the liquid with pure N_2 for 30 min, and then adjust the pH to 8.0 with the supernatant of the fresh supersaturated NaOH solution after centrifugation to attain BG11 carbon-free reaction solution (Cheng et al. 2008). Dispense the carbon-free reaction solution into 10 mL centrifugal tubes, cover tightly and seal with sealing membrane (making sure there is no residual bubble in the centrifugal tube) to prevent CO_2 in the air from dissolving into the reaction liquid again.

Marine algae can be cultured in seawater enriched with artificial seawater culture medium (e.g., f/2 culture medium) after 0.22 μm filtration. The process of preparing carbon-free reaction solution is similar to the above. Specific operations are as follows: adjust pH value of the seawater culture medium below 3.0 by adding HCl to convert the various inorganic carbon in seawater into CO_2, and then aerate the medium with pure N_2 for about 30 min (appropriately prolong the aerating time for larger volume of solution). Before stopping the N_2 aeration, add an appropriate pH buffer agent into the medium, then adjust the pH value with the supernatant of the fresh supersaturated NaOH solution to the required value (Gao et al. 1993; Chen et al. 2006).

According to the different requirements of pH values for specific experiments, suitable pH buffers can be selected. BTP, MES (4-Morpholineethanesulfonic acid hydrate, useful buffering range pH 5.5–6.7), HEPES (4-(2-hydroxyethyl)piperazine-1-ethanesulonic acid, useful buffering range pH 6.8-8.2), TRICINE (N-tris (hydroxymethyl) methylglycine, useful buffering range pH 7.4-8.8), TAPS (N-(Tris(hydroxymethyl)methyl)-3-aminopropanesulfonic acid, useful buffering range pH 7.7–9.1) and so on, are the common buffers that are used in the reaction solution for photosynthetic oxygen evolution determination. The concentration of the buffer is generally 20–50 mmol L^{-1}. The carbon-free reaction solution should be strictly protected from external "carbon pollution." It will prolong the carbon depletion time for the experimental materials when the incomplete carbon-free reaction solution is used, and may cause damage to photosystems in the process of carbon depletion.

15.3 Operation Procedures

15.3.1 Installation of the Liquid Oxygen Electrode

Before using, carefully clean the electrode with a cotton swab dipped in a special electrode cleaner (or toothpaste) until the electrode surface is bright to ensure the best work situation. Then install the electrode as follows:

(a) A drop of electrolyte (semi-saturated KCl solution, 17.5 mmol L^{-1}) is added to the top of the circular electrode (platinum electrode) to cover the electrode as much as possible without flowing away.
(b) Take a piece of salt bridge paper (or cigarette paper) with appropriate size to cover the electrolyte drop. Then take a piece of electrode membrane with similar size of salt bridge paper to cover the salt bridge paper. There should be no bubbles among the electrode, salt bridge paper, and electrode membrane.
(c) Fix the small "O" type rubber ring at the end of the membrane loader, and place the membrane loader perpendicular to the top of the circular electrode. Press the membrane loader coat downward, so that the O-ring is fixed on the electrode covered with the electrode membrane.

(d) Confirm whether the electrode membrane is smooth and that there are no bubbles between the salt bridge paper and electrode membrane. Then add a few drops of electrolyte into the groove of the electrode (silver electrode), and the cathode and the anode are connected through the electrolyte and salt bridge paper. Remove the bubbles carefully in the groove of the electrode with a pipette tip, and finally place the outer large "O" rubber ring in the groove outside the electrode.
(e) Remove the base of the electrode chamber counterclockwise, put the electrode into the electrode chamber, tighten the base clockwise, and make the cathode covered with the membrane the bottom of the sample chamber.
(f) Place the base of the sample chamber with the electrode on the magnetic stirrer above the electrode controller. Connect the electrode with the control box through the connecting wire to provide polarization voltage for the electrodes, and connect the electrode controller with the computer through the data wire.
(g) Connect the constant temperature circulating water bath to ensure the sample chamber with constant temperature during the process of determination.

15.3.2 Calibration of the Liquid Oxygen Electrode

Add a magnetic rotor and 2 mL deionized water to the sample chamber, and aerate air evenly into the distilled water. The oxygen saturated airline of the oxygen electrode is calibrated when the signal line is flattened. When the calibration is completed, a small amount of $Na_2S_2O_3$ or Na_2SO_3 powder is added into the sample chamber, and then seal the sample chamber (or high purity N_2 is evenly aerated into the sample chamber). The measured signal will drop rapidly, and the electrode will be calibrated after the signal line drops and stabilizes. Because the solubility of O_2 in water varies at different temperatures (Table 15.1), the temperature of the reaction system should be controlled by a constant temperature circulating water bath. Illumination is provided by a light source with a voltage stabilizing device, and

Table 15.1 Oxygen solubility in freshwater and seawater under different temperatures

Temperature (°C)	Oxygen solubility (mmol L^{-1})	
	Freshwater	Seawater
0	0.457	0.349
5	0.399	0.308
10	0.353	0.275
15	0.315	0.248
20	0.284	0.225
25	0.258	0.206
30	0.236	0.190
35	0.218	0.176
40	0.202	0.165
45	0.189	0.154
50	0.177	0.146

the light intensity can be adjusted by using neutral filters with different transmittance. The actual illumination is measured by a quantum sensor.

15.3.3 Determination of Dissolved Oxygen

A Clark liquid phase oxygen electrode can be used to measure the photosynthetic oxygen evolution rate and dark respiration rate of algae in solution (to avoid the influence of photorespiration, the experimental materials need to be kept in the dark for about 15 min, and then the stable oxygen consumption rate, i.e., dark respiration rate, is measured). In order to determine the oxygen evolution rate of isolated thylakoid membranes, artificial electron acceptors (such as potassium ferricyanide, quinone, and so on.) are needed. Excessive oxygen concentration in the reaction chamber may inhibit photosynthesis, and high purity N_2 can be bubbled into the reaction chamber to reduce the oxygen content. In this section, the photosynthetic oxygen evolution rates of *Nostoc sphaeroides* and *Synechococcus* sp. PCC 7942 were measured as examples. After centrifugation, the algal cells were collected and suspended with fresh reaction solution. The 2 mL sample was put into the sample chamber, agitated with the stirrer, and the measured signal was recorded.

The curves of photosynthetic response to irradiance (*P–I* curve) or inorganic carbon (*P–C* curve) can be obtained by measuring the change of photosynthetic oxygen evolution rate under different light intensities or inorganic carbon concentrations. In addition, the photosynthetic electron transport activity can be calculated by measuring the photosynthetic oxygen evolution or oxygen consumption rate with addition of specific photosynthetic electron transfer inhibitors, electron acceptors, and electron donors. These three aspects will be introduced as follows:

(a) *P–I* curve. Cells were collected by centrifugation and suspended with fresh BG11 reaction solution (added 10 mmol L^{-1} $KHCO_3$ carbon source). The photosynthetic oxygen evolution rates under different light intensities were measured (see Fig. 15.3a). Parameters for the photosynthetic response to irradiance were analyzed according to Henley (1993), the formula 15.1,

$$P = P_{\mathrm{m}} \times \tanh(\alpha \times I/P_{\mathrm{m}}) + R_{\mathrm{d}}, I_{\mathrm{k}} = P_{\mathrm{m}}/\alpha, I_{\mathrm{c}} = -R_{\mathrm{d}}/\alpha, \tag{15.1}$$

where I represents irradiance, P photosynthetic activity at certain irradiance, P_{m} light-saturated photosynthesis, I_{k} saturating irradiance for photosynthesis, and I_{c} light compensation point. The ascending slope at limiting irradiances, α was calculated to assess the photosynthetic efficiency.

(b) *P–C* curve. Cells were collected by centrifugation and suspended with fresh carbon-free BG11 solution. After carbon deletion for cells in the reaction chamber, the photosynthetic oxygen evolution rate of samples with additions of different DIC concentrations were measured (see Fig. 15.3b). Carbon deletion for cells was monitoring the oxygen evolution rate under 240 μmol photons m^{-2} s^{-1} (moderately decrease light intensity to avoid photodamage to photosystems during carbon limitation). When oxygen evolution ceased, the intracellular carbon of the sample in the reaction solution was determined to be depleted. Carbon depletion usually takes about 30 min. Then, the photosynthetic oxygen evolution rate was measured at 560 μmol photons m^{-2} s^{-1} (close to the saturated light intensity calculated from the light response curve) by adding $KHCO_3$ solution of known concentration (0, 5, 10, 20, 50, 100, 200, 400, and 800 μmol L^{-1}), and the concentration gradient was set according to different experimental materials. The net photosynthetic rate at different DIC concentrations was fitted by the Michaelis–Menten equation to obtain the different parameters. The formula is 15.2:

$$V = V_{\max} \times S/(K_m + S), \tag{15.2}$$

V denotes net photosynthesis, $V_{\max}$ denotes maximum net photosynthesis, S denotes DIC concentration, and K_m is the required DIC concentration when the net photosynthesis reaches a half of $V_{\max}$.

(c) Photosynthetic electron transport activity. Algal cells were collected and suspended with fresh BG11 reaction solution. H_2O was used as the electron donor and p-benzoquinone (p-BQ) (final concentration 1 mmol L^{-1}) as the electron acceptor in the determination of PSII oxygen evolution activity. PSI activity was determined by measuring the photodependent oxygen consumption rate. Reduced $DCPIPH_2$ was used as the electron donor and MV as the electron acceptor. 1 mmol L^{-1} NaN_3 (inhibiting respiration), 10 μmol L^{-1} 3-(3,4-dichlorophenyl-1,1-dimethylurea) DCMU (inhibiting PSII activity), 5 mmol L^{-1} ascorbate (reducing DCPIP), 0.1 mmol L^{-1} 2, 6-dichlorophenolindophenol (DCPIP) and 0.5 mmol L^{-1} methyl viologen (MV) were added to the reaction system. The whole chain electron transport rate is determined by measuring the oxygen consumption rate under illumination, in which H_2O is an electron donor and MV is an electron acceptor. The reaction system is measured by adding 1 mmol L^{-1} NaN_3 and 0.5 mmol L^{-1} MV (Fig. 15.2) (Zhou et al. 2006).

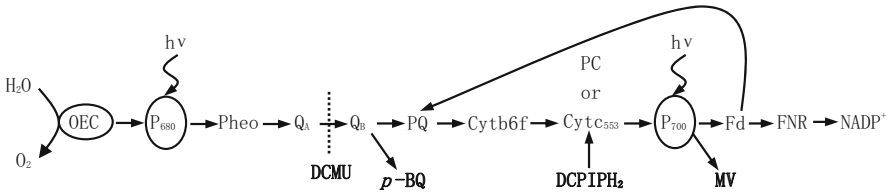

Fig. 15.2 Schematic representation of photosynthetic electron transport showing the action sites of inhibitor and different artificial electron donors and acceptors (Zhou et al. 2006)

15.3.4 Calculation of Oxygen Evolution/Oxygen Consumption Rate of Samples

According to the experimental requirement, a section of the recorded results with a stable slope was selected to calculate the rate of change of oxygen concentration (in the unit of μmol O_2 mL^{-1} min^{-1}). The photosynthesis or respiration rate was calculated according to the weight of the sample, the number of cells or the content of chlorophyll (Chl). For example, the measured photosynthetic oxygen evolution rate of *Synechococcus* sp. PCC 7942 was 0.0163 μmol O_2 mL^{-1} min^{-1} and the concentration of Chl *a* was 12 μg mL^{-1}, and the oxygen evolution rate expressed in terms of unit Chl *a* content was 1.36 μmol O_2 mg^{-1} Chl *a* min^{-1} (Cheng et al. 2008). Based on the calculated results, the *P–I* curve and *P–C* curve are shown in Fig. 15.3.

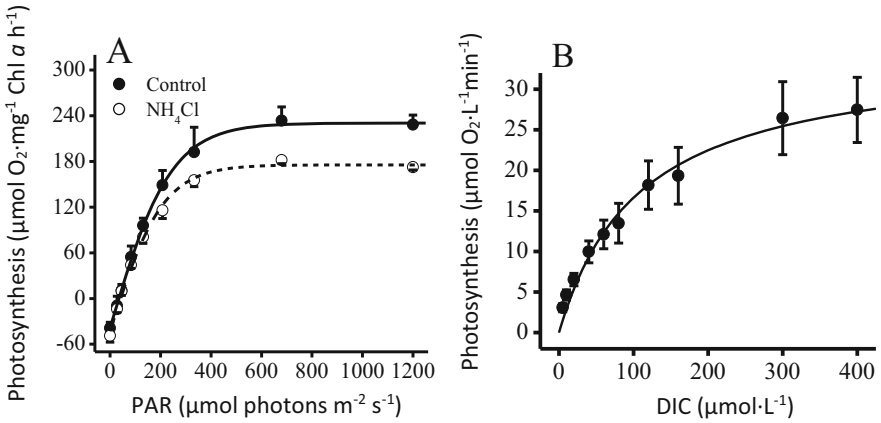

Fig. 15.3 Photosynthetic response to irradiance (*P–I* curve) or inorganic carbon (*P–C* curve) in *N. sphaeroides*. (**a**) *P–I* curve. Photosynthetic oxygen evolution of *N. sphaeroides* as a function of PAR irradiance with or without exposure of 1 mmol L^{-1} NH_4Cl for 96 h (Dai et al. 2008). (**b**) *P–C* curve. *N. sphaeroides* was carbon depleted in DIC-free reaction medium firstly, then the photosynthetic oxygen evolution rates under different concentrations of $KHCO_3$ were measured under 560 μmol photons m^{-2} s^{-1} and pH 8.0 (Qiu and Liu 2004)

In some cases, the experimental materials were not carbon depleted completely before *P–C* curve measurements, and the calculated *P–C* curve deviates from the true value and so needs to be corrected (Gao 1996). Three methods can be used to correct the *P–C* curve as follows: (a) Move the *P–C* curve horizontally along the *X*-axis (positive direction) until the intersection point with the *X*-axis coincides with the origin point. (b) Using the measured data under higher concentrations of inorganic carbon, convert them into reciprocal plots to avoid the large deviation between the actual values and the measured values at low concentrations of inorganic carbon. (c) Take the oxygen evolution rate measured before adding inorganic carbon as the background value, subtract this background value from the measured value under each concentration of inorganic carbon, and then redraw the *P–C* curve. This method will lead to a change of V_{max} value, but it is applicable to the calculation of K_m value.

15.4 The Advantages, Disadvantages, and Considerations

The photosynthetic oxygen evolution rate or respiration rate can be measured by liquid oxygen electrode. It is simple to operate and can quickly track the change of dissolved oxygen concentration. The measurement of one sample can be completed in a few minutes, and the whole process of the change of oxygen concentration can be recorded. However, this method is not very sensitive and requires a high concentration of cells. Thus, the samples collected in the field often need to be concentrated before they can be determined. In addition, compared with other photosynthetic analyzers, such as portable photosynthetic analyzers (infrared CO_2 gas analyzers), relatively few parameters can be measured with liquid oxygen electrodes simultaneously and it is not convenient to carry around. When using a liquid oxygen electrode to determine photosynthetic oxygen evolution rate, one should pay attention to the following points.

1. For the installation of the electrode, the electrode membrane cannot be directly touched by the hand, and must be free from wrinkles and breakage. The sample chamber should be sealed in the process of the measurements of oxygen evolution.
2. Oxygen electrodes are sensitive to temperature. Therefore, one should control the temperature of the sample chamber constant in the process of measuring. Meanwhile, the magnetic rod is stirring to facilitate oxygen diffusion in the reaction solution during the measurements; otherwise the signal will be unstable.
3. When the electrode is not used for a short period, 1 mL distilled water should be added to the sample chamber to prevent the evaporation of water in the electrode membrane and the precipitation of KCl. The electrode should be cleaned and stored in desiccator if it will not be used for a long time. During the working process of the electrode, an oxide film forms on the anode, which can affect the sensitivity of the electrode. It can be used for up to 1 week after a calibration. When finish the measurements, the electrode needs to be cleaned with a special cleaning agent (or toothpaste).

4. The response time and accuracy of different brands of oxygen electrodes are different, even the same brand of different oxygen electrodes are often also quite different. Therefore, attention should be paid to data comparison.

References

Chen XW, Qiu CE, Shao JZ (2006) Evidence for K^+-dependent HCO_3^- utilization in the marine diatom *Phaeodactylum tricornutum*. Plant Physiol 141:731–736

Cheng HM, Dai GZ, Yu L et al (2008) Influence of CO_2 concentrating mechanism on photoinhibition in *Synechococcus* sp. PCC7942 (Cyanophyceae). Phycologia 47:588–598

Dai GZ, Deblois CP, Liu SW et al (2008) Differential sensitivity of five cyanobacterial strains to ammonium toxicity and its inhibitory mechanism on the photosynthesis of rice-field cyanobacterium Ge-Xian-Mi (*Nostoc*). Aquat Toxicol 89:113–121

Gao KS (1996) Research techniques and methods in characterizing photosynthetic carbon fixation by algae. Mar Sci 6:37–41

Gao K, Aruga Y, Asada K et al (1993) Calcification in the articulated coralline alga *Corallina pilulifera*, with special reference to the effect of elevated CO_2 concentration. Mar Biol 117:129–132

Henley WJ (1993) Measurement and interpretation of photosynthetic light-response curves in algae in the context of photoinhibition and diel changes. J Phycol 29:729–739

Qiu BS, Liu JY (2004) Utilization of inorganic carbon in the edible cyanobacterium Ge-Xian-Mi (*Nostoc*) and its role in alleviating photoinhibition. Plant Cell Environ 27:1447–1458

Zhou WB, Juneau P, Qiu BS (2006) Growth and photosynthetic responses of the bloom-forming cyanobacterium *Microcystis aeruginosa* to elevated levels of cadmium. Chemosphere 65:1738–1746

Chapter 16
Photosynthetic Carbon Fixation

Gang Li, Yaping Wu, and Guang Gao

Abstract Many methods have been introduced to measure the photosynthetic rate of phytoplankton, while so far, the most common and sensitive one is to measure carbon fixation with radiocarbon (^{14}C) and to integrate the primary production throughout the water column, especially in oligotrophic pelagic oceans where phytoplankton abundance is very low. Therefore, we described in details here the estimation processes of photosynthetic carbon fixation, matters needing attention during the ^{14}C operations, and introduce some applications of the ^{14}C method in the laboratory.

Keywords Carbon fixation · Primary production · Radiocarbon (^{14}C) isotope tracer method

16.1 Introduction

Phytoplankton convert inorganic matter to organic matter by photosynthesis and produce oxygen, supplying foods and oxygen to higher trophic levels, and supporting the whole marine ecosystem. Therefore, measuring the photosynthetic rate of phytoplankton and estimating primary production of the water column are very helpful to better understand the variations of productivity, food chains, and ecosystems among different aquatic areas.

G. Li (✉)
Key Laboratory of Tropical Marine Bio-resources and Ecology, South China Sea Institute of Oceanology, Chinese Academy of Sciences, Guangzhou, China
e-mail: ligang@scsio.ac.cn

Y. Wu
College of Marine Life and Fishery, Jiangsu Ocean University, Lianyungang, China

G. Gao
State Key Laboratory of Marine Environmental Science and College of Ocean and Earth Sciences, Xiamen University, Xiamen, China

K. Gao et al. (eds.), *Research Methods of Environmental Physiology in Aquatic Sciences*, https://doi.org/10.1007/978-981-15-5354-7_16

Presently, there are many ways to estimate the photosynthetic rate of marine phytoplankton assemblages. Among them, the most direct and common methods are to measure the oxygen produced, and carbon fixation. Using the first method, higher algae biomass is often needed due to the detection limit of the oxygen electrode, such as chlorophyll *a* (Chl a) concentrations of 50–100 μg L^{-1} (Campbell et al. 2013). However, phytoplankton abundance is usually very low in the oceans. For instance, surface Chl a concentration is lower than 0.30 μg L^{-1} in the South China Sea (Li et al. 2011a, 2012a, 2016), whereas it is even lower than 0.10 μg L^{-1} in surface waters of the Indian Ocean (Li et al. 2012b, c). Therefore, there are limitations for the application of using oxygen measurement to determine the photosynthetic rate of in situ phytoplankton assemblages.

So far, the most common and sensitive method for marine primary production studies is to track photosynthetic carbon fixation by phytoplankton assemblages with radiocarbon (^{14}C), especially for in situ investigations. This method was used for the first time in the 1950s by Steeman Nielsen (1952), to estimate the photosynthetic rate on the basis of $^{14}CO_2$ absorption by phytoplankton during a certain time. Photosynthetic capacity can be used as an indicator for phytoplankton growth and physiology under in situ conditions, as well as the effects of environmental factors like temperature, salinity, nutrients, etc. (Li et al. 2011b). The amount of carbon fixation by phytoplankton communities can also reflect the productivity of different sea areas in different seasons, and indicate the dynamics of the food chain and the whole ecosystems.

16.2 ^{14}C Isotope Tracer Method

Determination of marine primary productivity with radiocarbon (^{14}C) is based on the equivalent absorption of $^{14}CO_2$ and $^{12}CO_2$ by phytoplankton, with the exception of a specific isotope difference factor (Steeman Nielsen 1952). In the marine carbonate buffer system, inorganic carbon exists in many forms, including CO_2, H_2CO_3, HCO_3^-, and CO_3^{2-}, among which HCO_3^- has the highest proportion, accounting for more than 90%. The radioactive ^{14}C isotope is thus introduced in the form of $H^{14}CO_3^-$. There are three steps to measure phytoplankton carbon fixation with the ^{14}C method, described as follows:

16.2.1 Sampling Protocols

The seawater samples with phytoplankton assemblages were taken with an acid-washed (1 mM HCl) polycarbonate bucket, and immediately transferred to the laboratory. Some samples like those from deep layers should be kept in darkness during sampling and transferring, to avoid light shock. In order to eliminate effects of zooplankton grazing, the seawater samples were filtered through a 180 μm-pore

nylon mesh to remove most zooplankton; however, during this treatment process some phytoplankton cells would also be removed, especially from eutrophic coastal waters where there are plentiful large and chain-forming phytoplankton species.

16.2.2 ^{14}C Inoculation and Incubation

The aliquot of seawater was dispensed into culture flasks, with some space left on top to prevent sample spillover when adding ^{14}C solution. The seawater volume dispensed into each flask should be approximately equal, but need not be exactly consistent. After this, a strictly consistent volume of $NaH^{14}CO_3$ working solution was added to each flask; simultaneously, 2–3 flasks were wrapped in foil to measure dark ^{14}C absorption.

After inoculation with ^{14}C solution, all the flasks with samples were fixed on a shelf and incubated in a water tank, with running surface seawater to control temperature at in situ levels. Fixing the flasks on shelves is more important in the onboard experiments, in order to avoid the influence of ship motion due to waves. There are two commonly used methods to control temperature: (1) The in situ incubation, that means putting the flasks with samples back into the ocean at the original sampling site and depth for incubation. This method can mimic the field condition, but the actual operation is very difficult, especially during the cruises. (2) The simulated in situ incubation, which means incubating the phytoplankton assemblage samples with ^{14}C solution in a tank, with running surface seawater to control the temperature. This method has been extensively used for field experiments, because it can mimic the in situ temperature and is easily operated in practice. However, using surface field water to control temperature for simulated in situ incubation has some drawbacks in some special areas. For instance, in the South China Sea the stratification in summer leads to an upper mixed layer (UML) that is less than 50 m, with temperature differences that reach 8–10 °C between the surface and bottom of UML (Fig. 16.1a, b). If such a vertical temperature difference is ignored, the estimation of marine primary production would be affected when using surface water for temperature control. In this case therefore, it is necessary to consider a corresponding correction of the measured productivity. In addition, since light drives photosynthetic carbon fixation of phytoplankton, light intensity and penetration need to be measured and considered during the estimation of marine primary production.

16.2.3 ^{14}C Collection, Treatment, and Measurement

After the incubation, seawater samples were immediately taken back to the laboratory and filtered through a Whatman GF/F filter under dim light conditions. To

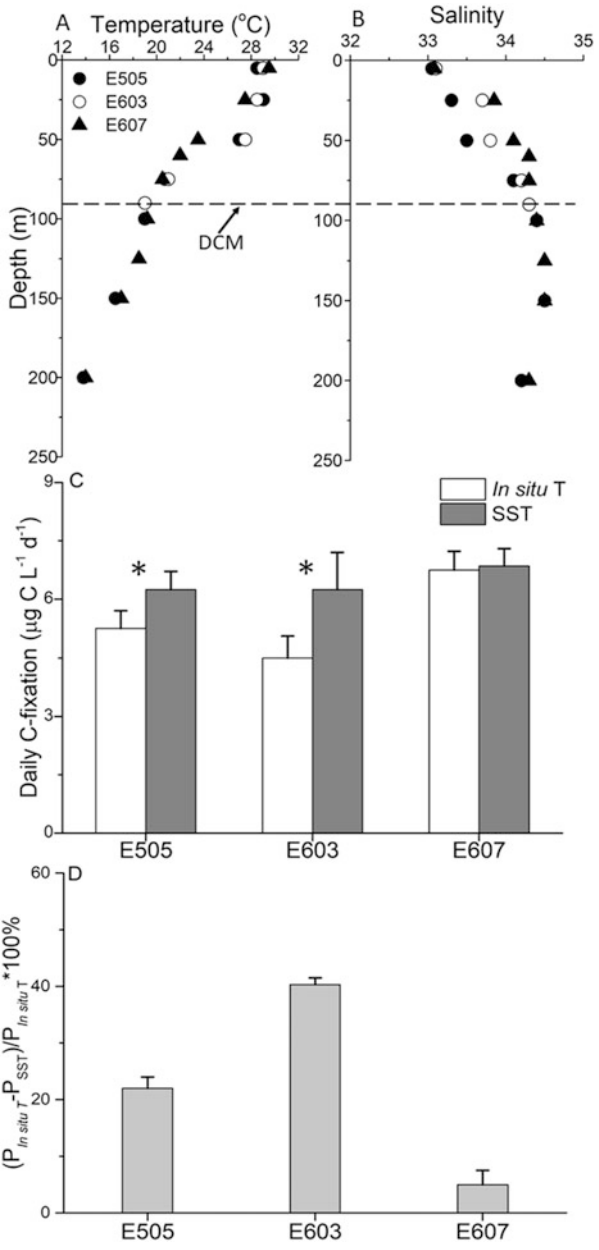

Fig. 16.1 Profiles of (**a**) temperature and (**b**) salinity in the South China Sea, with the dashed line indicating the depth of the chlorophyll a maximum (DCM); (**c**) Daily carbon fixation of phytoplankton assemblages from the DCM layer estimated at surface and in situ temperature, and (**d**) Overestimation of primary production under surface temperature condition. Sampling locations are E505 (18° 36′N, 113° 09′E), E603 (20° 07′, 112° 54′) and E607 (18° 30′, 114° 30′)

eliminate experimental errors, the filtration sequence should be from the dark sample to sample with low carbon fixation, then to high carbon fixation; this is very important for the estimation of photosynthesis versus light curve. And then, one filter with phytoplankton was put into each scintillation vial, and all the vials were

put into an acid box and exposed to hydrochloric acid (HCl) fumes, sealed and acidified overnight to remove the unfixed ^{14}C. After this, the acid box was opened and left in a hood for 15–20 min to vent off the acid, and dried in an oven for 3–5 h at 45–60 °C. Finally, 3–5 mL cocktail was dispensed into each vial and the incorporated ^{14}C was measured using a liquid scintillation counter. The carbon fixation rate by phytoplankton was calculated with the following equation (Holm-Hansen and Helbling 1995):

Carbon fixation ($\mu g\ C\,L^{-1}$) = $[(CPM_{(L)} - CPM_{(D)})/Ce] \times If \times DIC/[A \times (2.2 \times 10^6)]$, where $CPM_{(L)}$ and $CPM_{(D)}$ represent the number of counts per min of each sample under the light and dark (control) conditions, respectively; Ce indicates the counting efficiency derived from the ^{14}C standard; If indicates the isotope difference cofactor (1.06), derived from the 6% higher assimilation efficiency of ^{12}C than that of ^{14}C; DIC indicates the inorganic carbon concentration in samples, and A indicates the amount (μCi) of ^{14}C added to each sample.

The photosynthetic carbon fixation rate (assimilation rate) of phytoplankton can be calculated using the carbon fixation divided by the Chl a content and incubation time; and the daily carbon fixation per volume seawater can be approximately estimated by multiplying the dose ratio of solar radiation from sunrise to sunset to that of the incubation period. The daily primary production of the whole water column can also be obtained by integrating the daily carbon fixation at each layer throughout the depth of the water column. In this way, the estimation of daily primary production is conducted without considering the photoinhibition at high light level e.g., in middle of the day (Gao et al. 2007a). If considering the reduction of photosynthetic carbon fixation by high light at noon especially in surface water, it is more ideal to measure the light response curve of phytoplankton (*P–E* curve) and derive the photosynthetic parameters using the model of Eilers and Petters (1988):

$$P = E/\left(aE^2 + bE + c\right),$$

where P and E indicate the carbon fixation (μg C μg Chl a^{-1} h^{-1}) and light intensity (μmol photons m^{-1} s^{-1}), respectively; and a, b, and c are the adjustment factors.

Using these derived parameters (Gao et al. 2007b), the daily primary production throughout the water column can be estimated with the model of Behrenfeld and Falkowski (1997):

$$\sum \mathrm{PP} = \int_{t\,=\,\mathrm{sunrise}}^{\mathrm{sunset}} \int_{Z\,=\,0}^{\mathrm{Zeu}} E(t,z)/\left(a \times E^2(t,z) + b \times E(t,z) + c\right),$$

where ∑PP represents the integrated carbon fixation of the water column (mg C m^{-2} day^{-1}) from sunrise to sunset, t and Zeu indicate the time and the depth (m) of the euphotic zone, respectively.

In addition, some researchers like Fuentes-Lema et al. (2015) have divided the organic carbon produced by phytoplankton photosynthesis into two parts, and measured them separately. One part is stored within cells (particulate organic carbon,

POC) and the other is released into the environment (dissolved organic carbon, DOC). The sum of these two parts was considered to be the total organic carbon fixed by phytoplankton assemblages. Briefly, the seawater sample after incubation with ^{14}C was filtered through a 0.2 μm-pore polycarbonate filter, to collect the POC (particles or cells larger than 0.2 μm in effective diameter) settled on the filters as well as the DOC (<0.2 μm) within the filtrations; and then, both the POC and DOC samples were seperately put into each vial. The acid treatments and measurements for POC are same as described above. For DOC measurements, 200 μL HCl solution (50% HCl, v/v) was added into each vial with the filtrations, shaken overnight to remove the unfixed ^{14}C, and followed by adding 5 mL cocktails. The counting was performed with a liquid scintillation counter, and the DOC released by cells was calculated as described above.

16.3 Matters Needing Attention

16.3.1 Volume of Incubation Flask

The volume of incubation flasks varies greatly from 10 to 500 mL, and even to 2500 mL in the published studies of marine phytoplankton photosynthetic carbon fixation (Chen and Huang 1997; Huang et al. 1999; Chen 2000; Gao et al. 2007a, b; Li et al. 2011a, b, 2012a, c). In coastal and estuarine areas, phytoplankton are abundant, and it is proper to choose small volume (e.g., 30–50 mL) flasks. Because phytoplankton biomass is high in these areas, using smaller volumes of water samples is sufficient to detect strong ^{14}C signals. On the other hand, filtering smaller volumes of seawater could save time and eliminate experimental errors, especially in experiments with many samples, such as for the determination of a photosynthesis versus light curve (Gao et al. 2007a, b; Li et al. 2009). In the pelagic oceans however, the estimation errors would be larger if using the flask with smaller volumes for determination of primary production, as phytoplankton biomass is lower. In this case, flasks with larger volumes of e.g., 150–200 mL are ideal to use if one is again considering to save filtration time and lessen experimental errors.

16.3.2 Amount of ^{14}C Addition

To obtain strong ^{14}C signals and save experimental costs, the amount of ^{14}C solution added to each seawater sample should be considered when measuring the in situ phytoplankton productivity. The ^{14}C amount can be increased or decreased according to the Chl a concentration of field seawater. In coastal waters, for example, Chl a biomass usually varies from 2 to 5 μg/L, so an addition of 100 μL 5 μCi of ^{14}C solution is sufficient to detect strong ^{14}C signals after 2–4 h incubation (Gao et al. 2007a, b; Li et al. 2009, 2011a; Li and Gao 2012). To eliminate dilution effects of the

^{14}C solution, the volume of added ^{14}C solution should be much less than the volume of the seawater sample; so the ^{14}C stock solution is generally diluted to 50 μCi mL^{-1}. In eutrophic waters like in aquaculture areas or estuaries, the Chl a concentration is often higher than 5 μg L^{-1}; so 2–2.5 μCi of ^{14}C solution for each sample is enough to get strong ^{14}C signals after 2–3 h incubation (Li et al. 2011b). In the oligotrophic oceans, Chl a concentration is very low, so more ^{14}C solution and incubation time are often used to get strong enough ^{14}C signals; for example, 10 μCi of ^{14}C solution added to 250 mL seawater sample and 6–8 h incubation can be used get robust carbon fixation signals for primary production estimation in surface waters of the South China Sea (Li et al. 2012a, c).

16.3.3 Incubation Time

To determine phytoplankton primary productivity, the samples with ^{14}C were usually incubated in a tank and exposed to solar radiation, with running surface seawater to control temperature similar to the field condition. The processes of photosynthesis and respiration in phytoplankton occur simultaneously, but in opposite directions; so accumulation of oxygen during a long-term incubation will accelerate the respiration and cause "bottle effects," and subsequently affect the measured results (Gao et al. 2012). The smaller the culture bottle, the easier it is to cause "bottle effects"; the incubation time should thus not be too long when estimating the primary productivity in coastal waters, and it is ideal for 2–3 h (Gao et al. 2007a; Li et al. 2011a, b). In pelagic waters, the incubation time can be properly extended to obtain stronger ^{14}C signals. On the other hand, to overcome the difficulties in actual operation, the determination of offshore primary productivity usually involves incubating the water samples of different depth with ^{14}C in a tank, with running surface water to control temperature. However, the temperature often sharply decreases with water depth, such as in the South China Sea where severe stratification prevails in summer, which makes a thermocline depth of ~50 m and temperature differences of 8–10 °C between the surface and bottom of the UML (Fig. 16.1a). In this case, the temperature-caused effects on primary production need to be considered. It is estimated that the primary production of the chlorophyll a maximum layer is overestimated by 5–40% in the open waters of the South China Sea if using surface water to control temperature during the incubation (Fig. 16.1d).

16.4 Advantages and Disadvantages of the ^{14}C Method

Using radiocarbon (^{14}C) isotope to measure phytoplankton photosynthetic carbon fixation is a very classical and sensitive method; it has the advantages of simple operation and high sensitivity, etc., and is thus most commonly used for marine

primary production investigations. However, ^{14}C is radioactive and partly exists in the form of $^{14}CO_2$, so it is easy to enter the body through breathing and accumulate to cause harm due to its long half-life (5200 years). Secondly, ^{14}C is very expensive with 5 mCi $NaH^{14}CO_3$ solution costing ¥10,000 RMB, and the cost of using ^{14}C is much higher to measure marine primary productivity. Furthermore, processes of photosynthesis and respiration occur simultaneously within phytoplankton cells, but in opposite directions; so the amount of fixed carbon fixation using ^{14}C method is obtained under the balanced condition of these two physiological processes. If the incubation time is short enough, we often consider this carbon fixation as gross because the organic carbon produced by photosynthesis has not yet been consumed by respiration. But if the incubation time is long enough, photosynthesis and respiration metabolisms reach balance. In this condition, we can get the net primary production as part of the fixed carbon has been consumed by respiration.

16.5 Application of the ^{14}C Method in the Laboratory

Radioactive isotope (^{14}C) tracer technology is widely used not only in estimation of in situ marine primary production, but also in indoor physiological studies of photosynthetic carbon fixation. For example, Yang and Gao (2012) studied the responses of the model diatom species *Thalassiosira pseudonana* to light levels (*P–I* curve) and inorganic carbon concentrations (*P*–C curve) using the ^{14}C method, and Wu et al. (2010) also used this method to study the responses of the diatom *Phaeodactylum tricornutum* to the concentrations of inorganic carbon. Similarly, Xu et al. (2011) and Jin et al. (2013) used the ^{14}C method to study the photosynthetic carbon fixation of the coccolithophorids *Emiliania huxleyi* and *Gephyrocapsa oceanica* in the laboratory. The treatment processes are similar to those described above. Briefly, the algae samples were incubated with ^{14}C solution and collected with filters, acidified and dried to remove the unfixed ^{14}C; and then, an aliquot of cocktail is added to each vial and counted with a liquid scintillation counter. After this, the algae photosynthetic carbon fixation was calculated with the equation described above.

References

Behrenfeld MJ, Falkowski PG (1997) A consumer's guide to phytoplankton primary productivity models. Limnol Oceanogr 42:1479–1491

Campbell DA, Hossain Z, Cockshutt AM, Zhaxybayeva O, Wu H, Li G (2013) Photosystem II protein clearance and FtsH function in a diatom *Thalassiosira pseudonana*. Photosynth Res 115(1):43–54

Chen YL (2000) Comparisons of primary productivity and phytoplankton size structure in the marginal regions of southern East China Sea. Cont Shelf Res 20:437–458

Chen Q, Huang L (1997) Study on ecological process of nansha islands waters (I). Scientific Press, Beijing, pp 1–15. (in Chinese)

Eilers PHC, Petters JCH (1988) A model for the relationship between light intensity and the rate of photosynthesis in phytoplankton. Ecol Model 42:199–215
Fuentes-Lema A, Sobrino C, González N, Estrada M, Neale PJ (2015) Effect of solar UVR on the production of particulate and dissolved organic carbon from phytoplankton assemblages in the Indian Ocean. Mar Ecol Prog Ser 535:47–61
Gao K, Li G, Helbling EW, Villafañe VE (2007a) Variability of UVR-induced photoinhibition in summer phytoplankton assemblages from a tropical coastal area of the South China Sea. Photochem Photobiol 83:802–809
Gao K, Wu Y, Li G, Wu H, Villafañe VE, Helbling EW (2007b) Solar UV radiation drives CO2 fixation in marine phytoplankton: a double-edged sword. Plant Physiol 144:54–59
Gao K, Xu J, Zheng Y, Ke C (2012) Measurement of benthic photosynthesis and calcification in flowing-through seawater with stable carbonate chemistry. Limnol Oceanogr Meth 10:555–559
Holm-Hansen O, Helbling EW (1995) Técnicas para la medición de la productividad primaria en el fitoplancton. In: Alveal K, Ferrario ME, Oliveira EC, Sar E (eds) Manual de métodos ficológicos. Universidad de Concepción, Concepción, pp 329–350
Huang B, Hong H, Wang H (1999) Size-fractionated primary productivity and the phytoplankton-bacteria relationship in the Taiwan Strait. Mar Ecol Prog Ser 183:29–38
Jin P, Gao K, Villafañe VE, Campbell DA, Helbling EW (2013) Ocean acidification alters the photosynthetic responses of a Coccolithophorid to fluctuating ultraviolet and visible radiation. Plant Physiol 162:2084–2094
Li G, Gao K (2012) Variation in UV irradiance related to stratospheric ozone levels affects photosynthetic carbon fixation of winter phytoplankton assemblages in the South China Sea. Mar Biol Res 8:670–676
Li G, Wu Y, Gao K (2009) Effects of typhoon Kaemi on coastal phytoplankton assemblages in the South China Sea, with special reference to the effects of solar UV radiation. J Geophys Res 114: G04029
Li G, Gao K, Gao G (2011a) Differential impacts of solar UV radiation on photosynthetic carbon fixation from the coastal to offshore surface waters in the South China Sea. Photochem Photobiol 87:329–334
Li G, Gao K, Yuan D, Zheng Y, Yang G (2011b) Relationship of photosynthetic carbon fixation with environmental changes in the Jiulong River estuary of the South China Sea, with special reference to the effects of solar UV radiation. Mar Pollut Bull 62:1852–1858
Li G, Huang L, Liu H, Ke Z, Lin Q, Ni G, Yin J, Li K, Song X, Shen P, Tan Y (2012a) Latitudinal variability (6°S-20°N) of early-summer phytoplankton species composition and size-fractioned productivity from the Java Sea to the South China Sea. Mar Biol Res 8:163–171
Li G, Lin Q, Ni G, Shen P, Fan Y, Huang L, Tan Y (2012b) Vertical patterns of early-summer chlorophyll a concentration in the Indian Ocean, with special reference to the variation of deep chlorophyll maximum. J Mar Biol 2012:e801248
Li G, Ke Z, Lin Q, Ni G, Shen P, Liu H, Yin J, Li K, Huang L, Tan Y (2012c) Longitudinal patterns of spring-intermonsoon phytoplankton biomass, species compositions and size structure in the Bay of Bengal. Acta Oceanol Sin 31:121–128
Li G, Ni G, Shen P, Yi R, Huang L, Tan Y (2016) Spatial variability in summer phytoplankton community from offshore to coastal surface waters of the Northwestern South China Sea. Trop Geogr 36(1):101–107
Steeman Nielsen E (1952) The use of radiocarbon (^{14}C) for measuring organic production in the sea. J Cons Int Explor Mer 18:117–140
Wu Y, Gao K, Riebesell U (2010) CO_2-induced seawater acidification affects physiological performance of the marine diatom *Phaeodactylum tricornutum*. Biogeosciences 7:2915–2923
Xu K, Gao K, Villafañe VE, Helbling EW (2011) Photosynthetic responses of *Emiliania huxleyi* to UV radiation and elevated temperature: roles of calcified coccoliths. Biogeosciences 8:1441–1452
Yang G, Gao K (2012) Physiological responses of the marine diatom *Thalassiosira pseudonana* to increased pCO_2 and seawater acidity. Mar Environ Res 79:142–151

Chapter 17
Photorespiration and Dark Respiration

Dinghui Zou and Juntian Xu

Abstract Dark respiration (mitochondrial respiration) occurs both in the light and in darkness. Here the principle of determination of mitochondrial respiration in the light is described. The Kok method is introduced to estimate the rate of mitochondrial respiration in the light by using a LCA-4infrared gas analyzer with *Ulva lactuca* thalli as an example.

Keywords Dark respiration · The Kok method · Photosynthetic CO_2 exchange · *Ulva lactuca*

17.1 Introduction

Dark respiration (non-photorespiratory mitochondrial CO_2 release) is a pivotal metabolic activity during algal growth and maintenance, producing usable energy (ATP), reductants [NAD(P)H] and carbon skeleton intermediates to support other metabolic processes of the algae (Amthor 2000; Atkin et al. 2005). It has been well documented that plants or algae respire roughly half of their daily photosynthetic carbon gain, and therefore dark respiration plays an important role in the carbon budget of the algae. Dark respiration (mitochondrial respiration) occurs both in the light and in darkness. During the light, dark respiration may control stromal redox balance in the course of the photosynthetic process. At the same time, the respiration processes aid in minimizing the production of potentially damaging reactive oxygen species through re-oxidizing excess cellular redox equivalents generated by chloroplasts under excess irradiance conditions. Additionally, dark respiratory activity

D. Zou (✉)
School of Environment and Energy, South China University of Technology, Guangzhou, China
e-mail: dhzou@scut.edu.cn

J. Xu
School of Marine Science and Fisheries, Jiangsu Ocean University, Lianyungang, Jiangsu, China

K. Gao et al. (eds.), *Research Methods of Environmental Physiology in Aquatic Sciences*, https://doi.org/10.1007/978-981-15-5354-7_17

occurring in the light supplies ATP for the repair of photosynthetic proteins (in particular the D1 protein of PSII) degraded by photoinhibition, protecting against photoinhibitory damage of the photosynthetic apparatus.

It is generally assumed that dark respiration has the same rate in the light (R_L) as in darkness (R_D). However, in terrestrial higher plants there is growing evidence showed that R_L varies between 25% and 100% of dark respiration in darkness (R_D). This suggests that light partially inhibits dark respiration in photosynthetic tissue (Shapiro et al. 2004). The inhibition of dark respiration in the light is even evident at irradiances as low as 3–50 μmol photons m^{-2} s^{-1}, regardless of the red, blue, or white light (Atkin et al. 2005).

The Kok method can be used to determine the rate of R_L (Kok 1948; Shapiro et al. 2004). Under normal photosynthetic CO_2 conditions, the CO_2 exchange rates under a series of low light conditions are analyzed, and the R_L rate can be calculated. At very low light levels, the response rate of CO_2 exchange rate to light intensity is linear, and its slope (i.e., photosynthetic efficiency) is relatively steep. However, in the vicinity of the light compensation point (near the level of illumination at which the net photosynthetic rate is 0), a sudden break in this linear response occurs, i.e., the slope becomes smaller. This change is known as the "Kok effect." The physiological reason is that the inhibition of light to dark respiration gradually disappears (Kok 1948; Villar et al. 1994). Therefore, above the light compensation point, the linear section of the light curve above the break extrapolates to the *Y* axis to an estimate of R_L, while the line at irradiance below the break stretches to R_D, which is determined at zero irradiance.

17.2 Materials and Methods

17.2.1 Algal Materials

Thalli of *Ulva lactuca* L. were collected at low tide from the middle intertidal zone along coast of Nanao Islang, Shantou, China, and rinsed of accumulated sediments. Samples, sealed in plastic bags with some seawater in an insulated cooler (4 °C), were transported to the laboratory within 4 h, then were maintained in artificial seawater (450 mM NaCl; 10 mM KCl; 10 mM $CaCl_2$; 30 mM $MgSO_4$; 2.2 mM $NaHCO_3$) in glass aquarium containers. They received a light irradiance of about 100 μmol m^{-2} s^{-1} (PAR) from fluorescent tubes for 12 h out of every 24 h and a room temperature of 25 ± 1 °C. The seawater was aerated and renewed by half of the amount every day. Samples were used for the experiments within 2–5 days of laboratory maintenance, a period during which the thalli exhibited stable photosynthetic and respiratory activities. After 5 days of laboratory maintenance, the remaining algae were thrown away and fresh materials were collected again. For experiments, the algal thalli were taken out from the seawater and excess surface water drops on the thalli were gently removed with paper tissue.

17.2.2 Instruments

Infrared gas analyzer (LCA-4, Analytical Development Co., UK).

17.2.3 Method

Photosynthetic rates of the emersed *Ulva lactuca* thalli were measured as CO_2 exchange in an open-flow gas-exchange system, using an infrared gas analyzer (LCA-4, Analytical Development Co., UK) at ambient atmospheric CO_2 concentrations (Zou et al. 2007). The light source was a metal halide lamp (220/240 V, 150 W, Hikaric-J) suspended above the photosynthetic leaf chamber. Temperature was controlled at 25 °C by maintaining the chamber in a temperature-controlled cabinet. About 1.5 g fresh weight of algal thalli were spread out in the photosynthetic chamber. Net photosynthesis (P_n) [μmol CO_2 g(DW)$^{-1}$ h^{-1}] was calculated as follows:

$P_n = \Delta C \times F \times 60 \times 273/[(273 + T) \times 22.4 \times \mathrm{DW}]$,where ΔC is the difference in CO_2 concentration (ppm) between the inlet and outlet air, F is the gas flow rate (L/min), T is temperature (°C) and DW is the dry weight (g; which was determined after each experiment by oven drying, 80 °C for 24 h).

Eight irradiances between 0 and 120 μmol photons m^{-2} s^{-1} were used to analyze the photosynthetic responses at low irradiance. Irradiance was adjusted by altering the distance between the light source and the photosynthetic chamber. R_L was estimated by the Kok method described above. A representative light-response curve for emersed *U. lactuca* at low irradiance is presented in Fig. 17.1. R_D was

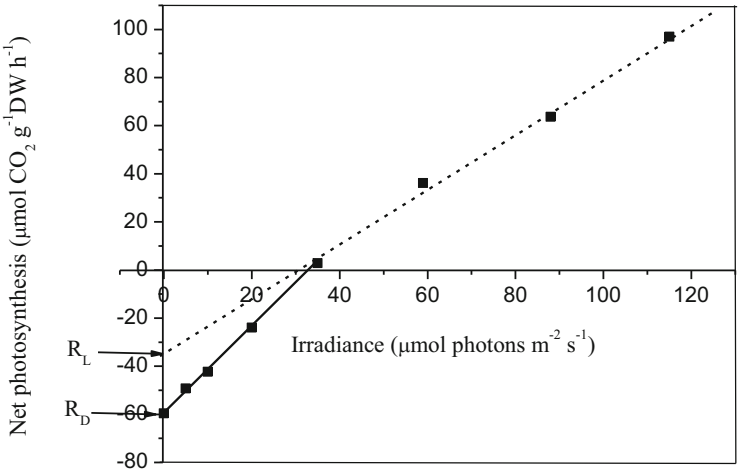

Fig. 17.1 The light–CO_2 exchange rates response curve at low levels light irradiance in *Ulva lactuca* thalli (Zou et al. 2007)

determined at zero irradiance by turning off the light source and covering the chamber with a black cloth.

References

Amthor JS (2000) The McCree-de Wit-Penning de Vries-Thornley respiration paradigms: 30 years later. Ann Bot 86:1–20

Atkin OK, Bruhn D, Hurry VM, Tjoelker MG (2005) The hot and the cold: unraveling the variable response of plant respiration to temperature. Func Plant Biol 32:87–105

Kok B (1948) A critical consideration of the quantum yield of *Chlorella* photosynthesis. Enzymology 13:1–56

Shapiro JB, Griffin KL, Lewis JD, Tissue DT (2004) Response of *Xanthium strumarium* leaf respiration in the light to elevated CO_2 concentration, nitrogen availability and temperature. New Phytol 162:377–386

Villar R, Held AA, Merino J (1994) Comparison of methods to estimate dark respiration in the light in leaves of two woody species. Plant Physiol 105:167–172

Zou DH, Gao KS, Xia JR, Xu ZG, Zhang X, Liu SX (2007) Responses of dark respiration in the light to desiccation and temperature in the intertidal macroalga, *Ulva lactuca* (Chorophyta) during emersion. Phycologia 46:363–370

Chapter 18
Carbon Dioxide vs. Bicarbonate Utilisation

Sven Beer, Mats Björk, and John Beardall

Abstract While CO_2 is the external inorganic carbon (C_i) form used for photosynthesis in terrestrial plants, the higher concentration of bicarbonate (HCO_3^-) in most water bodies renders this ionic C_i form the preferred external C_i source for most cyanobacteria, microalgae, and submerged macrophytes. The equilibrium concentrations of these two C_i forms depend largely on pH. For example, at today's average seawater pH of 8.1, the HCO_3^- concentration is approximately 120 times that of dissolved CO_2; in most lakes and streams pH values are lower so this ratio is reduced in favour of CO_2 (but this C_i form is seldom higher than that of HCO_3^-), and HCO_3^- utilisation becomes less advantageous. On the other hand, the affinity of aquatic phototrophs for CO_2 is much higher than that for HCO_3^-, and the preferred C_i form will thus be a compromise between the affinities for, and concentrations of, the two C_i forms. This chapter will outline ways to determine whether, and to what degree, external CO_2 or HCO_3^- is utilised by various aquatic phototrophs.

Keywords Aquatic plants · Photosynthesis · CO_2 · Bicarbonate utilisation · pH-drift · CCM

S. Beer (✉)
School of Plant Sciences and Food Security, Tel Aviv University, Tel Aviv, Israel
e-mail: svenb@ex.tau.ac.il

M. Björk
Department of Ecology, Environment and Plant Sciences, Stockholm University, Stockholm, Sweden
e-mail: mats.bjork@su.se

J. Beardall
School of Biological Sciences, Monash University, Clayton, VIC, Australia
e-mail: john.beardall@monash.edu

K. Gao et al. (eds.), *Research Methods of Environmental Physiology in Aquatic Sciences*, https://doi.org/10.1007/978-981-15-5354-7_18

18.1 Introduction

Today's (2019) average atmospheric CO_2 concentration is slightly above 400 ppm (or 18 μM, and will continue to rise). This corresponds to a 14 μM air-equilibrium concentration of dissolved CO_2 at 20 °C and a salinity of 35 (the latter of which is typical for seawater). As CO_2 dissolves in water, it also reacts with water molecules so as to form carbonic acid (H_2CO_3), which dissociates to form bicarbonate (HCO_3^-) and carbonate (CO_3^{2-}) ions according to

$$CO_2 + H_2O \leftrightarrow H_2CO_3 \leftrightarrow HCO_3^- + H^+ \leftrightarrow CO_3^{2-} + 2H^+.$$

As indicated by the protons, the equilibrium concentrations of the different forms of inorganic carbon (C_i) depend strongly on pH, while the CO_2 concentration in "open," air-equilibrated, systems depends mainly on that of the overlying atmosphere. At today's average open-sea water pH of 8.1, the concentration of HCO_3^- is ~1700 μM and that of CO_3^{2-} ~300 μM (while that of H_2CO_3 is negligible). Many freshwater and, especially, marine phototrophs (here summarily often referred to as "plants") can utilise HCO_3^- (but not CO_3^{2-}) as their external source of C_i for photosynthesis, and the advantage becomes clear when considering its ca. 120 times higher concentration in seawater than that of CO_2. In air-equilibrated freshwater lakes and streams, the concentration of HCO_3^- is higher than that of CO_2 at any pH value above ca. 6. Thus, HCO_3^- use may become advantageous in many natural aquatic settings (see however, below, the fact that the affinity for CO_2 is always higher than that for HCO_3^-). Before considering how to determine CO_2 vs. HCO_3^- use in aquatic phototrophs, a short explanation of the mechanisms of HCO_3^- utilisation is in order.

While many aquatic photosynthetic organisms can utilise HCO_3^- from the surrounding water, all ultimately use CO_2 for the fixation, via ribulose-1,5-bisphosphate carboxylase/oxygenase (Rubisco), and further reduction to carbohydrates in the Calvin cycle. This implies that somewhere along the way from the external medium, HCO_3^- has to be converted ("dehydrated," via H_2CO_3) to CO_2. This can happen extracellularly (in most macrophytes and in many microalgae), within diffusion boundary layers (including the cell wall), or intracellulary (in e.g., the macroalga *Ulva* spp. and many unicellular algae and cyanobacteria) after HCO_3^- has been taken up into the photosynthesizing cells. In both cases, the interconversion between CO_2 and HCO_3^- (via H_2CO_3) is catalysed by either extra- or intracellularly acting forms of the enzyme carbonic anhydrase (CA). For a comprehensive account of how marine plants utilise external C_i sources, see Beer et al. (2014).

18.2 Methodology

There is a range of techniques that can be used to distinguish between HCO_3^- and CO_2 use.

18.2.1 Isotope Disequilibria

The isotopic disequilibrium technique makes use of the relatively slow uncatalysed equilibration between CO_2 and HCO_3^-. To a suspension of cells in an alkaline medium (pH 8.5 is commonly used), a spike of a solution containing ^{14}C-labelled C_i in neutral pH solution is added. Samples are then taken at short intervals (we have found that 10 s intervals for the first minute, then longer intervals after that, works adequately). The slow interconversion between HCO_3^- and CO_2 following injection of the neutral pH ^{14}C-labelled spike into the alkaline pH cell suspension allows differential labelling of the carbon species with ^{14}C over time periods of a few minutes. In the neutral pH spike solution, $^{14}CO_2$ represents 20% of the total C_i pool. In contrast, in the cell suspension at alkaline pH, CO_2 at equilibrium accounts for only 0.4% (at pH 8.5) of the total C_i once equilibrium is reached. Consequently, the specific activity (dpm mol^{-1}) of CO_2 in the ^{14}Ci-spiked solution is initially high, but decays exponentially to an equilibrium value over the duration of the assay. If an algal species takes up CO_2 only, the ^{14}C incorporation rate should reflect these changes in the specific activity and rates of incorporation of ^{14}C will be initially high, but will gradually slow down to a lower, steady, rate as the system comes into equilibrium. Conversely, if the cells are taking up HCO_3^-, uptake is at a steady, linear rate. Experiments are run with cells with and without the addition of external CA such as acetazolamide or dextran-bound sulphonamide. The samples removed at various times are taken, treated with acid, and evaporated to dryness to drive off any remaining $^{14}C_i$. The radioactivity in the samples is then measured (see Chap. 16), fitted to the following equation, and solved for *f*. (Comparison of data with and without extracellular CA inhibitors can be used to quantify the external CA activity, see Elzenga et al. 2000 and Rost et al. 2007).

$$\mathrm{DPM_t} = V_t(1-f)(\alpha_1 t + (\Delta \mathrm{SA_{CO_2}}/\mathrm{SA_{DIC}})(1-\mathrm{e}^{-\alpha_1 t}))/\alpha_1$$
$$+V_t(f)(\alpha_2 t + (\Delta \mathrm{SA_{HCO_3^-}}/\mathrm{SA_{DIC}})\,(1-\mathrm{e}^{-\alpha_2 t}))/\alpha_2$$

where V_t is the total rate of C_i uptake, f is the fraction of uptake attributable to HCO_3^-, α_1 and α_2 are the first order rate constants for CO_2 and HCO_3^- hydration and dehydration, respectively, for the experimental temperature and salinity (calculated as described by Espie and Colman (1986), ΔSA_{CO_2} and $\Delta SA_{HCO_3^-}$ are the differences between the initial and equilibrium values of the specific ^{14}C activity of CO_2 and HCO_3^-, respectively, and SA_{DIC} is the specific activity of all C_i forms at equilibrium.

This approach is *quantitative*, and is sensitive enough for use in natural phytoplankton populations. It is, however, only really suitable to use with unicellular phototrophs as there would be complexities in macroalgae and seagrasses from equilibration of the ^{14}C spike through the tissue, potentially masking effects of equilibria between C_i species.

18.2.2 pH Dependence of $K_{0.5}$ Values

Examination of the pH dependence of photosynthesis vs. C_i curves (see Chap. 20) can give a *qualitative* indication of whether phototrophs are primarily using HCO_3^- or CO_2. In essence, photosynthesis vs. C_i concentration curves are performed in buffers at different pH values, and the C_i concentrations giving half-saturation rates of photosynthesis, $K_{0.5}$, are used to work out the corresponding $K_{0.5}$ values for CO_2 and HCO_3^-. If the values of $K_{0.5}CO_2$ are independent of pH, but $K_{0.5}HCO_3^-$ increases with pH, that is taken as indicating CO_2 use. Conversely, HCO_3^- use would be indicated by a large decrease in $K_{0.5}CO_2$ as pH increases, but little or no change in $K_{0.5}HCO_3^-$.

The above approach was used by Burns and Beardall (1987) to show HCO_3^- use in three marine microalgae, but would also be applicable to use with macroalgae (see below). It would *indicate* if cells can use HCO_3^- but would not allow determination of whether such HCO_3^- use occurred by direct uptake of via conversion to CO_2 via externally acting CA in the periplasmic space. It has the advantage of being relatively easy to carry out with established techniques of ^{14}C uptake or oxygen evolution, but the disadvantage that it does not allow quantitative measurements of uptake of the two C_i forms.

18.2.3 Photosynthetic Rates at Different pH Values

The most common way to determine CO_2 vs. HCO_3^- utilisation in macroalgae and seagrasses has been by changing pH values around a plant while measuring photosynthetic rates and calculating the distribution of the various C_i forms at those specific pHs. The pH can either be changed by the plants themselves (in so-called "pH-drift" experiments) or can be altered by injecting acids or bases into closed or open systems while measuring photosynthetic rates. Let's start with the latter approach, in closed systems.

Plants, or plant tissues (seagrass leaves, parts of algal thalli, microalgae, or cyanobacteria), are inserted into a photosynthesis-measuring system (e.g., a water-jacketed vial fitted with O_2 and pH electrodes, something like that pictured in Fig. 18.1). Then, during steady-state photosynthesis, small aliquots of an acid or base are injected into the system while recording the change in photosynthetic rates as well as pH. The concentrations of CO_2 and HCO_3^- can then be calculated for each

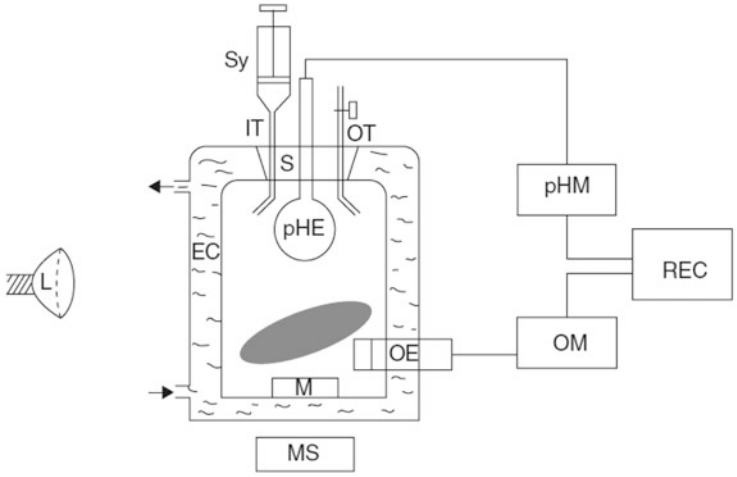

Fig. 18.1 Experimental setup for measuring rates of photosynthetic O_2 evolution at various pH values. This closed-system setup consists of a water-jacketed vial (EC) containing seawater and an *Ulva* disc (grey ellipse) irradiated by a light source (L), and a magnet (M) turned by a magnetic stirrer (MS), an O_2 and pH electrode (OE and pHE) connected to an O_2 and pH meter (OM and pHM) and a recorder (REC) or computer. Acids or bases, or CO_2-saturated water, are injected with a Hamilton syringe (Sy) via an inlet tube (IT) through a stopper (S) and overpressure is released via an outlet tube (OT) (Adapted from Beer et al. (1977); Copyright with permission from Journal of Experimental Botany)

pH value obtained (see below). When performing experiments in which rates of photosynthetic O_2 evolution are to be measured in such closed systems, it is important not to let the plants elevate the water concentration of O_2 too much. This is because O_2 itself may affect photosynthetic rates of some organisms via e.g., enhanced photorespiration (Buapet et al. 2013). Also, if O_2 bubbles form in the system, this will grossly underestimate the dissolved O_2 concentrations (because the bubbles will contain a much higher concentration of O_2 than an equal volume of water). For this, it may be advisable to sparge the seawater with N_2 for a short time period so as to lower initial O_2 concentrations just before closing the system. Secondly, one should be aware of the fact that photosynthesising organisms decrease the C_i concentration during, especially long-term, incubations, thus possibly limiting photosynthetic rates.

Alternatively, pH can be altered in open systems. If so, then the air-equilibrated CO_2 concentration will not depend on pH, but that of HCO_3^- will. (Again, CO_3^{2-} cannot be used by any aquatic phototroph investigated so far.) In such open systems, it is important to let the various C_i forms equilibrate after each pH alteration, and the resulting CO_2 concentration equilibrate with the air (enhanced e.g., by sparging with air), prior to measuring photosynthetic rates (by transferring both the plants and their media to a closed system for the actual measurement).

Examples of results from closed (a) and open (b) system pH experiments are depicted in Fig. 18.2 (from Beer and Eshel 1983). The starting point was normal

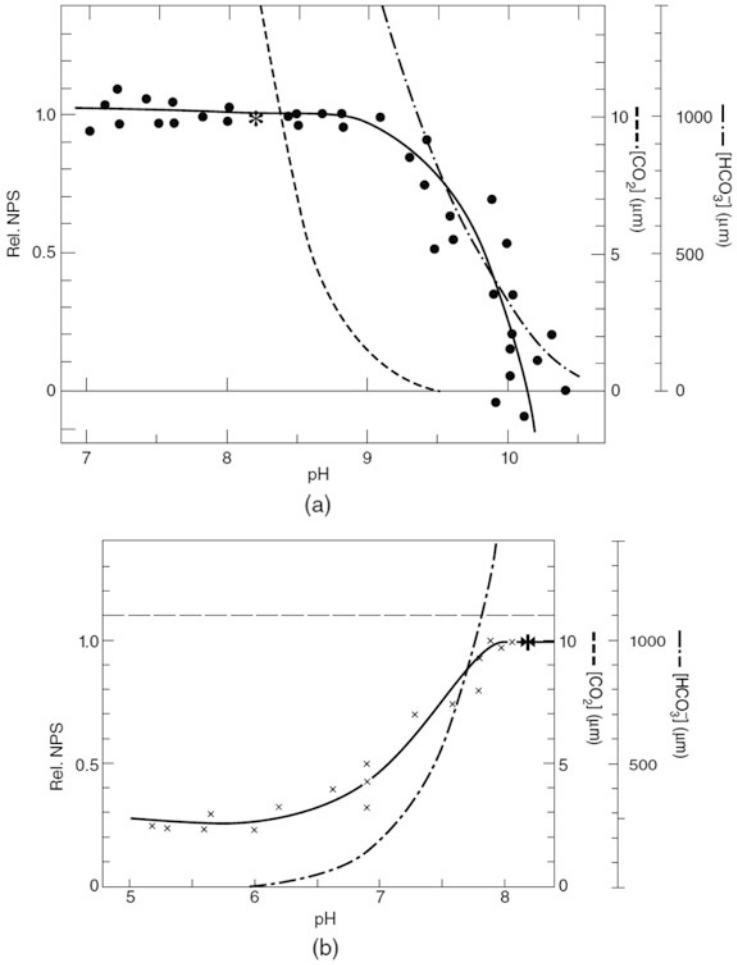

Fig. 18.2 Photosynthetic O_2 evolution responses of *Ulva* sp. to pH in a closed (**a**) and open (**b**) system. (**a**) Rates of apparent (net) photosynthesis (Rel. NPS, full line, as supported by the dot-data) at the various pH values generated in the closed system (Fig. 18.1). Inserted are also the calculated concentrations of CO_2 and HCO_3^- as a function of pH. (**b**) Rates of Rel. NPS (full line, as supported by the *x*-data) at various pH values in open beakers where the seawater had been equilibrated with air by bubbling following the pH changes. Inserted are also CO_2 and HCO_3^- concentrations (From Beer and Eshel (1983); Copyright with permission from Journal of Experimental Marine Biology and Ecology, Elsevier)

seawater at (in 1983) pH 8.2 and a total C_i concentration of 2.2 mM (asterisk in Fig. 18.2). The system was then closed with a piece of algal thallus inside (a). After steady-state photosynthesis was reached, HCl or NaOH was injected to result in various pH values (along the *x*-axis), and the changes in photosynthetic rates were recorded. The CO_2 (broken lines) and HCO_3^- (broken-dotted lines) concentrations were then calculated and the resulting photosynthesis vs. HCO_3^- concentration

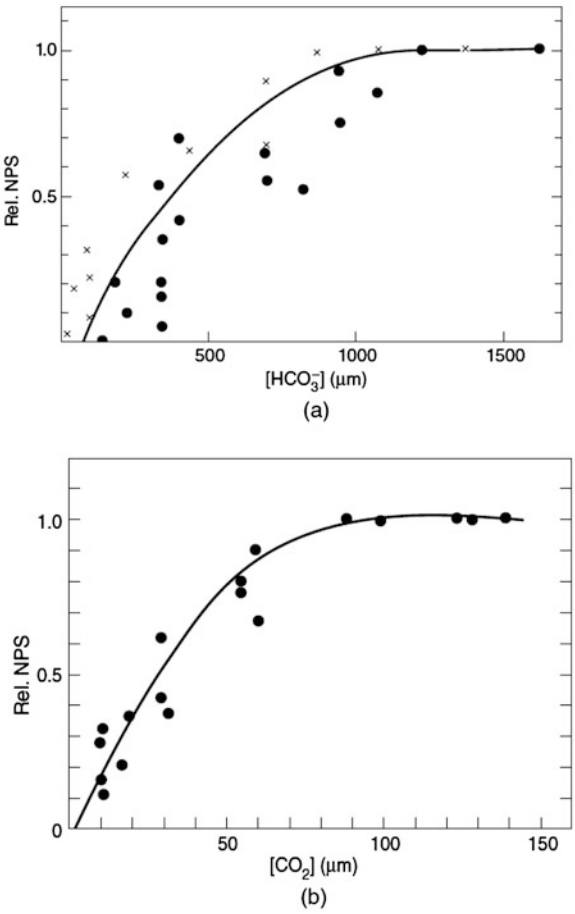

Fig. 18.3 Rates of photosynthetic O_2 evolution of the macroalga *Ulva* sp. as a function of HCO_3^- (**a**) and CO_2 (**b**) concentrations. (**a**) The same rates of apparent (net) photosynthesis (Rel. NPS) as obtained in Fig. 18.2 were plotted against calculated concentrations of HCO_3^-. (**b**) Rates were plotted against calculated concentrations of CO_2 after various amounts of a CO_2-saturated solution was injected into the closed system (From Beer and Eshel (1983); Copyright with permission from Journal of Experimental Marine Biology and Ecology, Elsevier)

plotted as in Fig. 18.3a. As can be seen in panel b of Fig. 18.2, photosynthetic rates did not reach 0 at pH values <6.0 (where HCO_3^- concentrations are virtually 0), meaning that rates there were supported by the CO_2 concentration in equilibrium with air. In order to obtain rates as a function of CO_2 concentration, another approach was taken. The system containing the plant sample was closed into C_i-free synthetic seawater (in which all C_i, including CO_2, had been removed by acidifying and sparging with N_2) and small aliquots of CO_2-saturated water were injected into the system while following O_2 evolution (see Beer and Eshel 1983). The result of such a closed-system experiment is depicted in Fig. 18.3b.

Calculations of the various C_i concentrations as a function of pH, carbonate alkalinity, temperature and salinity, and aerial partial pressures of CO_2 for open systems, can be carried out using the Excel program CO_2Sys.xls (Pierrot et al. 2006).

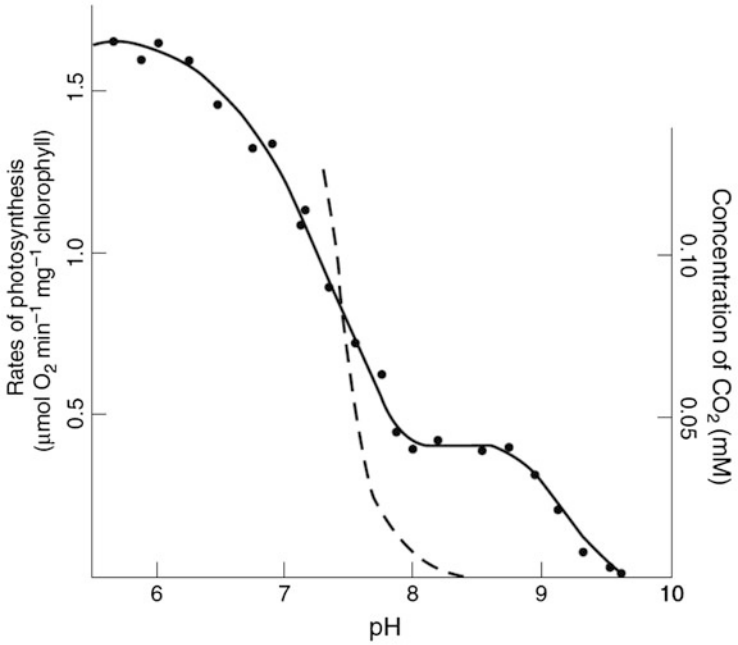

Fig. 18.4 Rates of photosynthetic O_2 evolution of the seagrass *Cymodocea nodosa* as a function of pH in a closed system such as depicted in Fig. 18.1. See text for details (From Beer and Waisel (1979); Copyright with permission from Aquatic Botany, Elsevier)

From the above example of *Ulva* sp., one can draw the conclusion that photosynthesis of this macroalga is saturated by today's seawater HCO_3^- concentration (~1700 µM) but that the affinity for CO_2 is much higher (saturation reached at ~100 µM, as compared to ~1000 µM for HCO_3^-). It seems to be the case for many marine macroalgae that the affinity for CO_2 is much higher than that for HCO_3^-, but given the low availability of CO_2 in seawater (~14 µM), together with the much lower diffusion rates of solutes in water than in air, HCO_3^- with its much higher concentration is still the main external C_i source for photosynthesis. This is not generally the case for seagrasses (or marine angiosperms), where the HCO_3^- utilisation system seems to be less effective. Therefore, when adding CO_2 to an already HCO_3^--saturated seawater medium, photosynthesis often increases. This is illustrated in Fig. 18.4 below: Photosynthetic rates were stable around the normal seawater pH at the time (8.2 rather than 8.1 today), i.e., at HCO_3^- saturation. As pH was altered in the closed system from 8.2 upward, photosynthesis decreases as a function of decreasing HCO_3^- concentrations (CO_2 concentrations, the dotted line, in this pH range are virtually nil). However, as pH was lowered, photosynthesis increased as a function of increasing CO_2 concentrations. This difference between marine macroalgae (saturated at today's oceanic C_i composition) and seagrasses (increasing their photosynthetic rates as CO_2 levels increase) has been interpreted as a likely scenario for future CO_2 level rises (e.g., Beer and Koch 1996).

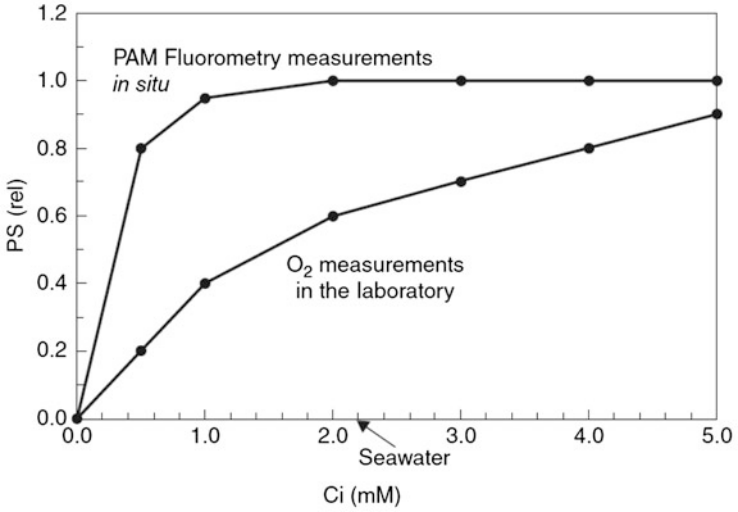

Fig. 18.5 Principal differences between O_2 evolution and PAM-fluorometry based electron transport rates for many seagrasses. See text for details (Drawing by Sven Beer; Copyright (2014) with permission from Wiley-Blackwell)

An additional, precautionary, note when performing experiments in order to determine photosynthetic responses to CO_2 vs. HCO_3^- is that the way photosynthesis is measured may affect the results. For example, when using pulse-amplitude modulated (PAM) fluorometry in situ (see Chaps. 25 and 26) rather than O_2 evolution in the laboratory, some tropical seagrasses that were previously thought to be C_i-limited in today's oceans were found to be C_i-saturated (Schwartz et al. 2000, see also Fig. 18.5). The general reason for this is most probably that measurements in laboratory-based experiments using excised leaves crammed into small measuring vials generate conditions that are very unnatural for the plants, while in situ measurements of whole plants, still attached to their natural substrates, reflect, well, more natural conditions.

Another, simpler but less detailed, way to determine CO_2 vs. HCO_3^- use is by pH-drift experiments. One advantage of this approach is that here the plants themselves alter the pH values around them due to photosynthesis and respiration and, thus, only the carbonate alkalinity decreases (and not the total alkalinity), which is closer to what happens in natural systems. Here, samples (cell suspensions or pieces of algal thalli or seagrass leaves) are incubated in closed containers in the light with periodic pH measurements taken until a steady state is reached. Final pH values greater than approximately 9 are taken as evidence of a capacity to use HCO_3^- as CO_2 concentrations at pHs above that value are vanishingly small. As a precaution, samples should be re-equilibrated with air afterward to ensure there is no change in total alkalinity for e.g., OH^- efflux associated with NO_3^- assimilation and acid–base balance by the cells/tissue.

There is a connection between HCO_3^- utilisation and CO_2 concentrating mechanisms (CCM): Most marine macroalgae possess CCMs. However, their CCM is (with very few exceptions) not based on the initial C_i fixation via phosphoenolpyruvate carboxylase and the final fixation and reduction of CO_2 in the bundle sheath cells as found in terrestrial C_4 plants. Also, Crassulacean Acid Metabolism (CAM) seems to be rare in aquatic, and even more so in marine, plants. Instead, their CCM is based on active utilisation of extracellular HCO_3^- (or, in some cyanobacteria, CO_2) as is described in Chap. 20.

18.2.3.1 Kinetics of O_2 Evolution vs. Uncatalyzed CO_2 Supply from HCO_3^-

In this qualitative approach, the data from photosynthesis vs. C_i curves are taken, and photosynthesis expressed as rates of O_2 evolution per mL per unit time (and can be further converted to rates of carbon assimilation using a photosynthetic quotient, PQ, of 1).

It is possible to also calculate the rates of uncatalyzed CO_2 supply from the dehydration of HCO_3^- using the equations of Miller and Colman (1980) and expressing rates of carbon-dependent O_2 evolution and CO_2 supply in the same units (e.g., nmol ml^{-1} min^{-1}), both as a function of C_i, which allows easy comparisons (see Burns and Beardall 1987, Fig. 2). If rates of oxygen evolution (= rates of C_i assimilation) are greater than rates of CO_2 supply, then this is taken as evidence that cells are using HCO_3^-.

The advantage of this approach is that photosynthesis vs. C_i curves can be used to gain information about CO_2 or HCO_3^- preferences. However, experiments must be run with sufficiently high biomass so that rates of photosynthesis are limited by, or exceed, rates of CO_2 supply, so some trial and error should be involved.

18.2.3.2 MIMS

The membrane inlet mass spectrometric (MIMS) technique also makes use of the chemical disequilibrium between CO_2 and HCO_3^- during light-dependent C_i uptake to differentiate between the fluxes of these two C_i species into algal cells (Badger et al. 1994; Rost et al. 2007). MIMS systems are described in Chap. 22.

Essentially, the MIMS is used to determine C_i fluxes from simultaneous measurements of O_2 and CO_2 during consecutive light and dark intervals. During the dark periods, known amounts of C_i are added just before the start of the following light period of ~2–5 min. Rates of O_2 consumption in the dark provide measurements of respiration and rates of O_2 production in the light are used as direct estimates of net carbon fixation, assuming a PQ of 1. Net CO_2 uptake is calculated from the steady-state rate of CO_2 depletion at the end of the light period, corrected for the CO_2/HCO_3^- interconversion in the medium. Bicarbonate uptake is derived by a mass balance equation, i.e., the difference between net carbon fixation and net CO_2

uptake. To do this, the data are processed using the equations given in Badger et al. (1994). As for all disequilibrium approaches, it is necessary that there is no external CA activity present, so acetazolamide or dextran-bound sulphonamide is added. This approach gives quantitative measures of CO_2 and HCO_3^- uptake. The technique has the advantage of being able to quantify both CO_2 and HCO_3^- fluxes into the cell and, with slight modification, CO_2 efflux rates (see Badger et al. 1994). With care, the technique can be applied in natural phytoplankton populations. The disadvantage is the high cost of MIMS instrumentation.

Also, with the recent advances in molecular biology it is possible to use genomics and transcriptomics to determine if genomes contain sequences encoding identified HCO_3^- transporters and CA, and examine their expression. Price et al. (2008), for example, summarised the evidence for C_i transporters and their regulation in cyanobacteria, while Tsuji et al. (2017) and Gao et al. (2015) reported on aspects of the molecular biology of C_i transport in diatoms and the model green alga *Chlamydomonas*, respectively.

18.3 Merits and Demerits

A common question is how to change the pH and C_i concentration in order to mimic future changes due to ocean acidification and increasing dissolved CO_2 levels. Here it is important to remember that an addition of CO_2 to water will lower the pH without changing the total alkalinity (TA) (Beer et al. 2014, Box 3.4). Thus it may not be advisable to simply add a strong acid or base to the water (since they will affect the TA, see e.g., Gattuso et al. 2010). Instead, the bubbling of air with a desired CO_2 content, the addition of already high-CO_2 water, or a combination of additions of acid and HCO_3^- and/or CO_3^{2-} is recommended (Gattuso et al. 2010). If the goal is to mimic ambient seawater of marine plants in a productive shallow area with highly fluctuating levels of pH, C_i, and O_2, it is also possible to use the approach of Buapet et al. (2013) where natural seawater was incubated in glass bottles with the green alga *Ulva intestinalis* and kept in the light for different time periods before the experiments. The photosynthetic C_i assimilation then caused a decrease in C_i levels and, subsequently, a rise in pH, while photosynthetic O_2 evolution simultaneously caused a rise in O_2 tension.

Another thing to consider in an experimental setup is that buffers, if added to the seawater of the experiment, can disturb the function of C_i-utilisation mechanisms in some marine plants, as shown in the seagrass *Zostera marina* where uptake rates were lower at normal C_i conditions, and saturation concentrations higher, in the presence of buffers (Hellblom et al. 2001).

References

Badger MR, Palmqvist K, Yu JW (1994) Measurement of CO_2 and HCO_3^- fluxes in cyanobacteria and microalgae during steady-state photosynthesis. Physiol Plant 90:529–536

Beer S, Eshel A (1983) Photosynthesis of *Ulva* sp. II. Utilization of CO_2 and HCO_3^- when submerged. J Exp Mar Biol. Ecol 70:99–106

Beer S, Koch E (1996) Photosynthesis of seagrasses vs. marine macroalgae in globally changing CO_2 environments. Mar Ecol Prog Ser 141:199–204

Beer S, Waisel Y (1979) Some photosynthetic carbon fixation properties in seagrasses. Aquat Bot 7:129–138

Beer S, Eshel A, Waisel Y (1977) Carbon metabolism in seagrasses. I. The utilization of exogenous inorganic carbon species in photosynthesis. J Exp Bot 106:1180–1189

Beer S, Björk M, Beardall J (2014) Photosynthesis in the marine environment. Wiley-Blackwell, Oxford. (ISBN: 978-1-119-97957-9)

Buapet P, Rasmusson LM, Gullström M, Björk M (2013) Photorespiration and carbon limitation determine productivity in temperate seagrasses. PLoS One 8(12):e83804

Burns DB, Beardall J (1987) Utilization of inorganic carbon by marine microalgae. J Exp Mar Biol Ecol 107:75–86

Elzenga JTM, Prins HBA, Stefels J (2000) The role of extracellular carbonic anhydrase activity in inorganic carbon utilization of *Phaeocystis globosa* (Prymnesiophyceae): a comparison with other marine algae using the isotope disequilibrium technique. Limnol. Oceanogr. 45:372–380

Espie GS, Colman B (1986) Inorganic carbon uptake during photosynthesis. Plant Physiol 80 (4):863–869

Gao H, Wang Y, Fei X, Wright DA, Spalding MH (2015) Expression activation and functional analysis of HLA3, a putative inorganic carbon transporter in *Chlamydomonas reinhardtii*. Plant J 82:1–11

Gattuso J-P, Lee K, Rost B, Schulz K (2010) Approaches and tools to manipulate the carbonate chemistry. In: Riebesell U, Fabry VJ, Hansson L, Gattuso JP (eds) Guide to best practices for ocean acidification research and data reporting. Office of the European Union, Luxembourg

Hellblom F, Beer S, Björk M, Axelsson L (2001) A buffer sensitive inorganic carbon utilisation system in *Zostera marina*. Aquat Bot 69:55–62

Miller AG, Colman B (1980) Evidence for HCO_3^- transport by the blue-green alga (cyanobacterium) *Coccochloris peniocystis*. Plant Physiol 63:397–402

Pierrot D, Lewis E, Wallace DWR (2006) MS Excel program developed for CO_2 system calculations. ORNL/CDIAC-105a. Carbon Dioxide Information Analysis Center, Oak Ridge National Laboratory, U.S. Department of Energy, Oak Ridge, TN

Price GD, Badger MR, Woodger FJ, Long BJ (2008) Advances in understanding the cyanobacterial CO_2-concentrating-mechanism (CCM): functional components, Ci transporters, diversity, genetic regulation and prospects for engineering into plants. J Exp Bot 59:1441–1461

Rost B, Kranz SQ, Richter K-U, Tortell PD (2007) Isotope disequilibrium and mass spectrometric studies of inorganic carbon acquisition by phytoplankton. Limnol Oceanogr Meth 5:328–337

Schwartz AM, Björk M, Buluda T, Mtolera M, Beer S (2000) Photosynthetic utilisation of carbon and light by two tropical seagrass species as measured *in situ*. Mar Biol 137:755–761

Tsuji Y, Nakajima K, Matsuda Y (2017) Molecular aspects of the biophysical CO_2-concentrating mechanism and its regulation in marine diatoms. J Exp Bot 68:3763–3772

Chapter 19
Action Spectra of Photosynthetic Carbon Fixation

Yaping Wu, Gang Li, and Kunshan Gao

Abstract Action spectrum is a method used to evaluate the effects of different wavelengths of light on a specific process. In the photosynthetic reaction, sunlight can be used both to drive photosynthetic carbon fixation (mainly visible light) or to inhibit it (mainly ultraviolet radiation). Therefore, action spectrum can be used to measure both the promotion effect of visible light of different wavelengths on photosynthetic carbon fixation and the inhibition of different wavelengths ultraviolet radiation on photosynthetic carbon fixation.

Keywords Action spectra · Biological weighting function · UV radiation · Carbon fixation · Photosynthesis

19.1 Introduction

The spectrum of incident sunlight radiation ranges from 199.5 to 10,075.0 nm. When penetrating the atmosphere, UVC with wavelength less than 280 nm is completely absorbed, while wavelength between 280 and 315 nm is partially absorbed. For photosynthetic organisms, usually visible light (PAR, 400–700 nm) and ultraviolet radiation (UVR, 280–400 nm) have a significant effect on them, so most studies are focusing on the impact of PAR and UVR. As the main energy source of photosynthetic organisms, the wavelength effect of visible light has been well studied. It is a significant milestone in the history of photosynthesis research that Emerson

Y. Wu (✉)
College of Marine Science and Fisheries, Jiangsu Ocean University, Lianyungang, China
e-mail: ypwu@jou.edu.cn

G. Li
South China Sea Institute of Oceanology, Chinese Academy of Sciences, Guangzhou, China

K. Gao
State Key Laboratory of Marine Environmental Science and College of Ocean and Earth Sciences, Xiamen University, Xiamen, China

K. Gao et al. (eds.), *Research Methods of Environmental Physiology in Aquatic Sciences*, https://doi.org/10.1007/978-981-15-5354-7_19

enhancement effect was discovered in the early action spectrum research and the important conclusion that there are two photosystems within photosynthetic organisms' cells. For UVR, a large number of studies have shown that it has obvious effects on organisms, and UVR is generally divided into two parts, namely UVA (315–400 nm) and UVB (280–315 nm), while effect of UVA is significantly greater than that of UVB in many cases, which obviously cannot reflect the fact that UVB is more damaging. Therefore, some researchers correlated the effects of UV with the radiation intensity of single-wavelength radiation to reflect the biological effects of different wavelengths. This section will begin with a brief overview of visible light action spectrum and, through specific experimental data, describe how to quantify the biological effects of UV radiation at different wavelengths.

19.2 Action Spectrum of Visible Light

19.2.1 Absorption Spectrum of Pigment

Photosynthetic organisms contain a variety of pigments, such as chlorophyll, carotenoids, cyanine, and so on. The light absorption of these pigments is wavelength dependent, and specific for some wavebands. Figure 19.1 shows the absorption spectra of several common pigments, and absorption peaks of different pigments are diverse. Photosynthesis relies on the absorption and transformation of light energy by pigments, while different wavelength, such as 445 nm, is more likely to be absorbed by chlorophyll a than 600 nm, although they may contain the same energy. Therefore, the effect of wavelength 445 nm on photosynthesis is much greater than that of 600 nm. Of course, this is also affected by other light-harvesting pigments within the cell. Therefore, scientists used different wavelengths of visible light to illuminate photosynthetic organisms and determine the rate of

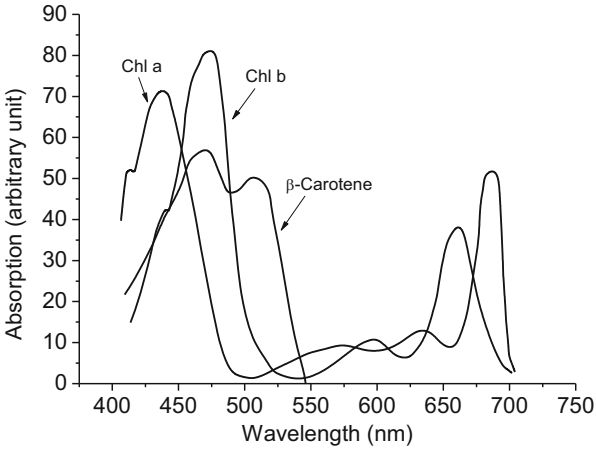

Fig 19.1 Schematic diagram of absorption spectra of chlorophyll a, b and beta carotene in acetone solution (Re-constructed from Moore et al. 1995)

photosynthesis during this period, thus obtaining the relationship between photosynthesis and wavelength, namely the action spectrum.

19.2.2 Production of Action Spectrum

Action spectrum of visible light generally using monochromator of narrow band of light to illuminate photosynthetic organisms, or through a variety of filters for different wavelengths of light, and simultaneous determination of photosynthesis rate, such as oxygen or carbon fixation, then photosynthetic rate is normalized to the unit light (photons), one can get the contribution of different wavelengths with same energy to photosynthetic rate because photosynthetic rate depends on pigment to absorb and convert light to energy. Thus the action spectrum of photosynthetic organisms is consistent with its pigment absorption spectrum. Figure 19.2 is the absorption spectrum and action spectrum of extract and thallus of *Pophyra*, who can see that the action spectrum and absorption spectrum of phycoerythrin extract are highly correlated between 480 and 570 nm.

19.3 Biological Weighting Function of UV Radiation

Biological weighting function (BWF) presented in this chapter is derived from carbon fixation rate of phytoplankton assemblage under different cutoff filters, that normalizes the relative inhibition of different wavebands of UVR to its intensity.

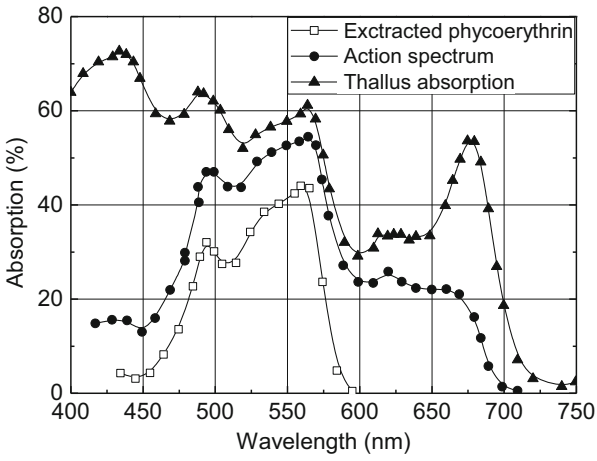

Fig. 19.2 Schematic diagram of action spectra, absorption spectra of phycoerythrin extract and thallus of *Phyphyra nereocystis* (Re-constructed from Haxo and Blinks 1950)

19.3.1 Sample Collection

BWF is suitable for various parameters, depends on the tested organisms, e.g., photosynthetic carbon fixation rate, growth rate, photosystem II activity, survival rate, and feeding rate. The following is an example of phytoplankton community in surface seawater.

19.3.2 Solar Radiation Monitoring

In this experiment, solar radiation was recorded by the ELDONET (Germany), which can simultaneously monitor the solar radiation intensity of PAR (400–700 nm), UVA (315–400 nm) and UVB (280–315 nm) in three bands, records the means over 1 min.

19.3.3 Ultraviolet Radiation Treatment

Six cutoff filters, WG280, WG295, WG305, WG320, WG350, and GG395, can be used for radiation treatments, which cutoff (50% maximum transmittance) sunlight radiation at 280, 295, 305, 320, 320, 350, and 395 nm, respectively (Fig. 19.3). These filters are covered on quartz tubes that containing seawater samples, each in triplicates, exposing the phytoplankton to different bands of ultraviolet radiation.

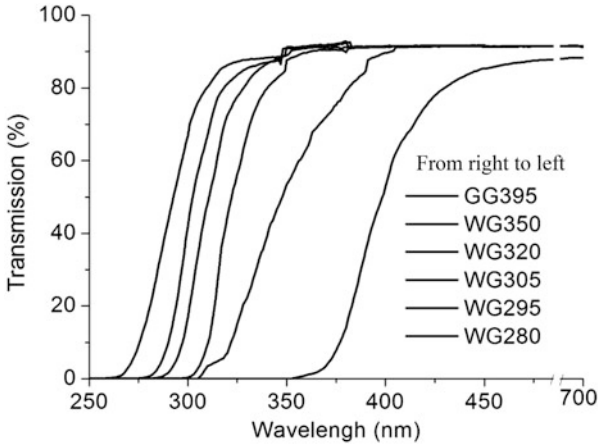

Fig. 19.3 Transmission characteristics of different filters (GG395, WG350, WG 320, WG 305, WG 295, WG 280) (From Wu and Gao 2011)

19.3.4 Determination of Photosynthetic Carbon Fixation Rate

The photosynthetic carbon fixation rate can be determined with carbon 14 (^{14}C) radioisotope method, as shown in Chap. 16.

19.3.5 Calculation of BWF

19.3.5.1 Photosynthetic Carbon Fixation of Phytoplankton

In this experiment, BWF is derived from the photosynthetic carbon fixation rate of phytoplankton under different cutoff filters (Table 19.1).

19.3.5.2 UV Intensity Between Filters

UV intensity between different filters: To quantify the relative contribution of different wavelength UV radiation to photosynthetic inhibition, UV intensity between filters (280–295, 295–305, 305–320, 320–350, and 350–395 nm) can be calculated from relative spectra of solar radiation (Ruggaber et al. 1994), in combination with the ELDONET data, and the transmission spectrum of the filter. Recently, spectrometer, such as Ocean Optics' optical fiber spectrometer, is developed to directly measure the intensity of UV radiation at different wavelengths.

19.3.5.3 Calculation of Biological Weight

The inhibition induced by UV radiation can be calculated as:

$$\mathrm{In}\, h = (P_{\mathrm{PAR}} - P_{\mathrm{UVx}})/P_{\mathrm{PAR}} \times 100\%.$$

P_{PAR} and P_{UVx} represent the carbon fixation rate under PAR and UVx treatment, e.g., for >280 and >295 nm treatment in day 1, the relative UV inhibition was:

Table 19.1 Photosynthetic carbon fixation rate of phytoplankton under different radiation treatments (μg C (μg Chl a)$^{-1}$ h^{-1})

Radiation treatment, nm	Day 1	Day 2	Day 3
>280	7.50	4.58	7.44
>295	10.16	4.98	8.71
>305	10.41	5.15	8.97
>320	11.42	5.31	9.72
>350	12.39	5.70	11.18
>395	13.31	6.47	12.79

$$\text{In } h_{280\text{nm}} = (13.31 - 7.50)/13.31 \times 100\% = 44\%$$
$$\text{In } h_{295\text{nm}} = (13.31 - 10.16)/13.31 \times 100\% = 24\%$$

While the inhibition induced by UV waveband (280–295 nm) is: 44–24% = 20%, meanwhile, the UV intensity of 289–295 nm was 1.27 mW m^{-2}, thus the biological weight is:

$$20\%/1.27 = 0.16\left(\text{mW m}^{-2}\right)^{-1}$$

Following the same procedure above, one can get the biological weight for different wavebands, then all biological weights can be fitted with polynominal function.

19.4 Advantages and Disadvantages

Action spectra of visible light is already very mature, the promotion space is relatively small at the technical level. However, the applied areas could be developed more, e.g., water bodies attenuates different wavelengths light differently, which leads to the change of spectra in water bodies with the increase of depth. If underwater spectra and action spectra can be combined, primary productivity can be estimated more accurately.

For ultraviolet radiation action spectrum, the method introduced in this paper is one of the simplified calculation methods of BWF, which can quantify the effects of ultraviolet radiation of different wavelengths, and can reflect the biological effects of ultraviolet radiation of different wavelengths more reliably. Compared with the *P–E* curve method under different ultraviolet radiation treatment proposed by Cullen et al. (1992), the present method has the advantages of simple operation, low requirement for experimental equipment and low cost. However, because the latter made *P–E* curve, it can reflect the effects of different intensity of ultraviolet radiation, so it can also find the appropriate intensity to more accurately reflect the inhibition rate of ultraviolet radiation.

References

Cullen JJ, Neale PJ, Lesser MP (1992) Biological weighting function for the inhibition of phytoplankton photosynthesis by ultraviolet radiation. Science 258:646–650

Haxo F, Blinks L (1950) Photosynthetic action spectra of marine algae. J Gen Physiol 33:389–422

Moore R, Clark WD, Stern K, Vodopich D (1995) Botany. Wm. C. Brown, Dubuque, IA

Ruggaber A, Dlugi R, Nakajima T (1994) Modelling of radiation quantities and photolysis frequencies in the troposphere. J Atmos Chem 18:171–210

Wu Y, Gao K (2011) Photosynthetic response of surface water phytoplankton assemblages to different wavebands of UV radiation in the South China Sea. Haiyang Xuebao 33:146–151

Chapter 20
Determination of the Inorganic Carbon Affinity and CO_2 Concentrating Mechanisms of Algae

Yaping Wu and Kunshan Gao

Abstract The rate of photosynthesis is measured mainly by changes in dissolved oxygen or inorganic carbon. The relationship between photosynthetic carbon fixation or oxygen evolution rate and inorganic carbon concentration is usually determined by changing the concentration of inorganic carbon in the reaction cuvette, while the photosynthetic rate under different concentrations of inorganic carbon are measured. Then the relationship curve (PC curve) between photosynthesis and inorganic carbon concentration is obtained and analyzed further. However, the inorganic carbon pool or concentration of inorganic carbon within cells needs to be determined and analyzed by silicon oil centrifugation.

Keywords Carbon concentrating mechanism · Algae · Phytoplankton · Silicon oil technique · CO_2

20.1 Introduction

The photosynthetic carbon fixation of algae is not only influenced by light, temperature, and nutrients, but also by pH, dissolved inorganic carbon (DIC), and dissolved oxygen in water. Inorganic carbon in seawater is mainly in the form of HCO_3^-, while dissolved aqueous CO_2, the only substrate for photosynthesis, is less than one percent. Therefore, most algae have evolved inorganic carbon concentrating mechanisms (CCMs) that actively absorb and concentrate inorganic carbon in order to improve the concentration of the CO_2 pool in cells. However, CCM operation is susceptible to environmental changes. Therefore, the study of CCMs of algae and

Y. Wu (✉)
College of Marine Life and Fisheries, Jiangsu Ocean University, Lianyungang, China
e-mail: ypwu@jou.edu.cn

K. Gao
State Key Laboratory of Marine Environmental Science and College of Ocean and Earth Sciences, Xiamen University, Xiamen, China

K. Gao et al. (eds.), *Research Methods of Environmental Physiology in Aquatic Sciences*, https://doi.org/10.1007/978-981-15-5354-7_20

their intracellular inorganic carbon pool is an important link to explain the process of carbon acquisition, physiological changes and the relationship with environmental changes. This chapter will introduce several methods for the study of the relationship between algal photosynthesis and DIC concentration, and analyzes their advantages and disadvantages.

20.2 Determination of Inorganic Carbon Affinity

20.2.1 Operation Steps

1. Preparation of DIC-free seawater: a certain amount of hydrochloric acid is added to seawater, to make the pH below 5.0, then the acidified seawater is bubbled with nitrogen gas for ~20 min (the time varies with the temperature), to completely expel the inorganic carbon in the form of CO_2 from seawater. Then a certain amount of buffer (optional) is added, and the pH is adjusted to the target value by adding hydrochloric acid or freshly prepared NaOH solution.
2. Algal cell collection: the algal cells are centrifuged or filtered onto a polycarbonate membrane, washed with the DIC-free seawater for three times, then suspended in DIC-free seawater. According to the sensitivity of the technique to be used the appropriate cell concentration should be pre-determined; thus for ^{14}C tracer or PAM based measurements, the cell concentration should be maintained at 1–5 μg chl a L^{-1}, while the oxygen electrode requires more than 500 μg chl a L^{-1}, so that reliable data can be obtained.
3. Intracellular inorganic carbon depletion when measuring the photosynthetic rate under different concentrations of inorganic carbon, although the algal cells were suspended in DIC-free seawater, they still contain a certain amount of inorganic carbon within the cells, which needs to be exhausted through photosynthesis. Therefore, it is necessary to place the cell suspension under light to allow its photosynthesis to continue until the photosynthetic oxygen release and respiratory oxygen consumption reach a balance, at which point it can be assumed that the intracellular inorganic carbon pool is fully depleted. Generally, the time required for intracellular inorganic carbon depletion is less than 30 min.
4. Photosynthetic rate at different inorganic carbon concentrations: The algal suspension is supplied with different concentrations of sodium bicarbonate solution within the concentration range of 50–4000 μmol L^{-1}, and various instruments used (see below) to measure its photosynthetic rate at different inorganic carbon concentrations.
5. Data processing and analysis: After the measurements, a series of photosynthetic rates under different inorganic carbon concentrations can be obtained. Data analysis software, such as Origin, can be used to fit the data to the Michaelis–Menten equation:
   $V = V_{max} \times S/(K_m + S)$,

where, V is the rate of photosynthesis, S is the concentration of substrate, which can be DIC (inorganic carbon), CO_2 or HCO_3^-. K_m is the substrate concentration when the photosynthetic rate is half of the maximum and reflects the affinity of algal cell photosynthesis for inorganic carbon. V_{max} is the maximum rate of photosynthesis when carbon is saturated.

20.2.2 Case Study

20.2.2.1 Comparison Between Different Measuring Techniques

As can be seen from Fig. 20.1, the cell photosynthetic rate or electron transport rate under both treatments increased with the increase of inorganic carbon concentration. After reaching a certain concentration, the trend gradually slowed down and rates finally remained stable (Fig. 20.1a, b). According to the fitting of results to the Michaelis–Menten equation, the K_m of cultured cells at 380 ppmv CO_2 was less than that of cells grown at 1000 ppmv, indicating that the affinity of cells to inorganic carbon decreased under high CO_2 (Fig. 20.1c). It was also found that although the photosynthetic rate increased significantly with the increase in DIC at low DIC concnetrations, at the DIC concentration of natural seawater (~2.2 mM), further addition of DIC would not significantly improve cells' photosynthetic rate (Fig. 20.1a, b). A PC curve can also be obtained by measuring the electron transport rate of photosystem II by pulse amplitude modulated (PAM) fluorometry. Although the K_m value obtained in this way is different from that using carbon fixation or oxygen evolution, it can accurately reflect the change of affinity of algae photosynthesis to inorganic carbon under different conditions, and is also a fast and effective method (Wu et al. 2010).

20.2.2.2 Solution for Incomplete Intracellular DIC Depletion

After the cells are washed by DIC-free seawater and intracellular DIC exhausted under light treatment, sometimes the photosynthetic oxygen release in the reaction cuvette is still positive for a long time, which indicates that there is residual DIC within the cells or in the reaction solution. In this case, if the cells are collected again, mechanical damage may be caused to the algae, and if the light treatment time is prolonged, light damage will possibly be incurred by the algae, affecting the subsequent PC curve measurement. Therefore, the following correction methods can be used to infer the key parameters of the PC curve. The first method is to shift the curve (solid line) along the horizontal axis so that the intersection of the curve and the X-axis coincides with the origin (dotted line), and then calculate the relevant parameters (Fig. 20.2). The second method is to subtract the photosynthetic rate at the concentration of each substrate from the photosynthetic rate without adding $NaHCO_3$, and then apply the Michaelis–Menten equation again for fitting. This will make V_{max} change, but an accurate K_m can be obtained. (Gao 1999).

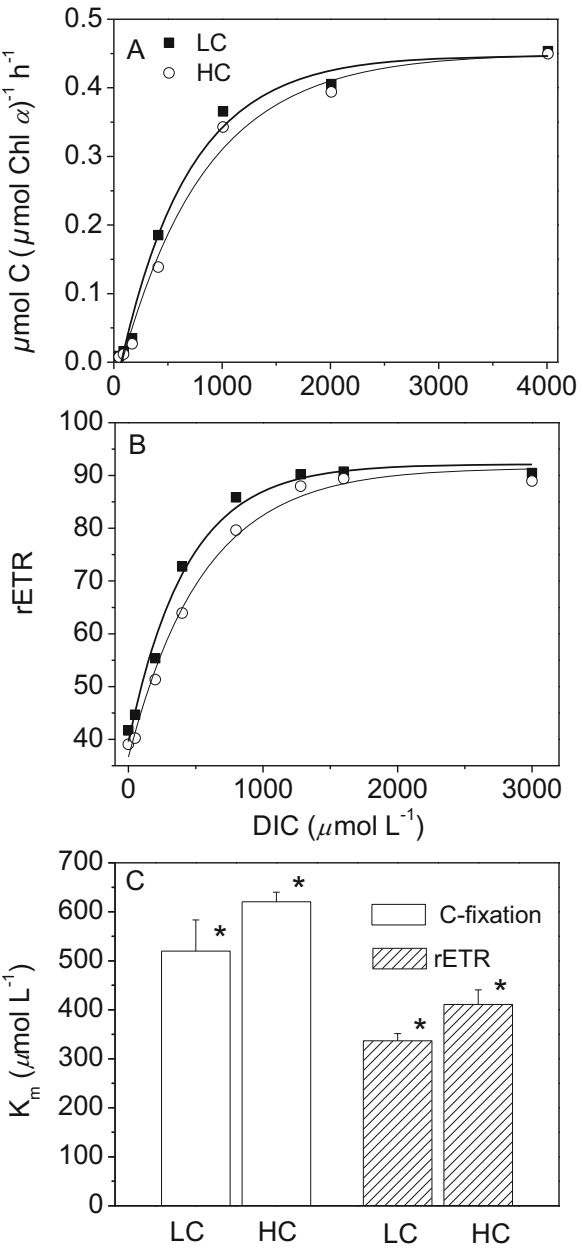

Fig. 20.1 Low CO_2 (LC, 380 ppmv) and high CO_2 concentration (HC, 1000 ppmv) grown *Phaeodactylum tricornutum*, suspended in DIC-free seawater at pH 8.15, then measured with addition of different concentrations of DIC under 400 μmol m^{-2} s^{-1} light intensity, the photosynthetic rate of carbon fixation (C-fixation, **a**), and the relative electron transport rate (rETR, **b**), the K_m (**c**) was obtained from PC curve fitting (Wu et al. 2010)

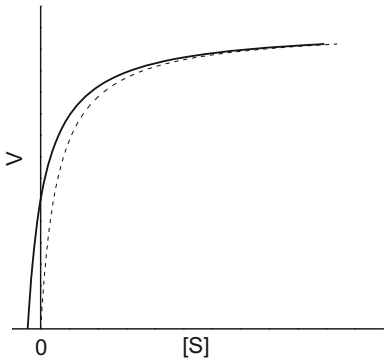

Fig. 20.2 Method to correct the incomplete inorganic carbon exhausting for PC curve

20.3 Determination of Intracellular Inorganic Carbon Pool

20.3.1 The Content of Intracellular Inorganic Carbon

20.3.1.1 Theoretical Basis

Before the determination of intracellular inorganic carbon pool, in order to eliminate the interference of the existing inorganic carbon in the intracellular, the cells should be suspended in carbon-free seawater and illuminated to use up residual inorganic carbon within cells, ^{14}C-labeled $NaHCO_3$ is then added and the cell suspension incubated under illumination. Extracellular CO_2 and HCO_3^- will penetrate the cell membrane through the carbon concentration mechanism (CCMs) or diffusion (CO_2), thus filling the intracellular DIC pool. This process takes a very short time; for instance for diatoms typically 10 s is sufficient to fully fill the intracellular pool. At this time, if the cell can be "removed" from the solution and the content of total carbon and organic carbon in the cell is measured, the difference between these measurements is the capacity of the intracellular inorganic carbon pool (i.e., the amount of inorganic carbon in the cell). However, how to quickly remove the cell from the solution while avoiding contamination from ^{14}C in the solution is a big problem. In 1957, Werkheiser and Bartley developed a method for centrifugation of cells using silicone oil (Werkheiser and Bartley 1957) and this approach was applied to the determination of intracellular carbon pools in algae (Badger et al. 1980; Tortell et al. 2000). The centrifuge tube is divided into three layers. The bottom layer is termination solution, which can instantly kill cells. The middle layer is silicone oil with a certain density, and the cells are suspended above the silicone oil layer (Fig. 20.3). Under high speed centrifugation, the cells pass through the silicone oil layer to the bottom, rapidly separating them from the solution. However, some inorganic carbon in the space around the cell membrane still exists, and some ^{14}C within the cell will be fixed to organic carbon through photosynthesis. These two factors can lead to overestimations of the inorganic carbon pool. Therefore, for the cells collected through silicone oil centrifugation half of the sample is treated with hydrochloric acid, to determine organic carbon content, and this value deducted from the total ^{14}C content.

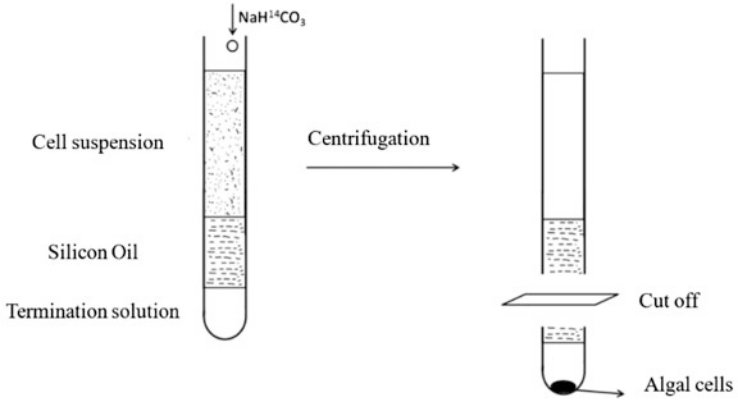

Fig. 20.3 Schematic diagram of silicone oil centrifugation for cell separation

20.3.1.2 Operational Steps

1. Silicone oil centrifuge tube: first, add the 100 μL termination solution (10% methanol solution containing 2.5 N NaOH) to the bottom of the 0.5 mL centrifuge tube, then add 150 μL mixed silicone oil (AR20 and AR200) above the termination solution. The proportion of the two silicone oils needs to be predetermined according to different algal cells.
2. Collection of algal cells: the determination of intracellular inorganic carbon content requires a high biomass, the ideal chlorophyll concentration is about 5 μg mL^{-1}. After algal cells are collected, they are washed and suspended in DIC-free seawater.
3. Inorganic carbon depletion: before adding ^{14}C, the algal suspension should be placed in an oxygen electrode reaction cuvette and illuminated at around 400 μmol m^{-2} s^{-1} until the oxygen evolution rate is 0. At this time, the light should be turned off immediately to prevent the algal cells from being photodamaged in the absence of inorganic carbon.
4. Radioactive labeling: carefully withdraw 200 μL algal suspension with a pipette and slowly add above the top of silicone oil layer, then add ^{14}C (5 μCi). After that, the centrifuge tube is placed under 400 μmol m^{-2} s^{-1} and illuminated for 10 s, then quickly retrieved and put into the centrifuge.
5. Centrifugation: centrifuge for 40 s at a centrifugation speed of more than 14,000 *g* (the specific time is set to ensure the algal cells are centrifuged completely to the bottom of the tube).
6. ^{14}C measurement: after the centrifugation, the bottom of the tubes (with cells) are cut off, half of the samples are treated with HCl overnight, and added to scintillation cocktail, while the rest of the samples are added to scintillation cocktail directly, then the ^{14}C content is calculated from scintillation counts.

20.3.2 Determination of Intracellular Volume

1. The theoretical basis for this determination is based on two isotopes, water labeled with ^{3}H and mannitol labeled with ^{14}C. The principle of this method is that tritiated water can penetrate the cell membrane in a short time (1–2 min), so that it is evenly distributed in the cell wall and cytoplasm. Mannitol cannot penetrate the cell membrane, but only into the space between the cell wall and the cell membrane. The difference between them is the intracellular volume for the inorganic carbon pool (see Fig. 20.4).
2. Operational steps.
   The procedure is basically the same as that for the determination of intracellular carbon content (only the isotopes are different). After adding tritiated water and mannitol, the cell suspensions in the centrifuge tubes are placed in low light for 2 min to ensure even distribution of the two isotopes inside and outside the cell. Then the cells are centrifuged and collected for radioisotope measurement.

20.4 Advantages and Disadvantages of the Methods

PC curves reflect the affinity of algal photosynthesis for inorganic carbon, and the photosynthetic rate can be obtained through oxygen evolution and DIC assimilation, and can also be measured by the ^{14}C tracer method. In addition, the chlorophyll fluorescence method can be used to determine the relationship between electron transport rate and inorganic carbon concentration. The advantages and disadvantages of these methods are as follows:

1. Photosynthetic oxygen evolution is simple and easy to measure but requires a large amount of algal biomass.
2. The determination of DIC changes requires special instruments, such as a total carbon analyzer, to determine dissolved inorganic carbon. This method is also

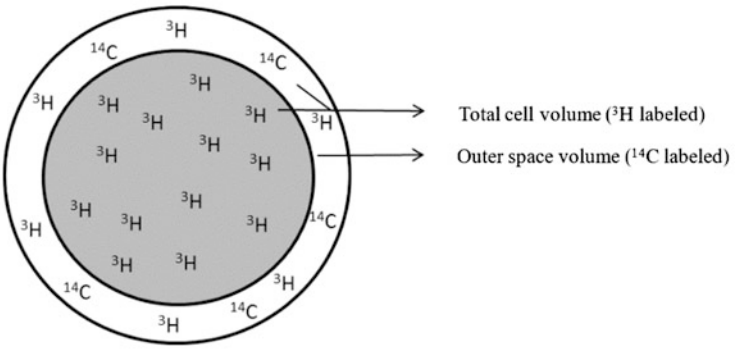

Fig. 20.4 Schematic diagram of intracellular distribution of $^{3}H_2O$ and ^{14}C-mannitol

simple, but requires a greater investment in instrumentation, a larger biomass of algae, and a knowledge of the best time to collect water samples (the linear change time must be taken).

3. The advantage of the ^{14}C tracer method is that it requires a short time and a small amount of cells (the amount of cells is inversely correlated with the culturing time). The disadvantage is that the operation is relatively complicated and accurate calculation is required. In addition, the measured carbon fixation reflects either gross photosynthetic rate or net photosynthetic rate, which is related to the culturing time and carboxylation efficiency of algae. Generally, ^{14}C values measured in minutes can be regarded as gross carbon fixation, while carbon fixation measured over hours can be regarded as the net value. Because of the high sensitivity of the ^{14}C tracer method, it is the best choice for the determination of photosynthetic carbon fixation in a relatively short time or in the case of extremely low chlorophyll concentration (such as seawater in oligotrophic areas).
4. For the determination of inorganic carbon concentration within algal cells, only the silicon oil centrifugation method is currently accepted. This method is only suitable for microalgae. If it is applied to macroalgae, preliminary experiments need to be done to remove the ^{14}C stored in tissues or between cells, and the number of cells in a unit algal body needs to be known. If cell number is indirectly replaced by unit weight or unit algal area, DIC concentration per unit algal amount can be given.

References

Badger MR, Kaplan A, Berry JA (1980) Internal inorganic carbon pool of *Chlamydomonas reinhardtii* – evidence for a carbon-dioxide concentrating mechanism. Plant Physiol 66:407–413

Gao K (1999) Research techniques and methods in characterizing photosynthetic carbon fixation by algae (In Chinese). Mar Sci 6:37–41

Tortell PD, Rau GH, Morel FMM (2000) Inorganic carbon acquisition in coastal Pacific phytoplankton communities. Limnol. Oceanogr. 45:1485–1500

Werkheiser WC, Bartley W (1957) The study of steady-state concentrations of internal solutes of mitochondria by rapid centrifugal transfer to a fixation medium. Biochem J 66:79–91

Wu Y, Gao K, Riebesell U (2010) CO_2-induced seawater acidification affects physiological performance of the marine diatom *Phaeodactylum tricornutum*. Biogeoscience 7:2915–2923

Chapter 21
Methods for Measuring Algal Carbon Fixation in Flow-Through Seawater

Kunshan Gao and Juntian Xu

Abstract Benthic algae and animals are generally in stirred or flowing seawater due to water currents and waves. It is hard to measure their photosynthetic or respiratory rates in a small closed container due to their large size and bottle effects. Seawater flow-through method can avoid bottle effects and be applied to large size organisms or benthic communities. By measuring the concentrations of dissolved oxygen or other parameters in the inlet and outlet of the tube simultaneously, one can calculate photosynthetic or respiratory rates using flow rate and biomass used and the difference in O_2 concentration between the inlet and outlet. This method can eliminate the effects of diffusion boundary layer surrounding the organisms, and overcome the bottle effects that lead to increasing accumulation of O_2 and decreasing availability of CO_2 and nutrients for marine plants. It can also be applied to measurements of respiration of animals and biological calcification.

Keywords Diffusion boundary layer · Flowing seawater · Photosynthesis · Respiration

21.1 Introduction

Photosynthetic rates of marine plants are usually determined on the basis of changes in dissolved oxygen or inorganic carbon within a certain time interval, the water volume, the duration of measurement and biomass or chlorophyll content. This is usually performed in a closed system, which can lead to significant variations of seawater carbonate chemistry (pH increase and pCO_2 decrease in light) and high

K. Gao (✉)
State Key Laboratory of Marine Environmental Science and College of Ocean and Earth Sciences, Xiamen University, Xiamen, China
e-mail: ksgao@xmu.edu.cn

J. Xu
College of Marine Life and Fisheries, Jiangsu Ocean University, Lianyungang, China

K. Gao et al. (eds.), *Research Methods of Environmental Physiology in Aquatic Sciences*, https://doi.org/10.1007/978-981-15-5354-7_21

concentration of dissolved oxygen due to photosynthesis. These chemical changes can on one hand cause the "bottle effect," on the other hand, they will stimulate production or accumulation of reactive oxygen species which damage photosynthetic apparatus and other metabolic pathways. Therefore, the rates obtained this way can hardly reflect the photosynthetic, calcification and respiration rates in a stable environment or in situ.

The seawater flow-through method introduced in this section can measure the photosynthetic rates of seaweeds and seagrasses meanwhile maintaining stable carbonate chemistry and accommodating more individuals and even community. For example, determination of photosynthesis or calcification is based on the changed amount of dissolved or total alkalinity between the inlet and outlet. One can obtain the calcification rate of coralline algae and even calcifying animal using this method based on the change of total alkalinity.

21.2 Outline of Seawater Flow-Through Open System

This system uses glass or quartz tubes as measuring vessels with high light transmission for photosynthetic measurements. It consists of water flowmeter, oxygen electrode, oxygen detection controller, seawater supplying tank, and water pump (Fig. 21.1).

The end of assimilation tube is better to be conically shaped, connected to plastic tube. The current speed in the tube is inversely proportional to the cross area of the assimilation tube. Seawater is incompressible liquid, the relationship between the flow speed in the assimilation tube (V, cm/s) and inner diameter (D, mm) and flow rate (F, L/min) can be expressed in the flowing equation:

$$V = 2123 \times D^{-2} \times F,$$

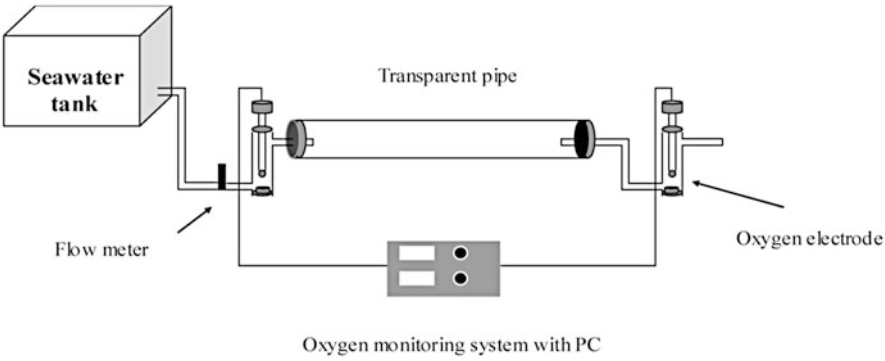

Fig. 21.1 Water flow-through system for determination of photosynthesis, calcification and respiration in benthic organisms (Gao and Xu 2008)

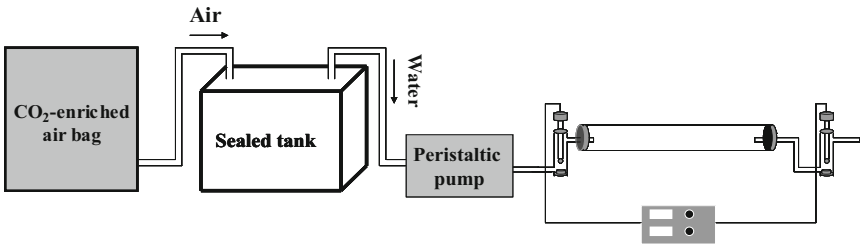

Fig. 21.2 schematic diagram for the flow system to control CO_2 partial pressure

where flow speed or current velocity is exponential function of the inner diameter of assimilation tube, enlarges as the inner diameter decreases.

If macroalgal individuals are used, they need to be fixed on something (to avoid being tangled) before being placed in the assimilation tube. Under a certain time and flow speed, the dissolved oxygen concentration of seawater flowing through the assimilation tube start to change and then reach a stable value under constant conditions, the oxygen concentration in the inlet and outlet water can be determined by oxygen electrode or Winkler method. The net photosynthetic oxygen evolution rate (Pn) can be calculated as:

$$\mathrm{Pn} = (B - A) \times F \times 60 \times W - 1,$$

where A and B represent oxygen concentrations of seawater in the inlet and outlet, F the flow rate (L/min), W the algal mass.

To get the high CO_2/low pH condition, the CO_2 control device can be connected to open system (Fig. 21.2). The seawater can be bubbled with CO_2 enriched seawater in advance; or the seawater with high CO_2 is stored in a closed tank, one end connected to the open system, and the other end connected to a gasbag with specific CO_2 concentration (Fig. 21.2), then the carbonate system can be stabilized in certain level. (It is suggested to control the temperature in the tank with constant temperature circulating water bath, at the same time the circulation can also play a mixing effect.)

21.3 Application of the Experimental System

The degree of accuracy to determine the photosynthesis and calcification rate with the flow system depends on the variation of oxygen concentration and total alkalinity between the inlet and outlet. If the biomass in the assimilation tube is not enough, the flow rate needs to be reduced in order to obtain detectable difference in oxygen concentration and total alkalinity between the inlet and outlet. If the volume of the assimilation tube is too large, it needs more time to see stable levels of the dissolved

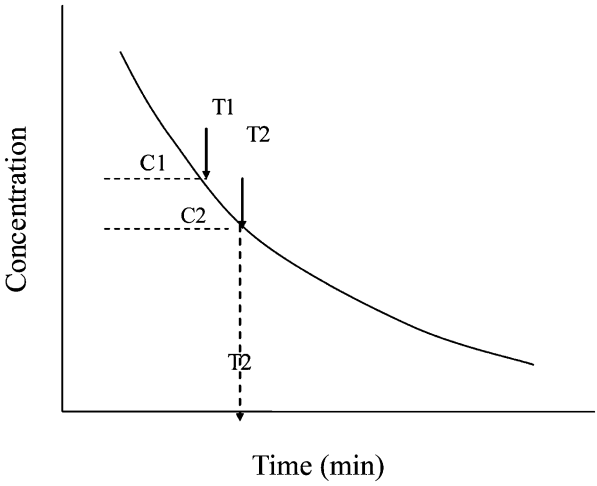

Fig. 21.3 Dissolved inorganic carbon (DIC) concentration (in the case of dissolved oxygen, it increases with time) or total alkalinity changes with time in a circulating closing system

oxygen in the outlet water (the decrease of the flow rate extends the residence time of seawater in the assimilation tube).

Under indoor constant light or outdoor fluctuating solar radiation, if the difference of the dissolved oxygen and total alkalinity between the inlet and outlet is too small, it will bring larger measuring error. Under this circumstance, the open flow-through system can be transformed to circulating open or circulating close systems. For the circulating open system, the seawater will be circulated from the outlet to inlet (an open container is in the middle to ease gas exchanges). For the circulating close system, the seawater keeps flowing through the system without gas exchanges. As a result, we can use the changes in dissolved oxygen or total alkalinity, seawater volume in the system (including seawater in the assimilation and connecting tube) and algae content to estimate the photosynthesis and calcification rate.

Though the nutrients become depleted with time in the closed systems, since the measuring time is not long enough to cause nutrient limitation effects, we still can get ideal results using these two systems, especially when measuring the change of total alkalinity and calcium concentration. For the closed system, rates of photosynthesis and calcification rate can be estimated as follows:

$$R = (C1 - C2)/(T2 - T1)/B,$$

where R is calcification or photosynthesis rate, $C1$ and $C2$ are the dissolved inorganic carbon concentration or total alkalinity at time $T1$ and $T2$ (Fig. 21.3), B the biomass.

With measuring time increasing, dissolved oxygen or total alkalinity gradually deviate the linear relationship, so it is necessary to finish measurement in a short time.

The calcification rate can be calculated as : $G = -\Delta TA/2$,

where ΔTA is the change of total alkalinity per biomass per time.

21.4 Cautions to Use the Measuring System

1. If the electrodes used in the inlet and outlet are different, the two electrodes might bring about measuring errors due to their difference in response and accuracy. Therefore, they must be calibrated. It is recommended to use the same electrode for the inlet and outlet measurement.
2. To make sure if the samples in the assimilation tube are shaded each other and subsequently affect light exposures.
3. Because it takes some time for the seawater in the assimilation tube to be turned over, it needs some minutes for the dissolved oxygen and total alkalinity to become constant in the outlet seawater. Different assimilation volume and flow rate result in different turn over time.
4. Make sure the dissolved oxygen between the inlet and outlet has apparent difference to decrease measuring error. Pre-experiment is needed to obtain suitable biomass and flow rate.
5. The light transparency between different materials is different, so the choice of assimilation tube material depends on experimental design. Glass, polycarbonate, and plastic material can't transmit UV radiation, while quartz can transmit whole spectrum of solar radiation.
6. When conducting experiment using this flow-through system under outdoor fluctuating conditions, the photosynthesis rate and solar radiation intensity should be measured at the same time, and diel photosynthetic performance can be analyzed with changing solar radiation.
7. The electrode must be calibrated with changing of seawater temperature.

21.5 The Advantages and Disadvantages of the Flowing-Through System

1. This system can effectively reduce the "bottle effect." Net photosynthetic rates of the red alga *Gracilaria lemaneiformis* was by 76% higher when measured in the flowing-through system than in the closed system, but no difference of respiratory rate was detected (Gao et al. 2012). The net photosynthetic rate of *Corallina sessilis* remained constant within 5 h, but decreased in the closed system over time (Fig. 21.4).
2. The stability of the seawater carbonate system can be effectively maintained (Table 21.1). In this system, the consumption of inorganic carbon by photosynthesis would cause a slight decrease in pCO_2 but a slight increase in pH. When the

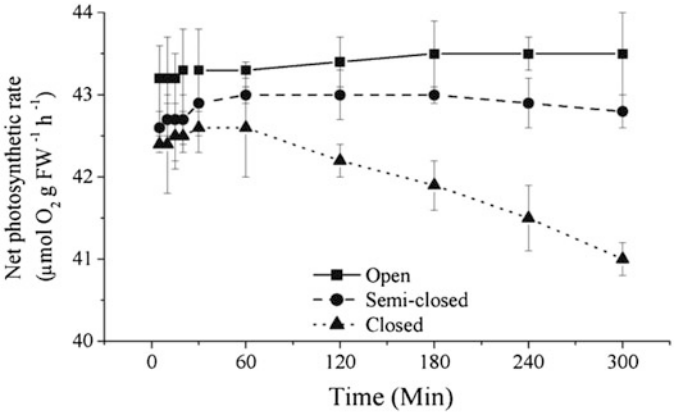

Fig. 21.4 The net photosynthetic rates of *Corallina sessilis* measured over 5 h in the open system (filled square), semi-closed system (filled circle), and closed system (v triangle) (Zheng 2009)

Table 21.1 Changes in the parameters of the seawater carbonate chemistry in the outlet and inlet seawater equilibrated with of 380 ppmv CO_2

	Inlet	Outlet
DIC (μM)	2036 ± 38[a]	2025 ± 45[a]
HCO_3^- (μM)	1845 ± 33[a]	1839 ± 40[a]
CO_3^{2-} (μM)	178 ± 12[a]	167 ± 120[a]
ρCO_2 (μM)	15 ± 2[a]	14 ± 3[a]
TA (μM)	2316 ± 22[a]	2310 ± 145[a]
Ω_c	3.7 ± 0.2[a]	3.7 ± 0.5[a]
pH	8.4 ± 0.1[a]	8.4 ± 0.2[a]

DIC dissolved inorganic carbon, *TA* total alkalinity, *Ωc* saturation of calcium carbonate (Gao et al. 2012). The same superscripted letters indicate insignificant changes

velocity of seawater and the biomass of the assimilation tube are kept constant, the carbonate system will stabilize at a certain level, and the dissolved oxygen concentration at the outlet and inlet differs by more than 20% (Gao et al. 2012).

3. By choosing reasonably sized transparent tubes that hold macroalgal individuals, photosynthesis of whole plants can be measured without punching and hurting the thalli, avoiding any negative effects and/or artifacts due to cutting. Additionally, this approach provides physiological information about a whole plant rather than using different parts that may possess different capacity of physiology.
4. The system shows longer response time of dissolved oxygen concentration and other indicators, compared with the traditional closed bottles or vessels.
5. Experimental operation is relatively complex and is not suitable for phytoplankton, but can be used for the study of benthic microalgae.
6. Although "air bag" can be used to maintain a stable CO_2 concentration to study the effects of elevated CO_2 levels or ocean acidification (Gao and Zheng 2010), the logistics are labor-consuming. At present, commercially available CO_2

enrichment device (Wuhan Ruihua) can be used to control the CO_2 concentrations in the air bubbled into the inlet seawater.

References

Gao K, Xu J (2008) Effects of solar UV radiation on diurnal photosynthetic performance and growth of *Gracilarialema neiformis* (Rhodophyta). Eur J Phycol 43:297–307

Gao K, Zheng Y (2010) Combined effects of ocean acidification and solar UV radiation on photosynthesis, growth, pigmentation and calcification of the coralline alga *Corallinasessilis* (Rhodophyta). Glob Chang Biol 16:2388–2398

Gao K, Xu J, Zheng Y, Ke C (2012) Measurement of benthic photosynthesis and calcification in flowing-through seawater with stable carbonate chemistry. Limnol Oceanogr Meth 10:555–559

Zheng Y (2009) Effects of CO_2 concentration and solar UV radiation on physiological and biochemical characteristics of coralline algae. Glob Chang Biol 16(8):2388–2398

Chapter 22
Application of Membrane-Inlet Mass Spectrometry to Measurements of Photosynthetic Processes

Kunshan Gao and Hualing Mi

Abstract Membrane-inlet mass spectrometer (MIMS) is used to simultaneously monitor changes of the concentrations of gases with different molecular weights in the solution. It can be used to measure the gas exchanges during photosynthesis and respiration of algae and other aquatic primary producers.

Keywords Gas exchanges · Isotopic gases · Photosynthesis

22.1 Introduction

MIMS is a set of devices developed by George Hoch and Bessel Kok based on mass spectrometry for the online analysis of volatile substances and gases in water and air (Hoch and Kok 1963). The gases can be directly sucked into the vacuum chamber from the solution using a reaction vessel or a sampling probe equipped with a gas-permeable membrane, and the composition and the relative concentration of gases of different molecular weights are obtained by ionization. The method is very sensitive and can be used to measure the concentration of gases dissolved in water quickly and accurately. It is widely used in the research of photosynthesis-related physiological processes (Fig. 22.1).

The injection of MIMS is through a semipermeable membrane (such as polydimethylsiloxane rubber), so that gases dissolved in the solution (such as O_2, CO_2, N_2, gaseous H_2O, etc.) go through, and then are detected. The application of MIMS in photosynthetic carbon fixation processes includes:

K. Gao (✉)
State Key Laboratory of Marine Environmental Science and College of Ocean and Earth Sciences, Xiamen University, Xiamen, China
e-mail: ksgao@xmu.edu.cn

H. Mi
National Key Laboratory of Plant Molecular Genetics, Institute of Plant Physiology and Ecology, Shanghai Institutes for Biological Sciences, Chinese Academy of Science, Shanghai, China

K. Gao et al. (eds.), *Research Methods of Environmental Physiology in Aquatic Sciences*, https://doi.org/10.1007/978-981-15-5354-7_22

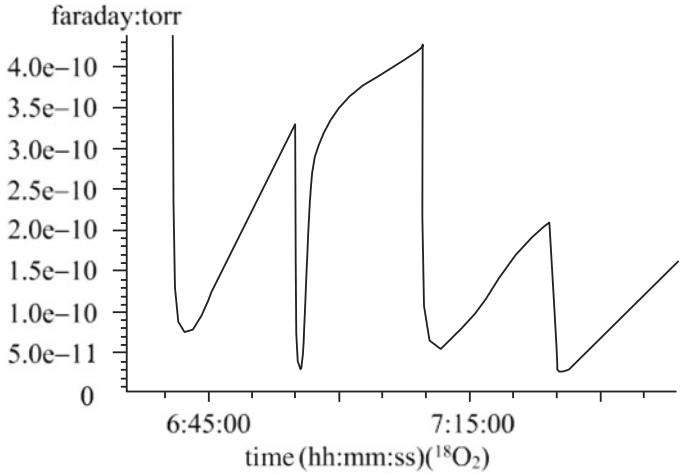

Fig. 22.1 Concentration of $^{18}O_2$ produced from the lysis of water in the medium mixed with $H_2{}^{18}O$ during photoreaction of photosynthesis. The lowest point indicates the value in darkness prior to the turn on of light, and the highest point is the value before the light is turned off

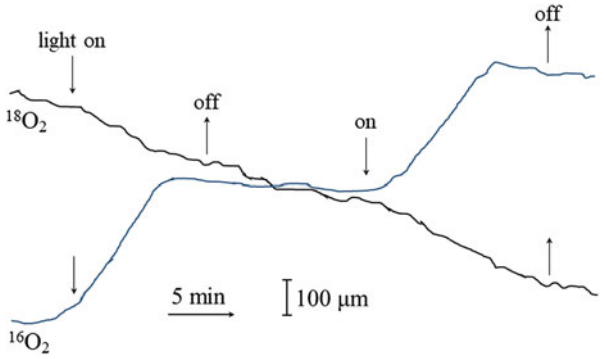

Fig. 22.2 Simultaneous determination of oxygen consumption and evolution in the red alga *Porphyra yezoensis*. Arrows indicate the time of turning on and off the light (Gao et al. 1992)

22.2 Real-Time Measurement of Oxygen Uptake and Evolution by Using Oxygen Isotopes

When the reaction medium containing algae is stripped off dissolved $^{16}O_2$ by sparging N_2 before $^{18}O_2$ is dissolved in it, $[^{16}O_2]/[^{18}O_2]$ ratio is very small. Therefore, during photosynthesis, decrease of $^{18}O_2$ can be viewed as oxygen uptake by photorespiration and mitochondrial respiration, that is respiratory consumption of O_2 in light; and increase of $^{16}O_2$ is considered as amount of photosynthetic oxygen evolution (Fig. 22.2). However, during the experiment, the solution is always unavoidably mixed with some $^{16}O_2$, so that a series of corrections are required to calculate the oxygen consumption and evolution rates (Radmer and Ollinger 1980).

22.3 Real-Time Measurement of Respiration and Photosynthetic Rate of Algae

CO_2 is evolved when algal cells respire and it is assimilated by cells when photosynthesis happens. When light is turned on, the CO_2 concentration in the solution changes, and other species of DIC (HCO_3^- and CO_3^{2-}) cannot go through the semipermeable membrane. Thus, MIMS can be used to measure the changes of CO_2 concentration in the solution in real time (Fig. 22.3). During the photosynthesis, the carbonate system in the solution changes and the pH rises if buffers are not added in the solution. Thus, the change in total DIC can only be obtained by taking the pH change into account, and then the actual photosynthetic or respiratory rate can be calculated on the basis of altered DIC concentration. If buffers are used, changes in CO_2 concentration can be directly used for the calculation of photosynthetic or respiratory rates.

22.4 Measurement of the Activity of Carbonic Anhydrase

The activity of carbonic anhydrase in microalgal cells can be calculated from the variation of the abundance of ^{18}O in double-labeled sodium bicarbonate $NaH^{13}C^{18}O_3$. Carbonic anhydrase catalyzes the reaction of $HCO_3^- + H^+ = H_2O + CO_2$ in two directions forth and back, thus leading to the exchange of oxygen between H_2O and HCO_3^- (Silverman 1982). The activity of carbonic anhydrase can be calculated by the change in $C^{18}O_2$ (from $NaH^{13}C^{18}O_3$), i.e., the changes in the decreasing rate in the presence or absence of carbonic anhydrase inhibitor (DBS) (Badger and Price 1989) (Fig. 22.4).

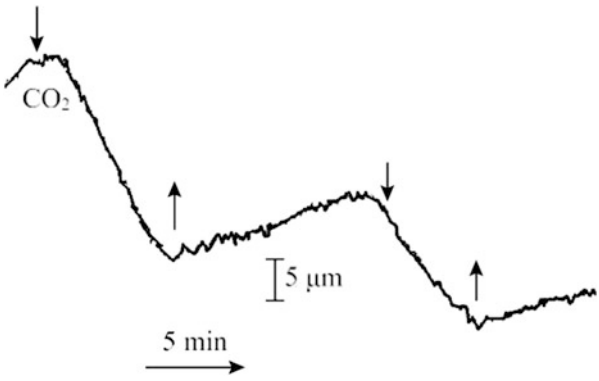

Fig. 22.3 Changes of pCO_2 in the solution holding the red alga *Porphyra yezoensis* when photosynthesis and respiration occur. Arrows indicate the time of turning on and off the light (Gao et al. 1992)

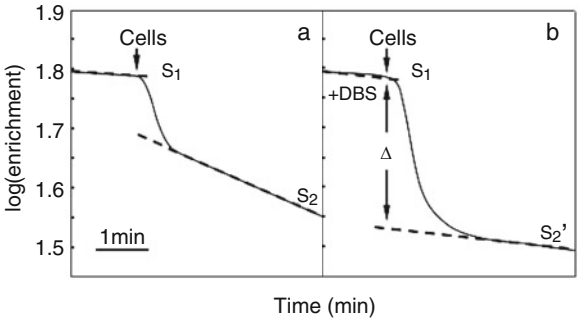

Fig. 22.4 The abundance of ^{18}O in double labeled CO_2 in the measurement of intracellular (a) and extracellular (b) carbonic anhydrase activity. DBS is an inhibitor of carbonic anhydrase, and S_1 and S_2 represent two kinds of changes. The newly added inorganic carbon (including the intracellular carbon pool, and the inorganic carbon in the added cell sample) instantly resulted in a decrease in the abundance of ^{18}O in the reaction chamber after adding cells. S_1 and S_2 represent the slope of the straight line before and after the addition of cells (reestablished from Rost et al. 2003)

^{18}O abundance in $C^{18}O_2$:

$$^{18}\text{O log (enrichment)} = \log \frac{\left(^{13}C^{18}O_2\right) \times 100}{^{13}CO_2}$$

$$= \log \frac{(49) \times 100}{45 + 47 + 49}.$$

45, 47, 49 are respectively the concentrations of CO_2 molecules that possess ^{13}C with corresponding atomic weights.

Carbonic anhydrase activity:

$U = \frac{(S_2 - S_1) \times 100}{S_1 \times mg\ Chl\ a}$

S_1 and S_2 represent the rate of change of the logarithmic ^{18}O abundance in CO_2 before and after adding cells. The exchange of ^{18}O will eventually reach equilibrium, but in a short period of time, the change of ^{18}O abundance in CO_2 is approximately a straight line, and Fig. 22.4 is the change during 5 min.

22.5 Measurement of the Production and Removal of H_2O_2 by MIMS

In the chloroplast, H_2O_2 is produced by the catalysis of superoxide anion by superoxide dismutase (SOD). Adada and Badger (1984) added $H_2{}^{18}O_2$ to the complete chloroplast, and the production ratio of $^{16}O_2$ and $^{18}O_2$ were detected. They found a light-dependent peroxidase pathway and it was independent of catalase-catalyzed reactive oxygen scavenging pathways. Photoreduction products ($e^- + H^+$) are used by peroxidase to reduce $H_2{}^{18}O_2$. The calculation is as follows:

$$2H_2{}^{16}O \rightarrow 4\,H^+ + 4(e^-) + {}^{16}O_2(\text{PS II})$$

$$2H_2{}^{18}O_2 + 4(e^-) + 4H^+ \xrightarrow{(\text{Peroxidase})} 4\,H_2{}^{18}O$$

$$2H_2{}^{16}O + 2\,H_2{}^{18}O_2 \rightarrow 4H_2{}^{18}O + {}^{16}O_2(\text{Total})$$

Miyake et al. (1991) used the same principle to study the clearance of reactive oxygen species by peroxidase in cyanobacteria.

22.6 Other Measurements

Methane produced during the metabolism of methanogens, N_2O released by organisms, the decrease of nitrogen (better to use isotopic N_2) caused by nitrogen fixation of phytoplankton, and the production of DMS by sea phytoplankton can be detected by MIMS.

Due to the detection principle of mass spectrometer and the characteristics of the semipermeable membrane, the impact of water vapor and the instrument itself must be excluded in the determination of oxygen and carbon dioxide in solutions. The background and the standard values must be calibrated because MIMS cannot directly provide the absolute concentration of gas in the solution. When measuring the dissolved gases in water, it is required that the reaction chamber is tightly sealed to avoid gas leakage. Silicone rubber film is very sensitive to the reaction temperature, so the temperature of the solution must be controlled.

22.7 Advantages and Disadvantages

MIMS can be used to simultaneously monitor the changes of gases in a long time period. Various compounds with different atomic weights can be used to explore new applications. The disadvantage is that the instrument is expensive, operation and concentration correction is time-consuming. In addition, due to the characteristics of the vacuum system of the instrument, it takes a long time to reach a relatively stable state, and as time goes on, the vacuum pressure of the system is reduced, which would influence the stability of the instrument. Thus, it is necessary to perform calibration twice at the beginning and the end of the measurement with a known concentration of a target gas.

References

Adada K, Badger MR (1984) Photoreduction of $^{18}O_2$ and $H_2{}^{18}O_2$ with concomitant evolution of $^{16}O_2$ in intact spinach chloroplasts: evidence for scavenging of hydrogen peroxide by peroxidase. Plant Cell Physiol 25:1169–2807

Badger MR, Price GD (1989) Carbonic anhydrase activity associated with the cyanobacterium *Synechococcus* PCC7942. Plant Physiol 89:51–60

Gao K, Aruga K, Ishihara T, Akano T, Kiyohara M (1992) Photorespiration and CO_2 fixation in the red alga *Porphyra yezoensis Ueda*. Jpn J Phycol 40:373–377

Hoch G, Kok B (1963) A mass spectrometer inlet system for sampling gases dissolved in liquid phases. Arch Biochem Biophys 101:160–170

Miyake C, Michihata F, Asada K (1991) Scavenging of hydrogen peroxide in prokaryotic and eukaryotic algae: acquisition of ascorbate peroxidase during the evolution of cyanobacteria. Plant Cell Physiol 32:33–34

Radmer R, Ollinger O (1980) Measurement of the oxygen cycle: the mass spectrometric analysis of gases dissolved in a liquid. Methods Enzymol 69:547–560

Rost B, Riebesell U, Burkhardt S (2003) Carbon acquisition of bloom-forming marine phytoplankton. Limnol Oceanogr 48:55–67

Silverman DN (1982) Carbonic anhydrase. oxygen-18 exchange catalyzed by an enzyme with rate-contributing proton-transfer steps. Methods Enzymol 87:732–752

Chapter 23
SIMS and NanoSIMS Techniques Applied to Studies of Plankton Productivity

Helle Ploug

Abstract During the past decade, secondary ion mass spectrometry (SIMS) has been introduced in phytoplankton ecology and microbiology. In principle, it combines the qualities of a microscope with those of a mass spectrometer with a high mass resolution and a spatial resolution of ca. 1 μm (SIMS) or even down to 50 nm (nanoSIMS). Thus, SIMS can provide images of stable isotopic composition of various elements at a sub-cellular spatial resolution of large phytoplankton (ca. >5 μm) while nanoSIMS is used to do stable isotopic imaging of smaller cells including individual bacteria. Combining SIMS with stable isotopic tracer incubations, we can study the cell-specific activities of phytoplankton and bacteria in mixed field communities at low nutrient concentrations while organism interactions remain intact. Methods are now established to investigate rates of, e.g., carbon fixation, nutrient acquisition of various nitrogen compounds including inorganic nitrogen fixation, and inorganic phosphorus assimilation in phytoplankton communities. Furthermore, transfer of nutrients and metabolites between different members of the community can be elucidated. Combining SIMS with elemental analysis isotope ratio mass spectrometry (EA-IRMS) the contribution of selected phytoplankton taxa to total community production can be analyzed and the quantitative role of various phytoplankton functional types revealed. This chapter presents an overview of the versatility of studies and experimental designs including SIMS as a powerful tool to quantify carbon and nutrient assimilation and transfer in phytoplankton field communities.

Keywords Isotopic tracers · Nutrient assimilation · Phytoplankton · Secondary ion mass spectrometry

H. Ploug (✉)
Department of Marine Sciences, University of Gothenburg, Gothenburg, Sweden
e-mail: helle.ploug@marine.gu.se

K. Gao et al. (eds.), *Research Methods of Environmental Physiology in Aquatic Sciences*, https://doi.org/10.1007/978-981-15-5354-7_23

23.1 Introduction

Secondary ion mass spectrometry (SIMS) is a well-established method to provide stable isotope images of organic and inorganic matter at high spatial resolution (>1 μm). It has a history spanning several decades where it has been applied in astrophysics and geology (e.g., Gnos et al. 2004; Whitehouse and Nemchin 2009; Zinner et al. 1989). Only during the past few years has it been introduced in biological oceanography, more specifically in phytoplankton ecology. This took place after nanoSIMS, with a spatial resolution down to 50 nm, had been developed to study in situ activities of uncultivated marine microbes and their symbioses (Lechene et al. 2006; Musat et al. 2008; Orphan et al. 2001). In principle, SIMS combines the qualities of a microscope with those of a mass spectrometer with high mass resolution and a spatial resolution at a subcellular level of single phytoplankton cells. Hence, the isotopic composition of single phytoplankton cells with known identity within mixed communities can be quantified after incubations with stable isotopic tracers, and hereby we can reveal their activities within field communities. The details of SIMS and nanoSIMS technology and measuring principles have been reviewed in depth previously (Lechene et al. 2006; Musat et al. 2012; Wagner 2009). In this chapter, recent examples of the applications of SIMS and nanoSIMS across various phytoplankton functional types are summarized, followed by a description of experimental designs and analysis of phytoplankton productivity and nutrient uptake by SIMS and nanoSIMS in field communities.

During the past decade, the applications of SIMS and nanoSIMS have given us an advanced mechanistic and quantitative understanding of the carbon (C), nitrogen (N), and phosphate (P) assimilation rates by various functional phytoplankton types and their interactions with other organisms within field communities. Much focus has been devoted to N_2 fixation and the fate of the newly fixed N within plankton communities. Using SIMS, the relative contributions of three different genera of large N_2 fixing cyanobacteria (*Nodularia*, *Aphanizomenon*, and *Dolichospermum*) to total CO_2 and N_2 fixation in the Baltic Sea were quantified during two years at a coastal and offshore station. Interestingly, the N_2 fixation by these three genera could explain 100% of total N_2 fixation while their combined contribution to the total CO_2 fixation was ca. 20% within the plankton community. The non-conspicuous *Aphanizomenon* contributed 70–80% to total N_2 fixation over the summer season (Klawonn et al. 2016). Using nanoSIMS, it has been shown that field populations of large filamentous cyanobacteria, e.g., *Trichodesmium*, *Nodularia*, *Aphanizomenon*, can grow solely on dissolved N_2 gas as inorganic N source in N depleted field communities (Martínez-Pérez et al. 2016; Ploug et al. 2010, 2011; Svedén et al. 2015). The same filamentous, N_2-fixing cyanobacteria have also been demonstrated to fix surplus N_2 relative to their CO_2 fixation. This surplus of freshly fixed N supports both the microbial and classical food web through release of ammonium and dissolved organic nitrogen (DON) that is quickly assimilated by other organisms within the coexisting plankton community, e.g., diatoms and picocyanobacteria (Adam et al. 2016; Bonnet et al. 2016; Caffin et al. 2018; Eichner et al. 2017;

Schoffelen et al. 2019). Hence, the transfer of diazotrophic nitrogen links various phytoplankton functional types within phytoplankton communities.

The development of nanoSIMS made it possible to study the exchange of carbon and fixed nitrogen in open ocean diatom-cyanobacterial symbioses (Foster et al. 2011) as well as in the recently discovered symbiosis between a unicellular prymnesiophyte and a unicellular cyanobacterium (UCYN-A). This symbiosis is highly abundant in the open oligotrophic ocean (Thompson et al. 2012; Martínez-Pérez et al. 2016). Extensive field experiments applying nanoSIMS as the main tool have shown that UCYN-A is at least as important as *Trichodesmium* for N_2 fixation in the subtropical ocean (Martínez-Pérez et al. 2016). These discoveries have stimulated much research of the role and rates of C- and N_2 fixation as well as utilization of various nitrogen sources (N_2, nitrate, ammonium, and DON) within plankton communities (e.g., Berthelot et al. 2015a, b, 2016, 2019; Klawonn et al. 2015, 2016, 2019).

SIMS has been applied to study the boron content and Si/C ratio, and their relationship to sea water pH and carbon acquisition in cultured chain-forming diatoms (*Thalassiosira)* (Mejía et al. 2013). Carbon and dissolved inorganic nitrogen (DIN) assimilation by diatoms have, so far, received less attention in studies involving SIMS and nanoSIMS as compared to N_2 fixation by cyanobacteria. Recently, the C and nitrate assimilation was measured in eight strains of the chain-forming diatom *Skeletonema marinoi*, which had been established in cultures from resting stages freshly isolated from sediment layers dating up to 80 years back in time. That study demonstrated a strong correlation between C and nitrate assimilation only during the exponential growth phase of these diatoms independent of age. A high strain-specific as well as cell-specific variation and diversity of assimilation rates also occurred in these diatoms independent of age (Olofsson et al. 2019a). High cell-to-cell variations of assimilation rates of C and nutrients are commonly observed in SIMS and nanoSIMS studies. This variation has now been demonstrated, both experimentally and mathematically by game theory, to support a population to adapt to variable growth limiting conditions and to support coexistence with other organisms in the field (Schreiber et al. 2016; Menden-Deuer and Rowlett 2018).

Diatoms are well-known to often base their primary production on nitrate as a DIN source as was also confirmed in two studies of field populations involving SIMS (Bergkvist et al. 2018; Olofsson et al. 2019b). These studies have shown that chain-forming diatoms can grow solely on nitrate in field communities and contribute ca. 50% to total nitrate assimilation in mixed phytoplankton communities both when their abundance is high during spring blooms (Bergkvist et al. 2018) as well as during summer when their abundance is low (Olofsson et al. 2019b). Interestingly, a comparison of measured cell-specific assimilation rates with those predicted by mass transfer theory indicated that when nitrate assimilation was diffusion-limited, ammonium uptake by chain-forming diatoms may be facilitated by microbial interactions in their phycosphere during summer when DIN concentrations are low (Olofsson et al. 2019b). Another SIMS study of C and nitrate assimilation at a single-cell level in chain-forming diatoms (*Skeletonema* and *Chaetoceros*) from spring bloom populations also demonstrated diffusion limitation of nitrate uptake, and CO_2

assimilation was increased in response to laminar shear which occur at small scale during turbulence as predicted by mass transfer theory (Bergkvist et al. 2018). Hence, diffusion-limited nitrate uptake in large chain-forming diatoms can occur both during the spring bloom maximum and in summer populations, and may be relatively common in field populations with nitrate concentrations <0.3 μM.

Mixotrophy has been demonstrated to boost primary production by up to 50% in oligotrophic areas (Stoecker et al. 2017), and it is therefore of high interest to accurately include its contributions to global nutrient budgets. Using SIMS in combination with isotopic tracers is an excellent approach to investigate both nutrient uptake and grazing of specific isotopically marked preys. The use of mixotrophy by large dinoflagellates has been analyzed both in cultures (Carpenter et al. 2018) and in the field (Olofsson et al. 2019b). These studies suggest that the C-demand in large dinoflagellates is covered by autotrophy whereas the N-demand is covered both by diffusion-limited DIN fluxes and grazing.

It has often been assumed that small cells grow faster than large cells due to diffusion limitation of nutrient uptake. SIMS and nanoSIMS studies in field communities, however, have shown that this is not always the case. Often large cells can grow as fast or even faster than small ones, and their large cellular biomass implies that the cell-specific assimilation rates of C and nutrients by large cells can be substantially higher than for small cells (Bergkvist et al. 2018; Klawonn et al. 2019; Musat et al. 2008; Martínez-Pérez et al. 2016; Olofsson et al. 2019b). Small cells do not grow as fast as they theoretically should do if they were perfect sinks of nutrients which means that they absorb nutrients as fast as they arrive at the cell surface and the steady-state concentration at the cell surface is close to zero (Adam et al. 2016; Bergkvist et al. 2018; Klawonn et al. 2019). These observations may be explained by the fact that smaller cells need a higher transporter density in their membranes compared to large cells, in order to maximize nutrient affinity during diffusion limitation when the nutrient concentration at the cell surface is very low. This cost of transporters is relatively higher for a small than for a large cell due to their high surface to volume ratio (Lindemann et al. 2016).

In addition to isotopically-labeled ^{15}N and ^{13}C, SIMS has also been applied to isotopes of phosphorous (P). However, as phosphorus only exists as one stable isotope, the quantification of its assimilation into biomass by SIMS and nanoSIMS is not trivial. A novel method was recently developed in which the phytoplankton community is incubated with the radioactive isotope ^{33}P, which decays to the stable isotope ^{33}S which can subsequently be measured together with ^{32}S by SIMS or nanoSIMS to quantify ^{33}P assimilation rates. This method has provided new insights into the P-source used by various coexisting N_2 fixing filamentous cyanobacteria (Schoffelen et al. 2018), and how inorganic P regulates the release of freshly fixed N_2 which is transferred to their epibionts (Schoffelen et al. 2019).

The effects of global warming and ocean acidification can now also be studied at a single-cell level in field population. Using SIMS and nanoSIMS it has been demonstrated that *Trichodesmium* colonies are not particular sensitive to ocean acidification, presumably due to the steep gradients of O_2 concentration and pH combined with a high cell-to-cell diversity of metabolic rates in *Trichodesmium* cells

as well as of their epibionts (Eichner et al. 2017). In another experimental study which focused on warming, it was shown that attachment and exchange of metabolites between phytoplankton and bacteria increase as a response to warming (Arandia-Gorostidi et al. 2017). Thus, SIMS and nanoSIMS can provide novel mechanistic understanding of consequences and adaptations to climate change at a small scale which are not possible with other techniques.

Conclusively, the application of SIMS has proven to be a powerful tool in experimental field studies to unravel carbon and nutrient assimilation at a single-cell level as well as their transfer through organism interactions in plankton communities. Using a thorough experimental design in combination with SIMS, we can address a wide range of fundamental questions in plankton physiology and productivity which were previously not possible.

23.2 Methodology

Incubations with isotopic tracers—it is relatively straight forward to study or examine the use of a specific nutrient by an organism if only a qualitative answer is needed. In such experiments, a tracer of the less abundant stable isotope of the nutrient of interest, e.g., ^{15}N-nitrate, ^{15}N-ammonium, or $^{15}N_2$, is added to the community during short-term incubations (a few hours) and a parallel incubation without any tracer addition is performed as control. Incubations including both ^{13}C and ^{15}N can be performed simultaneously. The incubations are ended by fixation of a sample in 2% PFA during ca. 24 h at 4 °C, e.g., in a fridge. The samples are subsequently filtered onto individual polycarbonate filters and washed with phosphate buffered saline (PBS, 10×, pH 7.4). Polycarbonate filters are available with different pore sizes, and must be chosen depending on the size of organisms of interest. For example, GTTP filters of 0.22 µm pore size can be used for bacteria and TTTP filters of 2.0 µm pore size for larger phytoplankton. Prior to the final filtration, it is important to examine how much volume should be filtered to produce a sample with several regions of evenly spread cells which do not overlap during the subsequent SIMS analysis. This can be done visually by light microscopy. Filters containing large phytoplankton can be stored dry at room temperature until SIMS analysis, whereas those for nanoSIMS analysis of bacteria should be treated with ethanol-PBS solution and stored at −20 °C.

Quantification of assimilation rates requires that the labeling % of the C and nutrient of interest in the ambient water are quantified during the incubations. This can be done by taking samples at various time points to be analyzed using GC-IRMS after conversion to CO_2 and N_2 gas (Füssel et al. 2012; Warembourg 1993). Furthermore, a sample from a non-labeled incubation is taken and analyzed as control. This can be limited to T_0 and T_{end} as long as no production of the nutrient of interest occurs during the incubation. Incubation with ^{15}N-ammonium is an example where much care must be taken to monitor the ^{15}N:^{14}N ratio of ammonium because its turnover time is short (usually a few hours) and its assimilation is tightly

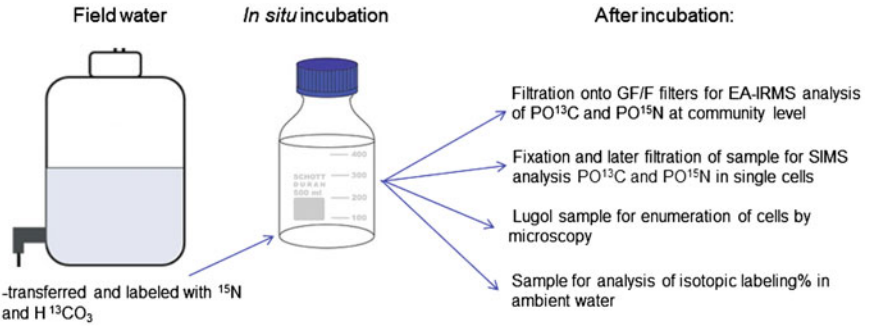

Fig. 23.1 Incubations, samples, and analysis needed for quantification of the contribution of a specific class or genera of organisms to the total C and nutrient fluxes in a phytoplankton community

coupled to its remineralization. The production of ^{14}N-ammonium during remineralization leads to a decrease in ^{15}N:^{14}N ratio during the incubation. Consequently, the ^{15}N:^{14}N ratio of ammonium decreases exponentially during the incubation time and often nearly all ^{15}N ammonium is assimilated in biomass after less than 5 h (Klawonn et al. 2019; Olofsson et al. 2019a).

Quantification of the contribution of specific taxa to total C and nutrient assimilation and transfer in a phytoplankton community requires, besides SIMS analyses, enumeration of the organisms in the community as well as measurements of total C and nutrient assimilation within the community. The enumeration of the phytoplankton organisms can be done by traditional microscopy in counting chambers after Lugol fixation. Determination of total C and nutrient assimilation by the mixed plankton community should be done in parallel with determination of the cell-specific assimilation rates. Here, the plankton community (ca. 500 mL in coastal environments) is filtered onto pre-combusted GF/F filters after incubation with the stable isotopic tracers. These filters are subsequently freeze-dried or dried at 60 °C, and decalcified in HCl fumes over night before subsamples are packed into tin cups for later determination of particulate organic carbon (POC) and nitrogen (PON) and the isotopic composition by Elemental Analysis Isotope Ratio Mass Spectrometry (EA-IRMS). An example of the experimental design to measure cell-specific activities of dissolved inorganic carbon (DIC) and DIN assimilation in field populations and their contributions to total DIC and DIN assimilation in a phytoplankton community is shown (Fig. 23.1).

SIMS analysis—Prior to SIMS analysis, the polycarbonate filters should be inspected by light or fluorescence microscopy to identify regions of interest with as many nonoverlapping cells of interest as possible. The regions are cut out of the filters in ca. 4 × 4 mm pieces and glued onto a filter holder and sputtered with gold to form a few nanometer thick layer covering the cells and which facilitates the conductivity of ions in the sample. The gold sputtered filters on the holder are subsequently loaded into a Secondary Ion Mass Spectrometer IMS 1280 (CAMECA, Gennevilliers, France). There is space for ca. 8 filter pieces on each

holder. Analysis on cells >5 μm can be performed using a Secondary Ion Mass Spectrometer IMS 1280 (CAMECA, Gennevillies, France) whereas smaller cells should be measured by a NanoSIMS 50L (CAMECA, Gennevilliers, France). In both cases, the cells are bombarded by cesium (Cs^+) ions from a primary beam producing secondary ions in the cell. The secondary ions produced during this bombardment are resolved at high mass resolution and spatial resolution to produce isotope images of the cell. One of the advantages of SIMS over nanoSIMS analysis of large cells is that the higher current from the primary Cs^+ beam of the SIMS facilitates the removal of consolidated cell walls, e.g., diatom frustules. Prior to analysis of diatoms, the cells are pre-sputtered by the primary Cs^+ beam of 10 nA for 5 min to remove the silicified cell wall. However, different intensities and durations must be tested to reach the CN-rich region within the cells. During analysis in the CN-rich region within the cells, the primary beam is reduced to 40–80 pA primary beam for 100 cycles corresponding to a sub-micrometer spatial resolution for data acquisition using a 50 × 50 μm primary beam raster. Secondary ion images can be collected for $^{12}C^{14}N^-$, $^{12}C^{15}N^-$, and $^{13}C^{14}N^-$ with dwell times of 1 s, 5 s, and 2 s, respectively (wt time 0.8 s, 100 cycles) at a mass resolution of 12,000 ($M/\Delta M$) using a peak-switching routine into the low-noise, ion counting electron multiplier detector of the SIMS. Alternative ions can be chosen for analysis, but the use of CN isotopomers has the advantage that they are bright and two isotope ratios can be measured from measurements of three isotopomers. Up to seven elements or isotopes of elements can be measured simultaneously by a NanoSIMS 50L. The lower spatial resolution of the SIMS as compared to nanoSIMS allows for a higher sample throughput of large cells. Several hundred phytoplankton cells can be analyzed by SIMS per day.

Data processing can be done using the CAMECA WinImage2 software, but alternative programs have been developed as well (Polerecky et al. 2012). The region of interest (ROI) of individual cells can be drawn manually in the image of $^{12}C^{14}N^-$ abundance, which reflects the biomass and shows highest intensity of the CN^- isotope images (Fig. 23.2). The average ^{15}N:^{14}N and ^{13}C:^{12}C isotope ratios within each ROI are calculated using theWinImage2 software and are returned in an Excel spread sheet.

The cell-to-cell variation is high both in phytoplankton monocultures and in field populations which are composed of many strains (Bergkvist et al. 2018; Olofsson et al. 2019b). Thus, it is important to do an analysis to examine if enough cells have been measured to achieve a representative average value of the assimilation rate of interest. This analysis can be done by plotting the average cell-specific assimilation rate as a function of number of cells analyzed. In such a plot the average cell-specific assimilation rate often reaches a stable value with a standard error of <5% after more than 50 cells have been measured (Svedén et al. 2015; Bergkvist et al. 2018). An example of such an analysis of C assimilation by *Chaetoceros* cells is shown (Fig. 23.3).

Calculations—the total C assimilation rates (nM h^{-1}) in the plankton community can be calculated from the ^{13}C-atom% excess of DIC above that of the natural isotope abundance in the ambient water measured by GC-IRMS after conversion to

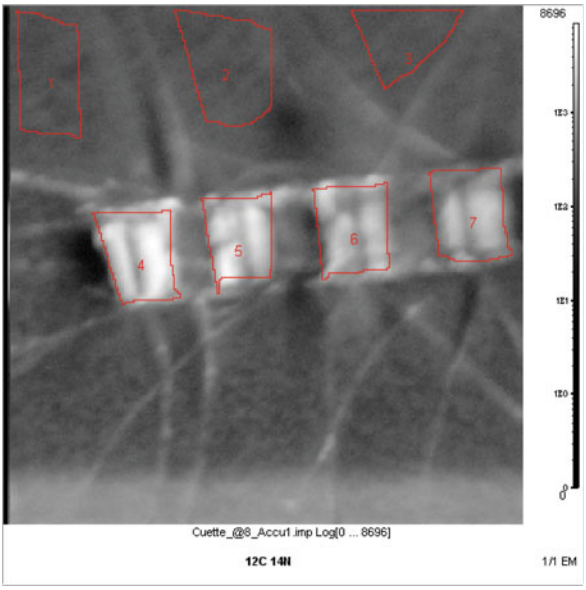

Fig. 23.2 SIMS ($^{12}C^{14}N^{-}$) image of *Chaetoceros* cell chain with regions of interest (ROI) around individual cells (4, 5, 6, 7)

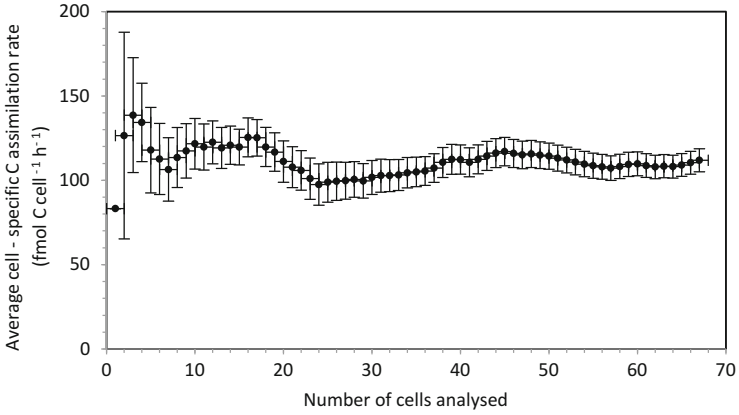

Fig. 23.3 Analysis of the average cell-specific C assimilation rate as a function of cells analyzed. The error bars represent standard error of the mean value

CO_2 and the change in excess isotopic composition of particulate organic carbon (POC) above that of the natural isotope abundance during the incubation time, *t*, measured by EA-IRMS (Montoya et al. 1996):

$$\text{C assimilation rate} = \frac{\Delta 13\text{C} - \text{atom\%excess}_{(\text{POC})} \times \text{POC}}{13\text{C} - \text{atom\%excess}_{(\text{DIC})} \times \Delta t} \tag{23.1}$$

Cell-specific C assimilation rates can be calculated analogously from the average POC content of single cells (Menden-Deuer and Lessard 2000) and the change in ^{13}C-atom% excess isotopic composition of single cells during the incubation time, t, measured by SIMS.

If no nitrification is detectable during the incubations, nitrate assimilation rates can be calculated from the ^{15}N-atom% excess of nitrate in the ambient water as measured by GC-IRMS after conversion to N_2 and the change in excess ^{15}N isotopic composition of particulate organic nitrogen (PON) measured by EA-IRMS during the incubation time, t (Montoya et al. 1996):

$$\text{Nitrate assimilation rate} = \frac{\Delta 15\text{N} - \text{atom\%excess}_{(\text{PON})} \times \text{PON}}{15\text{N} - \text{atom\%excess}_{(\text{nitrate})} \times \Delta t} \tag{23.2}$$

Similar to carbon assimilation, cell-specific N assimilation rates at a single-cell level can be calculated from the average PON content of single cells (Menden-Deuer and Lessard 2000) and the change in ^{15}N-atom% excess isotopic composition of single cells during the incubation time, t, measured by SIMS. N_2-fixation rates can also be calculated using Eq. 23.2 when the ^{15}N-atom% excess of dissolved N_2 gas is known (Klawonn et al. 2015).

Ammonium cycling is fast and the ^{15}N ammonium-atom% excess depends on regeneration of ^{14}N ammonium during the incubation. The ^{15}N:^{14}N ratio decreases exponentially in the ambient water with first-order kinetics concurrent with dilution of the ^{15}N from regenerated ^{14}N. Assimilation of ammonium must be calculated based on the average excess atom% during the incubation time, R (Glibert et al. 1982):

$$R = \frac{R_0}{kt}\left[1 - \exp\left(kt\right)\right] \tag{23.3}$$

where R_0 is the initial ^{15}N ammonium-atom% excess, t is the incubation time and k is the specific decrease in ^{15}N ammonium-atom% excess per unit time:

$$k = \frac{\ln\left(R_t/R_0\right)}{t} \tag{23.4}$$

The ammonium assimilation rate (nM h^{-1}) in the plankton community is calculated based on the average ^{15}N ammonium-atom% excess, R, during the incubation time (t) measured by GC-IRMS after conversion to N_2 (Warembourg 1993) and the change in excess ^{15}N isotopic composition of organic nitrogen measured by EA-IRMS during the incubation time:

$$\text{Ammonium assimilation rate} = \frac{\Delta 15\text{N} - \text{atom\%excess}_{(\text{PON})} \times \text{PON}}{R \times \Delta t} \quad (23.5)$$

Cell-specific ammonium assimilation rates can also be calculated from the average PON content of single cells (Menden-Deuer and Lessard 2000) and the change in ^{15}N-atom% excess isotopic composition of single cells measured by SIMS and the average ^{15}N ammonium-atom% excess, R, during the incubation time, t, measured by GC-IRMS using Eq. 23.5.

C and N growth rates at a single-cell level—assuming an evenly distribution of the isotope in the biomass during cell division, the C growth rate and the N growth rates (h^{-1}) based on DIC and DIN assimilation, respectively, can be calculated independent of cell size and POC or PON content of the single cells after SIMS measurements (Olofsson et al. 2019a, b; Schoffelen et al. 2018, 2019):

$$\text{C or N based growth rate } \left(h^{-1}\right) = \frac{\text{atom\%excess}_{(\text{POM})}}{\text{atom\%excess}_{(\text{dissolved})}} \times 2 \times 1/t \quad (23.6)$$

where atom% excess$_{(\text{POM})}$ represents the excess isotope ratio of the cell, atom% excess$_{(\text{dissolved})}$ represents the excess isotope ratio of DIC, nitrate or ammonium in the ambient water during the incubation, and t is the incubation time. The factor of 2 describes the dilution of the heavy isotope during assimilation into the cell with an original isotope composition equal to the natural background during cell division. C and N doubling times can be calculated as ln 2/k, assuming exponential growth.

23.3 Analysis of Merit and Demerit for the Method

Previously, studies of phytoplankton cell physiology have been limited to monocultures, where each strain has been isolated from a field population and grown under controlled light and temperature in a medium with high nutrient concentrations in the laboratory. The nitrate concentration in F/2 medium is as high as 880 μM whereas winter nitrate concentrations often are <5 μM in coastal seas (Guillard 1975). With such high nutrient concentrations, the phytoplankton growth often becomes light limited and the cells may adapt to higher nutrient concentrations than those occurring in the field, especially when kept in culture over several years. Applying SIMS technology as a culture-independent method, we can now measure cell-specific C and nutrient assimilation rates at naturally low nutrient concentrations in mixed communities with the interaction between organisms staying intact. In mixed communities, however, it is not possible to measure the absolute cell-specific content of C, N, and P while it can be relatively easily done in (axenic) monocultures. Instead, the cell-specific C and N content can be estimated from the cell volume (Menden-Deuer and Lessard 2000; Khachikyan et al. 2019). Cell-specific C:

N:P ratios in mixed communities can even be determined by energy dispersive X-ray spectroscopy (EDS) (Schoffelen et al. 2018, 2019).

The applications of SIMS and nanoSIMS technology were developed as a culture-independent method to study the activities of eukaryotic phytoplankton, Bacteria, and Archaea in the sea. However, we can also learn much from applications of SIMS technology in culture studies. Applying SIMS and nanoSIMS in culture studies of various strains of microorganisms as well as of chain-forming diatoms we have learned that even cells with monoclonal cells can show considerable variation in C and N assimilation rates under the same conditions (Olofsson et al. 2019a; Schreiber et al. 2016). Interestingly, all data published on C and nutrient assimilation at a single-cell level in phytoplankton as well as in phototrophic bacteria have shown a large cell-to-cell variability both in single strain cultures and in multi-strain field populations. Consequently, as mentioned earlier, a large number of cells need to be analyzed in order to achieve a representative cell-specific rate of C or nutrient assimilation. The high throughput by SIMS which can measure several hundred cells per day due to its lower spatial resolution makes SIMS superior to nanoSIMS when cells are >5 μm. However, the spatial resolution of ca. 1 μm for SIMS is not sufficient to do isotope imaging of single bacterial cells. To analyze such small cells, nanoSIMS with a spatial resolution of ca. 50 nm can be deployed with a similar high throughput as SIMS analysis of larger cells (Adam et al. 2016; Klawonn et al. 2016, 2019)

A clear advantage of SIMS and nanoSIMS to measure rates at a single-cell level combined with EA-IRMS to measure rates at a community level is that it provides insight into the life of plankton cells in natural complex communities where nutrient concentrations are usually low. With this new approach, we can now elucidate who is doing what and at which rates and even quantify how much selected organisms contribute to C fixation and assimilation of various nutrient sources within the community. Previously, size fractionations of field communities have been used before isotopic analysis to pursue similar questions. The latter method is simpler as compared to the elaborate analysis deploying various types of mass spectrometry. However, different phytoplankton functional types can have similar sizes but very different physiology and ecology which can be differentiated using SIMS (Berthelot et al. 2019; Klawonn et al. 2019; Olofsson et al. 2019a). Size fractionation also disrupts interactions between small and large cells, including nutrient transfer and grazing. Hence, SIMS can provide more realistic rates because nutrient concentrations remain low and organism interactions intact during the incubations.

The major drawback of studies involving SIMS, EA-IRMS, and GC-IRMS is that the generation of data and its analysis from these studies are elaborate and can be expensive. Few institutions across the world host all types of mass spectrometry at the same time. However, the number of SIMS and nanoSIMS facilities has increased substantially during the past decade, and many of these facilities are open for external users. As demonstrated in this chapter, SIMS technology offers a high versatility of new possibilities to study phytoplankton physiology and ecology in the field, and its use can advance of knowledge about plankton physiology and

ecology from the sub-micron microbes to micrometer-sized phytoplankton substantially.

Acknowledgements I am grateful to Marcel Kuypers and Niculina Musat for introducing me to nanoSIMS. I also wish to express my gratitude to Martin Whitehouse at the NORDSIM facility at the Natural History Museum in Stockholm and Niculina Musat who were open and supportive to initiate and develop protocols for SIMS analysis of large phytoplankton together with me and my students. I am grateful to John Beardall who invited me to contribute with this chapter. Thanks to Isabell Klawonn, Malin Olofsson, Rickard Stenow, and Elizabeth Robertson for reading and commenting a previous version of the manuscript.

References

Adam B, Klawonn I, Svedén J, Bergkvist J, Nahar N, Walve J, Littmann S, Whitehouse MJ, Lavik G, Kuypers MMM, Ploug H (2016) N_2-fixation, ammonium release, and N-transfer within the plankton community in the Baltic Sea. ISME J 10:450–459

Arandia-Gorostidi N, Weber PK, Alonso-Sáez L, Morán XAG, Mayali X (2017) Elevated temperature increases carbon and nitrogen fluxes between phytoplankton and heterotrophic bacteria through physical attachment. ISME J 11:641–650

Bergkvist J, Klawonn I, Whitehouse MJ, Lavik G, Brüchert V, Ploug H (2018) Turbulence simultaneously stimulates small-scale and large-scale CO_2 sequestration by chain-forming diatoms in the sea. Nat Commun 9(1):304

Berthelot H, Bonnet S, Camps M, Grosso O, Moutin T (2015a) Assessment of the dinitrogen released as ammonium and dissolved organic nitrogen by unicellular and filamentous marine diazotrophic cyanobacteria grown in culture. Front Mar Sci 2:80

Berthelot H, Moutin T, L'Helguen S, Leblanc K, Hélias S, Grosso O et al (2015b) Dinitrogen fixation and dissolved organic nitrogen fueled primary production and particulate export during the VAHINE mesocosm experiment (New Caledonia lagoon). Biogeoscience 12 (13):4099–4112

Berthelot H, Bonnet S, Grosso O, Cornet V, Barani A (2016) Transfer of diazotroph-derived nitrogen towards non-diazotrophic planktonic communities: a comparative study between *Trichodesmium erythraeum, Crocosphaera watsonii* and *Cyanothece* sp. Biogeoscience 13 (13):4005–4021

Berthelot H, Duhamel S, L'Helguen S, Maguer J-F, Wang S, Cetinic I, Cassar N (2019) NanoSIMS single cell analysis reveal the contrasting nitrogen sources for small phytoplankton. ISME J 13:651–662

Bonnet S, Berthelot H, Turk-Kubo K, Cornet-Barthaux V, Fawcett S, Berman-Frank I et al (2016) Diazotroph derived nitrogen supports diatom growth in the South West Pacific: a quantitative study using nanoSIMS. Limnol Oceanogr 61(5):1549–1562

Caffin M, Berthelot H, Cornet-Barthaux V, Barani A, Bonnet S (2018) Transfer of diazotroph-derived nitrogen to the planktonic food web across gradients of N_2 fixation activity and diversity in the western tropical South Pacific Ocean. Biogeoscience 15(12):3795–3810

Carpenter KJ et al (2018) Single cell view of carbon and nitrogen acquisition in the mixotrophic alga *Prymnesium parvum* (Haptophyta) inferred from stable isotope tracers and nanosims. Front Mar Sci 5:157

Eichner M, Klawonn I, Wilson ST, Littman S, Whitehouse MJ, Church MJ, Kuypers MMM, Karl DM, Ploug H (2017) Chemical microenvironments and single-cell carbon and nitrogen uptake in field-collected colonies of *Trichodesmium* under different pCO_2. ISME J 11:1305–1317

Foster RA, Kuypers MM, Vagner T, Paerl RW, Musat N, Zehr JP (2011) Nitrogen fixation and transfer in open ocean diatom-cyanobacterial symbioses. ISME J 5:1484–1493

Füssel J et al (2012) Nitrite oxidation in the Namibian oxygen minimum zone. ISME J 6:1200–1209
Glibert PM, Lipschultz F, McCarthy JJ, Altabet MA (1982) Isotope dilution models of uptake and remineralization of ammonium by marine plankton. Limnol Oceanogr 27:639–650
Gnos E, Hofmann BA, Al-Kathiri A, Lorenzetti S, Eugster O, Whitehouse MJ, Villa AJ, Jull T, Eikenberg J, Spettel B, Krähenbühl U, Franchi A, Greenwood RC (2004) Pinpointing the source of a lunar meteorite: Inplications for the evolution of the Moon. Science 305:657–659
Guillard RRL (1975) Culture of phytoplankton for feeding marine invertebrates. In: Smith W, Chanley M (eds) Culture of marine invertebrate animals. Springer, Boston, MA, pp 29–60
Khachikyan A, Milucka J, Littmann S, Ahmerkamp S, Meador T, Könneke M, Burg T, Kuypers MMM (2019) Direct cell mass measurements expand the role of small microorganisms in nature. Appl Environ Microbiol 85:e00493–e00419
Klawonn I, Lavik G, Böning P, Marchand H, Dekaezemacker J, Mohr W, Ploug H (2015) Simple approach for the preparation of $^{15\text{-}15}N_2$-enriched water for nitrogen fixation assessments: evaluation, application and recommendations. Front Microbiol 6:769
Klawonn I, Nahar N, Walve J, Andersson B, Olofsson M, Barthel Svedén J, Littmann S, Whitehouse MJ, Kuypers MMM, Ploug H (2016) Cell-specific N_2-fixation and primary production by cyanobacteria in a temperate marine system (the Baltic Sea). Environ Microbiol 18 (12):4596–4609
Klawonn I, Bonaglia S, Whitehouse MJ, Litmann S, Tienken D, Kuypers MMM, Brüchert V, Ploug H (2019) Untangling hidden nutrient dynamics: rapid ammonium cycling and single-cell ammonium assimilation in marine plankton communities. ISME J 13:1960–1974
Lechene C, Hillion F, McMahon G, Benson D, Kleinfeld AM et al (2006) High-resolution quantitative imaging of mammalian and bacterial cells using stable isotope mass spectrometry. J Biol 5:20
Lindemann C, Fiksen Ø, Andersen KH, Aksnes DL (2016) Scaling laws in phytoplankton nutrient uptake affinity. Front Mar Sci 3:26
Martínez-Pérez C et al (2016) The small unicellular diazotrophic symbiont, UCYN-A, is a key player in the marine nitrogen cycle. Nat Microbiol 1:16163
Mejía LM, Iseense K, Méndez-Vincente A, Pisonero J, Simizu N, González C, Monteleone B, Stoll H (2013) B content and Si/C ratio from cultured diatoms (*Thalassirosia pseudonana* and *Thalassirosira weissflogii*): relationship to sea water pH and carbon acquisition. Geochim Geocosm Acta 123:322–337
Menden-Deuer S, Lessard EJ (2000) Carbon to volume relationships for dinoflagellates, diatoms, and other protist plankton. Limnol Oceanogr 45:569–579
Menden-Deuer S, Rowlett J (2018) The theory of games and microbe ecology. Theor Ecol 12 (1):1–15
Montoya JP, Voss M, Kähler P, Capone DG (1996) A simple high-precision, high-sensitivity tracer assay for N_2-fixation. Appl Environ Microbiol 62:986–993
Musat N, Halm H, Winterholler B, Hoppe P, Peduzzi S et al (2008) A single-cell view on the ecophysiology of anaerobic phototrophic bacteria. Proc Natl Acad Sci U S A 105:17861–17866
Musat N, Foster R, Vagner T, Adam B, Kuypers MMM (2012) Detecting metabolic activities in single cells, with emphasis on nanoSIMS. FEMS Microbiol Rev 36(2):486–511
Olofsson M, Kourtchenko O, Zetsche EM, Marchant H, Whitehouse MJ, Godhe A, Ploug H (2019a) High single cell diversity in carbon and nitrogen assimilation by a chain-forming diatom across a century. Environ Microbiol 21:142–151
Olofsson M, Robertson EK, Edler L, Whitehouse MJ, Ploug H (2019b) Nitrate and ammonium fluxes to diatoms and dinoflagellates at a single cell level in mixed field communities in the sea. Sci Rep 9:1424
Orphan VJ, House CH, Hinrichs KU, McKeegan KD, DeLong EF (2001) Methane-consuming archaea revealed by directly coupled isotopic and phylogenetic analysis. Science 293:484–487
Ploug H, Musat N, Adam B, Moraru CM, Lavik G, Vagner T, Bergman B, Kuypers MMM (2010) Carbon and nitrogen fluxes associated with the cyanobacterium *Aphanizomenon* sp. in the Baltic Sea. ISME J 4:1215–1223

Ploug H, Adam B, Musat N, Kalvelage T, Lavik G, Wolf-Gladrow D, Kuypers MMM (2011) Carbon, nitrogen, and O_2 fluxes associated with the cyanobacterium *Nodularia spumigena* in the Baltic Sea. ISME J 5:1549–1558

Polerecky L, Adam B, Milucka J, Musat N, Vagner T, Kuypers MMM (2012) Look@nanosims – a tool for the analysis of nanoSIMS data in environmental microbiologyemi. Environ Microbiol 14:1009–1023

Schoffelen NJ, Mohr W, Ferdelman TG, Littmann S, Dürschlag S, Zubkov MV, Ploug H, MMM K (2018) Single cell imaging of phosphorus uptake shows that key harmful algae rely on different phosphorus sources for growth. Sci Rep 8:17182

Schoffelen NJ, Mohr W, Ferdelman TG, Littmann S, Dürschlag S, Ploug H, Kuypers MMM (2019) Phosphate availability affects fixed nitrogen transfer from diazotrophs to their Epibionts. ISME J 13:2701–2713

Schreiber F et al (2016) Phenotypic heterogeneity driven by nutrient limitation promotes growth in fluctuating environments. Nat Microbiol 16055

Stoecker DK, Hansen PJ, Caron DA, Mitra A (2017) Mixotrophy in marine plankton. Ann Rev Mar Sci 9:311–335

Svedén JB, Adam B, Walve J, Nahar N, Musat N, Lavik G, Whitehouse MJ, Kuypers MMM, Ploug H (2015) High cell-specific rates of nitrogen and carbon fixation by the cyanobacterium *Aphanizomenon* sp. at low temperatures in the Baltic Sea. FEMS Microbiol Ecol 91(12):fiv131

Thompson AW, Foster RA, Krupke A, Carter BJ, Musat N, Vaulot D, Kuypers MMM, Zehr JP (2012) Unicellular cyanobacterium symbiotic with a single-celled eukaryotic alga. Science 337 (6101):1546–1550

Wagner M (2009) Single-cell ecophysiology of microbes as revealed by Raman microspectroscopy or secondary ion mass spectrometry imaging. Annu Rev Microbiol 63:411–429

Warembourg FR (1993) In nitrogen isotopes techniques, nitrogen fixation in soil and plant systems. In: Knowles K, Blackburn TH (eds) . Academic, New York, NY, pp 157–180

Whitehouse MJ, Nemchin AA (2009) High precision, high measurement of oxygen isotopes in a large lunar zircon by SIMS. Chem Geol 261:31–41

Zinner E, Ming T, Anders E (1989) Interstellar SIC in the Murchison and Murray meteroites – isotopic composition of Ne, Xe, Si, C, and N. Geochim Cosmochim Acta 53:3272–3290

Chapter 24
Measurements of Photoinactivation and Repair of Photosystem II

Gang Li, Yahe Li, Wanchun Guan, and Hongyan Wu

Abstract Marine phytoplankton utilize the energy absorbed from natural sunlight through Photosystem II (PS II) complexes, to split water and convert the light energy into chemical energy; while excessive absorption of solar energy by the cells will result in the inactivation of PS II. Photoinactivation of PS II is an important component of the metabolic and eco-physiological processes in oxygen-evolving photoautotrophs; it is thus key to quantify the rate of PSII photoinactivation. This section describes in detail the methods and procedures for determination of PS II photoinactivation in phytoplankton, and particularly a method for estimating the rate constant of the damage to photosynthetic apparatus (k, in min^{-1}) and the corresponding repair rate constant (r, in min^{-1}) under inhibitory solar ultraviolet radiation (UVR), as well as matters needing attention during the operations.

Keywords Photoinactivation · Photodamage · Repair · Photosystem II · Phytoplankton

G. Li (✉)
Key Laboratory of Tropical Marine Bio-resources and Ecology, South China Sea Institute of Oceanology, Chinese Academy of Sciences, Guangzhou, China
e-mail: ligang@scsio.ac.cn

Y. Li
School of Marine Science, Ningbo University, Ningbo, China

W. Guan
School of Laboratory Medicine and Life Science, Wenzhou Medical University, Wenzhou, China

H. Wu
College of Life Science, Ludong University, Yantai, China

K. Gao et al. (eds.), *Research Methods of Environmental Physiology in Aquatic Sciences*, https://doi.org/10.1007/978-981-15-5354-7_24

24.1 Introduction

Phytoplankton utilize solar energy to assimilate inorganic carbon into organic matters and produce oxygen. For the first step, they use the light energy to split water in Photosystem II (PS II) complexes, and transfer the electrons from water splitting to plastoquinones (PQ). At the same time, the proton (H^+) gradient is established at two sides of thylakoid membrane, powered by the oxidation of water and reduction of Quinone (PQB^{2-}) to accumulate energy and for the formation of reductant (ATP and NADPH) (Albertsson 2001; Han et al. 2003). The PS II complex is primarily composed of the outer light harvesting pigment-protein complex II (LHC II), the inner light harvesting pigment-protein complex (CP43, CP47, etc.), the PS II reaction center (PS II-RC), the oxygen-evolving complex (OEC) and outer proteins (33 kDa, 17 kDa). The PSII reaction center is constituted of the core proteins of D1 and D2, the α- and β-subunits of Cytochrome b55 (Cyt b599), and the psbI gene product, as well as the pigments chlorophyll a (Chl a), Pheophytin (Pheo), and β-carotenoid (Car) (Han et al. 2003).

Light drives phytoplankton photosynthesis, while excessive light energy will cause PSII to be deactivated. Previous studies showed that high light or ultraviolet radiation (UVR) can damage the core protein subunits of the PSII reaction center of photosynthetic organisms, especially the D1 protein, enabling the photoinactivation of PSII to occur. When the photoinactivation rate over-exceeds the repair rate, photoinhibition occurs and leads to a decrease in photosynthetic capacity (Murata et al. 2007; Raven 2011). Therefore, photoinactivation of PSII is an indicator for the photophysiological status of photosynthetic organisms, reflecting their physiological responses and adaption to environments.

On the other hand, among all the available models, the Kok model that interprets the light effect as a balance between the damage and the corresponding repair to the photosynthetic apparatus (Kok 1956), is the simplest way to explain the light-caused effects on algal photosynthesis (Beardall et al. 2009). This model is applied to study the effects of light intensity including ultraviolet radiation (UVR) on the photosynthetic carbon fixation and photochemical efficiency of phytoplankton (Lesser et al. 1994; Heraud and Beardall 2000). The algae can synthesize UV-absorbing compounds such as mycosporine-like amino acids (MAAs), and activate a range of defense mechanisms to minimize the damage. To a certain extent, the ratio (r/k) of repair rate (r) to damage rate (k) reflects the overall responses to high light or UVR, with higher value showing lower inhibitory effects (Guan and Gao 2010). The effects of UVR on photosynthesis can be modulated by other environmental factors including light intensity or history, nutrient status, CO_2 level, and temperature (Guan and Gao 2008, 2010; Guan and Li 2017; Li et al. 2012). For example, the *Karenia mikimotoi* cells grown under the nitrogen (N): phosphorus (P) ratio of 16:1 showed the highest r:k ratio and thus weakest UVR-induced photoinhibition (Guan and Li 2017). The inhibitory effects of UVB on the effective photochemical quantum yield (F_V'/F_M') of *Phaeodactylum tricornutum* were eliminated by higher temperature and elevated CO_2, with a high r/k ratio being observed (Li et al. 2012).

24.2 Measurements of PS II Photoinactivation

Measuring the rate constant of PSII photoinactivation of phytoplankton is based on the repair process being blocked, such as inhibiting chloroplast protein translation with a certain concentration of the inhibitor lincomycin. Under illumination and especially under high light conditions, the activity of PSII, e.g., the maximum photochemical quantum yield (F_V/F_M) or active PSII (PSIIactive) amount decreases exponentially with increasing light exposure time or photons received by the cell (Campbell et al. 2013). The rate constant of PSII photoinactivation can be derived from the decrease of F_V/F_M or PSIIactive with the increased light exposure as described in the following sections.

24.2.1 Sample Treatment

To obtain stable physiological parameters, phytoplankton need to acclimate to their growth conditions. It is generally believed that phytoplankton reach a stable physiological status after more than 12 cellular generations of growth under a given condition (Wu et al. 2010; Li and Campbell 2013; Li et al. 2017). Then, the phytoplankton sample adapted to a specific growth condition was divided into two flasks; to one of the flasks was added a final concentration of 500 μg mL^{-1} lincomycin to inhibit chloroplast ribosome function to block PSII repair, and the other one served as an unmodified control (Wu et al. 2011, 2012; Li and Campbell 2013; Li et al. 2015, 2016, 2017). Both the flasks were then placed in the dark for 10 min to allow the antibiotic (if present) to penetrate cells and inhibit ribosome function.

24.2.2 Measurements of Chlorophyll Fluorescence Parameters

After 10 min dark-adaption, both flasks mentioned above were shifted back to the treatment light conditions, and the maximum photochemical quantum yield (F_V/F_M) of PS II were measured after a certain exposure to treatment light (Li and Campbell 2013; Wu et al. 2011, 2012). Generally, different levels of treatment light can be set according to different experimental aims, for example, growth light was set as the treatment light to probe the PS II photoinactivation under growth light conditions (Li et al. 2016). The treatment light level should be higher if you aim to explore the photoinactivation under higher light (light shift experiment) conditions (Wu et al. 2011, 2012; Li and Campbell 2013). Similarly, the exposure-time intervals are also changeable based on the sensitivity of phytoplankton to treatment light, for instance some studies used the interval of 0, 15, 30, 60, and 90 min (Li and Campbell 2013; Wu et al. 2011, 2012), and others used 0, 15, 30, 60, and 120 min (Li et al. 2016). At each time-point during the light exposure, 3–5 ml culture was taken and

dispensed into a cuvette and dark-adapted for a certain time in a temperature-controller; after this, the F_V/F_M was measured with a fluorometer (e.g., Xe-PAM, Waltz, Germany; or FL 3600, Photon Systems Instruments, Czech Republic). The recovery is usually detected after the high light treatment through returning the samples of lincomycin-treated or control to growth light conditions and measuring the changes of F_V/F_M within 30–60 min.

24.2.3 Rate Constant of PS II Photoinactivation

Under treatment light, the F_V/F_M of lincomycin-treated samples will decrease exponentially because the inhibitor blocks the chloroplast protein translation and thus the PSII repair. So, the constant (kpi) derived from the following equation is often used as the rate constant of PS II photoinactivation:

$$F_V/F_{M(t)} = F_V/F_{M(t0)} \times e^{-kpi \times t},$$

where $F_V/F_{M(t)}$ and $F_V/F_{M(t0)}$ represent the maximum PS II photochemical quantum yield at time t and 0; and t indicates the exposure time (Fig. 24.1).

The kpi (s^{-1}) derived from an exponential decrease in the F_V/F_M of lincomycin-treated samples per unit time can be used to compare the PS II photoinactivation of different species under the same treatment light condition, but may not be suitable for under different or variable light conditions. Therefore, another parameter σi, the target size was introduced as σi = kpi/Ji, wherein Ji represents the exposure quanta incident with the unit of quantum m^{-2} s^{-1}. Note that Ji times t is equal to the number of quanta incident received by the sample over time t (Nt), with the unit of m^2 $quantum^{-1}$. So, the formula can be transformed as:

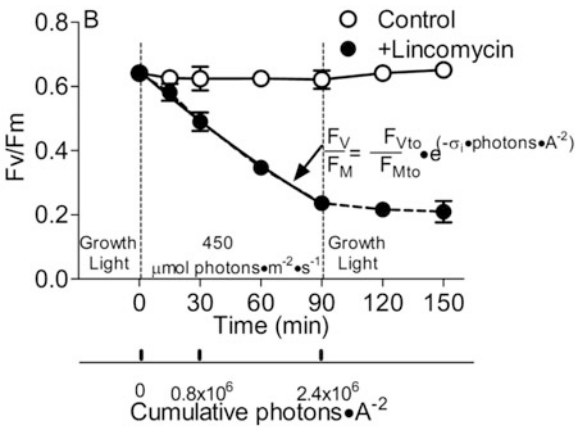

Fig. 24.1 PS II photochemical yield during and after an upward light shift. Susceptibility to photoinactivation (σi, A^2) was obtained by fitting an exponential decay curve to the decrease in F_V/F_M versus cumulative photons, in the subculture in which PSII repair was blocked by lincomycin (Li and Campbell 2013)

$$F_V/F_{M(t)} = F_V/F_{M(t0)} \times e^{-\sigma i \times Nt}$$

In this form, we can consider the σi as the functional absorption cross section of the photoreceptor(s) provoking photoinactivation or the functional size of a target that a photon must hit to cause photoinactivation, the larger σi indicating higher susceptibility to photoinactivation per incident photon.

Besides deriving from the decrease in F_V/F_M with the increased exposure incident quanta, the σi can also be derived from the decrease of active PS II reaction centers [PSIIactive]. The [PSIIactive] can be measured (Wu et al. 2012) as follows:

Firstly, sufficient culture density needs to be obtained in order to provoke detectable, short-term changes in oxygen concentration in the media. To do this, an aliquot volume of culture was concentrated by gentle centrifugation and resuspended in the residual growth media supernatant. A certain volume was loaded into a spectrophotometer cuvette to measure the oxygen content of the culture samples using an oxygen sensor (Foxy R Ocean Optics or Pyroscience, Germany), mounted in a lab-built epoxy gas tight cuvette plug that incorporates the oxygen sensor, a temperature probe and a thermostatted temperature control loop. The entire assembly was mounted into the SuperHead unit of a fluorometer (FL 3600, Photon Systems Instruments, Czech Republic), that contains LED light sources providing repetitive trains of light flashes of up to 90,000 μmol photons m^{-2} s^{-1} with duration as short as 2 μs. Before the oxygen flash yield experiments were carried out, the cuvette assembly with the concentrated sample was kept in the dark for 3–5 min until the inside temperature stabilized. After this, 1 min of low-level continuous preillumination (50 μmol photons m^{-2} s^{-1}) was applied to ensure induction of electron transport through both PS I and PS II (Kuvykin et al. 2008). Then, a train of flash lights was applied with the Superhead, and the changes of oxygen content in the culture were recorded. Following the flash trains, the sample was kept in the dark again and measurements of the oxygen decline were continued to derive the base rate of respiration that took place during the flash trains. As different algae species respond differentially to light, the pre-experiment was needed to verify that this flash train was sufficient to provide saturating, single-turnover flashes by varying the flash level, duration and dark spacing. For example, a train of 3,000 blue-light flashes of 20 μs duration, ~88,000 μmol photons m^{-2} s^{-1}, spaced by 50 ms dark intervals, giving a flash train lasting 150 s in total, was appropriate for the diatom *Thalassiosira pseudonana* grown under a light intensity of 30 μmol photons m^{-2} s^{-1} (Wu et al. 2012; Campbell et al. 2013). Finally, the net oxygen production was calculated by subtracting the dark respiration.

After the flash light experiment, the concentrated culture suspensions were harvested and extracted into 90%-magnesium carbonate-saturated acetone; after 24 h extraction in the dark at 4 °C, absorbance was measured and calculated with the equations of Jeffrey and Humphrey (1975) to estimate chlorophyll a content. The changes in oxygen concentration provoked by a series of single-turnover saturating flashes were used to estimate the content of active PS II per chlorophyll a following the method of Chow et al. (1989) as:

$$\begin{aligned}\left(\text{PSIIactive Chla}^{-1}\right) = &\left(\text{mol}\,O_2\,l^{-1}\,s^{-1}\right) \times \left(5 \times 10^{-2}\,\text{s flash cycle}^{-1}\right) \\ &\times \left(4\ \text{mol e} - \text{mol}\ {O_2}^{-1}\right) \\ &\times \left(1\ \text{flash cycle mol PSII mol e}-^{-1}\right) \\ &\times \left(1\ \text{mol Chl a}\ l^{-1}\right)^{-1}.\end{aligned}$$

Additionally, the initial chlorophyll fluorescence (Fo) often indicates chlorophyll a content, whereas the functional cross section for PSII photochemistry indicates the size of the PS II light harvesting pigment-protein complex. A new parameter Fo'/σ_{PSII} was introduced to represent the PSIIactive content (Oxborough et al. 2012; Silsbe et al. 2015). With this method, the PSIIactive content could thus be rapidly quantified with fluorescence technology (Chow et al. 1989; Murphy et al. 2017).

24.3 Measurement of Repair Rate

24.3.1 Materials and Treatments

A marine microalga *Phaeodactylum tricornutum*, Bohlin (CCMA 106) isolated from the South China Sea (SCS) in 2004 was used to describe how to measure the repair rate (*r*). The *P. tricornutum* cells were cultured at 20 °C under 70 μmol photons $m^{-2}\ s^{-1}$ for 20 generations, and were then exposed to the irradiance levels of 63.5 W m^{-2} (PAR, 290 μmol photons $m^{-2}\ s^{-1}$), 23.1 W m^{-2} (UV-A) and 1.20 W m^{-2} (UV-B) for 60 min at growth temperature under a solar simulator (Sol 1200 W; Dr. Hönle, Martinsried, Germany) (Li et al. 2012).

24.3.2 F_V'/F_M' and Repair Rate (r) Measurements

The effective quantum yield of PS II (F_V'/F_M') was measured every 3 min during the 60 min exposure with a Xenon-pulse amplitude modulated fluorometer (XE-PAM, Walz, Germany), and the data are shown in Table 24.1.

The rate constant of UVR-induced damage (*k*, in min^{-1}) and the corresponding repair rate constant (*r*, in min^{-1}) to the photosynthetic apparatus were estimated using the Kok model:

$$\frac{P}{P_0} = \frac{r}{r+k} + \frac{r}{r+k} e^{(-(r+k)\times t)}, \tag{24.1}$$

where *P* and P_0 indicate the F_V'/F_M' at time *t* and t_0, respectively.

The F_V'/F_M' data (Exposure-response curves) were fitted using a first-order exponential equation:

Table 24.1 Ratio (P/P_0) of P and P_0

Time (min)	P (F_v'/F_m')	P/P_0
0	0.62708	1
1	0.48475	0.773027365
4	0.3985	0.635485106
7	0.34175	0.544986286
10	0.3255	0.519072527
13	0.2855	0.455284812
16	0.2598	0.414301206
20	0.2595	0.413822798
23	0.2335	0.372360783
26	0.22225	0.354420489
30	0.2385	0.380334248
33	0.2282	0.363908911
37	0.20825	0.332094789
40	0.21925	0.34963641
43	0.2155	0.343656312
46	0.177	0.282260637
51	0.20575	0.328108056
54	0.19725	0.314553167
57	0.18225	0.290632774
60	0.22925	0.365583339

P and P_0 are F_v'/F_m' at time t_n (after light treatment) and t_0 (before light treatment), respectively

$$y = P1 + P2 \times e^{(-P3 \times t)} \tag{24.2}$$

where $P1$, $P2$, and $P3$ are adjustment parameters.

Comparing these two formulae, we can find:

$$P1 = \frac{r}{r+k}; P2 = \frac{k}{r+k}; P3 = r + k$$

then the r and k can be calculated as follows:

$$r = P1 \times P3; k = P2 \times P3 \tag{24.3}$$

Note: $P1 + P2 \neq 1$ during the fitting process; so, the Formula 24.3 can be only used to calculated r and k.

The ratio (P/P_0) of P and P_0 (Table 24.1) can be calculated at first as follows:

Then, copy the calculated data to the software (e.g. origin 7.5) as Fig. 24.2 as follows:

After this, select the appropriate first-order exponential equation and fit the data as shown in Fig. 24.3, and get the results as shown in Fig. 24.4.

And finally, the r and k were calculated as follows:

Fig. 24.2 The raw data into the origin worksheet

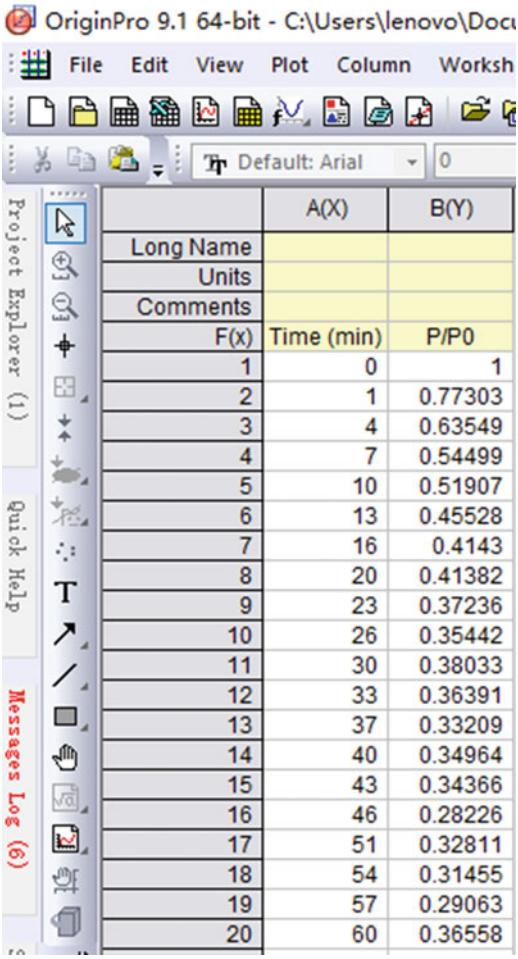

	A(X)	B(Y)
Long Name		
Units		
Comments		
F(x)	Time (min)	P/P0
1	0	1
2	1	0.77303
3	4	0.63549
4	7	0.54499
5	10	0.51907
6	13	0.45528
7	16	0.4143
8	20	0.41382
9	23	0.37236
10	26	0.35442
11	30	0.38033
12	33	0.36391
13	37	0.33209
14	40	0.34964
15	43	0.34366
16	46	0.28226
17	51	0.32811
18	54	0.31455
19	57	0.29063
20	60	0.36558

$$\mathrm{r} = P1 \times P3 = 0.33722 \times 0.13483 = 0.04547$$
$$k = P2 \times P3 = 0.58265 \times 0.13483 = 0.07856$$

24.4 Matters Needing Attention

1. Before measuring the maximum photochemical quantum yield (F_V/F_M) of PS II, a pre-experiment is needed to determine a sufficient dark-adaptation time for the algae species, because this time duration is species-specific and differs within different physiological status. For example, 5 min is enough for diatoms to obtain the maximal value of F_V/F_M (Li and Campbell 2013; Wu et al. 2012), while this

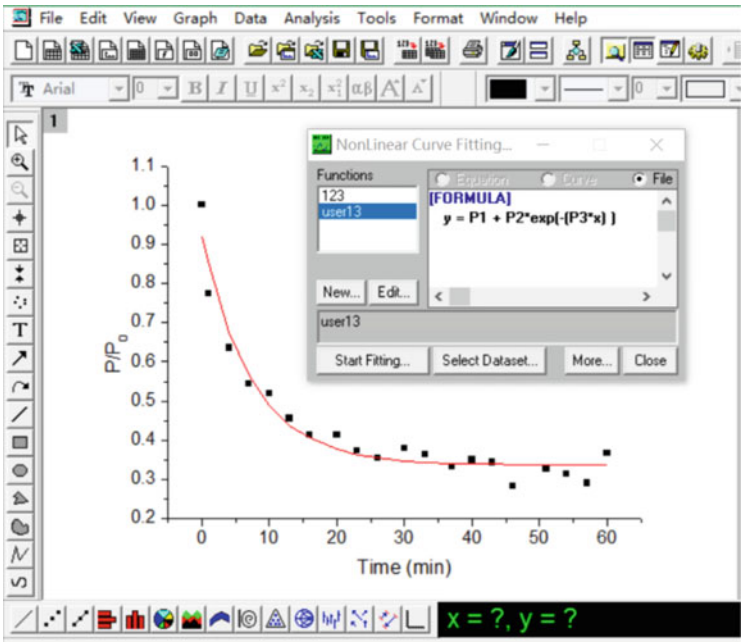

Fig. 24.3 Select the appropriate equation and fit the data

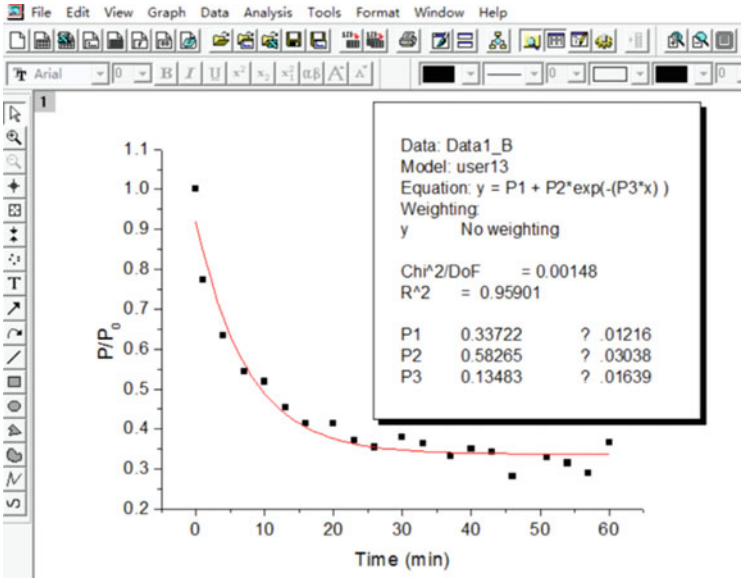

Fig. 24.4 Results from the fitted curve

time interval is not enough for cyanobacteria (Demmig-Adams et al. 1990). To obtain the F_V/F_M of cyanobacteria dithiothreitol (DTT) is often used to inhibit xanthophyll deepoxidase enzyme and thereby prevent induction of xanthophyll-dependent non-photochemical quenching (NPQ) (Ni et al. 2017).

2. The active PS II content can be derived from the oxygen production rate under the flash light condition, but the operation process is complex and time-consuming, and a large amount of culture is needed to obtain a high concentrated sample.
3. Quantifying PSIIactive with chlorophyll fluorescence technique is a newly developed method, with the properties of rapidity and simplicity; however, the accuracy of this quantification is often influenced by the high-light-caused photoinactivation that increases the initial fluorescence (Fo) (Ware et al. 2015). The Fo has also been calibrated by Oxborough and Baker (1997) through eliminating the effects of NPQ, which was testified effectively for PSIIactive quantification (Murphy et al. 2017).
4. The Kok model can only be used when obvious light or UVR-induced photoinhibition occurs; otherwise, the r and k cannot be calculated correctly. This is because the sum of adjustment parameters $P1$ and $P2$ is not equal to 1.

References

Albertsson P (2001) A quantitative model of the domain structure of the photosynthetic membrane. Trends Plant Sci 6(8):349–354

Beardall J, Sobrino C, Stojkovic S (2009) Interactions between the impacts of ultraviolet radiation, elevated CO2, and nutrient limitation on marine primary producers. Photochem Photobiol Sci 8 (9):1257–1265

Campbell DA, Hossain Z, Cockshutt AM, Zhaxybayeva O, Wu H, Li G (2013) Photosystem II protein clearance and FtsH function in a diatom Thalassiosira pseudonana. Photosynth Res 115 (1):43–54

Chow WS, Hope AB, Anderson JM (1989) Oxygen per flash from leaf disks quantifies photosystem II. Biochim Biophys Acta 973:105–108

Demmig-Adams B, Adams WW III, Czygan F-C, Schreiber U, Lange OL (1990) Differences in the capacity for radiationless energy dissipation in the photochemical apparatus of green and blue-green algal lichens associated with differences in carotenoid composition. Planta 180:582–589

Guan WC, Gao KS (2008) Light histories influence the impacts of solar ultraviolet radiation on photosynthesis and growth in a marine diatom, Skeletonema costatum. J Photochem Photobiol B Biol 91:151–156

Guan WC, Gao KS (2010) Impacts of UV radiation on photosynthesis and growth of the coccolithophore Emiliania huxleyi (Haptophyceae). Environ Exp Bot 67:502–508

Guan WC, Li P (2017) Dependency of UVR-induced photoinhibition on atomic ratio of N to P in the dinoflagellate Karenia mikimotoi. Mar Biol 164:31

Han B, Fu X, Han Z (2003) Mechanisms and models of algal photosynthesis. Beijing Press, Beijing

Heraud P, Beardall J (2000) Changes in chlorophyll fluorescence during exposure of Dunaliella tertiolecta to UV radiation indicate a dynamic interaction between damage and repair processes. Photosynth Res 63:123–134

Jeffrey SW, Humphrey GF (1975) New spectrophotometric equations for determining chlorophylls a, b, c1 and c2 in higher plants, algae, and natural phytoplankton. Biochem Physiol Pflanz 167:191–194

Kok B (1956) On the inhibition of photosynthesis by intense light. Biochim Biophys Acta 21:234–244

Kuvykin IV, Vershubskii AV, Ptushenko VV, Tikhonov AN (2008) Oxygen as an alternative electron acceptor in the photosynthetic electron transport chain of C3 plants. Biochemistry (Mosc) 73:1063–1075

Lesser MP, Cullen JJ, Neale PJ (1994) Carbon uptake in a marine diatom during acute exposure to ultraviolet B radiation: relative importance of damage and repair. J Phycol 30:183–192

Li G, Campbell DA (2013) Rising CO2 interacts with growth light and growth rate to alter Photosystem II photoinactivation of the coastal diatom Thalassiosira pseudonana. PLoS One 8(1):e55562

Li Y, Gao KS, Villafañ V, Helbling E (2012) Ocean acidification mediates photosynthetic response to UV radiation and temperature increase in the diatom Phaeodactylun tricornutum. Biogeoscience 9:3931–3942

Li G, Brown CM, Jeans JA, Donaher NA, McCarthy A, Campbell DA (2015) The nitrogen costs of photosynthesis in a diatom under current and future pCO2. New Phytol 205(2):533–543

Li G, Woroch A, Donaher N, Cockshutt AM, Campbell DA (2016) A hard day's night: diatoms continue recycling photosystem II in the dark. Front Mar Sci 3:218

Li G, Talmy D, Campbell DA (2017) Diatom growth responses to photoperiod and light are predictable from diel reductant generation. J Phycol 53:95–107

Murata N, Takahashi S, Nishiyama Y, Allakhverdiev SI (2007) Photoinhibition of photosystem II under environmental stress. Biochim Biophys Acta 1767:414–421

Murphy CD, Ni G, Li G, Barnett A, Xu K, Grant-Burt J, Liefer JD, Suggett DJ, Campbell DA (2017) Quantitating active photosystem II reaction center content from fluorescence induction transients. Limnol Oceanogr Meth 15:54–69

Ni G, Murphy CD, Zimbalatti G, Barnett AB, Arsenault CM, Li G, Cockshutt AM, Campbell DA (2017) Arctic micromonas uses non-photochemical quenching to cope with temperature restrictions on metabolism. Photosynth Res 131:203–220

Oxborough K, Baker NR (1997) Resolving chlorophyll a fluorescence images of photosynthetic efficiency into photochemical and non-photochemical components – calculation of qP and Fv′/Fm′; without measuring Fo′. Photosynth Res 54:135–142

Oxborough K, Moore CM, Suggett DJ, Lawson T, Chan HG, Geider RJ (2012) Direct estimation of functional PSII reaction center concentration and PSII electron flux on a volume basis: a new approach to the analysis of fast repetition rate fluorometry (FRRf) data. Limnol Oceanogr Meth 10:142–154

Raven JA (2011) The cost of photoinhibition. Physiol Plant 142:87–104

Silsbe GM, Oxborough K, Suggett DJ, Forster RM, Ihnken S, Komárek O, Lawrenz E, Prášil O, Röttgers R, Šicner M, Simis SGH, Van Dijk MA, Kromkamp JC (2015) Toward autonomous measurements of photosynthetic electron transport rates: an evaluation of active fluorescence-based measurements of photochemistry. Limnol Oceanogr Meth 13:138–155

Ware MA, Belgio E, Ruban AV (2015) Photoprotective capacity of non-photochemical quenching in plants acclimated to different light intensities. Photosynth Res 126:261–274

Wu Y, Gao K, Riebesell U (2010) CO2-induced seawater acidification affects physiological performance of the marine diatom Phaeodactylum tricornutum. Biogeoscience 7:2915–2923

Wu HY, Cockshutt AM, Campbell DA (2011) Distinctive PSII photoinactivation and protein dynamics in centric diatoms. Plant Physiol 156:2184–2195

Wu HY, Roy S, Alami M, Green BR, Campbell DA (2012) Photosystem II photoinactivation, repair and protection in marine centric diatoms. Plant Physiol 160:464–476

Part VI
Chlorophyll Fluorescence Techniques and Applications

Chapter 25
Basic Concepts and Key Parameters of Chlorophyll Fluorescence

Sven Beer, Mats Björk, and John Beardall

Abstract Photosynthetic rates can be measured in several different ways. Classically, phytoplankton productivity has been measured by uptake rates of ^{14}C-labelled inorganic carbon (C_i, i.e. CO_2 and HCO_3^-), which is a sensitive measure even for sparse phytoplankton assemblages. For macrophytes, gas exchange of CO_2 or O_2 have been used as preferred methods of photosynthetic productivity. All these above mentioned methods have the disadvantage of being slow (minutes to hours or days) and the need for enclosing the plants, the latter of which invariably alters their surroundings from natural ones in terms of light (both irradiance and spectrum), water flow and decreasing nutrient, such as C_i, levels, as well as increasing O_2 concentrations, which may impede on rates. For the last 20 years, chlorophyll fluorescence measurements have increasingly replaced the other methods as being both sensitive and speedy, and applicable under natural, non-enclosed, conditions. This chapter explains the background to chlorophyll fluorescence, as well as the principles of pulse-amplitude modulated (PAM) fluorometry and, briefly, fast repetition rate fluorometry (FRRF) measurements.

Keywords Aquatic plants · Photosynthesis · Chlorophyll fluorescence · PAM principles · Absorption factor

S. Beer (✉)
School of Plant Sciences and Food Security, Tel Aviv University, Tel Aviv, Israel
e-mail: svenb@ex.tau.ac.il

M. Björk
Department of Ecology, Environment and Plant Sciences, Stockholm University, Stockholm, Sweden
e-mail: mats.bjork@su.se

J. Beardall
School of Biological Sciences, Monash University, Clayton, VIC, Australia
e-mail: john.beardall@monash.edu

K. Gao et al. (eds.), *Research Methods of Environmental Physiology in Aquatic Sciences*, https://doi.org/10.1007/978-981-15-5354-7_25

25.1 Introduction

Chlorophyll fluorescence is a weak red light that is generated as part of the de-excitation of excited chlorophyll molecules. As photons of photosynthetically active radiation (PAR, 400–700 nm) are absorbed by chlorophyll, their energy elevates electrons of the latter to higher energy levels (excitation). Then, fractions of a second later, those excited electrons return to their original levels (de-excitation) while transferring the energy difference towards a little bit of heat, fluorescence, and photosynthesis (Fig. 25.1). If we ignore the minor component of heat formation, logic has it that there then is an inverse relationship between photosynthesis and fluorescence: the less efficient the photosynthetic process, the more energy is left to generate fluorescence, and vice versa—the more effective photosynthesis is, the less energy is dissipated as fluorescence: we say that photosynthesis under given conditions of irradiance *quenches* the fluorescence signal (or the fluorescence yield). Thus, the inverse relationship between photosynthesis and fluorescence can be used to estimate the photosynthetic performance.

Fluorescence is a weak light that under normal physiological conditions cannot be seen by the naked eye. It can, however, be measured by sensitive detectors in so-called fluorometers. Further, in modern fluorometers, the even weaker fluorescent light stemming from the de-excitation of chlorophyll excited by a very weak

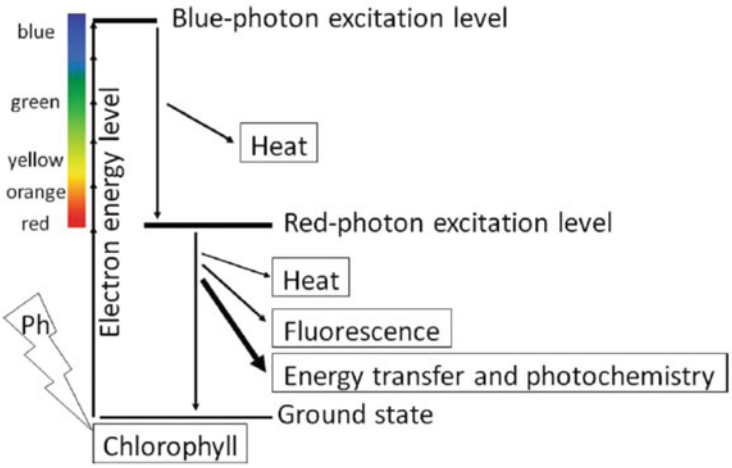

Fig. 25.1 Excitation and de-excitation of chlorophyll. As a photon (Ph) is absorbed by a chlorophyll molecule, one of its electrons is boosted up (excited) to a higher energy level: The more energetic the photon (i.e. towards blue light), the higher the energy, and the less energetic the photon (towards red light), the lower the energy level obtained. As electrons then loose energy during de-excitation from higher than the red-photon excitation level, that energy is dissipated as heat. However, from the red-photon excitation level, their energy is converted also to fluorescence and photochemistry (causing photosynthesis). The inverse relationship between fluorescence and photochemistry can be used for deriving quantum yields (Y) and photosynthetic electron transport rates (ETR). (Drawing by Sven Beer; Copyright (2014) with permission from Wiley-Blackwell)

modulated 'measuring light' can be separated from the usually much stronger fluorescence caused by the actinic (photosynthesis-causing) light absorbed by the photosynthesising plant parts, as well as from the usually immensely stronger actinic light itself reflected into the fluorometer, part of which is of the same wavelength as the fluorescence. (Also here we use the term 'plant' to include all aquatic phototrophs.) The technique mostly used to enable such a separation is called pulse-amplitude modulated (PAM) fluorometry. A second technique, used for less dense chlorophyll concentrations, e.g. for natural marine phytoplankton assemblages, is named fast repetition rate (FRR) fluorometry.

25.2 Methodology

PAM fluorometry works in the following principal way: The fluorometer sends out a weak (<1 µmol photons m^{-2} s^{-1}) beam of modulated (or pulsed, or pulse-amplitude modulated—hence the abbreviation PAM) measuring light (usually red, ~700 nm, or blue, ~450 nm, which are close to the absorption maxima of chlorophyll, but can be of any colour in between) at a high frequency (some 100–1000 Hz, obtained by a light-emitting diode, LED) through a flexible optical cable (see Fig. 25.2). The fluorescence caused by this modulated measuring light is then recorded by the fluorometer (marked as F in the figure and hereafter) as an increase in the total intensity of fluorescence. A PAM fluorometer not only manages to filter out fluorescence that was not generated by the measuring light, but also environmental light of the same wavelength that is reflected into the fibre-optical cable. As can be seen in the figure, F has a larger value at high (HL) than at low (LL) irradiances.

If we plot F as a function of time in a series of increasing irradiances interspersed with darkness, the following principal pattern can be seen (Fig. 25.3): F is at its lowest value in a dark-adapted leaf/thallus measured in virtual darkness (when all reaction centres of PSII are oxidised, or 'open', and can transfer electrons), and is accordingly called F_0. In this case the flow of electrons excited by the few photons of the measuring light flow freely through the open reaction centres (photosynthesis is very efficient) and fluorescence is effectively quenched. The fluorometer's internal light source (either a halogen lamp or the LED) then irradiates the leaf with a ~1 s photosynthesis-saturating light flash (some 10,000 µmol photons m^{-2} s^{-1}) by the touch of a button, whereby F arrives at its maximal value, F_m. This is because the many photons cause a very high proportion of the reaction centres to transfer electrons and are, thus, temporarily closed; photosynthesis is inefficient and much of the energy generated during de-excitation of the chlorophyll is emitted as fluorescence. The difference between these two extremes, i.e. $F_m - F_0$, is called the variable fluorescence, F_v. Now, it turns out that $(F_m - F_0)/F_m$, i.e. F_v/F_m, equals the quantum yield of PSII (termed Y in most fluorometer displays), defined as the portion of electrons passing through PSII per photons absorbed by the photosynthetic pigments. This would be the *maximal quantum yield* as measured in virtual darkness (again, with only the weak measuring light transferring the, albeit very few, electrons through PSII very efficiently).

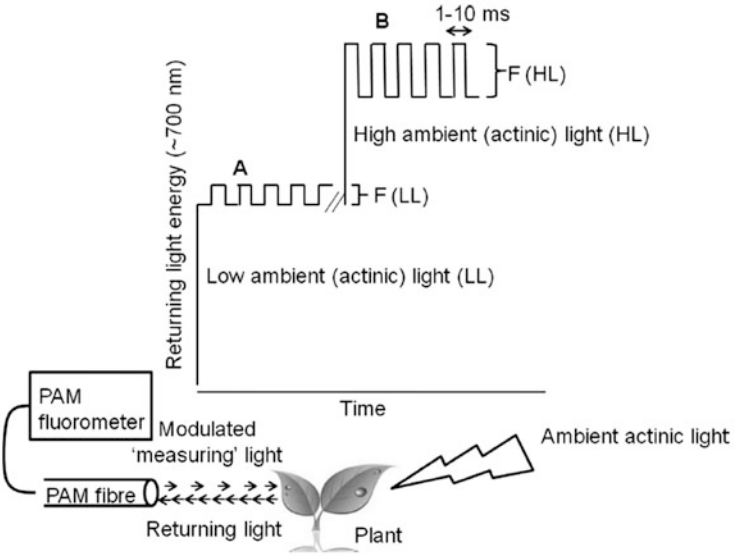

Fig. 25.2 The principle of PAM fluorometry. Ambient actinic (photosynthesis-causing) light generates fluorescence to be emitted from a green (chlorophyll-containing) plant part, and its intensity, as well as that part of the actinic light with the same wavelength as the fluorescence, enters the PAM fluorometer (lower left) and is recorded as a background. In addition, a pulse-modulated, very weak, measuring light emitted from the PAM fluorometer irradiates the same plant part, and its, albeit small, contribution to the fluorescence is also measured (*F* in the figure) at the time of the short pulses (typically 1–10 ms each). As can be seen, *F* increases as irradiance increases (because of less quenching by a lowered photosynthetic efficiency at high light; B in the figure). *F* would be at its minimum in virtual darkness, i.e. without any ambient light but only the very weak measuring light irradiating the plant. (Drawing by Sven Beer; Copyright (2014) with permission from Wiley Blackwell)

While F_v/F_m cannot be used for deducing photosynthetic rates (since it is measured in virtual darkness), it is often used as a measure of stresses other than actinic light directly affecting PSII. Such stresses include temperature, salinity, water and nutrient stresses, as well as high-light stresses experienced during periods of high irradiances prior to darkening the plant; the latter stresses can be called photoinhibition or downregulation of photosynthesis (a short-term, e.g. daily, decrease in photosynthetic efficiency) or photodamage (a longer-term damage to PSII).

As irradiances increase, so do the proportion of reduced reaction centres, and the fluorescence signal, now simply also called *F*, increases accordingly: from that in darkness, F_0, through low light, *F*(LL), to high light, *F*(HL), as marked in Fig. 25.3. After some adaptation periods at the various irradiances, we again let the fluorometer irradiate the leaf with the ~1 s flash of saturating light; reaction centres close, and a higher fluorescence value is obtained (F_m' in the figure). In these cases, i.e. in plant leaves exposed to light, ($F_m' - F$) is called ΔF. Similarly to the dark-adapted leaf, the quantum yield *Y* can now be calculated as $(F_m' - F)/F_m'$, or $\Delta F/F_m'$, which again

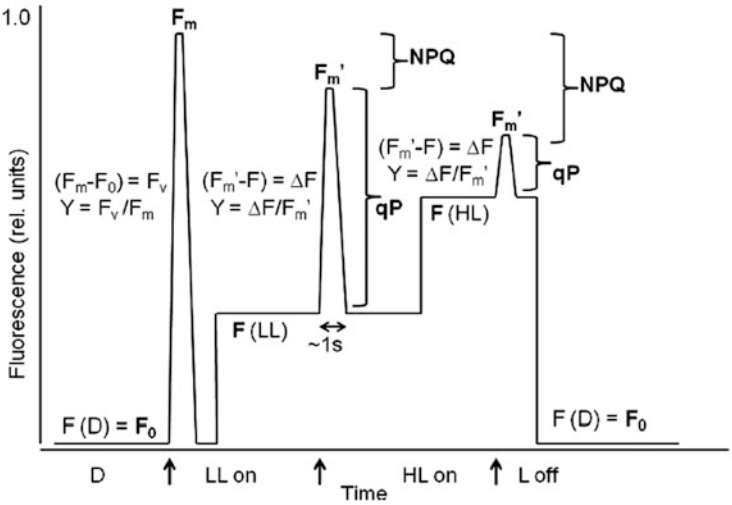

Fig. 25.3 A time course of fluorescence. In virtual darkness (*D*), the fluorescence stemming from the weak pulsed measuring light is the lowest, F_0 (left side). As a saturating light flash is applied (left up-arrow), *F* increases to its maximal value, F_m. $F_m - F_0$ is called the variable fluorescence, F_v, and $(F_m - F_0)/F_m$, or F_v/F_m, is accordingly the maximal quantum yield. As irradiances increase (towards the right, from darkness, *D*, through low light, LL to high light, HL), so does the fluorescence *F*. Again, a saturating flash of light is applied by the fluorometer after each irradiance increase (middle and right up-arrows), and *F* increases to a maximal value, now called F_m'. $F_m' - F$ is termed ΔF, and $(F_m' - F)/F_m'$, or $\Delta F/F_m'$, is called the effective quantum yield for each irradiance level. Note how the effective quantum yield decreases with increasing irradiance. This is due to decreased photochemical quenching (qP) and increased non-photochemical quenching (NPQ or qN). (Drawing by Sven Beer; Copyright (2014) with permission from Wiley Blackwell)

reflects the quantum yield of electron flow through PSII. We call this the *effective quantum yield* (as opposed to the maximal quantum yield, F_v/F_m, as measured in virtual darkness). As can be seen, $Y\ (\Delta F/F_m')$ decreases with increasing irradiance; a lower proportion of the photons stemming from the modulated measuring light causes photosynthesis because a higher proportion of reaction centres are temporarily closed for electron transport, which accordingly leads to a lower quantum yield.

The decrease in quantum yield with increasing irradiance as exemplified above and depicted in Fig. 25.3 is a general phenomenon caused by two types of fluorescence quenching: photochemical, qP ($qP = (F_m' - F)/F_m'$), and non-photochemical, NPQ ($NPQ = (F_m - F_m')/F_m'$). Non-photochemical quenching can also be termed qN, but this is calculated in a slightly different way than NPQ and ideally requires the knowledge of a term called F_0'; the latter term is obtained for fully oxidised reaction centres as generated by a far-red light source and will have a value lower than F_0—for this, see the instructions for those fluorometers that provide this option. If F_0' is not known, then qN can be estimated as $(F_m - F_m')/(F_m' - F_0)$. Photochemical quenching is of course the result of photochemistry quenching fluorescence signals. On the other hand, non-photochemical quenching is the result of plants finding ways other than photosynthesis to dissipate excess (photon) energy,

and the latter becomes more pronounced at higher irradiances. It is, however, not the purpose of this chapter to detail the mechanisms of non-photochemical quenching (or of the photosynthetic reactions altogether); for this, see the relevant literature on photosynthesis (with the risk of excessive self-citation, e.g. the book by Beer et al. (2014)).

The advantages of measuring photosynthetic parameters by fluorometry include that (a) it is faster than both O_2 and CO_2 gas exchange measurements; each individual measurement takes only a second and one can obtain a photosynthesis-irradiance (*P–I*, or *P–E*) response curve in minutes (see the next session), and (b) measurements can easily be performed in situ under natural conditions (see below) without the need for enclosures. The result of such measurements is the quantum yield (Y) of electrons flowing through PSII per photons absorbed by that photosystem. This can then be translated to electron transport rates (ETR) as will be explained below. These rates are true (or gross) rates of photosynthesis since fluorometry (as opposed to gas exchange measurements) does not take into account dark (mitochondrial) respiration and other components of the cell's metabolism, but only photosynthetic electron transport. Thus, apparent (or net) rates cannot be obtained using fluorometry alone.

One obvious question to ask of fluorometry is to what extent it can result in *quantitative* measures of photosynthetic rates comparable to those obtained in gas exchange measurements. In order to ask this, we must first learn to convert the effective quantum yields $(F_m' - F)/F_m'$, or $\Delta F/F_m'$, here termed Y, obtained by the fluorometer, to photosynthetic electron transport rates (ETR). This is done by the equation

$$\mathrm{ETR} = Y \bullet \mathrm{PAR_a(PSII)}$$

where $\mathrm{PAR_a(PSII)}$ is the amount of PAR (400–700 nm) photons absorbed by the photosynthetic pigments of PSII. $\mathrm{PAR_a}$ is thus expressed as incident irradiance ($\mathrm{PAR_i}$) multiplied by an absorption factor (AF). The above equation is often written as

$$\mathrm{ETR} = Y \bullet \mathrm{PAR_i} \bullet \mathrm{AF} \bullet 0.5$$

where $\mathrm{PAR_i}$ is easily measured by a PAR irradiance quantum meter held beside the leaf, 0.5 is an assumed equal distribution of photons absorbed between PSII and photosystem I (PSI), and AF (often assumed to be 0.84, which however is debatable, see the next chapter). (Incidentally, ETRs are best given as μmol electrons m^{-2} s^{-1}; this is because the accepted unit of PAR is μmol photons m^{-2} s^{-1}.) True AFs are often not available in calculations of ETR—thus the assumed AF of 0.84—but they can often be estimated quite easily (see the next section). Thus, without a given AF (i.e. $\mathrm{PAR_a}$ is not known), one cannot obtain quantitative rates of photosynthesis by PAM fluorometry. Instead, relative rates (rETR) may be given as

$$\mathrm{rETR} = Y \bullet \mathrm{PAR_i}$$

This measure is often good enough if one wants to e.g. compare the performance of a plant species growing under different environmental conditions.

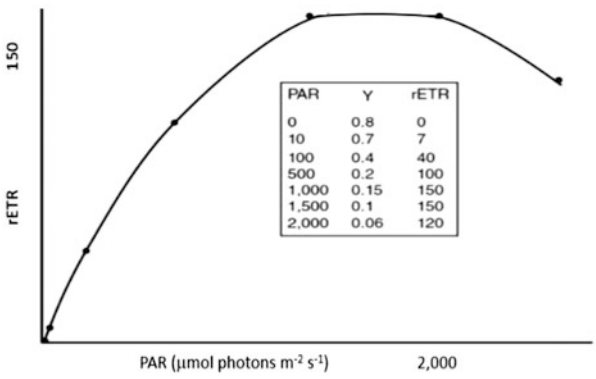

Fig. 25.4 Relations between quantum yield (*Y*), irradiance (PAR) and relative electron transport rates (rETR). See text for details. (Drawing by Sven Beer; Copyright (2014) with permission from Wiley Blackwell)

The fact that ETRs increase with irradiance (up to light saturation) although quantum yields (*Y*, which is a factor in the calculation of rETR or ETR) decrease can be clarified in the following simple example (as illustrated in Fig. 25.4): Since rETR is simply a multiple of $Y \bullet PAR_i$, it will increase as long as PAR_i increases more than *Y* decreases at each increasing irradiance. Thus, the reason that rETR increases from e.g. 500 to 1000 µmol photons m^{-2} s^{-1} is that PAR increases proportionally more than *Y* decreases. At 1000 and 1500 µmol photons m^{-2} s^{-1}, PAR and *Y* increase and decrease, respectively, at equal proportions, and so there is no change in rETR—photosynthetic electron transport has reached saturation. At even higher irradiances, *Y* decreases more than PAR increases, and so rETR decreases. This is a sign of downregulation of photosynthesis or photoinhibition.

If AF can be determined and if 0.5 is assumed to be a valid distribution factor of light absorption between PSII and PSI (which it usually is, but see also variations in the '0.5-factor' as a function of e.g. changes in the light spectrum along a depth gradient as exemplified in the next chapter), then comparisons of ETRs with true O_2 evolution can yield expected results. Figure 25.5 shows the expected relations between gas exchange (true O_2 evolution and CO_2 uptake, i.e. disregarding respiration) and electron transport in photosynthesis to be 1 mol O_2 = 1 mol CO_2 = 4 mol electrons. Thus, the molar O_2 (and CO_2)/ETR ratio is 0.25.

Several comparisons have been made between O_2 evolution and ETR, and in some cases the expected O_2/ETR ratio was found to be close to 0.25 (4 mol electrons per mol O_2). This is, for macrophytes, usually true for (a) flat-thallied algae or flat-leaved seagrass leaves, and (b) under relatively low irradiances. As illustrated in Fig. 25.6 for the simple thallus of the macroalga *Ulva* sp. (consisting of two layers of chloroplast-containing cells), the O_2/ETR ratio was close to 0.25 up to an irradiance of 500 µmol photons m^{-2} s^{-1} (~1/4 of full sunlight). The deviation from linearity of O_2 evolution as a function of ETR at higher irradiances seems to be a common phenomenon. The underlying reason is most probably that the O_2 evolution that is connected with, and regulated by, CO_2 fixation and reduction becomes saturated at high irradiances, but electron flow does not; the 'extra' electrons then reduce compounds other than CO_2 (e.g. O_2 to produce hydrogen peroxide as part of a

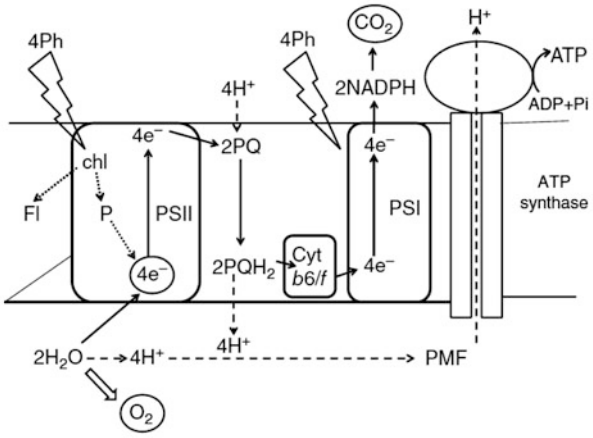

Fig. 25.5 Electron transport, and O_2 evolution and CO_2 uptake (in circles). The stoichiometry calls for 4 mol of electrons stemming from 2 mol of H_2O to reduce 1 mol of CO_2. At the same time, 1 mol of O_2 is released. For this to occur, 4 mol photons (Ph) are needed in each photosystem (i.e. 8 mol photons), but in practice there is a need for at least 10 mol photons for every mol O_2 released or CO_2 fixed and reduced. Abbreviated terms in the figure are according to accepted nomenclature in photosynthetic research. (Drawing by Sven Beer; Copyright (2014) with permission from Wiley Blackwell)

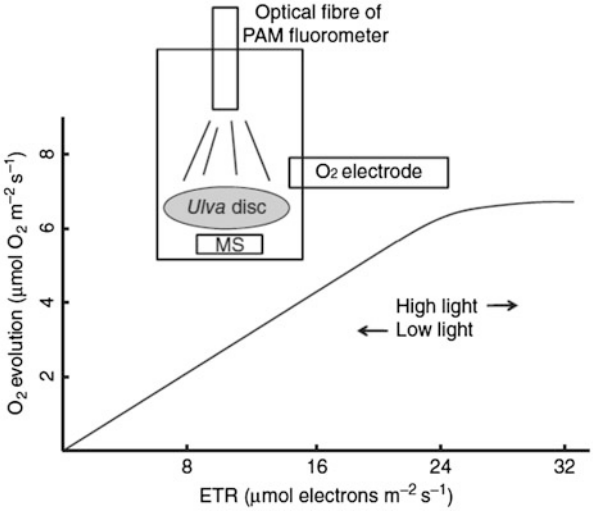

Fig. 25.6 Experimental setup (insert) and results of O_2 evolution vs. electron transport rates. O_2 exchange of *Ulva* sp. discs was measured in an O_2-electrode chamber while simultaneously measuring PAM fluorescence with a PAM fluorometer. Photosynthetic O_2 exchange was corrected for dark (mitochondrial) respiration following each level of irradiance (see Beer et al. 2000). (Drawing by Sven Beer; Copyright (2014) with permission from Wiley Blackwell)

water–water cycle). The best is of course to experimentally establish the correlation between ETR and O_2 evolution for each specific organism to be investigated, and the irradiances under which this relationship is linear, so as to determine the limits for which ETR can be used as a quantitative measure of photosynthetic rates.

Because of the differences in absorbance properties of the various pigments found in different groups of algae, some fluorometers can differentially excite characteristic pigments to excite chlorophyll specifically present in those groups and thus quasi-simultaneously probe the performance of particular algal classes in mixed populations. An example of this type of fluorometer is the Phyto-PAM-II by Heinz Walz GmbH, Germany. A more sophisticated version of this is the Multicolour-PAM, which also allows for wavelength-dependent determinations of the PSII absorption cross section and, hence, absolute ETRs. Dual-PAMs incorporate systems for determining PSI as well as PSII. More details are available from the Walz web pages on https://www.walz.com/products/chl_p700/overview.html.

25.3 Merits and Demerits

The *merits* of both PAM fluorometric and FRRF measurements of quantum yields and photosynthetic rates are that the measurements are fast (seconds) and can be performed in situ, under natural conditions, without the need of enclosures. The fact that only photosynthetic electron flow through PSII is measured, without any interference of other cellular activities, means that these methods yield true (or gross) rates of photosynthesis. While this may be a merit, e.g. when investigating the efficiency of the photosynthetic apparatus per se in response to environmental parameters, one should remember that plant growth is also a function of other metabolic activities such as respiration. Thus, one *demerit* of chlorophyll fluorometry could be that the resulting rates (ETRs) may not correlate well with productivity of the plants in terms of growth rates.

References

Beer S, Larsson C, Poryan O, Axelsson L (2000) Photosynthetic rates of *Ulva* (Chlorophyta) measured by pulse amplitude modulated (PAM fluorometry). Eur J Phycol 35:69–74

Beer S, Björk M, Beardall J (2014) Photosynthesis in the marine environment. Wiley-Blackwell, Oxford, UK. ISBN: 978-1-119-97957-9

Chapter 26
Fluorescence Measurement Techniques

Sven Beer, Mats Björk, and John Beardall

Abstract Chlorophyll fluorometers are constructed such that the immediate outcomes of the measurements provide information on quantum yields (*Y*) of electrons passing through photosystem II (PSII). If the photosynthetically active radiation (PAR) absorbed by PSII (PAR_a) is known, then photosynthetic rates can be calculated as electron transport rates (ETR). If only the incident irradiance (PAR_i) is known (which often is the case), then relative ETRs (rETR) can be calculated as the product of *Y* and PAR_i. There are sometimes easy ways to at least estimate PAR_a, and they will be described in this chapter, as will other practical means to measure photosynthetic parameters using fluorometry.

Keywords Aquatic plants · Photosynthesis · PAM fluorometers · PAM measurements · Quantum yield

26.1 Introduction

Many different fluorometers are available on the market, suitable for measurements with suspension of unicells, intact thalli or macrophytes and seagrass leaves, but here we will largely restrict ourselves to measurements using the (arguably) most relevant fluorometers for in situ measurements of aquatic macrophytic plants, i.e. the underwater adapted PAMs (e.g. the Diving-PAM, Walz, Germany, or the Aquation

S. Beer (✉)
School of Plant Sciences and Food Security, Tel Aviv University, Tel Aviv, Israel
e-mail: svenb@ex.tau.ac.il

M. Björk
Department of Ecology, Environment and Plant Sciences, Stockholm University, Stockholm, Sweden
e-mail: mats.bjork@su.se

J. Beardall
School of Biological Sciences, Monash University, Clayton, VIC, Australia
e-mail: john.beardall@monash.edu

K. Gao et al. (eds.), *Research Methods of Environmental Physiology in Aquatic Sciences*, https://doi.org/10.1007/978-981-15-5354-7_26

chlorophyll fluorometers). These instruments can also be used for terrestrial plants but have the advantage that they can be taken under water to depths of tens of metres.

26.2 Methodology

26.2.1 Quantum Yield Measurements

The recommended techniques used will depend on whether maximal (F_v/F_m) or effective ($\Delta F/F_m'$) quantum yields are to be measured, and if co-called rapid light curves (RLC) are to be obtained. Let's start with F_v/F_m: In order to achieve the highest possible values (showing the *maximal quantum yield*, or the highest *potential* for photosynthesis), the maximal proportion of PSII reaction centres should be oxidised (open). This occurs after prolonged periods of darkness. We often see F_v/F_m values measured after 5 or 10 min of dark adaptation, but have learned that additional periods of darkness can increase values significantly. So, in natural settings we often prefer to measure F_v/F_m in the early morning, before sunrise. If so, possible downregulation, photoinhibition, or photodamage during the preceding daylight cycle will largely have been amended, and PSII will then function optimally. A predawn F_v/F_m measurement can also be used later in the day for calculating non-photochemical quenching during the following day as $NPQ = (F_m - F_m')/F_m'$ or $qN = (F_m - F_m')/(F_m' - F_0)$ by using the stored minimum F_0 and maximum F_m values from that early F_v/F_m determination.

As mentioned in the previous chapter, F_v/F_m can be a good indicator of many stresses affecting PSII, and they really are many: desiccation stress in the intertidal, light stress during periods of irradiation preceding the dark-adaptation needed for the measurement, temperature stresses, etc. There are so-called 'dark-leaf clips' that can be clipped onto leaves or thalli, and a shutter is opened only prior to measurement(s), after the clip has been attached to the optical fibre of the fluorometer.

In order to obtain $\Delta F/F_m'$ (the *effective quantum yield* in light-adapted plants), so-called 'point measurements' can be performed. The distance between the tip of the optical fibre and the photosynthetic tissue to be measured should be such that a stable and high enough fluorescence signal (F) can be seen on a display (either on the fluorometer itself or on a connected computer). While the distance itself is unimportant, it is crucial to maintain that distance while employing the saturating flash. For this, there is a so-called 'leaf-distance clip' that can be attached to the tip of the optical fibre and that ensures that a stable distance is kept during the ca. 1 s measurement. It should also be ensured that the saturating light flash is really saturating. This can be done by increasing the saturating light flash intensity until the highest $\Delta F/F_m'$ values are obtained, or by shortening the distance between the end of the optical cable and the plant surface.

The effective quantum yield ($Y = \Delta F/F_m'$) describes, as mentioned above, the amount (mol) of electrons passing through PSII per amount (mol) of photons absorbed by the photosynthetic pigments of that photosystem. In a 100% efficient

plant, the value should be 1.0, and this value should be reached at very low irradiances, e.g. in virtual darkness where the only excitation is by the weak measuring light. However, this is a theoretical value, and the highest measured ever obtained is around 0.85 (again, at a low irradiance and otherwise optimal growth conditions).

26.2.2 Converting Effective Quantum Yields to ETR

In order to obtain *rates* of photosynthesis, effective quantum yields, Y ($\Delta F/F_m'$), must be converted to electron transport rates (ETR). For this, the absorbed (PAR_a, for determining absolute rates of ETR), or at least incident (PAR_i, for relative ETRs, rETR), irradiance must be known. Since PAR_a is often ignored or not known, let's first consider PAR_i.

PAR_i should be measured as close as possible to the site of the leaf or thallus where the PAM-fluorometric measurement is performed. There are many PAR meters available for this purpose. The easiest would be to use the PAR sensor usually supplied with the fluorometer, and the advantage is that it either is, or can be, connected to a leaf-distance clip or the like near the area to be measured. Some such meters are good (e.g. in the Mini-PAM, Walz, Germany), but the one of at least the older Diving-PAMs is not; it relies on an optical fibre leading the light into the instrument, where it is measured. The problem is that the resulting PAR reading is dependent on the curvature of the fibre, such that higher values are recorded when the fibre is held straight. In any case, those fibre-optically guided sensors should be calibrated against non-fibre-guided PAR sensors (such as those manufactured by e.g. LI-COR, USA). After Y and PAR_i have been measured, rETR can be calculated by multiplying the two. The instrument often does the calculation by applying the formula $ETR = Y \bullet PAR \bullet 0.84 \bullet 0.5$, assuming 0.84 to be an 'average' absorption factor (AF) for plant leaves and 0.5 to be the distribution of light absorption between PSII and PSI. While the latter may be close to the true value, 0.84 is almost never valid. Most thin macroalgae and seagrass leaves have much lower AFs while fleshy ones have higher values. Therefore, if AF is not measured, relative rates, rETR, should be presented by the simple calculation $rETR = Y \bullet PAR_i$.

For *quantitative* ETR calculations, the PAR absorbed by the photosynthetic pigments (PAR_a) of the area measured, i.e. the AF, must be known. As indicated above, assuming an AF of 0.84 (as included in some Walz fluorometers' software) is hardly acceptable. Instead, efforts should be made to determine a more correct AF for the tissue measured. There is an easy way to determine, or at least quickly estimate, AFs in flat-thallied algae and flat-leaved seagrasses simply by measuring the irradiance from a light source without and with the sensor covered by the tissue (see e.g. Beer et al. 1998; Sharon and Beer 2008). This should be done under water so as to minimise reflection from the leaf or thallus. The measurement rests on the assumption that most of the light is absorbed by the photosynthetic pigments. One can improve exactness by later extracting out (most of) the pigments (in e.g.

dimethyl formamide), remeasure the absorption of the plant part without the pigments, and make corrections accordingly. In some cases, and especially with thin-leaved seagrasses (e.g. several *Halophila* species) and thin-thallied macroalgae (e.g. *Ulva* spp.), this approach will yield ETRs which are stoichiometrically comparable to true (gross) O_2 evolution measurements, i.e. the molar O_2/ETR ratio is indeed close to 0.25 (such as illustrated in Fig. 25.6). For additional considerations regarding obtaining valid AFs so as to arrive at more quantitatively correct ETRs, see Chap. 8 in Beer et al. (2014). (Another way to estimate AFs in macrophytes is to use an integrating sphere, but this practice will not be covered here.)

One small caution regarding AF values: While most plants will maintain their AFs during the day, some can change them very quickly. For example, the seagrass *Halophila stipulacea* (as well as other *Halophila* spp.) can change AF values diurnally because of chloroplast clumping at high midday irradiances (Sharon and Beer 2008); this can lower the AF up to several tens of percent. Thus, if using the AF measured e.g. in the morning to be valid for midday measurements, ETRs would then be much overestimated during noontime (because of a higher than true AF taken into the calculation of ETR).

The exact value of the 0.5-factor is harder to achieve: it would require sophisticated methods for determining the proportional distribution of PAR_a between the two photosystems. This has in practice been done very rarely, and may be important mainly if the spectrum changes along a depth gradient (since PSI will absorb relatively more of the blue-shifted light at depth than PSII). One such example is given in Fig. 26.2 (in which the Dual-PAM, Walz, Germany, was used). However, we see the 0.5-factor as less critical to be corrected than the AF (since it will rarely deviate significantly from 0.5), and thus most authors will get away with using 0.5 for determining true ETRs.

The above describes how ETRs can be measured in larger, multicellular, photosynthetic organisms (e.g. macroalgae, seagrasses, corals and other photosymbiont-containing macroscopic organisms). Fluorometry can also be used for microalgae and cyanobacteria, but the techniques used may differ, especially in sparse, natural, assemblages.

26.2.3 FRRF (for Sparse Microalgal and Cyanobacterial Assemblages)

Although PAM fluorometry can be used for microalgae and cyanobacteria in culture, it is often not a sensitive enough method for sparse microscopic phototrophic assemblages such as are often found in nature (e.g. in oligotrophic ocean waters). Instead, fast repetition rate fluorometry (FRRF) can be used under such conditions. Here, very short (~1 μs), photosynthesis-saturating, light flashes (or "flashlets") generate single-turnover events of electron transport through PSII (rather than the multi-turnover events generated by the longer, ~1 s, saturating light in PAM

fluorometry). These short flashes will successively close reaction centres and reduce quinone-A until F_m has been reached. Thereafter, ca. 20 longer light flashlets of a lower frequency (~20 Hz) will reoxidise quinone-A. Algorithms will then treat the data so as to calculate F_m and F_o, and other parameters such as the effective cross-section area of the photosynthetic pigment-containing assemblage, the latter allowing calculation of absolute ETR. For further details of this method, see e.g. Huot and Babin (2011).

26.2.4 Rapid Light Curves

Much has been written about rapid light curves (RLC) regarding how they should be executed and how well the resulting ETRs along the irradiance axis can predict those under natural conditions of similar irradiances. So, first a few rules: (a) The irradiance span should be set such that the midpoint irradiance received by the plant sample is similar to the irradiance from which the plant was taken prior to the RLC measurement. If the plant previously grew at a low irradiance, then there is no need to extend the RLC to above 500 or 1000 μmol photons m^{-2} s^{-1} (the curve will simply saturate after the first or second irradiance), and if the plant grew in full sunlight, then very low initial irradiances of the curve are irrelevant: the best approach is to run a few trials with various start-points of irradiance to ensure that a nice curve is obtained, i.e. several points should be seen before light saturation and only a few after; (b) The RLC should be started immediately (within a second or so) after the plant sample has been attached to a (opened) leaf clip. A common flaw is that for some reason RLCs are often started 'after *x* seconds' or '*y* minutes of darkness' or the like. However, if so, then the plant is partly dark-adapted and will respond accordingly; (c) The duration of each irradiance should neither be too short nor too long: if too short (e.g. 2–5 s), then there will be a minimal adaptation time before each measurement—10 s may be a good compromise; if too long, then the light curve will take too long time to generate—it is after all called a *rapid* light curve!

Good correlations have been reported between in situ measured ETRs and those predicted by an RLC in which each irradiance was applied for 10 s only. One example is given in Fig. 26.1): The RLC was measured during midday at 6 m depth and 20–30 point measurements of ETR were taken at 09:15 and 13:00. Measured AFs were used in the calculations (but the 0.5-factor was assumed) so that (at least close to) true ETRs could be presented (Beer et al. 1998). As can be seen, the average ETRs at the two times of point measurements were close to those predicted from the RLC. This is not always so, but it gives an indication of the usefulness of RLCs even though the different irradiances were applied for only 10 s.

There are very few cases where the 0.5-factor has been challenged and the relative distribution of absorbed light between PSII and PSI has actually been measured. One such case includes, again, the seagrass *Halophila stipulacea* growing along a steep gradient in the northern Red Sea—from 1 to some 50 m depth (Sharon et al. 2011). At its depth limit, alongside with a much lower PAR irradiance, the spectrum is

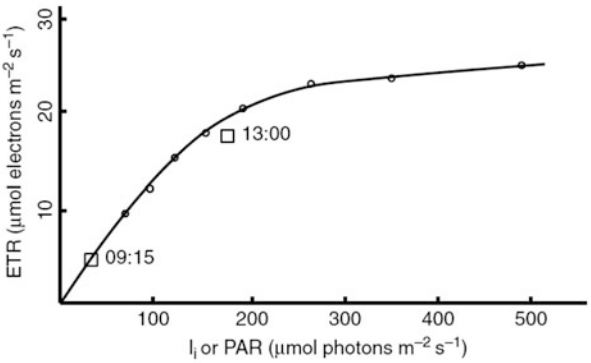

Fig. 26.1 Rapid light curve (RLC, circles) and average in situ electron transport rates (ETR, squares) as measured by point measurements. See text for details. (Adapted after Beer et al. (1998); "© Inter-Research 1998" with permission from Inter-Research)

strongly shifted towards bluish light. Thus, not only is the total chlorophyll content per leaf area higher, but so is the relative proportion of PSII/PSI (called FII in Fig. 26.2). If this is taken into account (as well as the different AF values at the two depths), then the RLCs attain the shapes as seen in Fig. 26.2, i.e. they and are more distanced from one another than if 0.5 would have been used for calculating ETR.

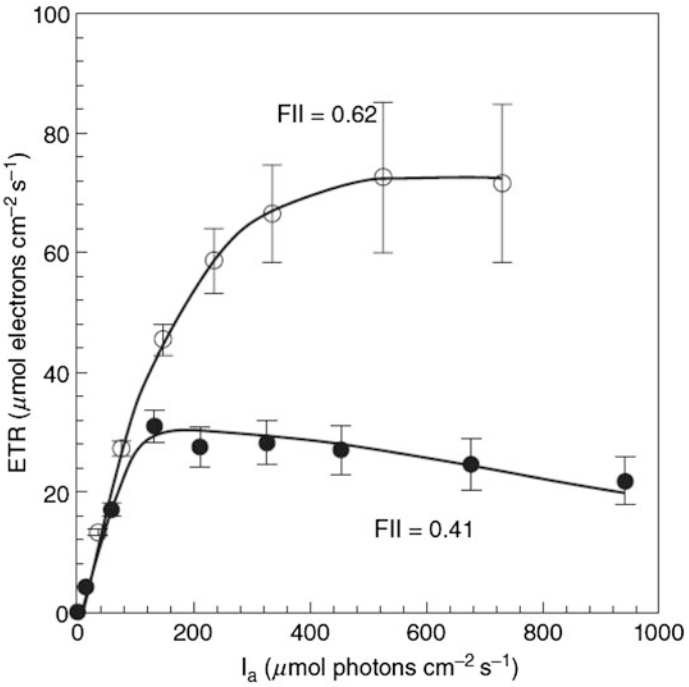

Fig. 26.2 ETR vs. absorbed irradiance (I_a) of *Halophila stipulacea* growing with two different PSII/PSI light absorption factors (FII). Rapid light curves (RLC) for plants growing at shallow (1 m, ~1.500 µmol photons m^{-2} s^{-1}, open circles) and deep (~50 m, ~100 µmol photons m^{-2} s^{-1}, closed circles). FII (the molar ratio of PSII/(PSI + PSII)) were 0.62 and 0.41 for the shallow and deep growing plants, respectively. (From Sharon et al. (2011); Copyright with permission from Limnology and Oceanography, John Wiley and Sons)

26.2.5 *Initial Slopes*—α

The initial slope (α) of a photosynthesis vs. irradiance (*P–I* or *P–E*) curve is often used as a measure of photosynthetic efficiency at low irradiances. In order for α to be quantitatively valid as a measure of quantum yield (Y), such curves should be generated using the *absorbed* irradiance, PAR_a (also termed I_a or E_a). However, PAR_a is often hard to measure (see above). Now, since fluorometry actually measures quantum yields, it is strange that those are not used more often for expressing α, but that α is still calculated by the initial slopes of *P–I* curves.

If Y of a plant acclimated to a certain irradiance is measured in low light (i.e. virtual darkness) before it has had time to dark-adapt, then logically this Y value should represent α. This was shown to be true by comparing calculated initial slopes of ETR vs. PAR_a curves with the initial Y values of RLCs, before the irradiance sequence starts (we call it Y_0), and the results show a good quantitative correlation (see Saroussi and Beer 2007; Fig. 26.3).

In practise, in order to obtain α, a plant sample should be placed, without delay, from its natural growth irradiance into the (open) dark-leaf clip, and the RLC should be started immediately (as always for RLCs). The first Y value obtained, i.e. that in virtual darkness (Y_0), will be equal to the initial slope α.

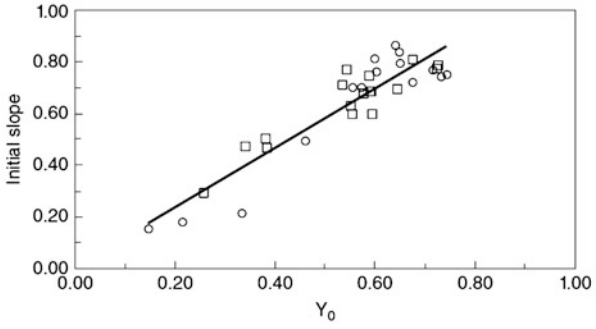

Fig. 26.3 Correlation between the calculated initial slope (α) of RLCs and Y derived from initial measurements of RLCs (Y_0). Circles and squares represent measurements of *Ulva* sp. growing under low (winter) and high (summer) conditions but acclimated to various irradiances in the laboratory. See text for details. (From Saroussi and Beer (2007); Copyright with permission from Aquatic Botany, Elsevier)

26.3 Merits and Demerits

The *merit* of fluorometry is, again, the speed and ease by which data can be obtained. Also, and at least equally importantly, measurements can be performed without even touching the plants. Thus, quantum yields and photosynthetic electron transport rates (ETRs or rETRs) can be obtained in situ under completely natural environmental situations. These are true (gross) rates, without any interference of respiration. This latter fact could also be seen as a demerit if ETRs are to be correlated with production in terms of growth rates. Thus, it is less straightforward to infer growth rates based on ETRs, and in this case gas exchange measurements may be a preferred alternative. We have found that fluorescence-based ETRs can favourably be used in order to evaluate the function of the photosynthetic apparatus per se in response to various environmental conditions, and especially its response to various irradiances. Furthermore, we seem to be the first to rapidly determine values for initial slopes (α) by PAM fluorometry, and hope this will be further developed and used by plant scientists.

References

Beer S, Vilenkin B, Weil A, Veste M, Susel L, Eshel A (1998) Measuring photosynthetic rates in seagrasses by pulse amplitude modulated (PAM) fluorometry. Mar Ecol Prog Ser 174:293–300

Beer S, Björk M, Beardall J (2014) Photosynthesis in the marine environment. Wiley-Blackwell, Oxford, UK. ISBN: 978-1-119-97957-9

Huot Y, Babin M (2011) Overview of fluorescence protocols: theory, basic conscepts and practice. In: Suggett DJ, Prasil MA, Borowitzka MA (eds) Chlorophyll fluorescence in aquatic sciences: methods and applications, Developments in applied phycology, vol 4. Springer, Netherlands, pp 31–74

Saroussi S, Beer S (2007) Alpha and quantum yield of aquatic plants as derived from PAM fluorometry. Aquat Bot 86:89–92

Sharon Y, Beer S (2008) Diurnal movements of chloroplasts in *Halophila stipulacea* and their effect on PAM fluorometric measurements of photosynthetic rates. Aquat Bot 88:273–276

Sharon Y, Levitan O, Spungin D, Berman-Frank I, Beer S (2011) Photoacclimations of the seagrass *Halophila stipulacea* to the dim irradiance at its 48-m depth limit. Limnol Oceanogr 56:357–362

Chapter 27
Carbon Assimilation Capacity and Blue-Green Fluorescence

Hualing Mi and Baosheng Qiu

Abstract Photosynthetic electron transfer produces reducing power in the form of NADPH for carbon assimilation. The carbon assimilation activity is closely related to the changes in NADPH concentration. In this chapter, we introduce a method for monitoring the change of carbon assimilation capacity in algae using blue-green fluorescence (460 nm) emission and kinetics of NADPH changes to estimate the fluctuation of light-dependent NADPH concentration, in combination with inhibitors of carbon assimilation and mutants.

Keywords Cyanobacteria · Carbon assimilation · Blue-green fluorescence · NADPH

27.1 Introduction

In the light reactions of oxygenic photosynthesis, light can be absorbed by light-harvesting antenna pigments (chlorophyll, carotenoids, and phycobilin), and energy transmitted to chlorophyll 680 (P680), the reaction center of photosystem II (PS II) and excited, causing charge separation, and capturing electrons from molecular water. On the one hand, it causes oxidation of molecular water to release oxygen and protons, on the other hand, electrons are transferred from molecular water to $NADP^+$ via a series of electron transporters in thylakoid membranes to produce NADPH. Accompanying this electron transfer, a proton gradient is established

H. Mi (✉)
National Key Laboratory of Plant Molecular Genetics, Institute of Plant Physiology and Ecology, Center for Excellence in Molecular Plant Sciences, Chinese Academy of Science, Shanghai, China
e-mail: mihl@cemps.ac.cn

B. Qiu
Hubei Key Laboratory of Genetic Regulation and Integrative Biology, School of Life Sciences, Central China Normal University, Wuhan, Hubei, China
e-mail: bsqiu@mail.ccnu.edu.cn

K. Gao et al. (eds.), *Research Methods of Environmental Physiology in Aquatic Sciences*, https://doi.org/10.1007/978-981-15-5354-7_27

across the thylakoid membrane. The electrochemical gradient is ultimately utilized for the synthesis of ATP by ATPase. NADPH and ATP are used as energy sources to drive CO_2 assimilation. When photosynthetic carbon assimilation is in full operation, NADPH will be used up and there will be no accumulation of photo-reductants. However, under environmental stress conditions, such as elevated temperature, high light, high salinity and limitation of inorganic carbon, the key enzymes of photosynthetic carbon assimilation will be inhibited, resulting in a decrease in the rate of photosynthetic carbon assimilation and a large accumulation of NADPH produced by the photoreactions. Thus, NADPH metabolism can indirectly reflect the activity of photosynthetic carbon assimilation. By detecting the dynamic changes of NADPH at the cellular level, we can investigate the status of photosynthetic carbon assimilation.

In early investigations, NADPH fluorescence was measured in algae and photosynthetic bacteria in vivo by Duysens and Amesz (1957), Olson et al. (1959), Olson and Amesz (1960), and more recently in intact chloroplasts and leaf segments of spinach (Cerovic et al. 1993). These studies did not use this method to investigate the complex reactions within cyanobacteria, in which NADPH plays a central role. Mi et al. (2000) first reported that light-induced changes in NADPH fluorescence display remarkable dynamics, which bear the potential of providing information on photosynthetic NADP reduction as well as dark reduction associated with the reductive pentose phosphate cycle, NADPH oxidation linked to Calvin cycle activity, thylakoid membrane-bound NAD(P)H dehydrogenase (NDH) mediated cyclic and respiratory electron transport as well as NADPH oxidation by oxidative phosphorylation and by active oxygen species, combined with the study of mutants and inhibitors.

27.2 Photo-Induced Change in Blue-Green Fluorescence

NADPH fluorescence is measured with a PAM chlorophyll (Chl) fluorometer featuring a modified version of the emitter-detector-cuvette unit ED-101PM (Heinz Walz GmbH, Effeltrich, Germany). The standard 650 nm measuring light LED is substituted by a blue LED (Nichia) with an emission peak at 440 nm and a shoulder extending into the UV-A. Wavelengths above 400 nm are eliminated by an optical filter (2 mm UG 11, Schott). The resulting measuring light displays a peak around 380 nm. It is applied at maximal intensity, i.e., intensity setting 12 at the PAM-101 unit and 100 kHz modulation frequency. The photomultiplier is protected by a combination of a long-pass filter (KV416, Schott), to eliminate the UV-measuring light and a short-pass filter (DT Cyan, Balzers), as well as a blue-green glass filter (BG39, Schott), to eliminate Chl fluorescence.

The sample is contained in a 10 × 10 mm quartz cuvette, with excitation and detection pathways at right angles, and the side opposite the detector being mirrored. Saturating actinic light (660 μmol quanta m^{-2} s^{-1}) is generated by an LED-array

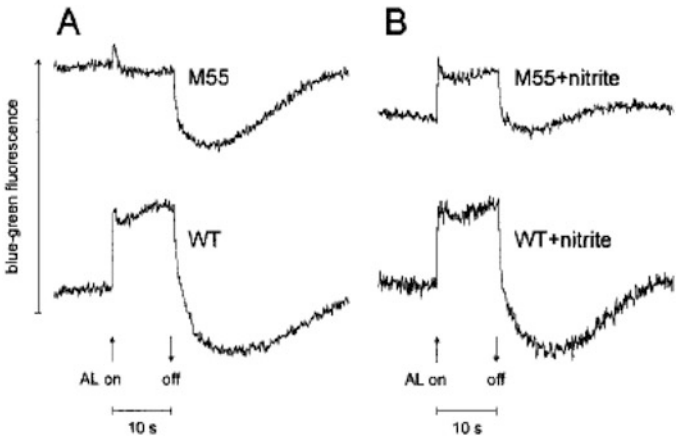

Fig. 27.1 The kinetics of blue-green fluorescence induced by dark–light–dark transitions in *Synechocystis* PCC6803 and its *ndhB*-defective mutant M55. (**a**) Comparison of wild-type cells (WT) and mutant cells (M55) in the absence of artificial acceptors. (**b**) Comparison in the presence of nitrite. KNO_2 was added to a final concentration of 5 mM at about 3 min before measurement (Mi et al. 2000)

cone with peak emission at 655 nm (High-Power-LED-Lamp, Walz). Chl concentration is around 18 g ml^{-1}. The suspension is kept at a constant temperature of 27 °C. The analog output signal of the PAM fluorometer is fed into a digital storage oscilloscope with signal averaging (Nicolet), from where the data are transferred to a PC for further processing.

In the given set-up a blue-green fluorescence signal is also observed in the absence of cyanobacteria, with the cuvette being filled with water. This background signal, which decreases with increasing concentrations of cyanobacteria (as both the excitation light and the fluorescence were absorbed) prevents a reliable quantitative assessment of absolute NADPH fluorescence levels. Therefore, the figures refer to "blue-green fluorescence" and no absolute units for NADPH fluorescence yield are given.

In Fig. 27.1, typical induction transients of blue-green fluorescence emission in response to illumination by saturating red light are shown, as measured with a standard PAM fluorometer equipped with a modified emitter-detector unit (see above). Fluorescence was excited by modulated UV light peaking around 380 nm. The signal did not contain any Chl fluorescence, as this was completely eliminated by the filter set in front of the photodetector. In Fig. 27.1a, the responses of wild-type cells of *Synechocystis* PCC 6803 and of its *ndhB*-defective mutant M55 upon illumination with a 10 s saturating light pulse are compared. In both cases complex dark–light–dark induction transients are observed. In the wild type, the response is dominated by a rapid fluorescence increase which is followed by a dip and a slower rise phase. Upon light-off there is a biphasic fluorescence decline leading to a level distinctly below the initial dark level (undershoot) followed by a slow rise back to the dark level. In the mutant M55 upon onset of illumination there is only a small,

rapid fluorescence rise which is followed by a dip phase leading below the initial level. Upon light-off there is a pronounced further fluorescence decline (undershoot) before the signal slowly returns to its original level.

Nitrite is known to be reduced by ferredoxin at the acceptor side of PSI, thus competing with NADP for electrons. In the dark, nitrite causes slow oxidation of NADPH via ferredoxin-$NADP^+$ oxidoreductase (FNR) and ferredoxin. Figure 27.1b shows that in the presence of nitrite the kinetic response of M55 becomes more similar to that of wild-type cells, as the amplitude of the initial positive transient is distinctly increased. Nitrite has practically no effect on the wild-type induction kinetics. This reflects the exhaustion of NADPH, which is partially oxidized by the Calvin cycle and thus withdrawn from cyclic flow around PSI. In M55 cells, which are deficient in NDH, there is no dark reduction of the intersystem electron transport chain and no NDH-mediated cyclic electron flow. Hence the mutant cells are lacking a donor for PSI and, therefore, will prevent NADP reduction. In the presence of artificial electron acceptors, some of the electrons from the photosystem I flow to NO_2^-, which decreases the accumulation of NADPH. Meanwhile, NADPH is utilized by carbon assimilation, thus producing enough $NADP^+$ as the acceptor, and the process of NADPH synthesis is detectable.

The data in Fig. 27.1 were interpreted as follows.

1. First rapid rise: light-driven reduction of NADP.
2. Dip phase: oxidation of NADP via Calvin cycle activity, which sets in as soon as the ribulose bisphosphate carboxylase is activated and ATP becomes available.
3. Secondary rise phase: accumulation of NADPH as its oxidation in the Calvin cycle becomes limited, possibly concurrent with a limitation in ATP supply.
4. Stationary phase: matched rates of light-driven NADP reduction and NADPH oxidation via the Calvin cycle; electron storage in reduced carbon.
5. Rapid decay phase: dark-oxidation of NADPH via the Calvin cycle or alternative acceptor systems, as, for example, active oxygen species.
6. Slow decay phase: NADPH oxidation during oxidative phosphorylation. There was no significant difference in this process between wild type and NDH-1 inactivated mutant M55.
7. Slow rise phase: dark reduction of NADP associated with reductive pentose phosphate cycle.

27.3 Relationship Between NADPH Fluorescence Kinetics and Carbon Assimilation

Figure 27.2 shows that in the presence of IAA, an inhibitor of Calvin cycle activity, the amplitude of rapid NADP reduction is approximately doubled in wild type but not in M55 cells. In both types of cells the dip phase is suppressed. Furthermore, particularly in the wild-type cells, there is a distinct suppression of the transient post-illumination drop (undershoot) of the blue-green fluorescence signal below the base

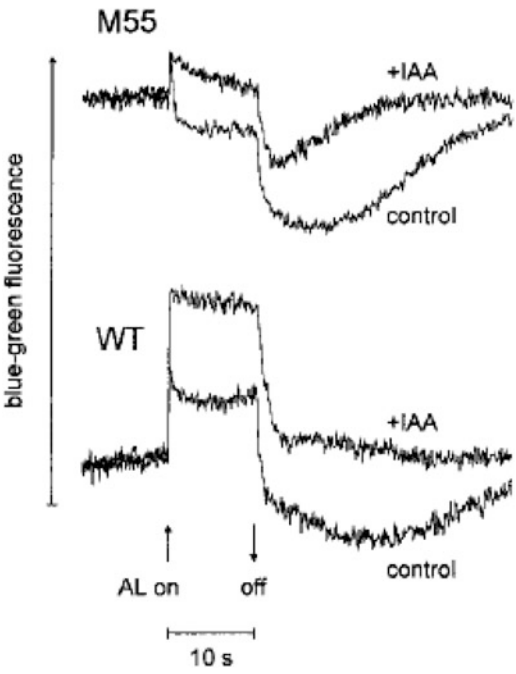

Fig. 27.2 Effect of iodoacetic acid (IAA) on induction transients of blue-green fluorescence in wild-type and mutant cells (Mi et al. 2000)

line. The result suggests that the Calvin cycle is limited by ATP supply in the absence of NDH-mediated cyclic photophosphorylation.

Therefore, we can indirectly estimate the carbon assimilation ability of algae by analyzing the fluorescence dynamics of NADPH, combining mutant and inhibitor studies.

27.4 The Advantage and Demerits of the Method and Its Misunderstandings

The advantage of this method is that it is rapid and can be used to evaluate the carbon assimilation capacity under various physiological conditions. Because the changes of NADPH are closely related to environmental factors such as light and dark periods, temperature, chlorophyll concentration, etc., the experimental conditions need to be strictly controlled.

References

Cerovic ZG, Bergher M, Goulas Y, Tosti S, Moya I (1993) Simultaneous measurement of changes in red and blue fluorescence in illuminated isolated chloroplasts and leaf pieces: the contribution of NADPH to the blue fluorescence signal. Photosynth Res 36:193–204

Duysens LNM, Amesz J (1957) Fluorescence spectrometry of reduced phosphopyridine nucleotide in intact cells in the near-ultraviolet and visible region. Biochim Biophys Acta 24:19–16

Mi H, Klughammer C, Schreiber U (2000) Light-induced dynamic changes of NADPH fluorescence in *Synechocystis* PCC6803 and its ndhB-defective mutant M55. Plant Cell Physiol 41:1129–1135

Olson JM, Amesz J (1960) Action spectra for fluorescence excitation of pyridine nucleotide in photosynthetic bacteria and algae. Biochim Biophys Acta 37:14–24

Olson JM, Duysens LNM, Kronenberg GHM (1959) Spectrofluorometry of pyridine nucleotide reactions in *Chromatium*. Biochim Biophys Acta 36:125–131

Chapter 28
In Situ Measurement of Phytoplankton Photochemical Parameters

Guang Gao, Peng Jin, and Kunshan Gao

Abstract Chlorophyll fluorescence techniques, apart from the application in laboratory measurements of photosynthesis, are widely used in field studies on marine primary production, referring to biomass of phytoplankton, photochemical reaction, photosynthetic carbon fixation, pathway of energy utilization and dissipation. This section introduces the use of chlorophyll fluorescence techniques in oceanographic survey.

Keywords Carbon fixation · Chlorophyll fluorescence · Climate change · Ocean acidification · Photosynthesis · Phytoplankton

28.1 Introduction

In marine science, chlorophyll fluorescence techniques are first used to estimate concentration of chlorophyll *a* as chlorophyll *a* is most commonly used to estimate biomass of photosynthetic organisms in marine ecosystem. The level of chlorophyll *a* is very low in oceans, 0.02–20 μg/L in the upper 200 m ocean with a mean value of 0.31 μg/L (Falkowski et al. 2004). Such low levels of chlorophyll *a* require a large amount of seawater volume to measure and 500 ml seawater is required even if fluorescence spectrophotometer is used. In addition, organic solvent is involved in the measurement of chlorophyll *a* for the method of spectrophotometer. In 1960s, chlorophyll fluorescence techniques were used to measure chlorophyll *a* in phytoplankton. In 1966, Carl Lorenzen pumped in situ seawater into a Chlorophyll Fluorometer and measured concentration of chlorophyll *a* by fluorescence signal.

G. Gao · K. Gao (✉)
State Key Laboratory of Marine Environmental Science and College of Ocean and Earth Sciences, Xiamen University, Xiamen, China
e-mail: ksgao@xmu.edu.cn

P. Jin
School of Environmental Science and Engineering, Guangzhou University, Guangzhou, China

K. Gao et al. (eds.), *Research Methods of Environmental Physiology in Aquatic Sciences*, https://doi.org/10.1007/978-981-15-5354-7_28

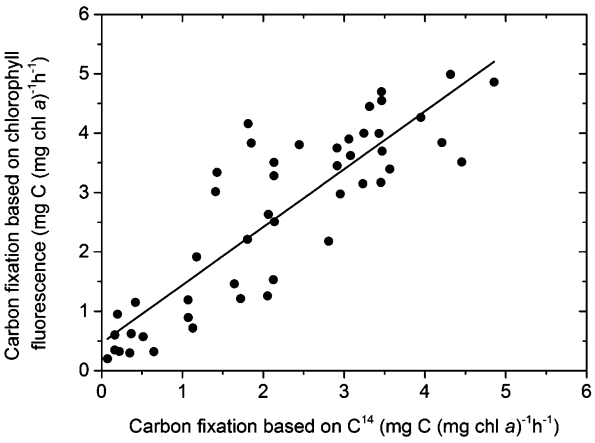

Fig. 28.1 Correlation between fluorescence-based and radiocarbon-based estimates of carbon fixation for 55 discrete samples taken from the North Atlantic over a period of 2 years (after Falkowski et al. 1991)

This technique reduced the time, raised efficiency, and is widely used in measurement of in situ chlorophyll *a*.

Chlorophyll fluorescence techniques have been used to measure maximal photochemistry efficiency of PSII, effective photochemistry efficiency of PSII, electron transport rate, functional absorption cross section of PSII, etc., since the 1980s. Research focuses on the effects of light (Kishino et al. 1986; Morrison 2003; Alderkamp et al. 2010; Yuan et al. 2018), nutrient (Kolber et al. 1990; Babin et al. 1996; Liu et al. 2010; Gao et al. 2017), iron (Kolber et al. 1994; Behrenfeld et al. 1996; Coale et al. 2004; Peloquin et al. 2011) on maximal photochemistry efficiency of PSII and electron transport rate. In addition, chlorophyll fluorescence techniques have been used in response of phytoplankton to ocean acidification (Gao et al. 2012, 2018; Wu et al. 2012; White et al. 2020). Jin et al. (2016) used in situ FIRe to map the northern South China Sea. They found that functional absorption cross section of PSII was relatively conservative which increased with depth at nearly all stations while effective photochemistry efficiency was higher at upwelling station and lower at pelagic stations. Therefore, in situ FIRe can be used to investigate photophysiological response of phytoplankton to environmental changes.

Chlorophyll fluorescence is also used to estimate marine primary productivity and carbon fixation of phytoplankton (Gilbert et al. 2000; Jakob et al. 2005). Kolber and Falkowski (1993) obtained a good line relationship between C^{14}-estimated carbon fixation and fluorescence-estimated carbon fixation (Fig. 28.1). It is worth noting that photorespiration can affect this relationship (Genty et al. 1990). The ratio of fluorescence-estimated to C^{14}-estimated carbon fixation would rise when photorespiration increases because photorespiration consumes the products of electron transport, such as ATP and NADPH, and thus reduces carbon fixation. Apart from estimating marine primary productivity, chlorophyll fluorescence techniques are used to analyze the fate of photons absorbed by phytoplankton (Lin et al. 2016). There are three possible fates for solar energy absorbed by any photosynthetic organism: (1) generate photochemical reactions to produce organic matter, (2) be

dissipated as heat, (3) be emitted back to the environment via fluorescence. Lin et al. (2016) constructed an extremely sensitive sea-going instrument measuring chlorophyll fluorescence lifetimes that can be quantitatively related to absolute quantum yield of fluorescence. Combined with photochemistry efficiency, the portion of heat can be calculated. Based on this technology, Lin et al. (2016) calculate that, on average, ~60% of absorbed photons are converted to heat, only 35% are directed toward photochemical water splitting, and the rest are reemitted as fluorescence. Lin et al. (2016) also found that quantum yields obtained from satellite-based measurements are not corroborated by in situ lifetime measurements. Two reasons can explain this discrepancy. In the central ocean gyres, where surface chlorophyll concentrations are very low (<0.1 mg m^{-3}), the fluorescence signals propagated to space are extremely weak. As a result, the current algorithms used to calculate quantum yields of fluorescence become increasingly uncertain whereas the in situ lifetime measurements remain extremely precise (within 5%), even at the lowest chlorophyll concentrations found in the upper ocean. Another reason is the effect of pigment packaging within a phytoplankton cell (Behrenfeld et al. 2009), which is most pronounced in larger cells and reduces the observed quantum yields, as compared to their true "molecular" values inferred from lifetime. Accordingly, this fluorescence lifetime technique has noticeable advantages in future oceanography research.

28.2 Select and Use of In Situ Fluorometer

According to operation principle, in situ fluorometer can be catalyzed to PAM-based and Fast Repetition Rate-based instruments. The main products for PAM are PAM from German WALZ and the main products for FRR are FIRe from Satlantic Canada and Fast Repetition Rate Fluorometer from CTG UK. There are differences in absolute values of parameters between these two kinds of instruments. For instance, the effective photochemistry efficiency measured by PAM can be 20% higher than that measured by FRRF under lower light intensity although they tended to be the same under higher light intensity (Suggett et al. 2003). Falkowski et al. (2004) found that viable fluorescence measured by PAM was 50% higher than FIRe and maximal photochemistry efficiency measured by PAM was 10–15% higher than FIRe. Furthermore, Röttgers (2007) reported that the parameters measured by these two kinds of instruments can be mutually converted.

According to characters, in situ fluorometer can be divided into deck and underwater. Deck-based instrument cannot be used in seawaters but be mounted in the deck and measure phytoplankton by pumping or transferring seawater into its cuvette. This instrument can be used for deck incubation experiments. Underwater instruments collect data in seawaters and are used for in situ oceanography investigation.

The selection of instrument should be based on design and aim of experiments. PAM can be used for in situ experiments in coastal waters as it is easy to operate and works well in coastal macro-algae and phytoplankton research. If in situ incubation

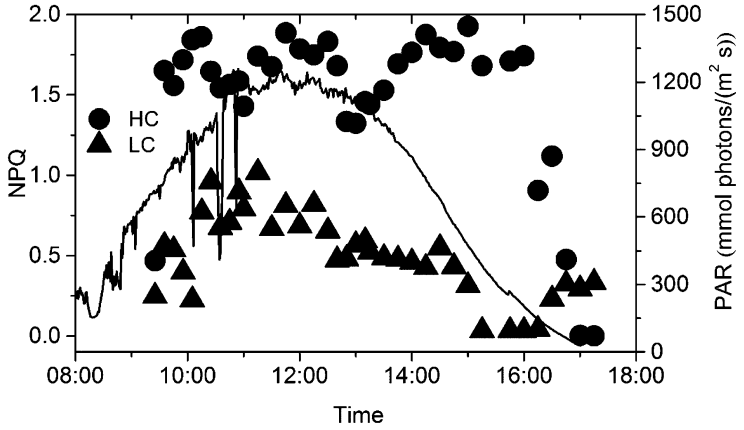

Fig. 28.2 The NPQ of phytoplankton assemblages at station E606 in the South China Sea grown under low pCO_2 (385 μatm, triangle) and high pCO_2 (800 μatm, circle) in the microcosms on day six. The black curve represents the visible light intensity of that day (Gao et al. 2012)

experiments are conducted in pelagic waters, FIRe can be used as it has higher sensitivity for chlorophyll *a* level despite of its DOS operation system (Fig. 28.2). If in situ photochemistry parameters of phytoplankton at different depths are required, in situ FIRe can be chosen as it can give out photochemistry parameters very fast and has even higher sensitivity to chlorophyll *a* level compared to FIRe (Fig. 28.3).

28.3 The Do's and Don'ts

Compared to lab measurements, there are some significant differences in using in situ fluorescence measurements. The operations for deck and underwater instruments are also different. Therefore, careful reading of manuals before using is compulsory.

1. Deck instruments must be fixed before use as shake of research vessels can remove instruments that are not fixed. The cuvettes are fragile so operation must be careful.
2. When chlorophyll *a* concentration is very low, particularly in summer, the ratio of signal to noise dramatically decreases, resulting in poor data. To increase the ratio of signal to noise, repetitive measurements are needed.
3. For underwater fluorometer, ensure the cast time after discussing with the leading scientist. Meanwhile, ensure there are no other instruments in the sea before casting and prevent other instruments casting when your instrument is in the sea.
4. Control the cast speed (0.5–1.5 m s^{-1}) to obtain reliable data.

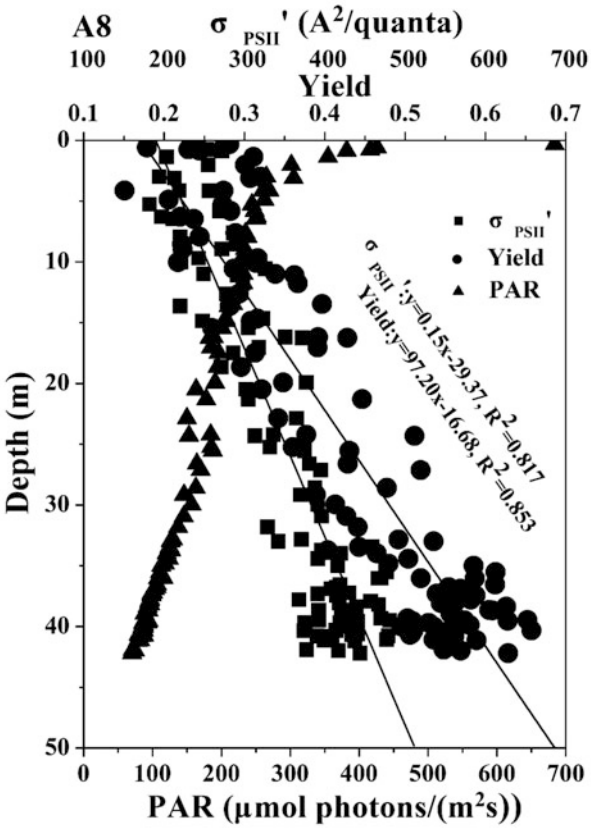

Fig. 28.3 Vertical profiles of photosynthetic parameters of functional absorption cross section of photosystem II ($\sigma PSII'$) (A^2 $quanta^{-1}$, square) and effective photochemical efficiency of photosystem II (PSII) (Yield, circle) and photosynthetically active radiation (PAR, triangle) irradiance at station A8 in South China Sea

5. Each research vessel has its own mooring direction, please acquire the mooring direction and release instruments at the windward side of vessel in case the instrument goes under the vessel due to wind.
6. The time when a vessel moors may be different between stations, leading to low possibility for comparison in photochemistry parameters between stations due to the change of solar radiation.
7. At stations where a vessel moors for more than 1 day, continuous monitoring can be conducted to investigate the dial variation of photochemistry parameters.
8. The instruments must be rinsed thoroughly with fresh water after use to avoid corrosion.

28.4 Case Study in Using In Situ Fluorometer

This section takes in situ FIRe as an example and introduces how to use in situ Fluorometer.

1. Connect the instrument to a computer via the supplied USB programming cable, click FIReeCom and open Operation Settings dialog and set the following:
   - Set Operation Mode to Continuous.
   - Enable Transmit Raw Data on External Interfaces checkbox.
   - In SerialPort section, select Active Port to match the selected connection (RS-232 or RS-422).
   - For long cable RS-422 profiling, recommended baud rate is 9600.
2. After applying above settings, remove USB and power. Leave instrument unpowered for at least 20 s and then restart the instrument. Connect RS-422 cable to FIRe and connect deck unit to computer running FIReCom software. Wait 60 s after repowering FIRe then use FIReCOm to establish data connection. Observe data as it is emitted in real time to confirm FIRe is configured correctly.
3. Click Acquisition button and start to collect data.
4. Release the instrument into seawater with a rope in a speed of 0.5–1.5 m s^{-1} and withdraw the instrument in the same speed when it arrives at the target depth.
5. After the instrument comes back to the deck, close software and disconnect instrument and computer. Rinse the instrument immediately with fresh water to avoid corrosion.

References

Alderkamp A-C, de Baar HJW, Visser RJW, Arrigo KR (2010) Can photoinhibition control phytoplankton abundance in deeply mixed water columns of the Southern Ocean? Limnol Oceanogr 55:1248–1264

Babin M, Morel A, Claustre H, Bricaud A, Kolber ZS, Falkowski PG (1996) Nitrogen- and irradiance-dependent variations of the maximum quantum yield of carbon fixation in eutrophic, mesotrophic and oligotrophic marine systems. Deep-Sea Res Part I 43:1241–1272

Behrenfeld MJ, Bale AJ, Kolber ZS, Aiken J, Falkowski PG (1996) Confirmation of iron limitation of phytoplankton photosynthesis in the equatorial Pacific Ocean. Nature 383:508–511

Behrenfeld MJ, Westberry TK, Boss ES, O'Malley RT, Siegel DA, Wiggert JD, Franz BA, McLain CR, Feldman GC, Doney SC, Moore JK (2009) Satellite-detected fluorescence reveals global physiology of ocean phytoplankton. Biogeosciences 6:779–794

Coale KH, Johnson KS, Chavez FP, Buesseler KO, Barber RT, Brzezinski MA, Cochlan WP, Millero FJ, Falkowski PG, Bauer JE et al (2004) Southern Ocean iron enrichment experiment: carbon cycling in high-and low-Si waters. Science 304:408–414

Falkowski PG, Ziemann D, Kolber Z, Bienfang PK (1991) Role of eddy pumping in enhancing primary production in the ocean. Nature 352:55–58

Falkowski PG, Koblížek M, Gorbunov M, Kolber Z (2004) Development and application of variable chlorophyll fluorescence techniques in marine ecosystems. In: Papageorgiou GC, Govindjee (eds) Chlorophyll *a* fluorescence: a signature of photosynthesis. Springer, Dordrecht, pp 757–778

Gao KS, Xu JT, Gao G, Li YH, Hutchins DA, Huang BQ, Wang L, Zheng Y, Jin P, Cai XN et al (2012) Rising CO_2 and increased light exposure synergistically reduce marine primary productivity. Nat Clim Change 2:519–523

Gao G, Xia J, Yu J, Zeng X (2017) Physiological response of a red tide alga (*Skeletonema costatum*) to nitrate enrichment, with special reference to inorganic carbon acquisition. Mar Environ Res 133:15–23

Gao G, Shi Q, Xu Z et al (2018) Global warming interacts with ocean acidification to alter PSII function and protection in the diatom *Thalassiosira weissflogii*. Environ Exp Bot 147:95–103

Genty B, Harbinson J, Baker NR (1990) Relative quantum efficiencies of the two photosystems of leaves in photorespiratory and nonphotorespiratory conditions. Plant Physiol Biochem 28:1–10

Gilbert M, Domin A, Becker A, Wilhelm C (2000) Estimation of primary productivity by chlorophyll a in vivo fluorescence in freshwater phytoplankton. Photosynthetica 38:111–126

Jakob T, Schreiber U, Kirchesch V, Langner U, Wilhelm C (2005) Estimation of chlorophyll content and daily primary production of the major algal groups by means of multiwavelength-excitation PAM chlorophyll fluorometry: performance and methodological limits. Photosynth Res 83:343–361

Jin P, Gao G, Liu X, Li FT, Tong SY, Ding JC, Zhong ZH, Liu NN, Gao K (2016) Contrasting photophysiological characteristics of phytoplankton assemblages in the Northern South China Sea. PLoS One 11(5):e0153555

Kishino M, Okami N, Takahashi M, Ichimura S (1986) Light utilization efficiency and quantum yield of phytoplankton in a thermally stratified sea. Limnol Oceanogr 31:557–566

Kolber Z, Falkowski PG (1993) Use of active fluorescence to estimate phytoplankton photosynthesis in situ. Limnol Oceanogr 38:1646–1665

Kolber Z, Wyman KD, Falkowski PG (1990) Natural variability in photosynthetic energy conversion efficiency: a field study in the Gulf of Maine. Limnol Oceanogr 35:72–79

Kolber ZS, Barber RT, Coale KH, Fitzwateri SE, Greene RM, Johnson KS, Lindley S, Falkowski PG (1994) Iron limitation of phytoplankton photosynthesis in the equatorial Pacific Ocean. Nature 371:145–149

Lin HZ, Kuzminov FI, Park J, Lee SH, Falkowski PG, Gorbunov MY (2016) The fate of photons absorbed by phytoplankton in the global ocean. Science 351:264–267

Liu HC, Gong GC, Chang J (2010) Lateral water exchange between shelf-margin upwelling and Kuroshio waters influences phosphorus stress in microphytoplankton. Mar Ecol Prog Ser 409:121–130

Lorenzen CJ (1966) A method for the continuous measurement of in vivo chlorophyll concentration. Deep-Sea Res Oceanogr Abstr 13(2):223–227

Morrison JR (2003) In situ determination of the quantum yield of phytoplankton chlorophyll *a* fluorescence: a simple algorithm, observations, and a model. Limnol Oceanogr 48:618–631

Peloquin J, Hall J, Safi K, SmithJr WO, Wright S, van den Enden R (2011) The response of phytoplankton to iron enrichment in Sub-AntarcticHNLCLSi waters: results from the SAGE experiment. Deep-Sea Res Part II 58:808–823

Röttgers R (2007) Comparison of different variable chlorophyll *a* fluorescence techniques to determine photosynthetic parameters of natural phytoplankton. Deep-Sea Res Part I 54:437–451

Suggett DJ, Oxborough K, Baker NR, MacIntyre HL, Kana TM, Geider RJ (2003) Fast repetition rate and pulse amplitude modulation chlorophyll *a* fluorescence measurements for assessment of photosynthetic electron transport in marine phytoplankton. Eur J Phycol 38:371–384

White E, Hoppe CJ, Rost B (2020) The Arctic picoeukaryote *Micromonas pusilla* benefits from ocean acidification under constant and dynamic light. Biogeosciences 17:635–647

Wu XJ, Gao G, Giordano M, Gao KS (2012) Growth and photosynthesis of a diatom grown under elevated CO_2 in the presence of solar UV radiation. Fund Appl Limnol 180:279–290

Yuan W, Gao G, Shi Q, Xu Z, Wu H (2018) Combined effects of ocean acidification and warming on physiological response of the diatom *Thalassiosira pseudonana* to light challenges. Mar Environ Res 135:63–69

Part VII
Biochemical and Molecular Methods

Chapter 29
Biochemical Inhibitors for Algae

Yaping Wu and Kunshan Gao

Abstract Biochemical inhibitors are usually used to study the mechanisms or pathways of cellular metabolism; these inhibitors are able to bind to a specific site of enzymes or ion channels, and interrupt a certain reaction in which enzymes are involved, while there are no direct effects to other biochemical reactions. This chapter will introduce typical inhibitors that are used in algal research.

Keywords Inhibitor · Photosynthesis · Carbon concentrating mechanism · Photosystem · Electron transport chain

Acetazolamide, (AZ): This inhibitor can specifically bind to carbonic anhydrase and disable it. The inhibitor cannot penetrate the cell membrane, so it can only act on enzymes secreted to the outside of the cell. The reference final concentration is 100 μmol L^{-1} (Chen and Gao 2004a, b).

Dextran-bound sulfonamide, (DBS): This inhibitor can specifically bind to carbonic anhydrase. The inhibitor cannot penetrate the cell membrane, so it can only act on enzymes secreted to the outside of the cell. The reference final concentration is 200 μmol L^{-1} (Nimer et al. 1999).

4,4′-Diisothiocyano-2,2′-stilbenedisulfonic acid, (DIDS): This is an anion exchange protein inhibitor, can specifically disable the anion exchange protein on the cell membrane, thus preventing anions from entering the cell. Generally, this inhibitor can be used to study the mechanism of ion absorption of bicarbonate in inorganic carbon. The final reference concentration is 200 μmol L^{-1} (Chen and Gao 2004a, b).

Y. Wu (✉)
College of Marine Life and Fisheries, Jiangsu Ocean University, Lianyungang, China
e-mail: ypwu@jou.edu.cn

K. Gao
State Key Laboratory of Marine Environmental Science and College of Ocean and Earth Sciences, Xiamen University, Xiamen, China

K. Gao et al. (eds.), *Research Methods of Environmental Physiology in Aquatic Sciences*, https://doi.org/10.1007/978-981-15-5354-7_29

1-Hydroxyethylidene-1,1-bisphosphonic acid, (HEBP): Inhibit the formation of crystal, e.g., the calcium carbonate skeleton of coral, the final reference concentration is 0.5 mmol L^{-1} (Herfort et al. 2008).

Ethoxyzolamide, (EZ): This inhibitor binds specifically to carbonic anhydrase and deactivates its catalytic activity. Because the inhibitor can penetrate the cell membrane, it acts on both intracellular and extracellular carbonic anhydrase. The final reference concentration is 100 μmol L^{-1} (Chen and Gao 2004a, b).

Lincomycin: This inhibitor can specifically inhibit protein synthesis in chloroplast, thereby blocking the turnover of photosystem II protein. This inhibitor is generally dissolved in distilled water with a reference final concentration of 500 μg mL^{-1} (Wu et al. 2011).

3-(3,4-Dichlorophenyl)-1,1-dimethylurea, (DCMU): Also known as diuron, it inhibits the electron transfer from Q in PSII to PQ, and the reference final concentration is 50 μmol L^{-1} (Msilini et al. 2011).

Atrazine: This inhibitor can specifically bind to plastoquinone of photosystem II, thereby blocking photosynthetic electron transport, with a reference final concentration of 6 μmol L^{-1} (SchÄFer et al. 1992).

3,3-Dichloro-2-dihydroxyphosphinoylmethyl-2-propenoate, (DCDP): Similar to phosphoenolpyruvate (PEP) in structure, this inhibitor can specifically inhibit the activity of phosphoenolpyruvate carboxylase, which has been repeatedly used in the study of C4 carbon fixation pathway. The reference final concentration is 750 μmol L^{-1} (Reinfelder et al. 2004).

Rotenone: It inhibits electron transfer in NADH-Q reductase, thus blocking electron transfer from NADH to CoQ. The reference final concentration is 0.4 μmol L^{-1} (Ernster et al. 1963).

Amytal: This inhibitor specifically bind to NADH-Q reductase, and the electron transfer from NADH to CoQ was blocked. The reference final concentration is 2 mmol L^{-1} (Ernster et al. 1963).

Antimycin A: It inhibits the transfer of electrons from reduced CoQ (QH2) to cytochrome C1, by referring to the final concentration of 2 μg mL^{-1} (Walther et al. 2010).

Vanadate: it inhibits H^+-ATPase, the reference final concentration is 0.5 mmol L^{-1} (Araie et al. 2011).

GeO_2: This chemical can specifically inhibit the formation of silicon shells of diatoms, which is generally used to inhibit the adhesion of diatoms on the surface of macroalgae. The reference final concentration is 0.1–0.5 mL of saturated GeO_2 L^{-1} (Shea and Chopin 2007).

Erythromycin: This inhibitor binds to the 50s ribosome and inhibits protein synthesis, leading directly to cell death, and a series of concentration gradients are commonly used in studies (Champney and Burdine 1996).

References

Araie H, Sakamoto K, Suzuki I, Shiraiwa Y (2011) Characterization of the selenite uptake mechanism in the coccolithophore *Emiliania huxleyi* (Haptophyta). Plant Cell Physiol 52:1204–1210

Champney WS, Burdine R (1996) 50S ribosomal subunit synthesis and translation are equivalent targets for erythromycin inhibition in *Staphylococcus aureus*. Antimicrob Agents Chemother 40:1301–1303

Chen XW, Gao K (2004a) Photosynthetic utilisation of inorganic carbon and its regulation in the marine diatom *Skeletonema costatum*. Funct Plant Biol 31:1027–1033

Chen XW, Gao KS (2004b) Roles of carbonic anhydrase in photosynthesis of *Skeletonema costatum*. J Plant Physiol Mol Biol 30:511–516

Ernster L, Dallner G, Azzone GF (1963) Differential effects of rotenone and amytal on mitochondrial electron and energy transfer. J Biol Chem 238:1124–1131

Herfort L, Thake B, Taubner I (2008) Bicarbonate stimulation of calcification and photosynthesis in two hermatypic corals. J Phycol 44:91–98

Msilini N, Zaghdoudi M, Govindachary S, Lachaâl M, Ouerghi Z, Carpentier R (2011) Inhibition of photosynthetic oxygen evolution and electron transfer from the quinone acceptor QA^- to QB by iron deficiency. Photosynth Res 107:247–256

Nimer NA, Brownlee C, Merrett MJ (1999) Extracellular carbonic anhydrase facilitates carbon dioxide availability for photosynthesis in the marine dinoflagellate *Prorocentrum micans*. Plant Physiol 120:105–112

Reinfelder JR, Milligan AJ, Morel FM (2004) The role of the C4 pathway in carbon accumulation and fixation in a marine diatom. Plant Physiol 135:2106–2111

SchÄFer C, Simper H, Hofmann B (1992) Glucose feeding results in coordinated changes of chlorophyll content, ribulose-1,5-bisphosphate carboxylase-oxygenase activity and photosynthetic potential in photoautrophic suspension cultured cells of *Chenopodium rubrum*. Plant Cell Environ 15:343–350

Shea R, Chopin T (2007) Effects of germanium dioxide, an inhibitor of diatom growth, on the microscopic laboratory cultivation stage of the kelp, *Laminaria saccharina*. J Appl Phycol 19:27–32

Walther T, Novo M, Rossger K, Letisse F, Loret M-O, Portais J-C, Francois J-M (2010) Control of ATP homeostasis during the respiro-fermentative transition in yeast. Mol Syst Biol 6:344

Wu H, Cockshutt AM, McCarthy A, Campbell DA (2011) Distinctive photosystem II photoinactivation and protein dynamics in marine diatoms. Plant Physiol 156:2184

Chapter 30
Measurements of Particulate Organic Carbon, Nitrogen, and Phosphorus

Kai Xu, Kunshan Gao, Fei-xue Fu, and David A. Hutchins

Abstract Carbon, nitrogen, and phosphate are three macroelements of organisms. These elements are core components of organic matter and biological macromolecules. For this reason, interest in the measurement of particulate organic carbon (POC), nitrogen (PON), and phosphorus (POP) is becoming a hot research topic. In this section, the measurement methods for marine POC, PON, and POP, such as theory of operation, sampling and measuring procedures, and calculation, were introduced so that the data are of high quality and comparable.

Keywords Elemental ratio · Particulate organic carbon · Particulate organic nitrogen · Particulate organic phosphorus · Phytoplankton

30.1 Introduction

All life on earth is carbon based, so the concentration of carbon in organisms is higher than that of any other element. Alfred C. Redfield found that the molar C:N:P of marine plankton is relatively conservative at approximately 106:16:1 (Redfield 1958). This Redfield ratio is one of the most important concepts for understanding C, N, and P cycles in all kinds of marine ecosystems, and even the whole Earth system. About one-fourth of anthropogenic atmospheric emissions of CO_2 have been absorbed by the ocean (the biggest carbon pool on Earth), and about one-third has been released to the atmosphere (Doney et al. 2009; Feely et al. 2009; Prentice

K. Xu
Fisheries College, Jimei University, Xiamen, People's Republic of China

K. Gao (✉)
State Key Laboratory of Marine Environmental Science and College of Ocean and Earth Sciences, Xiamen University, Xiamen, China
e-mail: ksgao@xmu.edu.cn

F.-x. Fu · D. A. Hutchins
Marine and Environmental Biology, Department of Biological Sciences, University of Southern California, Los Angeles, CA, USA

K. Gao et al. (eds.), *Research Methods of Environmental Physiology in Aquatic Sciences*, https://doi.org/10.1007/978-981-15-5354-7_30

et al. 2001; Sabine et al. 2004). Thus, marine phytoplankton are likely to be influenced by increased CO_2 in the oceans in many ways. Moreover, although the total biomass of marine phytoplankton is only about 0.2% of terrestrial plants, but they have roughly equal contributions to global net primary production (Field et al. 1998). The sinking of phytoplankton exports a large amount of organic compounds to be remineralized in the deep sea, driving the marine C, N, and P cycles. In open oceans, phytoplankton are generally growth-limited by low concentrations of N and P, which reflects on their C:N:P ratio relative to dissolved ratios (Moore et al. 2013; Tyrrell 1999). Thus, the C:N:P ratio of seawater samples could be used to analyze the nutrient limitation of phytoplankton. Different algae have quite different nutrient requirements, which indicates that marine nutrient composition could be used to predict the dynamics of phytoplankton composition (Hutchins et al. 2009; Quigg et al. 2003).

30.2 POC and PON

Generally, the C and N contents of a solid sample can be measured by running a single test using a combustion method with an elemental analyzer. In the combustion tube of the elemental analyzer, the sample is combusted in pure oxygen, and the products of combustion are passed through specialized reagents to assure complete oxidation. In the reduction tube, oxides of nitrogen are converted to molecular nitrogen. Thus, total C and N contents of sample are finally converted to CO_2 and N_2, respectively. It must be recognized that some elemental analyzers are designed only to measure either C or N content of the sample, in which case duplicate samples are needed to ensure both POC and PON can be measured. An analysis day should start with the establishment of a standard curve. The most commonly used standard is acetanilide, which has a C:N ratio close to the Redfield ratio. A standard curve should contain at least five standards with different weights which cover the expected ranges of C and N contents in the samples. Some instruments are designed so they can only measure inorganic N, and thus inorganic chemicals cannot be used to establish a N standard curve for PON measurement. While the samples are running, insert a system blank after every five samples to check the stability of the instrument.

For phytoplankton samples without calcifying algae, collect the sample onto precombusted Whatman GF/F filters (500 °C, 3 h) under low pressure (~200 mbar) and rinse three times with fresh medium or 0.22-μm filtered seawater. Then fold the filter in precombusted aluminum foil (500 °C, 3 h), and store individually at −20 °C until analysis. Dry the filter at 60 °C for 12 h before analysis. Treat unused precombusted GF/F filters in the same way, and use as filter blank. For C and/or N analysis, fold the filter in tin foil and compress into a small pill, then place the pill into the combustion tube of an elemental analyzer. Record reads and calculate cellular POC and PON contents based on the standard curve and cell concentration. Use the following formula to calculate the POC and PON production rates:

$$\text{POC production rate} = \text{POC per cell} \times \mu \tag{30.1}$$

$$\text{PON production rate} = \text{PON per cell} \times \mu \tag{30.2}$$

where μ is the specific growth rate. For samples contain calcifying phytoplankton, to correctly determine POC, the inorganic carbon needs to be removed as CO_2 by exposing the filter to fumes of HCl (37%, w/w) for 12 h, and then the filter is rinsed, dried, and analyzed as described above.

30.3 POP

For POP analysis, high temperature combustion is used to completely oxidize the particulate matter, which converts all the organic phosphorus matter into orthophosphate. Then the dissolved orthophosphate is measured by colorimetric analysis. The inorganic phosphorus quantitatively reacts with a mixture of reagents to form a blue complex that can be determined with a spectrophotometer (Solorzano and Sharp 1980). The mixture of reagents consists of molybdic acid, ascorbic acid, H_2SO_4, and antimonyl-tartarate.

30.3.1 Reagents

Solution 1: 0.024 mol/L ammonium molybdate solution. Store in a dark glass bottle at room temperature. This reagent is stable.

Solution 2: 2.4 mol/L H_2SO_4 solution. This reagent is stable.

Solution 3: 0.31 mol/L ascorbic acid solution. This reagent must be made fresh daily.

Solution 4: 0.004 mol/L potassium antimonyl-tartarate solution. Store in a dark glass bottle. This reagent is stable.

Mixture of reagents: mix Solution 1, Solution 2, Solution 3 and Solution 4 at a volume proportion of 2:5:2:1.

30.3.2 Standard Curve

Phosphate standard: 5 mmol/L KH_2PO_4. This reagent is stable. A secondary standard of 50 μmol/L is made and stored at 4 °C. A daily standard curve is established using 1, 5, 10 and 15 μmol/L KH_2PO_4. Prepare 5 mL (10 mL if 10 cm cell is used on the spectrophotometer) aliquots of the standard (triplicate), Milli-Q water blank (triplicate), and samples (duplicate). Add 0.5 mL of mixed reagent to each tube.

Wait 1 h for color development. Read optical density in spectrophotometer at 885 nm. The formula of the standard curve is:

$$Y = aX + b \tag{30.3}$$

where X is the absorbance, Y is the concentration of standards, a is the slope, and b is the intercept. The ideal value of a is 50 for a 1 cm cuvette.

30.3.3 Procedure

GF/F filters used for sampling are combusted at 500 °C for 3 h to remove organic contamination. Similarly, organic contamination in glass scintillation vials is removed by capping with foil, combusting in a muffle furnace at 500 °C for 2 h, rinsing with 0.2 mol/L HCl after cooling and Milli-Q water and dried. Filter sample onto the precombusted GF/F filter (500 °C, 3 h) under low pressure (~200 mbar). Rinse filter twice with 2 mL 0.17 mol/L Na_2SO_4 and place in the clean glass scintillation vial. Add 2 mL of 0.017 mol/L $MgSO_4$ and evaporate to dryness in a 95 °C oven. Afterward, recover the vial with foil and combust at 500 °C for 2 h. Add 5 mL of 0.2 mol/L HCl after cooling, capped with the plastic cap and place in a water bath at 80 °C for 30 min. Add Milli-Q water to ensure sample volume is 5 mL if water was evaporated. Add 0.5 mL of mixed reagent to 5 mL sample after cooling, Wait 1 h for color development. Read optical density in spectrophotometer at 885 nm. For a blank determination, treat a GF/F filter like a sample. The calculation formula is:

$$\mathrm{POP/cell} = (a \times (A_s - A_b) + b) \times 10/\text{cell number} \tag{30.4}$$

where a is the slope and b is the intercept of standard curve (equation). A_s is the absorbance of sample and A_b is the absorbance of blank.

30.4 Notices and Suggestions

Due to experimental design, bottle effects, and stressful conditions, biomass budget is commonly tight for the measurements of particulate organic C, N, and P. However, the organic C, N, and P contents in a sample should to be much higher than the lower limit of analytical range of the measurement, and the measured change should to be higher than analytical precision. This can be assured by adjusting biomass per sample and length of time period between the initial and final samples. Phytoplankton accumulate organic components via photosynthesis during the light period, and consume the organic components via respiration during the dark period. Besides, cell division will strongly decrease the organic C, N, and P

contents per cell. Thus, data are comparable only when the samples are collected at the same time point under the same light/dark cycle. Otherwise, POC, PON and POP data need to be analyzed and interpreted together with other data such as growth rate, cell number, and cell size.

References

Doney SC, Fabry VJ, Feely RA, Kleypas JA (2009) Ocean acidification: the other CO_2 problem. Annu Rev Mar Sci 1:169–192

Feely RA, Doney SC, Cooley SR (2009) Ocean acidification: present conditions and future changes in a high-CO_2 world. Oceanography 22:36–47

Field CB, Behrenfeld MJ, Randerson JT, Falkowski P (1998) Primary production of the biosphere: integrating terrestrial and oceanic components. Science 281:237–240

Hutchins DA, Mulholland MR, Fu F-X (2009) Nutrient cycles and marine microbes in a CO_2-enriched ocean. Oceanography 22:128–145

Moore CM, Mills MM, Arrigo KR, Berman-Frank I, Bopp L, Boyd PW, Galbraith ED, Geider RJ, Guieu C, Jaccard SL, Jickells TD, La Roche J, Lenton TM, Mahowald NM, Marañón E, Marinov I, Moore JK, Nakatsuka T, Oschlies A, Saito MA, Thingstad TF, Tsuda A, Ulloa O (2013) Processes and patterns of oceanic nutrient limitation. Nat Geosci 6:701–710

Prentice IC, Farquhar GD, Fasham MJR, Goulden ML, Heimann M, Kheshi HS, Quere L (2001) The carbon cycle and atmospheric carbon dioxide. In: Climate change: the scientific basis—contribution of working group I to the third assessment report of the intergovernmental panel on climate change. Cambridge University Press, Cambridge, UK, pp 183–237

Quigg A, Finkel ZV, Irwin AJ, Rosenthal Y, Ho TY, Reinfelder JR, Oscar S, Morel FMM, Falkowski P (2003) The evolutionary inheritance of elemental stoichiometry in marine phytoplankton. Nature 425:291–294

Redfield AC (1958) The biological control of chemical factors in the environment. Am Sci 46:205–221

Sabine CL, Feely RA, Gruber N, Key RM, Lee K, Bullister JL, Wanninkhof R, Wong CS, Wallace DWR, Tilbrook B, Millero FJ, Peng T-H, Kozyr A, Ono T, Rios AF (2004) The oceanic sink for anthropogenic CO_2. Science 305:367–371

Solorzano L, Sharp JH (1980) Determination of total dissolved phosphorus and particulate phosphorus in natural waters1. Limnol Oceanogr 25:754–758

Tyrrell T (1999) The relative influences of nitrogen and phosphorus on oceanic primary production. Nature 400:525–531

Chapter 31
Isolation of Organelles

Min Xu and Hualing Mi

Abstract Algae organelles such as chloroplasts and thylakoid membranes are the basic materials for the study of physiological and biochemical reactions in photosynthesis. In this section, we briefly introduce the methods of separating the cytoplasmic membrane and thylakoid membrane from the prokaryotic cyanobacteria and the isolation of chloroplasts from the eukaryotic alga *Chlamydomonas reinhardtii*.

Keywords Cyanobacteria · Organelle · Chloroplast · Thylakoid · Cytoplasmic membrane

31.1 Introduction

The chloroplast is the organelle of energy conversion and the location of photosynthesis in cells of eukaryotic algae. Like mitochondria, the chloroplast contains circular DNA, and is a semiautonomous organelle. Isolation of chloroplasts, cytoplasmic membranes, and thylakoid membranes are common techniques for studying the physiological and biochemical reactions in photosynthesis. Such studies are helpful for the investigation of the localization and function of new proteins, and is also the basis for the study of chloroplast genetics.

M. Xu · H. Mi (✉)
National Key Laboratory of Plant Molecular Genetics, Institute of Plant Physiology and Ecology, Center for Excellence in Molecular Plant Sciences, Chinese Academy of Science, Shanghai, China
e-mail: mxu@sibs.ac.cn; mihl@cemps.ac.cn

K. Gao et al. (eds.), *Research Methods of Environmental Physiology in Aquatic Sciences*, https://doi.org/10.1007/978-981-15-5354-7_31

31.2 Isolation of Chloroplasts from *Chlamydomonas reinhardtii*

CW-15 cells at the middle and late logarithmic stage are centrifuged for 5 min at 3000 × *g* at 4 °C. The pellet (cells) is collected and washed with pre-cooled buffer A [0.45 mol/L sorbitol, 10 mmol/L HEPES-NaOH, 5 mmol/L sodium phosphate (pH 7.5), 10 mmol/L $MgCl_2$, 10 mmol/L NaCl, 5 mmol/L EDTA]. After recentrifugation under the same conditions, the cells are suspended in buffer A containing 20% glycerol. The cell suspension is then placed in a pre-cooled Yeda Press chamber for cell breakage. After raising the pressure to 140 kg/m^2, the valve is slowly loosened to allow the compressed sample to flow out, drop by drop, into a container in an ice bath. The broken cells are carefully placed on the top of a concentration gradient of Percol (40% and 60%). The intact chloroplasts are collected in the layer between 40–60% Percol after 10 min of centrifugation at 4000 × *g*. A horizontal rotor is recommended.

31.3 Isolation of the Raw Thylakoid Membranes

The raw thylakoid membranes are prepared using the method described by Mi et al. (2001). Cells of the cyanobacterium *Synechocystis* PCC 6803 at the middle to late logarithmic phase are collected by centrifugation at 5000 × *g* for 10 min. The pellet (cells) is washed twice with buffer B [25% (v/v) glycerol, 10 mM $MgCl_2$, 10 mM NaCl, and 20 mM sodium phosphate buffer (pH 7.5)] and resuspended in buffer B at a concentration of 1.5 mg Chl/ml. After incubation on ice for 1 h, the suspension is passed through a French pressure cell at 147,000 kPa, and the resultant suspension is centrifuged at 5000 × *g* for 10 min to remove unbroken cells. The supernatant is centrifuged at 140,000 × *g* for 1 h, and the pelleted thylakoids are re-suspended in medium B and stored at −80 °C. All the processes are carried out at 4 °C.

31.4 Isolation of Thylakoid Membranes and Cytoplasmic Membranes

Ten liters of *Synechocystis* cells are used for the isolation. The cells are cultured at 2% CO_2 until middle to late logarithmic phase (OD_{730nm} = 0.6–0.8), shifted to air for 1 day and finally harvested by centrifugation at 5000 × *g* for 5 min, re-suspended in 30 ml of buffer C (20 mmol/L KH_2PO4/K_2HPO4, pH 7.5), broken by shaking with glass beads (150–212 mm) and then centrifuged at 2000 × *g* for 10 min. The membrane fraction containing both thylakoid membranes (TM) and cytoplasmic membranes (CM) is obtained by centrifugation of the supernatant at 150,000 × *g* for 40 min. Highly purified preparations of CM and TM can be produced from low CO_2

Table 31.1 Formulation of two-phased partitioning method

	Polymer Systems	
Stock solutions	5.8% 10 g-system	5.8% 40 g-system
Dextran T-500 (18.87%)	3.0737 g	12.295 g
PEG 3350 (40%)	1.45 g	5.80 g
Sucrose (1 M)	1.5630 g	10.0 g
H_2O	0.1633	11.905 g
Sample (membrane)	3.75 g	–

grown cells of *Synechocystis* 6803 with the two-phased partitioning method described by Norling et al. (1998) with modifications (Xu et al. 2008).

Preparation of six 40 g-separation systems and one 10 g-separation system is carried out according to Table 31.1. The final concentrations of water-soluble polymer dextran (Dextran T-500) and polyethylene glycol (PEG-3350) are 5.8%. All steps must be completed at temperatures below 2 °C. Firstly, the 40 g-system without samples is centrifuged for 10 min at 5000 × *g*. After stratification, all the upper layers are transferred to the new tubes, labeled T1, T2, T3, T4, T5, and T6, respectively. The lower layers are labeled B1, B2, B3, B4, B5, and B6, respectively, and placed on ice before use.

When preparing the 10 g-separation system according to Table 31.1, add 3.75 g pre-stored membrane protein sample, mix 30–40 times and centrifuge at 5000 × *g* for 10 min at 4 °C. The separated two phases are labeled as upper T0 (orange-brown, with cytoplasmic membranes) and lower B0 (dark green, with thylakoid membranes); T0 was transferred into the prepared tube. In B1, after mixing and carrying out the centrifugal stratification with the same method, the upper layer is named T1′, and the lower layer is discarded. By repeating the previous steps, the components T2′, T3′, T4′, T5′, T6′ are obtained. At this time, the lower layer should gradually become colorless, and T6′ is the purified component containing cytoplasmic membrane (orange). If the green colour can still be extracted from the lower layer at this time, a 40 g-system is prepared according to the need, and the extraction will be colorless according to the above process. In addition, the lower B0 is transferred to the prepared T1. After centrifugation, the upper layer is discarded and the lower layer is named B1′. Repeat this step to obtain components B2′, B3′, B4′, B5′, and B6′, respectively. At this time, the discarded upper layer should gradually fade into colorless, and B6′ is the purified thylakoid membrane component (green). If the upper layer can still extract orange at this time, further extraction and separation are needed. The separation process is shown in Fig. 31.1.

The final samples T6′ and B6′ are centrifuged at 35,000 *g* for 10 min at 4 °C. The pellets are cytoplasmic membrane (CM) and thylakoid membrane (TM), respectively. After adding a small amount of potassium phosphate buffer, the samples can be stored in the dark at −80 °C.

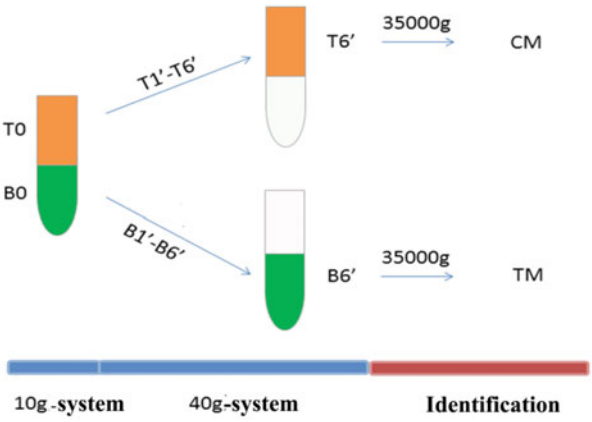

Fig. 31.1 Basic Process Diagram of Separation by two-phased partitioning method

31.5 The Advantage and Demerits of the Method and Misunderstandings

The two-phase partitioning method can effectively separate the cytoplasmic membrane and thylakoid membrane, but the following points should be paid attention to: Firstly, all the mixed extraction processes are needed to be kept below 2 °C. Secondly, a small amount of cytoplasmic membrane or thylakoid membrane remains in the two phase (Dextran and PEG-3350), so it is necessary to identify the residual components in the samples with the corresponding labeled protein antibodies to help determine the location of the target protein.

References

Mi H, Deng Y, Tanaka Y, Hibino T, Takabe T (2001) Photo-induction of an NADPH dehydrogenase which functions as a mediator of electron transport to the intersystem chain in the cyanobacterium *Synechocystis* PCC 6803. Photosynth Res 70:167–173

Norling B, Zak E, Andersson B, Pakrasi H (1998) 2D-isolation of pure plasma and thylakoid membranes from the cyanobacterium *Synechocystis* sp. PCC 6803. FEBS Lett 436:189–192

Xu M, Ogawa T, Pakrasi HB, Mi H (2008) Identification and localization of the CupB protein involved in constitutive CO_2 uptake in the cyanobacterium, *Synechocystis* sp. strain PCC 6803. Plant Cell Physiol 49(6):994–997

Chapter 32
Measurements of Calcification and Silicification

Kai Xu, Kunshan Gao, and David A. Hutchins

Abstract Calcification and silicification are two major kinds of biomineralization on the Earth. Coccolithophore and diatom are major calcifier and silicifier in the oceans, respectively. Thus, these marine phytoplankton play important roles in global cycle of carbon, silicon, and calcium. In this section, the standard measurement methods for calcification and silicification, such as measuring principles, sampling and measuring procedures, and calculation, were introduced using coccolithophore and diatom as examples, respectively.

Keywords Calcification · Coccolithophore · Diatom · Phytoplankton · Silicification

32.1 Introduction

Biomineralization, such as calcification and silicification, is closely related to the evolution history, which offers protection to alive organisms by forming skeletons or shells, and involves organisms into global elemental cycle by depositing dead organisms as sediment (Knoll 2003; Leadbeater and Riding 1986). Calcifying autotrophs distributed in all kinds of water all over the world. The most common calcifying algae include marine macroalgae and single-celled coccolithophores (Raven and Giordano 2009). Diatoms are the most common silicifying algae in all kinds of water in the world, and most diatom species absorb environmental Si to build cell wall (Raven and Waite 2004). Diatoms and coccolithophores contributed

K. Xu
Fisheries College, Jimei University, Xiamen, China

K. Gao (✉)
State Key Laboratory of Marine Environmental Science and College of Ocean and Earth Sciences, Xiamen University, Xiamen, China
e-mail: ksgao@xmu.edu.cn

D. A. Hutchins
Marine and Environmental Biology, Department of Biological Sciences, University of Southern California, Los Angeles, CA, USA

K. Gao et al. (eds.), *Research Methods of Environmental Physiology in Aquatic Sciences*, https://doi.org/10.1007/978-981-15-5354-7_32

about 50% and 1–10% of the marine primary production, respectively (Field et al. 1998; Poulton et al. 2007). In the oceans, coccolithophres contribute more than half of the marine calcifying production, but calcifying macroalgae are the major contributors in the coastal waters (Milliman 1993; Mazarrasa et al. 2015). The transportation of dissolved silicon from surface seawater to deep sea is mainly through deposition of diatoms (Conley 2002).

In addition, biomineralization resulted in high sinking rates of marine phytoplankton. Thus, organic carbon sinking fluxes in the oceans correlate tightly with mineral fluxes (Armstrong et al. 2002; Klaas and Archer 2002). The global changes due to human activities may strongly influence calcification and silicification which in turn will change competition ability of biomineralized organisms and shift ecological structures, then impact the global elemental cycles.

32.2 Measurement of Calcification

Coccolithophores are tiny single-celled phytoplankton which produce calcite ((Ca, Mg)CO_3), termed coccoliths, that cover their cell surface. Thus, the calcification can be measured either as the increase in (Ca, Mg)CO_3, or removal of dissolved [Ca^{2+}, Mg^{2+}] and/or total alkalinity.

32.2.1 Increase in Mass of (Ca, Mg)CO_3

32.2.1.1 Particulate Inorganic Carbon (PIC)

Two subsamples for total carbon (TC) and particulate organic carbon (POC) are collected onto precombusted Whatman GF/F filters (500 °C, 3 h) under low pressure (~200 mbar) and rinsed three times with fresh medium or 0.22-μm filtered seawater. The filters are folded in precombusted aluminum foil (500 °C, 3 h) and stored individually at −20 °C until analysis. The filters are then dried at 60 °C for 12 h before analysis. In order to remove inorganic carbon as CO_2, the filters used for the determination of POC are exposed to fumes of HCl (37%, w/w) for 12 h, rinsed three times and dried. Unused precombusted GF/F filters can be treated in the same way and used as filter blanks. Filters are to be folded with tin foil and compressed into small pills and analyzed by combusting method using an elemental analyzer. The difference in the carbon values of non-acidified filters (contain TC) and acidified filters (only POC) is the PIC content. The PIC content per cell and production rates of PIC can be calculated as following formulae:

$$\text{PIC per cell} = \frac{\text{TC} - \text{POC}}{\text{Cell number}} \tag{32.1}$$

$$\text{PIC production rate} = \text{PIC per cell} \times \mu \tag{32.2}$$

where μ is the specific growth rate. As for calcifying macroalgae, ground the macroalgal tissue into powder and then expose to HCl fumes to remove PIC; and the PIC content can be derived from mass changes between the organic mass and the total. In general, acetanilide is used as the calibration standard and at least five standards are run for every analysis day and a system blank after every five samples.

32.2.1.2 Contents of Ca and Mg

Many kinds of machines can be used to analyze contents of Ca and Mg, such as Atomic Absorption Apectrometer, Inductively Coupled Plasma Spectrometer, High-Pressure Liquid Chromatography (Gao et al. 1993; Müller et al. 2008; Katagiri et al. 2010). Phytoplankton samples are collected on polycarbonate filter (0.8 μm) which have been presoaked in 0.05 mol/L HCl for 24 h, then rinsed with milli-Q water and placed into milli-Q water until sample collection. Macroalgae powder could be directly used for Ca and Mg measurement after dissolution. Another method to evaluate calcification is by measuring the removal of dissolved [Ca^{2+}] and [Mg^{2+}].

In general, calcite has been classified as high-Mg and low-Mg calcite which represents a mol percentage of Mg/(Ca + Mg) over and below 4%, respectively (Stanley 2008). The amount of Mg in calcite increases with ambient Mg/Ca ratio, which means that low-Mg calcite should be the major form in modern seawater (Mg/Ca = 5.2). However, when grown in seawater mimicing the Mg/Ca ratio of modern ocean, the Mg in calcite of some coccolithophores species showed pretty high values (large than 18%) (Stanley 2008). Thus, whether measure the content of Mg in calcite depending on the research purpose. For high-Mg calcite with a high percentage of Mg substituting for Ca (e.g., 18%), Ca contents could not be used for evaluation of calcification.

32.2.1.3 Notices and Suggestions

The energy consumed by calcification is originated from photosynthesis. Generally, the PIC contents increase with expose time of light during the light phase (Zondervan et al. 2002). Thus, PIC data are comparable when the samples are collected at the same time point under the same light conditions, or comprehensively analyze PIC data with growth rate, cell size, cell number, etc. Samples from laboratory cultures or natural seawater with high concentration of coccolithphores usually have better data repeatability. For natural seawater samples with low abundance of coccolithphores, data can be even negative values due to using two big

values (TC and POC) to calculate a much small value (PIC). Similarly, other reasons which decrease the calcification could also affect the data quality, such as, low light, nutrient limitation, low-calcifying strain or even noncalcifying strain.

32.2.2 Isotope Methods

Isotopic tracer method is a quick and high sensitive method which can be used to measure calcification rate, especially suitable for field samples with low abundance of coccolithophores. Following is a brief protocol using ^{14}C tracer to measure calcification rate: add a small amount of ^{14}C labeled $NaH^{14}CO_3$ to two subsamples, and incubate the samples for a short time (e.g., hours) at the original culture conditions or specific conditions according to research purpose. Afterward, filter the samples onto Whatman GF/F filters under low pressure (~200 mbar), rinse three times with fresh medium or 0.22-μm filtered seawater and put in scintillation vials. To remove inorganic ^{14}C, one filter is fumed with HCl (37%, w/w) for 12 h, then rinsed three times and dried. Before count each filter for ^{14}C activity, the filters need to be digested with scintillation cocktail. The calcification rate is estimated from the difference between two filters, pigment concentration/cell concentration and incubation time as following.

$$\text{Calcification rate} = \frac{\text{CPM}_\text{T} - \text{CPM}_\text{P}}{C_\text{e}} \times I_\text{f} \times \frac{\text{DIC}}{\text{CPM}_\text{W} \times \text{Chl}\ a \times \text{time}} \tag{32.3}$$

where CPM_T and CPM_P are ^{14}C activities of total (photosynthetic fixation and calcification) and photosynthetic fixation (fumed filter), respectively. C_e is the counting efficiency, I_f is the isotope discrimination factor, DIC is total dissolved inorganic carbon in the culture, Chl *a* is the concentration of chlorophyll *a*, *time* represents the incubation time. The $NaH^{14}CO_3$ working liquid is a seawater diluent of technical liquid. CPM_W is the ^{14}C activities in the $NaH^{14}CO_3$ working liquid added to each sample. Due to the big difference in ^{14}C between working liquid and atmosphere, ^{14}C would outgas with time which could significantly lower the ^{14}C activity of working liquid (Gattuso et al. 2010). Thus, the CPM_W should be measured rather than estimated from the ^{14}C activity of technical liquid and dilution factor. For safety reason and measurement reliability, the incubation system should be sealed to stop gas exchange with outside and incubation time should be not too long to decrease the outgas of ^{14}C during the incubation. For the same purposes, the working liquid should be sub-packed with several small vials and sealed with parafilm. The calcification rate could also be normalized to cell concentration by replacing the Chl a with cell concentration in Eq. (32.3).

In theory, calcification rate could also been measured using ^{45}Ca uptake method. However, ^{45}Ca tracer was less frequently used relative to ^{14}C due to two reasons: unincorporated ^{45}Ca is difficult to be rinsed from samples, $MgCO_3$ is also a part of products of calcification (Fabry and Balch 2010).

32.2.2.1 Notices and Suggestions

In laboratory conditions, incubating *Emiliania huxleyi* (with PIC/POC ≈ 1) cultures for 2 h at a cell concentration of ~5 × 10^4/mL is enough to get a good data repeatability. Besides, as same as PIC, data repeatability is not good when volume-normalized calcification rate is low, and the cultures should be incubated at the same time period. The biomass for ^{14}C incubation and incubation time should be increased to enhance data repeatability when the calcification rate is low. Paasche and Brubak (1994) suggested an improved method which directly measures the fixed ^{14}C by calcification. Briefly, samples collect on GF/F filter, then place the filter at bottom of a scintillation vial, add a small volume of 1% phosphoric acid to the bottom which drives the ^{14}C–PIC into the head space as ^{14}C–CO_2. A small GF/F filter is positioned on the inside of the vial cap which containing a CO_2-absorbant. Then, transfer the latter filter to a new scintillation vial and counted for ^{14}C activity which then is used to calculate calcification rate. The advantage of this method is that the value of calcification rate is always a positive one.

32.2.3 Decrease of Total Alkalinity

Deposit 1 mol $CaCO_3$ result in decrease of 2 mol total alkalinity (A_T). Meanwhile, other metabolic processes (e.g., photosynthesis, respiration, absorption, and utilization of N, etc.) only have negligible effects on A_T (Zeebe and Wolf-Gladrow 2001). Thus, calcification rate can be evaluated from the decrease of A_T (Gao et al. 2012; Gao and Zheng 2010; Gattuso et al. 1999). In general, seawater A_T can be measured using potentiometric titration (Dickson et al. 2003; Zeebe and Wolf-Gladrow 2001). Following is a brief protocol: collect A_T sample by filtering the cultures or natural seawater through 0.6 μm polycarbonate filter; add $HgCl_2$ at a final concentration of 0.05–0.10%; then store the sample in borosilicate bottles at 4 °C. Titrant is a solution of ~0.1 mol/kg HCl in 0.6 mol/kg NaCl (Dickson et al. 2003). Before titration, the HCl concentration need to be calibrated using standard seawater (certified by Scripps Institution of Oceanography, USA) or high purity Na_2CO_3.

As same as measurement of PIC and ^{14}C, to obtain an accurate measurement of the calcification, the measured change in A_T needs to be at least 6 μmol/kg (London et al. 2010). This can be assured by adjusting biomass per volume of seawater and length of time period between the initial and final A_T samples. Although it is desirable to have a large change in A_T during the incubation, it must be recognized that other seawater carbonate parameters (i.e., pH, DIC, HCO_3^-) may change significantly at the same time except using the approach to measure calcification of calcifying macroalgae in flow-through seawater (see Chap. 21).

32.3 Measurement of Silicification

Diatoms absorb and convert seawater $Si(OH)_4$ into $SiO_2 \cdot nH_2O$ which is the major component of cell wall of diatoms. Similar to calcification, two methods can be used to measure silicification: the change in mass of $SiO_2 \cdot nH_2O$ and isotope method. The mass of $SiO_2 \cdot nH_2O$ can be measured by spectrophotometry which is much easier than the latter in terms of the complexity of operation (Brzezinski and Nelson 1995; Thamatrakoln and Hildebrand 2008). Following is the protocol of measurement of biogenic silica (BSi) by spectrophotometry:

32.3.1 Reagents for Standards and Processing

Solution 1: 0.006 mol/L ammonium molybdate in 0.29 mol/L HCl, this solution needs to be stored in a dark bottle and prepared monthly.

Solution 2: 0.01 mol/L Na_2SO_3 and 0.058 mol/L p-methylaminophenol sulfate (dissolve Na_2SO_3 first and then add p-methylaminophenol sulfate), this solution needs to be stored in a dark bottle and prepared monthly.

Solution 3: 0.79 mol/L oxalic acid, this solution is stable when stored in a dark bottle.

Solution 4: 9 mol/L H_2SO_4, this reagent is stable.

Reducing reagent: mix Milli-Q water, *Solution 2*, *Solution 3* and *Solution 4* at a volume proportion of 4:5:3:3.

32.3.2 Processing Procedure

Collect samples onto 0.8 μm (can be changed according to the size of diatoms) polycarbonate filters, rinse twice with fresh medium or filtered seawater, fold the filters and place each filter in a clean and labeled plastic tube. Open the tubes and put in drying oven (50 °C) overnight. Close the tubes and store until ready to run test. Prepare two unused filters as blanks.

Prepare a series of 5 mL aliquots of silicon standard solutions (0–35 μmmol/L) in duplicate (silicon standard is available from Fisher or Sigma-Aldrich). Add 2 mL *Solution 1* to each standard solution, mix immediately and let stand for 10 min. Add 3 mL *Reducing reagent*, mix immediately and let the color (blue) develop for 2–3 h. Using the recorded absorbance at 810 nm of each solutions to establish a standard curve.

As for samples, add 4 mL of 0.25 mol/L NaOH to the tube to submerse the filter, place the tube in a boiling bath for 30–40 min. SiO_2 could be dissolved in the hot strong base solution and produce Na_2SiO_3: $SiO_2 + 2NaOH = Na_2SiO_3 + H_2O$. Add 1 mL of 1 mol/L HCl, mix the solution to neutralize excessive NaOH. Dilute 1 mL of the supernatant with 4 mL milli-Q water into a clean and labeled plastic vial (transfer

vial). Add 2 mL of *Solution 1* to the transfer vial. After 10 min, add 3 mL *Reducing reagent*, mix and stand for 2–3 h. Calculate the BSi contents on the basis of the standard curve and the recorded absorbance at 810 nm of each sample. According to the analysis purpose, BSi can be normalized to per cell, per cell per time, or per volume per time. BSi production rate can be calculated as

$$\text{BSi production rate} = \text{BSi per cell} \times \mu \tag{32.4}$$

where μ is the specific growth rate.

32.3.3 Notices and Suggestions

Similar to calcification, the energy consumed by silicification is originated from photosynthesis. Thus, BSi data are comparable when the samples are collected at the same time point under the same light conditions, therefore one can comprehensively analyze BSi data with growth rate, cell size, cell number, etc. Samples with high concentration of diatom cells usually have better data repeatability. For natural seawater samples, any reasons that may inhibit the silicification rate, can affect the data quality, such as, low abundance of diatoms, low light, nutrient limitation, low-silicifying strain or even nonsilicifying strain.

References

Armstrong RA, Lee C, Hedges JI, Honjo S, Wakeham SG (2002) A new, mechanistic model for organic carbon fluxes in the ocean based on the quantitative association of POC with ballast minerals. Deep-Sea Res II Top Stud Oceanogr 49(1):219–236

Brzezinski MA, Nelson DM (1995) The annual silica cycle in the Sargasso Sea near Bermuda. Deep-Sea Res I Oceanogr Res Pap 42:1215–1237

Conley DJ (2002) Terrestrial ecosystems and the global biogeochemical silica cycle. Global Biogeochem Cycles 16(4):1121

Dickson A, Afghan J, Anderson G (2003) Reference materials for oceanic CO_2 analysis: a method for the certification of total alkalinity. Mar Chem 80:185–197

Fabry VJ, Balch WM (2010) Direct measurements of calcification rates in planktonic organisms. In: Guide to best practices in ocean acidification research and data reporting. Publications Office of the European Union, Luxembourg, pp 41–52

Field CB, Behrenfeld MJ, Randerson JT, Falkowski P (1998) Primary production of the biosphere: integrating terrestrial and oceanic components. Science 281(5374):237–240

Gao K, Aruga Y, Asada K, Ishihara T, Akano T, Kiyohara M (1993) Calcification in the articulated coralline alga Corallina pilulifera, with special reference to the effect of elevated CO2 concentration. Mar Biol 117(1):129–132

Gao K, Zheng Y (2010) Combined effects of ocean acidification and solar UV radiation on photosynthesis, growth, pigmentation and calcification of the coralline alga *Corallina sessilis* (Rhodophyta). Glob Chang Biol 16:2388–2398

Gao K, Xu J, Zheng Y, Ke C (2012) Measurement of benthic photosynthesis and calcification in flowing-through seawater with stable carbonate chemistry. Limnol Oceanogr Methods 10:555–559

Gattuso J-P, Frankignoulle M, Smith SV (1999) Measurement of community metabolism and significance in the coral reef CO_2 source-sink debate. Proc Natl Acad Sci U S A 96:13017–13022

Gattuso JP, Gao K, Lee K, Rost B, Schulz KG (2010) Approaches and tools to manipulate the carbonate chemistry. In: Riebesell U, Fabry VJ, Hansson L, Gattuso JP (eds) Guide to best practices in ocean acidification research and data reporting. Publications Office of the European Union, Luxembourg, pp 41–52

Katagiri F, Takatsuka Y, Fujiwara S, Tsuzuki M (2010) Effects of Ca and Mg on growth and calcification of the coccolithophorid pleurochrysis haptonemofera: Ca requirement for cell division in coccolith-bearing cells and for normal coccolith formation with acidic polysaccharides. Mar Biotechnol 12(1):42–51

Klaas C, Archer DE (2002) Association of sinking organic matter with various types of mineral ballast in the deep sea: implications for the rain ratio. Global Biogeochem Cycles 16(4):63-61–63-14

Knoll AH (2003) Biomineralization and evolutionary history. Rev Mineral Geochem 54 (1):329–356

Leadbeater B, Riding R (eds) (1986) Biomineralization in lower plants and animals. Clarendon Press, Oxford

London C, Gattuso JP, Andersson A (2010) Measurements of calcification and dissolution of benthic organisms and communities. In: Riebesell U, Fabry VJ, Hansson L, Gattuso JP (eds) Guide to best practices in ocean acidification research and data reporting. Publications Office of the European Union, Luxembourg, pp 41–52

Mazarrasa I, Marbà N, Lovelock CE, Serrano O, Lavery PS, Fourqurean JW, Kennedy H, Mateo MA, Krause-Jensen D, Steven ADL, Duarte CM (2015) Seagrass meadows as a globally significant carbonate reservoir. Biogeosciences 12(16):4993–5003

Milliman JD (1993) Production and accumulation of calcium carbonate in the ocean: budget of a nonsteady state. Global Biogeochem Cycles 7(4):927–957

Müller MN, Antia AN, La Roche J (2008) Influence of cell cycle phase on calcification in the coccolithophore Emiliania huxleyi. Limnol Oceanogr 53:506–512

Paasche E, Brubak S (1994) Enhanced calcification in the coccolithophorid Emiliania huxleyi (Haptophyceae) under phosphorus limitation. Phycologia 33:324–330

Poulton AJ, Adey TR, Balch WM, Holligan PM (2007) Relating coccolithophore calcification rates to phytoplankton community dynamics: regional differences and implications for carbon export. Deep-Sea Res II 54(5):538–557

Raven JA, Giordano M (2009) Biomineralization by photosynthetic organisms: evidence of coevolution of the organisms and their environment? Geobiology 7(2):140–154

Raven JA, Waite AM (2004) The evolution of silicification in diatoms: inescapable sinking and sinking as escape? New Phytol 162(1):45–61

Stanley SM (2008) Effects of global seawater chemistry on biomineralization: past, present, and future. Chem Rev 108:4483–4498

Thamatrakoln K, Hildebrand M (2008) Silicon uptake in diatoms revisited: a model for saturable and nonsaturable uptake kinetics and the role of silicon transporters. Plant Physiol 146:1397–1407

Zeebe RE, Wolf-Gladrow DA (2001) CO_2 in seawater: equilibrium, kinetics, isotopes. Elsevier, Amsterdam

Zondervan I, Rost B, Riebesell U (2002) Effect of CO_2 concentration on the PIC/POC ratio in the coccolithophore *Emiliania huxleyi* grown under light-limiting conditions and different daylengths. J Exp Mar Biol Ecol 272:55–70

Chapter 33
Use of the Fluorochrome Calcein to Measure Growth and Calcification in Marine Organisms

Sam Dupont

Abstract Accurate observations of calcified structures and measurements of growth and calcification rates are key to evaluate fitness of marine calcifiers. These are critical as many marine calcifiers are now challenged by global changes such as ocean acidification. There are a wide range of available techniques to measure calcification, but many are costly, require specialized and advanced equipment and training, and can be invasive or lethal. Here we present calcein staining as a cheap, easy, nontoxic, and noninvasive alternative. This technique can be used to observe newly formed calcified structures, quantify growth, calcification, and dissolution rates as well as understanding underlying mechanisms. Calcein staining can be used both in the laboratory and in the field, and observations can be made on live or fixed specimens. The use of this versatile technique is illustrated by case studies evaluating the impact of ocean acidification on a range of calcifiers from phytoplankton to animals.

Keywords Calcein · Skeletogenesis · Calcification · Dissolution · Growth

33.1 Introduction

Growth and calcification rates are key parameters to evaluate the fitness of marine calcifiers. Individual growth rate can be calculated using multiple measurements over time of the same individual or increased size over a given period of time. These methods often require mark-and-recapture using different labeling techniques. Many of these techniques (e.g., tagging, painting, edge notching) are invasive and require handling of the individuals with potential consequences on their fitness. For calcification, a wide range of techniques are available to observe skeletogenesis, skeletal properties, measure calcification rates, and investigating underlying mechanisms (reviewed by Fitzer et al. 2019). The selection of a technique depends on the

S. Dupont (✉)
Department for Biological and Environmental Sciences, University of Gothenburg, The Kristineberg Centre for Marine Infrastructure, Fiskebäckskil, Sweden
e-mail: Sam.dupont@bioenv.gu.se

K. Gao et al. (eds.), *Research Methods of Environmental Physiology in Aquatic Sciences*, https://doi.org/10.1007/978-981-15-5354-7_33

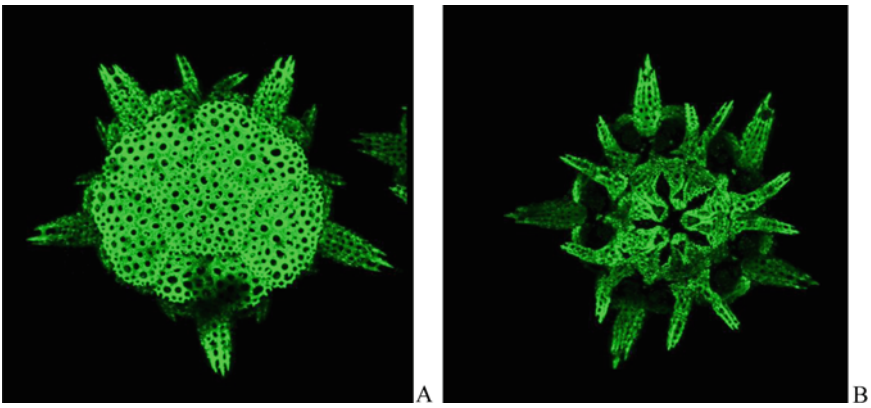

Fig. 33.1 Example of calcein-labeled skeletal structure. Aboral (**a**) and oral (**b**) sides of a freshly settled juvenile of the brittlestar *Amphiura filiformis* exposed for 3 days to calcein (25 µg/mL). Pictures from fixed juveniles (in buffered 4% paraformaldehyde solution in filtered seawater) examined under a confocal microscope, analyzed by collecting stacks of images and projecting them in the *Y*-axis

scientific question but also practical aspects. Many of these methods require well-equipped and sometimes specialized laboratory and can be costly. An easy, low-cost, nontoxic, and noninvasive alternative is the use of fluorochrome such as calcein.

Calcein is a fluorescent organic dye synthesized through the modification of fluorescein with ethylenediaminetetraacetic acid analog. It forms a bond with Ca^{2+} and emits a green fluorescence (~520 nm) when the calcein complex is excited by blue light (~488 nm; Magnabosco et al. 2018). When incorporated into newly formed mineralized calcium carbonate, it leads to a bright green fluorescent mark on freshly calcified skeletal structures that is visible under fluorescent light (Fig. 33.1).

Calcein has been extensively used to study the growth and calcification in many taxa (see Fox et al. (2018) for review) but can also be used to track the location of calcifying structure or resolve morphology. Creative use of calcein can also allow to quantify dissolution (e.g., Ventura et al. 2016) or design complex physiological or ecological experiments.

33.2 Methodology

33.2.1 Stock Solution (Yajima and Kiyomoto 2006)

Calcein powder can be ordered from major chemical companies (e.g., C0875 SIGMA). A stock solution at 2.5 mg/mL can be prepared by dissolving calcein in filtered seawater. Dissolution can be facilitated by using a magnetic stirrer and slowly increasing the pH with NaOH solution. The final pH of the stock solution

must be adjusted to the pH of the seawater used for the experiment. The solution is kept at 4 °C in the dark. This stock solution can be maintained for several week. However, some authors documented better results with freshly made solutions (Fox et al. 2018).

33.2.2 Concentration and Exposure

A wide range of concentration of calcein (1.25–2000 μg/mL) and exposure time (20 min to 4 months) has been documented in the literature (Fox et al. 2018 for review). The literature can be a valuable source of information to identify the right combination of concentration and exposure time for the species and life history stage. If no information is available, it is recommended to perform a pilot experiment.

33.2.3 Storage

Observation can be performed on living or fixed animals. Samples can be stored in 4% paraformaldehyde (PFA) in filtered seawater and in the dark. PFA 4% can be prepared by dissolving PFA powder in seawater, spin using a magnetic stirrer, and slowly warm the solution till the solution is clear (up to max 50 °C). It is important to buffer the solution (e.g., pH 8.3) to avoid dissolution of the fixed calcified structures and lose the calcein signal. The calcein signal is stable, and the samples can be stored for several months (van der Geest et al. 2011; Fox et al. 2018).

33.2.4 Observation and Pictures

Calcein signal can be observed under an epi-fluorescence or confocal microscope. Green calcein (Sigma, C0875) emits fluorescence at 509 nm (green) after excitement at 470 nm (blue). Green calcein is the most used, but other calcein can also be used. For example, blue calcein (Sigma, M1255) emits fluorescence at 455 nm (blue) after stimulation at 322 nm (UV). It is also possible to combine several types of calcein within the same experiment to mark at different times (e.g., Ventura et al. 2016).

33.3 Example of Calcein Uses in the Context of Ocean Acidification

Anthropogenic CO_2 emissions are acidifying the world's oceans, leading to perturbation of the carbonate system inclusing a decrease in pH, a phenomenon known as ocean acidification. The associated reduction in saturation states (Ω) has implication on the dissolution of exposed calcium carbonate ($CaCO_3$) structures. When Ω is lower than 1, seawater is corrosive and leads to the dissolution of $CaCO_3$. Many marine organisms are calcifiers, use calcium carbonate structures for their shells or skeleton, and are considered at risk when facing ocean acidification. Numerous studies have demonstrated the negative impact of ocean acidification on skeletal development and growth (Wittmann and Pörtner 2013). However, some calcifiers are able to thrive and calcify in corrosive waters (Thomsen et al. 2010), but underlying mechanisms are still poorly understood. Here are a few examples of different uses of calcein to study growth and calcification in the context of ocean acidification.

33.3.1 Skeletogenesis

Larvae and juveniles of the seastar *Crossaster papposus* cultured in two pH_{nbs} (high 8.1 vs. low 7.7) were exposed to a 1–7 days exposure to calcein (50 µg/mL). Species were examined under a confocal microscope, analyzed by collecting stacks of images and projecting them in the *Y*-axis. Combined with the measures of the growth rate, it was shown that larvae and juveniles grew faster when cultured at low pH with no visible effects on survival or skeletogenesis. Calcein staining allowed to identify the first signs of calcification (day 7) in the superficial layer of the dermis and the formation of the first spines at day 38 (Fig. 3 in Dupont et al. 2010).

33.3.2 Measurement of Growth

Juveniles of the infaunal bivalve *Macoma balthica* were maintained in aerated calcein solution (250 µg/mL) for 24 h prior to a 29-day exposure to two pH_{nbs} treatments (high 7.9 vs. low 7.3) and two oxygen levels (high 8.3 vs. low 3.0 mg/L). Fixed individuals were examined using a confocal microscope. A clear fluorescent band was visible and allowed to calculate the relative growth as (see Fig. 2 in Jansson et al. 2015):

$$\text{Relative growth } (\%) = \frac{\text{Shell initial size}}{\text{Length of newly growth part of the shell}} * 100$$

Positive growth was observed in all treatments with a 2.4 times higher growth observed in the low pH and low oxygen treatment as compared to the high pH and high oxygen.

33.3.3 Qualitative Observation of Calcification/Dissolution

The formation and maintenance of a skeleton is a dynamic process between biologically controlled precipitation of calcium carbonate and dissolution (e.g., when exposed to unfavorable conditions). Gross calcification is the overall formation of calcium carbonate structures through physiological mechanisms while net calcification is the net effect of gross calcification and dissolution (Cyronak et al. 2016).

Calcein was used to qualitatively observe the relative contribution of calcification and dissolution in the formation and maintenance of the skeleton of the crustose coralline alga *Phymatolithon lenormandii* at early life stages exposed to pH_T ranging from 8.00 to 7.55. Evaluation of net calcification as well as dissolution was performed in a two-step procedure: (1) After 3 weeks, live thalli were exposed to calcein (25 μg/mL) for 24 h, rinsed, and examined under a confocal microscope to collect a stack of images that were projected in the *Y*-axis. This allowed to observe the net calcification over 24 h. (2) Slides were then transferred into calcein-free seawater for 24 h, and new stacks of pictures were taken for the same individuals. Comparing the calcein signal before and after this 24 h exposure allowed to visualize dissolution in the different pH treatments (Fig. 7 in Bradassi et al. 2013). After the 24 h calcein exposure, individuals raised in pH 8.0 showed clear signs of calcification on the margin of the thalli. On the other hand, when exposed to lower pH, the whole thalli were labeled with calcein. When the labeled thalli were transferred to calcein-free seawater, the signal was stable at pH 8.0 (no obvious sign of dissolution) while most of the signal disappeared at lower pH (strong dissolution). It could be concluded that maintenance of the skeleton at low pH is possible through a dynamic dissolution and re-calcification process.

33.3.4 Quantitative Measurement of Calcification/Dissolution

Tambutté et al. (2012) evaluated the potential of calcein labeling as a quantitative method to measure calcification rate. After calcein labeling (12.4 μg/mL for 20 min), tissues were removed chemically, the skeleton dissolved in HCl, and the solution neutralized with NaOH. Calcein concentration was measured in the solution using a confocal microscope. They showed that the rate of calcein incorporation was lower

but linearly correlated to calcification rate measured using the total alkalinity anomality technique, demonstrating that this method may be a useful tool to estimate coral calcification.

Net calcification and dissolution rates using calcein labeling were measured on mussel larvae (Ventura et al. 2016). Using two different types of calcein (calcein and blue calcein, 25 µg/mL), two different endpoints were measured on mussel larvae acutely exposed to different pH_T (high 8.1 vs. low 7.0). Larvae were exposed to calcein for 48 h at the two tested pH. They were then transferred to seawater at the same pH or the other pH (full crossed design) containing blue calcein for an extra 48 h.

Relative net calcification was calculated after 48 h and 96 h as:

$$\text{Relative calcification } (\%) = \frac{\text{Length of the newly formed calcein band}\ (\text{Green after 48 h, Blue after 96 h})}{\text{Maximum shell length}} * 100$$

After 96 h, *relative net dissolution* was calculated as:

$$\text{Relative dissolution } (\%) = \frac{\text{LGB1} - \text{LGB2}}{\text{LGB1}} * 100$$

where LGB1 is the length of the newly formed green band after 48 h and LGB2 is the length of the remaining green band after 96 h. This demonstrated the existence of a compensatory calcification mechanisms in mussel larvae as increased dissolution observed under low pH is compensated by increased calcification (Figs. 4 and 5 in Ventura et al. 2016).

Another strategy to maintain skeleton in corrosive seawaters is to invest energy into mechanisms that prevent dissolution by maintaining favorable conditions around the skeleton. Using a similar assay combining two forms of calcein, we could show that sea urchin pluteus larvae exposed to low pH seawater for 3 days ($pH_T = 7.4$) were able to prevent skeleton dissolution and maintain positive but reduced calcification compared to larvae raised in high pH seawater ($pH_T = 8.0$). Three-day-old gastrula larvae of the green sea urchin (*Strongylocentrotus droebachiensis*) were exposed to green calcein (25 µg/mL) at high pH_T (8.0) for a duration of 3 days. Over that period of time, they started calcifying and developed into a pluteus larvae. At that stage, the whole skeleton was labeled in green. Larvae were rinsed three times with calcein-free filtered seawater and transferred to seawater with blue calcein (25 µg/mL) for 3 more days at either high (8.0) or low pH_T (7.4). Larvae were fixed in buffered 4% paraformaldehyde solution in filtered seawater, examined under a confocal microscope, and analyzed by collecting stacks of images and projecting them in the *Y*-axis. As illustrated in Fig. 33.2, there was no overlap between the green calcein signal (calcification over the first 3 days) and the blue calcein signal (calcification over the following 3 days). New calcification occurs only at the edge of the skeleton (red signal), and the comparison between the green

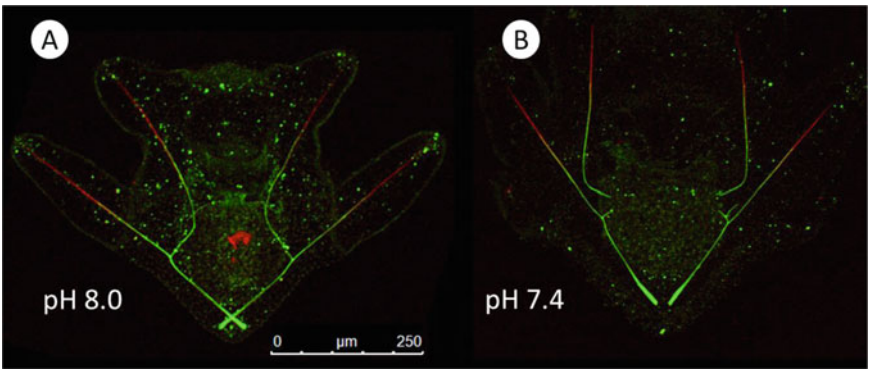

Fig. 33.2 Fluorescence of pluteus larvae exposed to both calcein (green) and blue calcein (red) under two different pH_T (**a**. 8.0 vs. **b**. 7.4)

signal after 3 and 6 days showed that no dissolution or compensatory calcification could be observed at the two tested pH (personal observation).

33.3.5 Cellular Imaging (e.g., Fox et al. 2018) and Mechanistic Understanding

Calcein microscopy can be used to visualize calcification compartment and track the calcification process. An exposure to calcein (125 µg/mL) allowed for the detection of heterogeneous patterns of calcification, growth, and cell division in a population of coccolithophores (Fig. 3 in Fox et al. 2018). The authors also showed the usefulness of calcein labeling for flow cytometry.

Tambutté et al. (2012) used calcein (up to 160 µg/mL for 20 min) to determine the permeability properties of coral cells and tissues to molecule and how it is incorporated into the skeleton. They showed that calcein passes through coral tissues by a paracellular pathway and highlighted the importance of intercellular junctions controlling and restricting the diffusion of molecules.

33.4 Limitations

A vast majority of studies demonstrate that calcein is a suitable marker as it is noninvasive, nondestructive, and nontoxic. For example, calcein in concentration ranging from 1 to 8 µg/mL produced a clear and long-lasting (3 months) fluorescent mark in the burrowing bivalve *Loripes lacteus* exposed to calcein in situ for up to 2.6 h. The calcein exposure had no measurable effects on survival, shell growth rate, or body condition index (van der Geest et al. 2011). Laboratory-based studies did not

detect effects of calcein labeling on growth or survival. For example, five species of coccolithophore exposed for 8 days to calcein 125 μg/mL were not impacted for photosynthetic physiology, external calcite morphology, or growth rate (Fox et al. 2018). One study suggests that calcein has an impact on the form of calcium carbonate that is formed in vitro. When present in concentrations used in experimental studies (2.5–250 μg/mL), calcein modifies the shape and morphology of the aragonite and calcite polymorphs, and in the presence of Mg^{2+}, aragonite formation is inhibited in favor of magnesium calcite (Magnabosco et al. 2018). However, authors admit that no such change in deposition was observed in vivo and that organisms may have mechanisms to overcome the interference caused by calcein.

References

Bradassi F, Cumani F, Bressan G, Dupont S (2013) Early reproductive stages in the crustose coralline alga *Phymatolithon lenormandii* are strongly affected by mild ocean acidification. Mar Biol 160:2261–2269

Cyronak T, Schulz KG, Jokiel PL (2016) The omega myth: what really drives lower calcification rates in an acidifying ocean. ICES J Mar Sci 73:558–562

Dupont S, Lundve B, Thorndyke M (2010) Near future ocean acidification increases growth rate of the lecithotrophic larvae and juvenile of the seastar *Crossaster papposus*. J Exp Zool B 314B:382–389

Fitzer SC, Chan VBS, Meng Y, Rajan KC, Michio S, Not C, Toyofuku T, Falkenberg L, Byrne M, Harvey BP, de Wit P, Cusack M, Gao KS, Taylor P, Dupont S, Hall-Spencer J, Thiyagarajan V (2019) Established and emerging techniques for characterizing the formation, structure and performance of calcified structures under ocean acidification. Oceanogr Mar Biol Annu Rev 57:89–126

Fox E, Meyer E, Panasiak N, Taylor AR (2018) Calcein staining as a tool to investigate coccolithophore calcification. Front Mar Sci 5:326

Jansson A, Norkko J, Dupont S, Norkko A (2015) Growth and survival in a changing environment: combined effects of moderate hypoxia and low pH on juvenile bivalve *Macoma balthica*. J Sea Res 102:41–47

Magnabosco G, Polishchuk I, Erez J, Fermani S, Pokroy B, Falini G (2018) Insights on the interaction of calcein with calcium carbonate and its implications in biomineralization studies. CrystEngComm 20:4221

Tambutté E, Tambutté S, Segonds N, Zoccola D, Venn A, Erez J, Allemand D (2012) Calcein labelling and electrophysiology: insights on coral tissue permeability and calcification. Proc Biol Sci 279:19–27

Thomsen J, Gutowska MA, Saphörster J, Heinemann A, Trübenbach K, Fietzke J, Hiebenthl C, Eisenhauer A, Körtzinger A, Wahl M, Melzner F (2010) Calcifying invertebrates succeed in a naturally CO_2-rich coastal habitat but are threatened by high levels of future acidification. Biogeosciences 7:3879–3891

Van der Geest M, van Gils JA, van der Meer J, Olff H, Piersma T (2011) Suitability of calcein as an *in situ* marker in burrowing bivalves. J Exp Biol Ecol 399:1–7

Ventura A, Schulz A, Dupont S (2016) Maintained larval growth in mussel larvae exposed to acidified undersaturated seawater. Sci Rep 6:23728

Wittmann AC, Pörtner HO (2013) Sensitivities of extant animal taxa to ocean acidification. Nat Clim Chang 3:995–1001

Yajima M, Kiyomoto M (2006) Study of larval and adult skeletogenetic cells in developing sea urchins larvae. Biol Bull 211:183–192

Chapter 34
The Application of Transcriptomics, Metagenomics, and Metatranscriptomics in Algal Research

Xin Lin

Abstract This chapter introduces the basic principles of transcriptomics and its application in algal research. The latest studies demonstrate how to use transcriptomic techniques to investigate the molecular mechanisms of algae in response to environmental changes. The successful application of transcriptome techniques in algal research has shown its importance and its supportive role for algal physiological mechanism research. In addition, this chapter briefly introduces the metagenomic and metatranscriptomic techniques which have been widely used in marine ecology research.

In the post-genome era, various omics techniques such as transcriptomics, proteomics, and metabolomics provide powerful technical support for interpreting molecular mechanisms of biological processes. Among these omics techniques, transcriptomics is the first and most widely used technique. In addition, in recent years, the roles of metagenomics and metatranscriptomics in marine ecology research have become increasingly important. This section introduces some basic concepts and application examples of transcriptomics, metagenomics, and metatranscriptomics.

Keywords Algae genome · Transcriptomics · Metagenomics · Metatranscriptomics · Sequencing

34.1 The Basic Principles of Transcriptomics

Messenger RNA (mRNA) transmits biological information from DNA to proteins, which is the first step in gene expression and the key step in gene expression regulation. Therefore, mRNA is considered to be a "bridge" between them. All mRNAs are collectively referred to as the transcriptome (Wang et al. 2009).

X. Lin (✉)
State Key Laboratory of Marine Environmental Science, College of Ocean and Earth Sciences, Xiamen University, Xiamen, China
e-mail: xinlinulm@xmu.edu.cn

K. Gao et al. (eds.), *Research Methods of Environmental Physiology in Aquatic Sciences*, https://doi.org/10.1007/978-981-15-5354-7_34

RNA-Seq (transcriptome sequencing) uses high-throughput sequencing technology to sequence cDNA libraries (mRNA is not stable) that are reverse transcribed from all mRNA in tissues or cells, followed by statistical analysis. The transcriptomes are very different under different growth stages and growth conditions. Comparing the transcriptomes under different growth conditions and growth stages can reveal differentially expressed genes and explore the molecular mechanisms under different growth conditions and growth stages. Transcriptomes can provide expression profiles of a particular gene under specific conditions (Qi et al. 2011). Based on the transcriptomic information, the functions of certain genes could be deduced, which is helpful for revealing the mechanisms of action of specific genes under specific conditions (Mutz et al. 2013). The transcriptome study mainly includes the following steps: (1) All mRNAs of a certain organism or tissue are extracted at a specific time (Mutz et al. 2013). (2) A cDNA library is constructed and subjected to high-throughput sequencing. (3) Bioinformatics analysis is performed. After a series of bioinformatics analyses, mRNAs that are differentially expressed in different periods, different tissues, or different individuals can be identified, and a gene expression network can be obtained based on the gene annotations.

34.2 The Algae Genome

Whole-genome information can support in-depth transcriptomic analysis, although the transcriptome technique does not rely on it. As the cost of sequencing declines, many model algae species have been successfully sequenced, including the green algae *Chlamydomonas reinhardtii* (Merchant et al. 2007), the diatoms *Thalassiosira pseudonana* (Armbrust and Palumbi 2015) and *Phaeodactylum tricornutum* (Bowler et al. 2008), the model coccolithophore species *Emiliania huxleyi* (Von Dassow et al. 2009), and the cyanobacterium *Trichodesmium erythraeum* IMS 101 (Walworth et al. 2015). The completion of more and more algae genome sequences will further promote the application of transcriptomics techniques in algal research (Tirichine and Bowler 2011).

34.3 The Application of Transcriptomics Technique in Algal Research

Transcriptomics can be used for analyzing the underlying molecular mechanisms of algae with reference genomes or no reference genomes in response to environmental changes. Investigating the molecular mechanisms of carbon sequestration and nitrogen fixation is helpful for better understanding the role of algae in the carbon and nitrogen cycles. Therefore, many studies have focused on the molecular mechanisms of carbon fixation and nitrogen fixation in algae.

As a model diatom, the cost of transcriptome sequencing of *P. tricornutum* is relatively lower due to its small genome. Therefore, it is convenient to investigate the molecular mechanisms of *P. tricornutum* in response to different environmental changes using transcriptomic techniques. The *P. tricornutum* genome encodes the genes involved in C3 and C4 pathways, based on whole-genome information. Valenzuela et al. (2012) found that *P. tricornutum* uses different carbon utilization mechanisms at different DIC concentrations using transcriptomics techniques. When the dissolved inorganic carbon (DIC) concentration is high, the genes involved in the C3 pathway are active, whereas the genes involved in the C4 pathway with higher carbon utilization efficiency are activated when the DIC concentration is low.

Coccolithophores are the major calcareous phytoplankton group in the modern ocean. *E. huxleyi* is a model coccolithophore species which has been investigated in physiological and ecological aspects. Von Dassow et al. (2009) identified a series of genes potentially involved in calcification based on the transcriptome of haploid and diploid *E. huxleyi.* This laid a foundation for revealing the molecular mechanism of calcification and further exploring the molecular responses of *E. huxleyi* to environmental changes, such as ocean acidification. Benner et al. (2013) found that the genes probably associated with calcification in a previous study did not show pronounced responses under ocean acidification conditions for 700 generations using transcriptomics techniques.

The nitrogen-fixing cyanobacterium *T. erythraeum* has a very important influence on nitrogen and carbon cycling in tropical and subtropical oceans. An analysis of *T. erythraeum* showed that only 60% of the genome encodes proteins. In the transcriptome of *T. erythraeum,* besides a large number of known transposons, there are a large number of non-coding transcripts (Walworth et al. 2015). Under long-term ocean acidification, the genes encoding DNA methytransferases responsible for DNA methylation to control the activity of transposons were significantly upregulated (Hutchins et al. 2015). Therefore, the activity of transposons may be closely related to long-term acidification responses. This study using transcriptomic techniques showed that the genes responsive to ocean acidification are not limited to carbon sequestration and nitrogen fixation genes, which fully demonstrates that transcriptomics technique can help us to better understand the molecular mechanisms of algae in response to environmental changes.

As the cost of sequencing declines, more and more algal genomes have been fully sequenced. However, most algal genomes have still not been fully sequenced. Transcriptomics techniques can also be applied to algal research without reference genomes. *Skeletonema* is a widely distributed diatom species and a common non-toxic diatom bloom causing species. The carbon sequestration pathway of *Skeletonema marinoi* can be analyzed based on transcriptome information, even though its genome has not yet been fully sequenced. A total of 34 genes encoding 18 enzymes in the carbon metabolic pathway of *S. marinoi* were detected. The carbon metabolic pathway network of *S. marinoi* was constructed, and it was found that it contains all the enzymes for a CO_2 concentration mechanism like that in terrestrial C4 plants. Therefore, it was speculated that *S. marinoi* has a C4 like CO_2 concentration mechanism. This may explain why this species can still have high

primary productivity in a CO_2 concentration limited environment (Liu et al. 2016). Furthermore, by comparing the transcriptome data of *S. marinoi* at different grwoth phases, it was found that the gene encoding fructose diphosphate aldolase which determines the final distribution of carbon in the C3 pathway was significantly upregulated in the decline phase, while the gene encoding pyruvate phosphodikinase was also significantly upregulated during the stationary phase. These results help us to better understand algal carbon sequestration mechanisms and the biogeochemical cycle of carbon in the marine ecosystem (Liu et al. 2016).

34.4 Metagenomics and Metatranscriptomics

Metagenomics is the study of genetic material recovered directly from environmental samples, including the genetic composition and community function of all organisms in the natural samples. Metatranscriptomics studies the genome-wide transcription and transcriptional regulation of all organisms in a given environment or at a specific time, by extracting RNA from all organisms directly from environmental samples (Fig. 34.1). With the development of molecular biology techniques and the decline in sequencing costs, metagenomics and metatranscriptomics are becoming more widespread and applied in different fields. For marine ecology

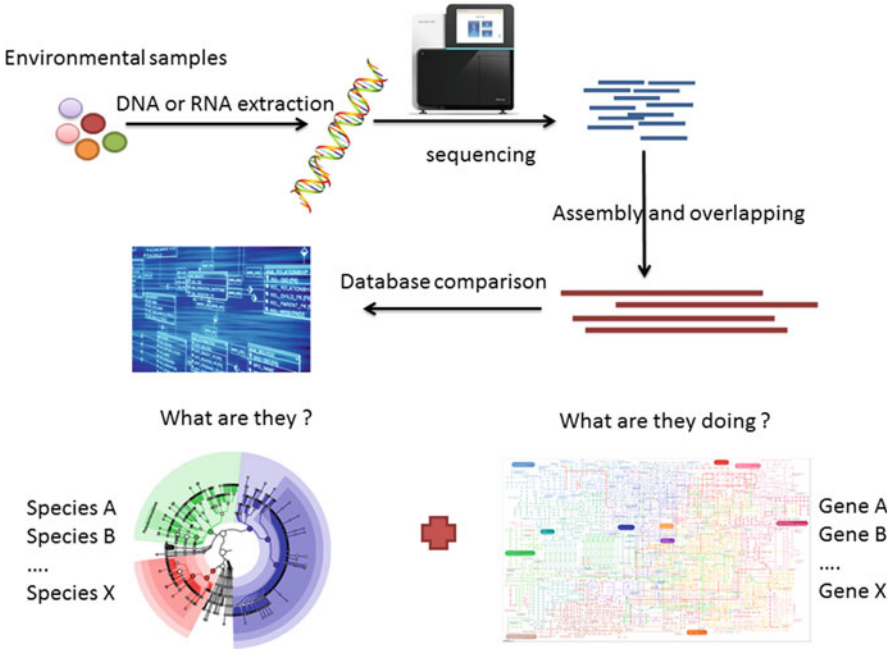

Fig. 34.1 Main experimental procedures for metagenomics and metatranscriptomes

research, metagenomics and metatranscriptomics techniques have incomparable advantages over traditional research methods, especially for some difficult-to-cultivate species. In general, a metagenome can provide information on species composition in the environment, and a metatranscriptome can provide information about active genes and metabolic pathways in the environment. As the primary producers in marine ecosystems, using metagenomics and metatranscriptomics techniques in phytoplankton studies has achieved fruitful research results.

The most prominent examples of metagenomics and metatranscriptomics technique applications are from 2009 to 2013, when scientists from all over the world sampled during a circum-global research cruise aboard the French scientific research vessel Tara. In all, they collected over 35,000 samples including marine viruses, phytoplankton, and zooplankton during the voyage. The samples were sequenced and analyzed by metagenomic and metatranscriptomic techniques, and millions of new genes were obtained. The marine microbial diversity in the global ocean was analyzed, and the relationships between them and how they are affected by the environmental factors were explored. These databases are huge, providing the scientific community with an unprecedented new resource that is changing the way scientists study oceans and environmental changes. Related research has been published in a special issue of *Science* magazine on May 22, 2015 (Sunagawa et al. 2015; Lima-Mendez et al. 2015; Armbrust and Palumbi 2015; Brum et al. 2015).

34.5 Advantages and Disadvantages of this Method

The transcriptomics technique has many advantages over the microarray chip technique:

1. There is no cross-reaction and background noise, compared to the traditional microarray chip technique.
2. The sequence of each transcript fragment can be directly determined with the accuracy of single-nucleotide resolution.
3. With high sensitivity, it can detect rare transcripts of as few as a few copies per cell.
4. Transcriptome analysis can be carried out on any species without having whole genome information.
5. Transcriptomics techniques can simultaneously detect rare transcripts (transcripts with low expression) and normal transcripts (transcripts with relatively higher expression). In contrast, the microarray chip technique is not sensitive to over-highly expressed and over-lowly expressed genes.

For transcriptomes with reference genomes, you can also map transcripts back to the genome and obtain information about transcript location, gene splicing, other genetic information. Furthermore, detection of the expression of different transcripts due to alternative splicing can help us discover new transcripts. In all, transcriptomics techniques can provide more accurate digital signals and a wider

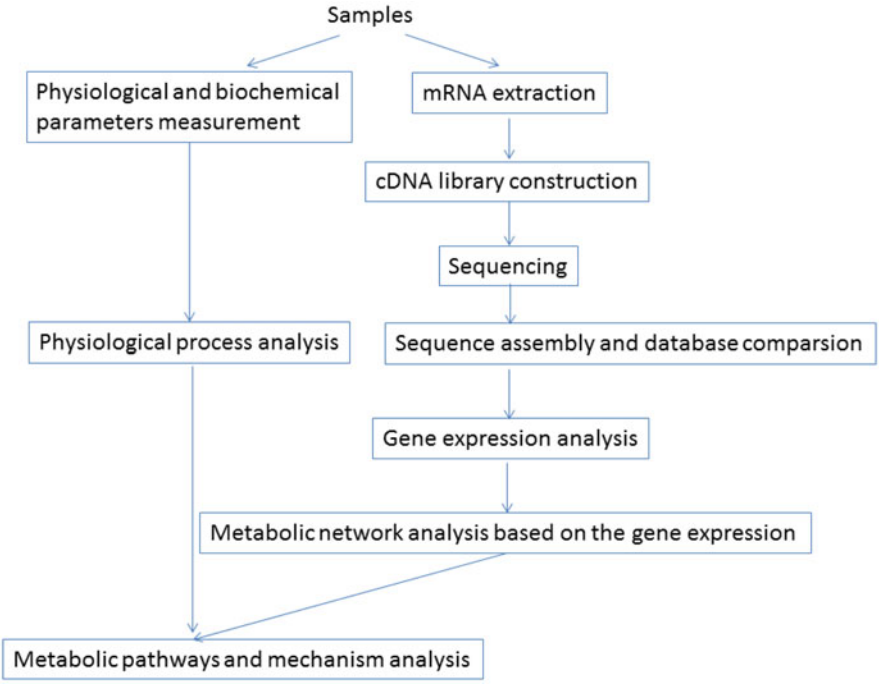

Fig. 34.2 The diagram of how transcriptomics technique supports physiological mechanism research

range of detection with higher information influx to support physiological mechanism studies (Fig. 34.2).

References

Armbrust EV, Palumbi SR (2015) Uncovering hidden worlds of ocean biodiversity. Science 348:865–867

Benner I et al (2013) Emiliania huxleyi increases calcification but not expression of calcification-related genes in long-term exposure to elevated temperature and p CO_2 Emiliania huxleyi increases calcification but not expression of calcification-related genes in long-term e. Philos Trans R Soc B Biol Sci 368:20130049

Bowler C et al (2008) The Phaeodactylum genome reveals the evolutionary history of diatom genomes. Nature 456:239–244

Brum JR et al (2015) Ocean viral communities. Science 348:1261498-1–1261498-11

Hutchins DA et al (2015) Irreversibly increased nitrogen fixation in Trichodesmium experimentally adapted to elevated carbon dioxide. Nat Commun 6:1–7

Lima-Mendez G et al (2015) Determinants of community structure in the global plankton interactome. Science 348:1262073–1262073

Liu Q, Mi TZ, Zhen Y et al (2016) Description of carbon fixation pathway based on *Skeletonema marinoi* transcriptome (in Chinese). Chin Sci Bull 61:2483–2493. (in Chinese)

Merchant SS et al (2007) The Chlamydomonas genome reveals the evolution of key animal and plant functions. Science 318:245–250

Mutz K-O, Heilkenbrinker A, Lönne M, Walter J-G, Stahl F (2013) Transcriptome analysis using next-generation sequencing. Curr Opin Biotechnol 24:22–30

Qi YX, Liu YB, Rong WH (2011) RNA-Seq and its applications: a new technology for transcriptomics. Hereditas 33(11):1191–1202. (in Chinese)

Sunagawa S et al (2015) Structure and function of the global ocean microbiome. Science 348:1–10

Tirichine L, Bowler C (2011) Decoding algal genomes: tracing back the history of photosynthetic life on Earth. Plant J 66:45–57

Valenzuela J et al (2012) Potential role of multiple carbon fixation pathways during lipid accumulation in *Phaeodactylum tricornutum*. Biotechnol Biofuels 5:40

Von Dassow P et al (2009) Transcriptome analysis of functional differentiation between haploid and diploid cells of Emiliania huxleyi, a globally significant photosynthetic calcifying cell. Genome Biol 10:R114

Walworth N et al (2015) Trichodesmium genome maintains abundant, widespread noncoding DNA in situ, despite oligotrophic lifestyle. Proc Natl Acad Sci U S A 112:201422332

Wang Z, Gerstein M, Snyder M (2009) RNA-Seq: a revolutionary tool for transcriptomics. Nat Rev Genet 10:57–63

Chapter 35
Methods for Nitrogen Fixation Measurement

Feixue Fu and Pingping Qu

Abstract This chapter introduces the acetylene reduction assay (ARA) and $^{15}N_2$ technique, two commonly used methods for the measurement of N_2-fixation rates of aquatic samples in the field and laboratory. As a simple, low-cost, and relatively sensitive technique, the AR assay determines the acetylene (C_2H_2) reduction or ethylene (C_2H_4) production rate in samples using gas chromatography and yields the N_2-fixation rate by converting the C_2H_4 production rate. A detailed protocol of the ARA is described in this chapter, including the principles, acetylene preparation, sample collection and incubation, and quantification and conversion of the C_2H_4 production rate.

The $^{15}N_2$ tracer assay directly measures the N_2-fixation rate of aquatic samples, which can be amended with the $^{15}N_2$ tracer by direct $^{15}N_2$ gas bubble injection or $^{15}N_2$-enriched seawater addition. The comparison and detailed procedures of the two tracer enrichment methods are introduced here. With the development of high-precision isotope ratio mass spectrometers, the $^{15}N_2$ assimilation technique is commonly used for the measurements of aquatic samples.

Keywords Nitrogen fixation · Acetylene reduction assay (ARA) · Gas chromatography · $^{15}N_2$ tracer technique · $^{15}N_2$ bubble-addition method · $^{15}N_2$ dissolution method · Mass spectrometry

F. Fu (✉)
Department of Biological Sciences, University of Southern California, Los Angeles, CA, USA
e-mail: ffu@usc.edu

P. Qu
Department of Biological Sciences, University of Southern California, Los Angeles, CA, USA

Department of Psychiatry and Behavioral Sciences, School of Medicine, University of Stanford, Stanford, CA, USA

K. Gao et al. (eds.), *Research Methods of Environmental Physiology in Aquatic Sciences*, https://doi.org/10.1007/978-981-15-5354-7_35

35.1 Acetylene Reduction Assay (ARA)

Acetylene reduction assay (ARA) is a commonly used method to detect biological N_2 fixation activities and determine the N-fixation rate of marine diazotrophs. This method was developed based on the discovery that nitrogenase, the enzyme for biological N_2-fixation processes, can also reduce acetylene (C_2H_2) to ethylene (C_2H_4). This reduction reaction can be very sensitively detected by gas chromatography (Capone 1993). In the application of the ARA, diazotrophic phytoplankton is tricked into breaking carbon bonds in acetylene with nitrogenase instead of breaking nitrogen bonds in dinitrogen (N_2). In this way, N_2 fixation rates can be indirectly determined by quantifying the ethylene production rate.

The AR assay does not relate directly to N_2 fixation, but instead measures the electron flux in the C_2H_2 reduction with nitrogenase. To directly determine the N_2-fixation rates, $^{15}N_2$ techniques should be used (described in Sect. 35.2). However, the AR assay is a classical way to determine N_2 fixation since this method is simple, low-cost, and relatively sensitive. The application of the AR method to aquatic samples has been proposed in detail in Capone (1993). This ARA protocol is adapted based on the methods and modifications described in Wilson et al. (2012) and Capone (1993).

35.1.1 Preparation of Acetylene Gas

C_2H_2 is commercially available as a compressed gas in the laboratory and can also be prepared freshly prior to use through the reaction of calcium carbide (CaC_2) with water in the fieldwork, which is described as follows. The gas preparation system is composed of a 250-mL side-arm glass flask as a reaction vessel, a sealed glass serum bottle half-filled with distilled water as a collection container, 1/8-in Tygon or polytetrafluoroethylene (PTFE) tubing, and a transfer pipette (Wilson et al. 2012). The tubing connects the side arm of flask and the pipette, which is inserted through the septum of the serum collection bottle. A gas pathway is thus built up from the reaction vessel to the gas collection container. In the field and laboratory work, the serum bottle can also be replaced with a medium size inner tire tube for a longer-time gas storage.

To produce ~0.1 mol of C_2H_2 gas, 6.4 g of CaC_2 is added to 150 mL of deionized water in the glass flask according to the following reaction formula:

$$CaC_2 + 2H_2O \rightarrow C_2H_2 + Ca(OH)_2$$

Once CaC_2 is added and the reaction begins, cover the flask opening immediately with a rubber stopper. Let the flask vent for several seconds to remove remnant air in the reaction vessel before connecting the reaction flask to the serum bottle and transferring the produced C_2H_2 gas into the collection bottle. It should be noted

that the reaction of CaC_2 with water does not yield pure C_2H_2 gas. Contaminants including C_2H_4 are present (Hyman and Arp 1987). To purify the generated C_2H_2, the produced gas is actively bubbling in DI water in the serum bottle, which is afterward shaken vigorously for 5 min. Purified C_2H_2 can be withdrawn with a syringe by inserting the needle through the septum of the serum bottle. The presence of residual contaminant C_2H_4 is calibrated by carefully measuring the concentration of C_2H_4 in the sample vial at time zero (T_0) and in the triplicated blank controls at selected time points through the entire incubation period, together with incubated samples.

When employing commercially prepared C_2H_2, the compressed gas tank, instead of the reaction flask, is connected to a sealed glass serum bottle containing DI water with a similar setting of tubing and a pipette as described above. After the C_2H_2 gas tank is switched on, let the C_2H_2 gas bubbles the DI water in the serum bottle for at least 30 s before the withdrawal of C_2H_2 gas. The calibration of contaminant C_2H_4 is carried out in the same way as described above. After the injection of C_2H_2 is completed, switch off the C_2H_2 gas tank.

35.1.2 Sample Collection and Incubation

Seawater samples or cultures are collected and transferred to acid-washed and combusted Wheaton serum vials/borosilicate glass vials/clear polycarbonate bottles, filling up approximately half to two thirds of the sample vial/bottle inner volume and leaving headspace. Wheaton serum vial/borosilicate vials are afterward air tightened with round bottom rubber stoppers and aluminum cap seals. The polycarbonate bottle can be sealed with white open-top screw caps and PTFE-faced silicone septa. An appropriate volume of C_2H_2 gas is injected to each sample vial through the rubber stopper or septum with a gas-tight syringe. Aliquots of the gas phase are analyzed for the C_2H_4 concentration at selected intervals during the sample incubation period or at the predetermined endpoint.

To better illustrate the procedure and help determine the volumes of samples and C_2H_2 gas, here we use a 25-mL serum vial as an example for the sample vial. After transferring 10 mL of seawater or culture sample to the serum vial, air-tighten the vial, extract 2 mL of air from the vial headspace, and inject 2 mL of acetylene into it with a syringe. Let acetylene equilibrate with the sample solution by gently shaking the vial.

Triplicated controls, or blanks, are prepared by adding the same volume of 0.2 μm-pore-size filtered seawater or medium used as the samples to the serum vials. Afterward, the control vials are air-tightened, replace 2 mL of air with 2 mL of C_2H_2 in the same way as sample vials. Controls are measured and analyzed along with samples (Fu et al. 2014).

As noted above, the zero-time measurement of C_2H_4 in the headspace of vials is important in order to correct the background C_2H_4 in the injected C_2H_2 in the headspace of vials. Experimental and control treatments are incubated under the

experimental conditions. In order to get a decent reading, the typical incubation period is 2 h, although it can be extended up to 6 h or overnight on a few occasions.

Multiple measurements can be taken from each sample like time-course sampling to determine the variation in the N_2 fixation rate over time. In order to avoid the side effect of C_2H_2 or sample dilution, a fresh sample should be taken from the experimental cultures, inoculated with 2 mL of C_2H_2 and analyzed again every 2-h incubation period.

35.1.3 Gas Chromatography Analysis of C_2H_4 Production

C_2H_4 production is analyzed by gas chromatography (GC) (e.g., Shimadzu gas chromatograph GC-8a, from Shimadzu Scientific Instruments) equipped with flame ionization detector (FID) or photoionization detector (PID) (Hutchins et al. 2015). For the purpose of C_2H_4 measurement, the GC column used is 2.1 mm ID × 1/8 in OD stainless column tubing, packed with Porapak polymer (R or N) and 100/120 mesh.

Turn on and warm up the GC device for 30–45 min before use. Make a serial dilution of standard 100 ppm ethylene (4.016 nmol/mL of C_2H_4; product base code: GMT10325TC, supplied by Matheson Gas Products) and inject ethylene gas of a standard range of concentrations to the GC device to establish a standard curve. A highly linear and repeatable standard gas curve indicates a good condition of the GC device for the following sample analysis.

After an incubation period, 200 μL of the gas from the headspace of each vial is sampled using a calibrated 250 μL gas-tight syringe and injected to the GC device. Importantly, the injection volume of the headspace of samples and controls can vary between measurement batches but should be consistent at all selected time points during the entire incubation period for each batch. Record the reading of the height or area of the C_2H_4 peak generated in the GC analysis. Inject the same volume (200 μL) of standard 100 ppm ethylene as samples to the GC device and use the reading to quantify the amount of C_2H_4 produced in samples. Detailed calculation instructions are described in the section below.

35.1.4 Determination of C_2H_4 Production Rate

The ethylene production rate is expressed as mole of C_2H_4 formed per hour per unit culture volume. First, the concentration of C_2H_4 in the equilibrated headspace of an assay vessel at any time point T, represented as $\{C_2H_4\}_T$, is calculated with the following formula:

$$\{C_2H_4\}_T = (\text{peak height or area of samples}/\text{peak height or area of standard } C_2H_4) * \text{standard } C_2H_4 \text{ concentration},$$

where peak height or area of samples and standard C_2H_4 gas are obtained from the GC analysis on the same volume (in our case, 200 μL) of headspace air from samples and 100 ppm C_2H_4 gas, and standard C_2H_4 concentration is 4.016 nmol/mL given that 100 ppm ethylene is used.

Second, the total amount of C_2H_4 accumulated in the assay vessel at any time point T, represented as C_T, is calculated as follows:

$$C_T = \{C_2H_4\}_T * \text{GPV} * \text{SC},$$

where GPV represents gas phase volume (mL), calculated by extracting the volume of the liquid solution from the total volume of the assay vessel. SC refers to the solubility correction for C_2H_4 in aqueous phase in the assay vessel since a fraction of the produced C_2H_4 is dissolved in the liquid solution. SC is calculated by determining the ratio of the total volume of produced C_2H_4 in the vessel to the volume of C_2H_4 in the gas phase with a converted formula as follows:

$$\text{SC} = 1 + (\alpha * p * \text{the aqueous volumein the vessel}/\text{the gas phase volume in the vessel}),$$

where α (mL of C_2H_4/mL of liquid/atm) represents the Bunsen solubility coefficient of C_2H_4 at the temperature and atmospheric pressure of measurement (Battino and Clever 1966; Breitbarth et al. 2004), and p is atmospheric pressure (atm) of dry air under the condition of measurement. Taking together, multiplying the concentration of C_2H_4 in the gas phase by GPV and SC generates a total amount (nmol) of C_2H_4 formed in the vessel during the incubation period.

Third, the C_2H_4 production rate of samples is quantified as nmol C_2H_4 per incubation time per unit volume of culture with the following formula:

$$C_2H_4 \text{ production rate} = [(C_{sf} - C_{bf}) - (C_{si} - C_{bi})]/(T_f - T_i)/\text{culture volume in the vessel},$$

where C_{sf} and C_{si} represent nmol C_2H_4 in the sample vessel at the end time T_f and initial time T_i of the incubation period, respectively, while C_{bf} and C_{bi} are the amount of background C_2H_4 in the blank or control treatment at T_f and T_i (Wilson et al. 2012). The culture volume refers to the liquid volume in the assay vessel.

35.1.5 Conversion to Nitrogen Fixation Rate

Nitrogen fixation rate is commonly expressed as mole of N fixed per hour per biomass and can be converted from the C_2H_4 production rate (C_2H_2 reduction) obtained in Sect. 35.1.4 by using the following formula:

$$\begin{aligned}\text{Nitrogen fixation rate} = &(C_2H_4 \text{ production rate}/3)\\ &* \ 2/\text{unit biomass of culture.}\end{aligned}$$

The interpretations of the coefficient and constant in the formula are as follows. A theoretical 3:1 ratio (mol C_2H_2 reduced to mol N_2 fixed) is used to convert the C_2H_4 production rate (C_2H_2 reduction) obtained in the section above to dinitrogen fixation rate (Montoya et al. 1996), due to the different requirements of hydrogen ions in two reactions. Namely, two hydrogen ions are required to reduce one C_2H_2 molecule and generate one C_2H_4 molecule while six hydrogen ions needed to reduce one N_2 molecule to two NH_3 molecules, which is shown in the following formulas:

$$C_2H_2 + 2H^+ \rightarrow C_2H_4$$
$$N_2 + 6H^+ \rightarrow 2NH_3$$

A ratio of 4:1 between C_2H_4 production and N_2 fixation has also been proposed since the reduction reaction of a N_2 molecule also incorporates the evolution of a H_2 molecule (Capone and Montoya 2001), as shown in the formula below:

$$N_2 + 8H^+ \rightarrow 2NH_3 + H_2$$

Generally, the theoretical reduction ratio (C_2H_2:N_2 = 3:1) has been validated by the $^{15}N_2$ fixation rate in multiple ecosystems and scenarios, although exceptions do exist (Postgate 1982; Montoya et al. 1996; Wilson et al. 2012). In our case here, the theoretical 3:1 ratio is applied to convert the C_2H_4 production rate to dinitrogen fixation rate. Since one dinitrogen is composed of two nitrogen atoms, multiplying one third of C_2H_4 production rate by a factor of 2 generates the gross fixation rate of nitrogen atom. The nitrogen fixation rate is normalized to biomass by dividing the gross nitrogen fixation rate by the unit biomass, which can be the cell number, particulate organic carbon/nitrogen, and dry weight per unit sample volume in the assay vessel.

35.2 $^{15}N_2$ Tracer Assay

The rate of N_2 fixation can be measured directly using ^{15}N tracer techniques (Montoya et al. 1996). However, the application of tracer techniques in the N_2 fixation measurement of aquatic samples has been largely limited over the last

several decades, due to the complexity of the involved mass spectrometric analysis and the difficulty in detecting the relatively low levels of ^{15}N enrichment resulting from short-term $^{15}N_2$-added incubations. With the development of high-precision isotope ratio mass spectrometers, now $^{15}N_2$ assimilation technique can be carried out on aquatic samples efficiently with minimal disruption to the incubation system.

Aquatic samples can be amended with the $^{15}N_2$ tracer by direct $^{15}N_2$ gas bubble injection (Montoya et al. 1996) or $^{15}N_2$-enriched seawater addition (Klawonn et al. 2015). Notably, significant differences have been discovered in the quantity of ^{15}N recovered in the particulate nitrogen formed between those two $^{15}N_2$ introducing methods. Underestimated $^{15}N_2$ assimilation rates were observed in research where $^{15}N_2$ was added as a gas bubble to open ocean seawater samples containing natural diazotrophic assemblages or cultures of the nitrogen fixer *Crocosphaera watsonii* (Mohr et al. 2010; Großkopf et al. 2012; Wilson et al. 2012; Klawonn et al. 2015; Böttjer et al. 2017). In another word, adding $^{15}N_2$ in dissolved form increases the recovery of ^{15}N in samples compared to the bubble addition. On the other side, the $^{15}N_2$ dissolution assay may cause changes in the concentration of trace elements in the incubation samples (Klawonn et al. 2015), which should be taken into consideration when applying it to the research on nutrient-limited diazotrophs. In this section, both the methods are introduced as follows.

35.2.1 $^{15}N_2$ Fixation Rate Measurement with the Modified $^{15}N_2$ Bubble-Addition Method

The modified *$^{15}N_2$ bubble-addition* approach is recommended in the application of the $^{15}N_2$ assimilation technique since it avoids the usage of pre-prepared $^{15}N_2$-enriched stock solutions and hence can lower the risk of trace element contaminations. When employing the modified bubble-addition method, $^{15}N_2$ gas is added to sterile-filtered water samples exceeding the standard N_2 solubility. $^{15}N_2$ fixation samples are incubated in sterile Pyrex or clear polycarbonate bottles, the volume of which is determined based on the experimental design and biomass density. Here we take the 250 mL bottle as an example. The incubation bottles are filled with sample solutions to overflowing and afterward carefully sealed with a septum cap (Teflon-lined butyl rubber). A 0.5 mL of $^{15}N_2$ (98.9 atom% ^{15}N, Cambridge Isotope Laboratories, Tewksbury, MA, USA) is injected into the sealed bottle using a gas-tight syringe (Bonnet et al. 2016). To balance the pressure across the septum, the same volume of solution (0.5 mL, in our case) is extracted from the incubation bottle with the syringe (Montoya et al. 1996). Notably, the suggested volume ratio of $^{15}N_2$ gas injected to the incubation bottle is 1:500 in Montoya et al. (1996) while a lower ratio, from 1:800 to 1:1500, has been applied in some shipboard incubation experiments (Mohr et al. 2010; Klawonn et al. 2015; Bonnet et al. 2016; Böttjer et al. 2017).

Sample bottles are vigorously shaken to fragment the gas bubble before the incubation and gently shaken three times a day during the incubation period, which can help ensure a small variability of ^{15}N-atom% among experiments (Bonnet et al. 2016). In order to determine the amount of initially dissolved $^{15}N_2$ gas after the agitation, triplicated control bottles should be prepared in the same way as samples but are sampled with the vacuum filtration immediately after the gas injection and agitation (Mohr et al. 2010).

The incubation time can last from hours to days based on the species composition and condition of samples. For instance, shipboard incubation time for natural *Trichodesmium* colonies is commonly 24–36 h and for unicellular diazotroph community is 2–4 days. At the end of the incubation period, the suspended particles in each bottle are collected by gentle vacuum filtration through a 25-mm pre-combusted (450–500 °C for 2–4 h) GF/F filter. The filters are frozen immediately and stored in a freezer prior to analysis (Bonnet et al. 2016).

35.2.2 *$^{15}N_2$ Fixation Measurement with the $^{15}N_2$ Dissolution Method*

35.2.2.1 Seawater Degassing by Pressure Reduction

As suggested in Klawonn et al. (2015), a 4-L vacuum filtration flask which can work at low pressures is filled with 2 L of 0.2 μM-filtered seawater with a clean magnetic stirring bar (40 × 8 mm) added. Afterward the flask is gas tightened by plugging a rubber stopper in the top opening and connecting the side arm to a vacuum pump (Diaphragm Pump, N 026.3AN.18, KNF Neuberger Inc., Freiburg, Germany) with gas-tight tubing (Tygon R, 8 mm o.d., 5 mm i.d.). In order to thoroughly agitate the seawater, the flask is placed on a magnetic stirring block (Heidolph MR Hei-Mix L), which is set to its maximum (1400 rpm) during the seawater degassing. The vacuum pump is set at 950 mbar below atmospheric pressure (atm. pressure) for 10 min to conduct the degasification process. The stirring system is stopped once the degassing is finished, and the vacuum pump is turned off immediately after the seawater is settled.

35.2.2.2 Preparation for the $^{15}N_2$-Enriched Seawater

The degassed seawater is siphoned from the filtration flask into borosilicate glass serum bottles via gas-tight tubing. To minimize the exposure of degassed seawater to air, make sure that the two tubing ends are placed at the bottom of the serum bottle and the filtration flask, respectively. The fully filled serum bottles are crimp-sealed with overpressure-tolerant thick rubber stoppers with no headspace. To avoid introducing air into the bottles, a syringe without plunger is inserted through the rubber stopper as an outlet when sealing the bottle.

To prepare $^{15}N_2$-enriched seawater, $^{15}N_2$ gas (98.9 atom% ^{15}N, Cambridge Isotope Laboratories) is injected into the degassed seawater in sealed serum bottles with a gas-tight syringe. Given the volume of a serum bottle is 160 mL, 2.5–7 mL of $^{15}N_2$ gas can be added to exceed the standard solubility of N_2 in water (Klawonn et al. 2015). In order to dissolve the gas into the seawater, the serum bottles need to be hand-shaken for 30 s and vortex-mixed vigorously for more than 5 min. After the thorough agitation, the vapor–liquid equilibrium in the serum bottles still leaves a fraction of injected $^{15}N_2$ in the gaseous phase. To further force the dissolution of $^{15}N_2$ gas into the solution, 0.5 mL of degassed sterile seawater can be carefully pressed into each serum bottle to compress the gas bubble.

With the maximal $^{15}N_2$ gas addition (7 mL) to a 160-mL serum bottle, the final $^{15}N_2$ concentration in the solution is 1200 μmol L^{-1} (Klawonn et al. 2015). In this case, replacing 2% of the incubation volume with the $^{15}N_2$-enriched seawater (1200 μmol L^{-1}) can yield a ^{15}N-atom excess of 5% in the samples (at 24 °C). For instance, for 1 L of incubation samples, 20 mL of $^{15}N_2$-enriched seawater is sufficient to be applied. Additionally, the salinity and temperature of incubation samples need to be considered to accurately determining the amount of $^{15}N_2$-enriched water used (Klawonn et al. 2015). After the incubation samples are amended with an appropriate amount of $^{15}N_2$-enriched seawater, the sample bottles are sealed with no headspace, well mixed, and incubated under the experimental condition.

35.2.2.3 Calculation of $^{15}N_2$ Enrichment

At time zero (T_0), triplicated controls need to be collected by filtering the same volume of samples without $^{15}N_2$ amended to the pre-combusted (450–500 °C, 2–4 h) GF/F filters with the vacuum filtration system. At the end of the incubation period, the seawater or culture samples amended with $^{15}N_2$ are collected in the same way. The GF/F filters containing samples are dried at 60 °C overnight and pelletized into tin capsules (Costech Analytical Technologies Inc., 5 × 9 mm). Pellets are analyzed on an elemental analyzer coupled to an isotopic ratio mass spectrometer to quantify the organic carbon and nitrogen (POC, PON) of samples and determine the amount of ^{15}N incorporated into biomass (Montoya et al. 1996; Bonnet et al. 2016).

Atmospheric N_2 gas is used as the reference standard ($^{15}N/^{14}N = 0.0036765$) in the mass spectrometry analysis (Junk and Svec 1958; Montoya et al. 1996). N_2 fixation rates are calculated with the following equation:

$$N_2 \text{ fixation rates} = \frac{\left(A^{PN}_{sample} - A^{PN}_{control}\right)}{\left(A_{N2} - A^{PN}_{control}\right)} \times \frac{PN}{\Delta T} \times \frac{1}{2},$$

where PN is the concentration of particulate N in samples, A_{N2} is the ^{15}N atom% in the total dissolved N_2 pool, which refers to the sum of naturally abundant and added ^{15}N, and A^{PN} refers to the ^{15}N atom% in the ^{15}N-PN content of incubated ^{15}N

amended samples (*A*PN sample) and unamended controls (*A*PN control). ΔT is the incubation time and a factor of 2 is included in the equation since one molecule of N_2 is composed of two N atoms (Montoya et al. 1996; Capone and Montoya 2001; Klawonn et al. 2015).

References

Battino R, Clever HL (1966) The solubility of gases in liquids. Chem Rev 66(4):395–463

Bonnet S, Berthelot H, Turk-Kubo K, Cornet-Barthaux V, Fawcett S, Berman-Frank I, Barani A, Grégori G, Dekaezemacker J, Benavides M, Capone DG (2016) Diazotroph derived nitrogen supports diatom growth in the South West Pacific: a quantitative study using nanoSIMS. Limnol Oceanogr 61(5):1549–1562

Böttjer D, Dore JE, Karl DM, Letelier RM, Mahaffey C, Wilson ST et al (2017) Temporal variability of nitrogen fixation and particulate nitrogen export at station ALOHA. Limnol Oceanogr 62(1):200–216

Breitbarth E, Mills MM, Friedrichs G, LaRoche J (2004) The Bunsen gas solubility coefficient of ethylene as a function of temperature and salinity and its importance for nitrogen fixation assays. Limnol Oceanogr Methods 2(8):282–288

Capone D (1993) Determination of nitrogenase activity in aquatic samples using the acetylene reduction procedure. In: Kemp PF, Sherr BF, Sherr EB, Cole JJ (eds) Handbook of methods in aquatic microbial ecology. Lewis Publishers, Boca Raton, FL, pp 621–631

Capone DG, Montoya JP (2001) Nitrogen fixation and denitrification. Methods Microbiol 30:501–515

Fu FX, Yu E, Garcia NS, Gale J, Luo Y, Webb EA, Hutchins DA (2014) Differing responses of marine N_2 fixers to warming and consequences for future diazotroph community structure. Aquat Microb Ecol 72(1):33–46

Großkopf T, Mohr W, Baustian T, Schunck H, Gill D, Kuypers MM, Lavik G, Schmitz RA, Wallace DWR, LaRoche J (2012) Doubling of marine dinitrogen-fixation rates based on direct measurements. Nature 488(7411):361

Hutchins DA, Walworth NG, Webb EA, Saito MA, Moran D, McIlvin MR, Gale J, Fu FX (2015) Irreversibly increased nitrogen fixation in *Trichodesmium* experimentally adapted to elevated carbon dioxide. Nat Commun 6:8155

Hyman MR, Arp DJ (1987) Quantification and removal of some contaminating gases from acetylene used to study gas-utilizing enzymes and microorganisms. Appl Environ Microbiol 53(2):298–303

Junk G, Svec HJ (1958) The absolute abundance of the nitrogen isotopes in the atmosphere and compressed gas from various sources. Geochim Cosmochim Acta 14(3):234–243

Klawonn I, Lavik G, Böning P, Marchant H, Dekaezemacker J, Mohr W, Ploug H (2015) Simple approach for the preparation of $^{15-15}N_2$-enriched water for nitrogen fixation assessments: evaluation, application and recommendations. Front Microbiol 6:769

Mohr W, Grosskopf T, Wallace DW, LaRoche J (2010) Methodological underestimation of oceanic nitrogen fixation rates. PLoS One 5(9):e12583

Montoya JP, Voss M, Kahler P, Capone DG (1996) A simple, high-precision, high-sensitivity tracer assay for N_2 fixation. Appl Environ Microbiol 62(3):986–993

Postgate JR (1982) The fundamentals of nitrogen fixation. Cambridge University Press, London

Wilson ST, Böttjer D, Church MJ, Karl DM (2012) Comparative assessment of nitrogen fixation methodologies, conducted in the oligotrophic North Pacific Ocean. Appl Environ Microbiol 78 (18):6516–6523

Chapter 36
Trace Metal Clean Culture Techniques

Yuanyuan Feng, Feixue Fu, and David A. Hutchins

Abstract Trace metals are involved in many metabolic pathways of marine phytoplankton, and are involved in regulating their growth and productivity, thereby influencing the community structure and function of the marine ecosystem. As such, trace metals play important roles in the marine biogeochemical cycles of carbon and nitrogen. However, due to the low solubility in seawater, the bio-availability of trace metals such as Zn, Co, and especially Fe may limit the growth of phytoplankton in many oceanic areas.

On the one hand, shipboard and laboratory culture environments are very likely to cause trace metal contamination. Therefore, trace metal clean culture techniques are necessary during studies of phytoplankton uptake of trace metals and trace metal limited culture experiments, and during the sampling and analysis procedures in these experiments. On the other hand, trace metal ion buffer reagents are usually required in seawater media in order to provide a sufficient but nontoxic supply of trace metals necessary for phytoplankton growth, and to precisely adjust the trace metal availability in the laboratory culturing experiments. This chapter is primarily intended to set forth trace metal clean culture techniques for the study of trace metal–phytoplankton interactions. In addition, the chapter also provides information on how to prepare seawater culture media used in laboratory and shipboard trace metal clean incubation experiments.

Keywords Algae · Marine phytoplankton · Culture technique · Trace metal clean · Seawater medium

Y. Feng (✉)
College of Marine and Environmental Sciences, Tianjin University of Science and Technology, Tianjin, China
e-mail: yyfengcocco@126.com

F. Fu · D. A. Hutchins
Marine and Environmental Biology, Department of Biological Sciences, University of Southern California, Los Angeles, CA, USA

K. Gao et al. (eds.), *Research Methods of Environmental Physiology in Aquatic Sciences*, https://doi.org/10.1007/978-981-15-5354-7_36

The growth of phytoplankton requires not only a sufficient supply of elements of macronutrients (C, N, P, and Si), but also a variety of micronutrient metals (such as Fe, Mn, Co, Cu, Mo, Zn, and Co). The solubility of some metal elements tends to be low, with only low concentrations of free ions present in seawater environment, and so they are classified as micro- or trace elements (concentrations lower than 50 and 0.05 μmol kg^{-1}, respectively). Among these trace metals, Fe is required by all photosynthetic organisms and has been most studied by oceanographers, as it plays important roles in phytoplankton biochemical electron transfer. Fe is involved in reactions of both photosynthesis and respiration, and the reduction of nitrate, nitrite and sulfate, as well as nitrogen fixation processes. In high-nutrient and low-chlorophyll (HNLC) regions, such as the Southern Ocean, subpolar and equatorial Pacific, and some Pacific eastern boundary upwelling regions, the bioavailability of iron is the limiting factor of phytoplankton growth and regulates primary productivity and ecosystem structure, thus influencing the global carbon cycle (Martin et al. 1993; Sunda and Huntsman 1995a; Coale et al. 1996; Hutchins and Bruland 1998; Boyd et al. 2000). The trace metal Mn is an essential element in the water-oxidizing complex of photosystem II (PSII), and so is required for the growth of all marine phytoplankton groups. It has been observed that the availability of Mn can limit phytoplankton growth, especially under low irradiance conditions (Sunda and Huntsman 1998). Zn is an important component in carbonic anhydrase synthesis, and so is essential in the processes of inorganic carbon transport and fixation, and is also involved in the production of alkaline phosphatase for organic phosphorus uptake (Morel et al. 1994). Co (and Cd) can be used as a substitute element for Zn in the alkaline phosphatase synthesis (Morel et al. 1994; Sunda and Huntsman 1995b), and are essential for the growth of some cyanobacteria and haptophytes (Sunda and Huntsman 1995b; Saito et al. 2002). Unlike Fe, these other trace metals such as Zn, Co, and Mn only limit marine phytoplankton growth in certain oceanic regions or under particular environmental conditions. Because the requirements of trace metals are species specific among different phytoplankton groups, the bioavailability of these trace metals may also play important roles in shaping natural phytoplankton community structure.

With the development of analytical chemistry and modern instrumental analysis techniques such as atomic absorption spectrometry, electrochemical technology, and inductively coupled plasma (ICP) mass spectrometry, chemical oceanographers are able to analyze seawater trace metal concentrations more precisely. In contrast to the low concentrations of trace metals in seawater, these metals are ubiquitous in the shipboard or laboratory environment from dust, rust, paint, etc., easily contaminating the seawater samples or the culture media used for incubation. Therefore, in order to precisely determine or control the concentrations of trace metals in seawater samples or culture experiments, it is important to adopt trace metal clean sampling and culture techniques in the studies of trace metal–phytoplankton interactions. These techniques include but are not limited to separating a clean operational space, using experimental containers made of special materials, special cleaning of the labware, and removing the trace metal residues in the chemicals used for the incubation media with ion-exchange methods.

In addition, seawater is a weak alkaline solution containing various salts, with low concentrations of free metal ions. A major fraction of many trace metals in

natural seawater are present as chelates with organic ligands. The presence of these organic ligands also increases the solubility and bioavailability of trace metals in the marine environment (Bruland and Lohan 2003). Eukaryotic phytoplankton mainly take up dissolved inorganic metal elements (such as Fe, Cu, Zn, and Mn) from the seawater medium through cell membrane-bound transport proteins. These transporters on the surface of the cell membranes are able to bind to either the free metal ions, or metals bound to organic ligands in the seawater through ligand exchange processes. The metal can then be transported into cells across the membrane to be utilized in different metabolic pathways. As a result, the degree to which the chelators bind to trace metals can affect the uptake and utilization efficiency of these elements by phytoplankton. Therefore, in order to provide sufficient trace metal elements for phytoplankton growth, or to precisely control the trace metal concentrations in the study of trace metal limitation or enrichment experiments, it is necessary to add ligands (chelators) to the seawater medium in marine phytoplankton cultures (Morel et al. 1979; Price et al. 1989; Sunda 1988). Ethylenediaminetetraacetic acid (EDTA) is the most widely used inorganic chelator in these studies. The addition of EDTA and metal ions in culture medium can be treated as a trace metal ion buffer system to regulate the trace metal ion concentration and bioavailability. On the one hand, EDTA binds the free metal ions in the solution through the chelation process. On the other hand, as the free metal ions are utilized by phytoplankton, the complex can release metal ions back to the seawater medium.

This chapter mainly summarizes the trace metal clean culture techniques and the preparation of seawater culture media used in laboratory and shipboard trace metal clean incubation experiments. This is mainly intended to benefit readers who are especially interested in the study of trace metal uptake by marine phytoplankton, the mechanisms of trace metal limitation in phytoplankton, and trace metal enrichment incubations.

36.1 Methods

36.1.1 Trace Metal Clean Culture Techniques

36.1.1.1 Setup of Clean Laboratory Space

The concept of a "trace metal clean" laboratory was first established by Professor Patterson at the California Institute of Technology. It is well known that ambient air tends to contain high numbers of particles. The concentration of airborne particles in a laboratory without cleaning procedures is about 200 μg m^{-3} and even higher in industrial areas, with percentages of the metal elements of 10%, 3%, 1.5%, 1.5%, and 0.5% for Ca, Fe, Al, Ni, and Cu, respectively. In contrast, the concentrations of some metals in seawater are extremely low, with units of ppm or even ppb. Therefore, the ubiquitousness of trace metals in the regular shipboard or laboratory environments may easily cause trace metal contamination of seawater. In order to lower the chance of contamination, some of the algal culture operations need to be performed in a special clean laboratory area. These procedures include the preparation of seawater culture medium, and the sampling and analyses of seawater and

phytoplankton samples. The clean laboratory/room is a contained space with a high-efficiency particulate air (HEPA) filtration system to trap the airborne particles that are 0.3 μm or larger in size. Especially for the procedures involved in trace metal analyses, a class 100 HEPA filter is usually required (less than 100 particles with size larger than 0.3 μm in an air volume of 1 m^3). All of the air delivered to a clean laboratory/room should pass through the HEPA filters, with positive pressure in the whole clean space. It needs special attention that the degree of cleanliness usually decreases with the airflow direction, which is also the principle used to decide the position for HEPA filter installation. If restrained by space or logistical conditions, a laminar flow hood mounted with HEPA filters may be used in substitution of a clean laboratory. In shipboard incubation experiments, a separate trace metal clean laboratory container is the best option. In some circumstances, a temporary clean laboratory container established by wrapping trace metal clean plastic with HEPA-filters/laminar flow can also be used.

In general, metal labware is not allowed in a clean laboratory/room. The walls and ceilings of the laboratory should be kept tightly closed, and the materials such as the test benches that come into contact with the samples should be relatively clean and made of inert materials, such as polypropylene (PP), polyethylene (PE), or polytetrafluoroethylene (PTFE, also known as Teflon). No metal materials should be exposed in the whole laboratory space; therefore, the walls, ceilings, faucets, and cabinet handles should be replaced with plastic fixtures, otherwise metal-free plastic wraps or a relative clean and inert epoxy paint are needed for the best coverage, to avoid metal contamination. The personnel who work in the clean laboratory/room are also required to wear clean attire, including clean-room shoes, hats, gowns, and plastic gloves. These clothes should not be worn outside the clean room. Plastic gloves should be replaced regularly whenever they come in contact with possible contamination sources. Clean-room apparel is usually lint-free and non-shedding, and mostly made of Tyvek, microporous (MP) fabric and Spunbond–Meltblown–Spunbond (SMS) tri-laminate materials. Cosmetics and hair spray are not recommended to wear in the clean room. When feasible, a separate changing room should be constructed between the trace metal clean room as a transitional place for personnel who enter the clean room or for materials/samples transported from the dirty general laboratory environment.

36.1.1.2 The Requirements and Cleaning of Labware

Trace metal clean incubation should avoid the use of metal utensils. The culture flasks and reagent bottles used in the experiments should be made of PE, PP, polycarbonate (PC), or PTFE as needed. The water for making solutions and cleaning should be ultrapure such as Milli-Q water, with a resistivity of 18.2 MΩ cm^{-1} at 25 °C. Prior to use, the reagent bottles and culture flasks and all the other labware that directly contact the samples and cultures need to be soaked and acid-washed to remove contaminants that may be adsorbed onto the surface. These major procedures are described below.

Newly purchased appliances should be cleaned first with solvents or special detergents such as Decon®-Clean and Micro® reagents. After removal of coarse impurities, all utensils require further cleaning by acid washing. In phytoplankton culture experiments, a 10% HCl solution is generally used. All utensils need to be immersed in a 10% HCl acid bath at least for 3 days, and then rinsed with ultrapure water about five times until the HCl remaining on the surface of the container is removed. For the tubing used in some continuous culture devices, which are difficult to clean by soaking, 10% HCl solution is usually pumped into the lines for rinsing, and then ultrapure water is thoroughly pumped through for cleaning. For field research work, in order to avoid contamination during the transportation for scientific expedition cruises, these instruments are generally brought in small sealed containers and kept immersed in 10% HCl solution, until they are washed with ultrapure water in the shipboard clean laboratory just before the beginning of the culture experiment. For the culture flasks and experimental tubing directly used in the culture experiment, it is necessary to use uncontaminated filtered in situ seawater for the final rinsing step right before the culture experiment.

For some extremely strict analysis experiments, according to the NBS standard, multi-step acid-washing procedures are required:

For PTFE containers, after washing with detergent at 77 °C, add concentrated HCl, concentrated HNO_3, and ultrapure water in a mixed solution with volume ratio of 12:5:18 for several days and then rinse several times with ultrapure water.

For PE containers, after soaking them in concentrated HCl for 3 days at room temperature and washing with ultrapure water, immerse them in 1% HCl solution at 55 °C for 3 days, followed by rinsing with ultrapure water and soaking in 1% HCl solution at room temperature for 3 days, and finally rinse the containers with ultrapure water.

36.1.1.3 Trace Metal Clean Procedures During Incubation and Sampling

The sampling of seawater (including phytoplankton) used in shipboard incubation experiments also requires trace metal clean operations. PTFE-lined water samplers should be used to avoid potential metal contamination. The hydro-wire rope should be painted with non-metallic materials (such as PTFE and PE) or replaced with plastic line. In order to minimize contamination from the steel body of the research vessel, the sampling should be conducted while the ship is facing upwind and upstream. Another method is to rapidly throw a sample collector at the bow to immerse it in the water for sample collection, which should be conducted after the engine of the research vessel has been shut down but while the hull is still slowly moving forward. To collect large volumes of seawater, a trace metal clean pumping system is generally used, made by attaching trace metal clean hose to a towfish that is deployed at the desired depth of seawater. Special devices (such as supporting rods) are applied to keep the water inlet as far away as possible from the hull to minimize possible contamination. When feasible, a small boat sampling method can be used

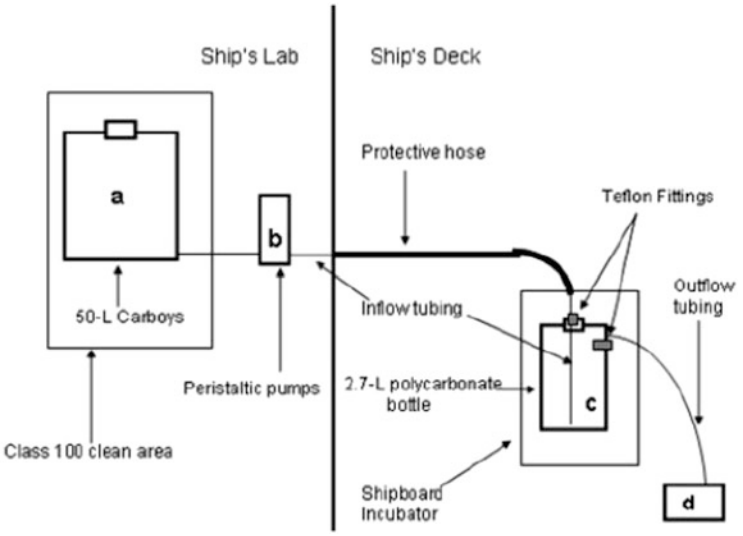

Fig. 36.1 The schematic diagram of a trace metal clean shipboard natural community continuous incubation system (Hutchins et al. 2003). The system is composed of the following parts: (a) Carboys are used to contain culture medium made of cleanly collected filtered seawater in a class 100 clean area. (b) Adjustable peristaltic pumps are used to pump medium from the carboys through Teflon tubing to the incubation bottles located inside the shipboard incubators. (c) The shipboard incubator is mounted with Plexiglas holders to hold polycarbonate bottles for phytoplankton incubation. The Teflon fittings are placed on the cap for inflow and neck for outflow of each incubation bottle. These incubation bottles are shaken periodically by an air-pressurized arm. (d) The outflow collecting bottles are connected outside the incubator

by sailing a Zodiac made of non-metallic materials hundreds of meters away from the research vessel for sample collection, and then taking the collected water back to the shipboard laboratory for incubation experiments.

In both shipboard and laboratory culture experiments, culture systems especially need to be sealed to reduce metal contamination from the surrounding environment. During the sampling process, any opening of the culture caps need to be performed only in a clean laboratory or a clean hood. Plastic apparatus that directly come into contact with the samples must be acid-washed in advance. For shipboard incubations, Hutchins et al. (2003) designed a temperature-controlled continuous culture device (Fig. 36.1), which is appropriate for trace metal clean incubations.

36.1.1.4 Trace Metal Clean Operations in Reagent Preparation

The reagents used in trace metal clean culture experiments need to be prepared with ultrapure water. Chemicals with high purity (guaranteed reagent, chromatographically pure or ultrapure reagent, etc.) are preferred as well. The solutions used for making seawater culture medium require special metal removal treatments, usually by the use of a chelating ion exchange resin. The most commonly used in practice is

Chelex® 100 ion exchange resin, which has good selectivity for heavy metal ions such as iron and copper. Chelex® 100 ion exchange resin is a copolymer of divinylstyrene containing iminodiacetic acid ions that acts as a chelation group to bind multivalent metal ions. Due to its carboxylic acid group, Chelex® 100 ion exchange resin has weak acidity, good metal ion selectivity, and strong binding ability, which is an advantage over other conventional exchange resins.

Special purification processes are required before the use of Chelex® 100 ion exchange resin (Price et al. 1989), as listed as below.

1. Weigh a certain amount of Chelex® 100 ion exchange resin as needed. The general rule is to use 5 g of resin for every 100 mL of solution. Soak it in methanol at room temperature (with resin mass to methanol volume ratio of 1:5 w/v) 3–4 h, and then rinse with 750 mL of Milli-Q water.
2. Next, soak the rinsed resin in 1 M HCl solution overnight and rinse with 1 L Milli-Q water.
3. Soak the resin in 3 M NH_4OH solution for 1 week, and then rinse with 1 L Milli-Q water.
4. After soaking for 10 min in 0.1 M HCl solution, rinse with 2 L Milli-Q water, and then rinse with 200 mL of artificial seawater.
5. Add 200 mL of the solution to be purified, resuspend the resin, and slowly titrate the medium solution to pH 8.1 with 1 M NaOH solution.
6. Finally transfer the resin to the container using a batch method or column method for the final purification of solutions.

   (a) Batch method: Directly add the Chelex® 100 ion exchange resin purified after the steps 1–5 to the solution requiring removal of heavy metal ions and stir or shake the mixture continuously for 1 h using a magnetic stir plate or laboratory shaker. Finally, the resin is filtered away to obtain the trace metal clean solution. Special attention should be paid to maintain clean operations during filtration (e.g., acid washing of containers and stirrers in a clean room).

   (b) Column method: The purified resin suspension is filled in an exchange column, which can be performed in several steps to ensure there are no air bubbles in the column. Then gently pour the solution to be purified into the packed column, taking care to avoid agitation of the resin in the column. Finally, discard the initial 500 mL of solution has passed through the column, and then start collecting the purified solution from the outflow of the packed column.

The applications of Chelex® 100 ion exchange resin for the removal of specific metals is referred to in the reference list in Table 36.1.

Table 36.1 The application of Chelax® 100 ion exchange resin in the seawater medium

Metals to be removed from seawater medium	Reference
Cd, Co, Cu, Fe, Mn, Ni, Pb, Zn	Kingston et al. (1978)
Cd, Zn, Pb, Fe, Mn, Cu, Ni, Co, Cr	Sturgeon et al. (1980)
Fe, Cd, Zn, Cu, Ni, Pb, U, Co	Mykytiuk et al. (1980)
Cd, Pb, Ni, Cu, Zn	Rasmussen (1981)
Cd, Ce, Co, Cu, Fe, Mn, Mo, Ni, Pb, Sc, Sn, Th, U, Zn	Kingston and Greenberg (1984)
Fe, Mn, Cu, Ni, Cd, Pb, Zn	Paulson (1986)

Table 36.2 Preparation of synthetic ocean water (SOW) used for Aquil* medium

Component	Quantity to be added to each liter of final volume (g)	Final concentration (M)
Anhydrous salts		
NaCl	24.5400	4.2×10^{-1}
Na_2SO_4	4.0900	2.88×10^{-2}
KCl	0.7000	9.39×10^{-3}
$NaHCO_3$	0.2000	2.38×10^{-3}
KBr	0.1000	8.4×10^{-4}
H_3BO_3	0.0030	4.85×10^{-4}
NaF	0.0030	7.14×10^{-5}
Hydrous salts		
$MgCl_2 \cdot 6H_2O$	11.0900	5.46×10^{-2}
$CaCl_2 \cdot 2H_2O$	1.5400	1.05×10^{-2}
$SrCl_2 \cdot 6H_2O$	0.0170	6.38×10^{-5}

36.1.2 Preparation of Seawater Media in Trace Metal Clean Culture Experiments

36.1.2.1 Aquil* Medium

The Aquil* medium is a one of the most commonly used synthetic seawater culture media. The preparation of Aquil* medium usually includes enriching the artificial seawater with macro- and micronutrients used to support the growth of many coastal and oceanic phytoplankton taxa. The Aquil* medium described here is a modification by Sunda et al. (2005) from the original Aquil medium (Morel et al. 1979; Price et al. 1989). The modification contains a final concentration of 100 μM of EDTA and eightfold lower iron concentration to minimize the precipitation of hydrous ferric oxides. In the preparation of Aquil* medium, all the stock solutions except for the trace metal and vitamin solutions need to pass through the Chelax® iron exchange column to remove potential metal contamination. The addition of EDTA is used to control the metal speciation and concentrations.

Synthetic ocean water (SOW) is prepared by mixing separate solutions of anhydrous salts and hydrous salts, with a final salinity of 35, as listed in Table 36.2.

Table 36.3 Preparation of major nutrients for Aquil* medium

Component	Concentration of stock solution (g L^{-1})	Volume to be added to SOW for 1 L of medium (mL)	Final concentration in medium (M)
$NaH_2PO_4 \cdot H_2O$	1.38	1	1.00×10^{-5}
$NaNO_3$	8.50	1	1.00×10^{-4}
$Na_2SiO_3 \cdot 9H_2O$	28.40	1	1.00×10^{-4}

Table 36.4 Preparation of metal/metalloid stock solution for Aquil* medium (add 1 mL of the stock solution to SOW for preparing each liter of final Aquil* medium)

Component	Concentration of stock solution (g L^{-1})	Quantity to be added to each liter of final volume	Final concentration in medium (M)
EDTA	–	29.200 g	1.00×10^{-4}
$FeCl_3 \cdot 6H_2O$	–	0.2700 g	1.00×10^{-6}
$ZnSO_4 \cdot 7H_2O$	–	0.0230 g	7.97×10^{-8}
$MnCl_2 \cdot 4H_2O$	–	0.0240 g	1.21×10^{-7}
$CoCl_2 \cdot 6H_2O$	–	0.0120 g	5.03×10^{-8}
$Na_2MoO_4 \cdot 2H_2O$	–	0.0242 g	1.00×10^{-7}
$CuSO_4 \cdot 5H_2O$	4.9	1 mL	1.96×10^{-8}
Na_2SeO_3	1.9	1 mL	1.00×10^{-8}

For making the SOW, first dissolve each of the anhydrous salts individually into 600 mL of Milli-Q water. And then use 300 mL of Milli-Q water to dissolve each of the hydrous salts. For the best dissolution, the salts need to be added into the solutions in order. Only add new salt into the solution after the previous salt is fully dissolved. Then combine the two salt solutions and bring the final volume to 1 L using Milli-Q water.

The preparation of macro-nutrient solution described in Table 36.3 includes making stock solutions of each individual nutrient. Add 1 mL of each of the stock solutions into SOW for each 1 L final volume of Aquil* medium.

For the preparation of trace metal stock solutions (Table 36.4), prepare the individual stock solutions using Milli-Q water first. Then dissolve EDTA in 950 mL of Milli-Q water and add 1 mL of each stock solution. Next bring the volume to 1 L for the trace metal stock solution, and use 1 mL of the stock solution for preparing each liter of final Aquil* medium.

The preparation of mixed vitamin stock solution is listed in Table 36.5. First, the stock solutions of vitamin B_{12} and vitamin H are prepared individually. 1 mL of each of the vitamin B_{12} and vitamin H solutions are added next into 950 mL of Milli-Q water. Then add 100 mg vitamin B_1 into the solution and use Milli-Q water to bring the final volume up to 1 L. Use 1 mL of the stock solution for 1 L of Aquil* medium.

Table 36.5 Preparation of mixed vitamin stock solution for Auqil* medium (add 1 mL of the mixed vitamin stock solution for each liter of Aquil* medium)

Component	Concentration of stock solution (g L^{-1})	Quantity to be added to each liter of final volume of stock solution	Final concentration in medium (g L^{-1})
Thiamine HCl (vitamin B_1)	–	100 mg	1.00×10^{-4}
Biotin (vitamin H)	0.5	1 mL	5.00×10^{-7}
Cyanocobalamin (vitamin B_{12})	0.55	1 mL	5.50×10^{-7}

Table 36.6 Artificial seawater preparation for YBC-II medium

Component	Content in each liter of seawater (g)	Final concentration (M)
NaCl	24.55	4.20×10^{-1}
KCl	0.75	1.00×10^{-2}
$NaHCO_3$	0.21	2.50×10^{-3}
H_3BO_3	0.036	5.80×10^{-4}
KBr	0.1157	9.72×10^{-4}
$MgCl_2 \cdot 6H_2O$	4.07	2.00×10^{-2}
$CaCl_2 \cdot 2H_2O$	1.47	1.00×10^{-2}
$MgSO_4 \cdot 7H_2O$	6.18	2.50×10^{-2}

36.1.2.2 YBC-II Medium

The YBC-II medium is an artificial seawater culture medium, developed for culturing the nitrogen-fixing cyanobacterium *Trichodesmium* without a nitrogen source (Chen et al. 1996). To make the artificial seawater used for the medium, first fully dissolve all the salts listed in Table 36.6 using 900 mL of Milli-Q water, next add the metal and f/2 vitamin stock solutions into the artificial seawater, and finally bring the volume to 1 L with Milli-Q water. Adjust the pH of the medium to 8.15–8.2 by adding NaOH solution. The medium is sterilized by filtration instead of autoclaving (Tables 36.7 and 36.8).

It requires special attention that the seawater growth medium used in laboratory culture experiments in general needs to be autoclaved. However, in order to avoid metal contamination from the autoclave, in the trace metal clean incubations culture media are usually sterilized using a microwave, or by filtration through 0.2 μm pore-size filters.

Table 36.7 Preparation of metal stock solutions used for YBC-II medium

Component	Content used for each liter of 1° stock solution (g)	Concentration in 1° stock solution (M)	Volume of 1° stock solution to add to 1 L of medium (mL)	Final concentration in the medium (M)
NaF	2.94	7.00×10^{-2}	1	7.00×10^{-5}
$SrCl_2 \cdot 6H_2O$	17.4	6.50×10^{-2}	1	6.50×10^{-5}
KH_2PO_4	6.8	5.00×10^{-2}	1	5.00×10^{-5}
Na_2EDTA	0.74	2.00×10^{-3}	1	2.00×10^{-6}
$FeCl_3 \cdot 6H_2O$	0.11	4.07×10^{-4}	1	4.07×10^{-7}
$MnCl_2 \cdot 4H_2O$	0.04	2.00×10^{-4}	0.100	2.00×10^{-8}
$ZnSO_4 \cdot 7H_2O$	0.012	4.00×10^{-5}	0.100	4.00×10^{-9}
$Na_2MoO_4 \cdot 2H_2O$	0.027	1.10×10^{-4}	0.100	1.10×10^{-8}
$CoCl_2 \cdot 6H_2O$	0.06	2.50×10^{-4}	0.010	2.50×10^{-9}
$CuSO_4 \cdot 5H_2O$	0.025	1.00×10^{-4}	0.010	1.00×10^{-9}
f/2 vitamin stock solution			0.5	

Table 36.8 Preparation of f/2 vitamin solutions for the YBC-II medium. To prepare the final mixed vitamin stock solution, begin with making the vitamin H and vitamin B_{12} stock solutions separately, then dissolve vitamin B_1 with 950 mL of Milli-Q water, add certain volumes of vitamin H and vitamin B_{12} solutions indicated as below, and bring the final volume to 1 L with Milli-Q water (Guillard 1975; Guillard and Ryther 1962)

Component	Concentration of the primary stock solution (g L^{-1})	Amount to be added to each of 1 L of f/2 vitamin stock solution	Final concentration in medium when add 1 mL per liter (M)
Thiamine HCl (vitamin B_1)	–	200 mg	2.96×10^{-7}
Biotin (vitamin H)	1.0	1 mL	2.05×10^{-9}
Cyanocobalamin (vitamin B_{12})	1.0	1 mL	3.69×10^{-10}

36.2 Problems and Precautions

Due to the higher concentration of trace metals in atmospheric particulate matters compared to the oceanic environment, and the ubiquitousness of trace metal contamination in many laboratory and shipboard incubation areas, phytoplankton cultures and samples are easily exposed to potential contamination. Therefore, the culture bottles need to be kept sealed during the incubation experiments to minimize contamination. All the operations that require exposure of cultures or seawater to the ambient air should be carried out in the class 100 clean area, such as the processes of inoculation, filling seawater and cultures into bottles, nutrient enrichment and sampling.

Moreover, in the same incubation experiment, the culture flasks should be from similar batches, and the acid-washing processes of these containers should also be

uniform to minimize the errors caused by contamination between different treatments and duplicate samples. This is mainly because the culture flasks are made of different materials that may have different capacities to adsorb/release trace metal ions, and the new ones are generally more contaminated.

During the whole experimental process, it should be always kept in mind that potential metal contamination can be ubiquitous. Thus, the personnel should take caution to prevent and minimize the contamination from each step of the experimental operations.

Last but not least, the requirement of trace metals by phytoplankton may also be affected by other environmental conditions. For example, it has been reported that the irradiance and light/dark cycle affected phytoplankton uptake and utilization of Fe and Mn; that the nitrogen source played an important role in the Fe, Mo, and Ni uptake; and that the CO_2 supply may regulate Zn limitation and uptake in marine diatoms and iron availability to marine phytoplankton (Sunda 1988; Sunda and Huntsman 1995a, b, 1998, 2005; Shi et al. 2010). Therefore, in future research and new experimental designs to study trace metal and phytoplankton interactions, the condition of these other environmental parameters are also needs to be carefully considered.

References

Boyd PW, Watson AJ, Law CS et al (2000) A mesoscale phytoplankton bloom in the Polar Southern Ocean stimulated by iron fertilization. Nature 407:695–702

Bruland KW, Lohan MC (2003) Controls of trace metals in seawater. Treatise Geochem 6:23–47

Chen Y-B, Zehr JP, Mellon M (1996) Growth and nitrogen fixation of the diazotrophic filamentous nonheterocystous cyanobacterium *Trichodesmium* sp. IMS 101 in defined media: evidence for a circadian rhythm. J Phycol 32:916–923

Coale KH, Johnson KS, Fitzwater SE et al (1996) A massive phytoplankton bloom induced by a ecosystem-scale iron fertilization experiment in the equatorial Pacific Ocean. Nature 383:495–501

Guillard RRL (1975) Culture of phytoplankton for feeding marine invertebrates. In: Smith WL, Chanley MH (eds) Culture of marine invertebrate animals. Plenum Press, New York

Guillard RRL, Ryther JH (1962) Studies of marine planktonic diatoms. I. *Cyclotella nana* Hustedt and *Detonula confervacea* Cleve. Can J Microbiol 8:229–239

Hutchins DA, Bruland KW (1998) Iron-limited diatom growth and Si:N uptake in a coastal upwelling regime. Nature 393:561–564

Hutchins DA, Pustizzi F, Hare CE et al (2003) A shipboard natural community continuous culture system for ecologically relevant low-level nutrient enrichment experiments. Limnol Oceanogr Methods 1:82–91

Kingston HM, Greenberg RR (1984) An elemental rationing technique for assessing concentration data from a complex water system. Environ Int 10(2):153–161

Kingston HM, Barnes IL, Brady TJ et al (1978) Separation of eight transition elements from alkali and alkaline earth elements in estuarine and seawater with chelating resin and their determination by graphite furnace atomic absorption spectrometry. Anal Chem 50(14):2064–2070

Martin JH, Fitzwater SE, Gordon RM et al (1993) Iron, primary production and carbon–nitrogen flux studies during the JGOFS North Atlantic Bloom Experiment. Deep-Sea Res 40:115–134

Morel FMM, Reuter J, Anderson D et al (1979) Aquil: a chemically defined phytoplankton culture medium for trace metal studies. Limnol Oceanogr 36:27–36
Morel FMM, Reinfelder JR, Roberts SB et al (1994) Zinc and carbon co-limitation of marine phytoplankton. Nature 369:740–742
Mykytiuk AP, Russell DS, Sturgeon RE (1980) Simultaneous determination of iron, cadmium, zinc, copper, nickel, lead, and uranium in sea water by stable isotope dilution spark source mass spectrometry. Anal Chem 52(8):1281–1283
Paulson AJ (1986) Effects of flow rate and pretreatment on the extraction of trace metals from estuarine and coastal seawater by Chelex-100. Anal Chem 58(1):183–187
Price NM, Harrison GI, Hering JG et al (1989) Preparation and chemistry of the artificial algal culture medium Aquil. Biol Oceanogr 6:443–461
Rasmussen L (1981) Determination of trace metals in sea water by chelex-100 or solvent extraction techniques and atomic absorption spectrometry. Anal Chim Acta 125:117–130
Saito MA, Moffett JW, Chisholm SW, Waterbury JB (2002) Cobalt limitation and uptake in *Prochlorococcus*. Limnol Oceanogr 47:1629–1636
Shi D, Xu Y, Hopkinson BM, Morel FMM (2010) Effect of ocean acidification on iron availability to marine phytoplankton. Science 327:676–679
Sturgeon RE, Berman SS, Desaulniers JAH et al (1980) Comparison of methods for the determination of trace elements in seawater. Anal Chem 52(11):1585–1588
Sunda WG (1988) Trace metal interactions with marine phytoplankton. Biol Oceanogr 6:411–442
Sunda WG, Huntsman SA (1995a) Iron uptake and growth limitation in oceanic and coastal phytoplankton. Mar Chem 50:189–206
Sunda WG, Huntsman SA (1995b) Cobalt and zinc inter replacement in marine phytoplankton: biological and geochemical implications. Limnol Oceanogr 40:1404–1407
Sunda WG, Huntsman SA (1998) Interactive effects of external manganese, the toxic metals copper and zinc, and light in controlling cellular manganese and growth in a coastal diatom. Limnol Oceanogr 43:1467–1475
Sunda WG, Huntsman SA (2005) Effect of CO_2 supply and demand on zinc uptake and growth limitation in a coastal diatom. Limnol Oceanogr 50:1181–1192
Sunda WG, Price N, Morel FMM (2005) Trace metal ion buffers and their use in culture studies. In: Andersen RA (ed) Algal culturing techniques. Academic Press/Elsevier, Amsterdam, pp 35–63

Part VIII
Research Methods for Animals and Viruses

Chapter 37
Electrophysiological Recording in Fish

Xiaojie Wang

Abstract Electrophysiological recording is a useful method to study the basic physiological activities of fish, such as respiration and nerve conduction. Neuroelectrophysiological recordings have been widely used to investigate the effects of physical factors (sound, light, electricity, and pH) and chemical factors (chemical pollutants) on the sensory system and behavior of fish. This chapter mainly introduces the development of neural electrophysiology in fish, including the basic equipment and the basic process.

Keywords Extracellular recording · Fish · Neurophysiology · Perfusion system · Craniotomy

37.1 Introduction

The first experimental understanding of bioelectricity was obtained in the 1770s, when John Walsh described electric sparks and electric shocks generated by live animals, such as electric eels and electric rays. Then, Galvani began to study the effects of electricity on frogs. Galvani's work led to the foundation of a new science called electrophysiology (Piccolino 1998). As a branch of physiology, electrophysiology is the study of the electrical properties of biological cells and tissues. With the development of the concept of bioelectricity, the tools and methods of electrophysiology were developed, ranging from Galvani's experiments using the Leyden jar to those of Neher and Sakmann using the gigaseal patch-clamp approach (Verkhratsky and Parpura 2014). It is possible to measure voltage changes, electric currents, and manipulations on a wide variety of scales from single ion channel proteins to whole organs using the modern electrophysiological techniques.

X. Wang (✉)
Institute for Marine Biosystem and Neurosciences, Shanghai Ocean University, Shanghai, China
e-mail: xj-wang@shou.edu.cn

K. Gao et al. (eds.), *Research Methods of Environmental Physiology in Aquatic Sciences*, https://doi.org/10.1007/978-981-15-5354-7_37

Bioelectricity in animals is involved in fundamental physiological processes, such as nerve conduction and muscle contraction. Noninvasive methods can be employed to monitor the physiological condition of fish. It is common to measure the electric signals associated with the heart rate and ventilating activity (Spoor et al. 1971). Using the methods of electrocardiography and electropneumography, the effects of temperature and the level of illumination on cardiac and respiratory rhythms have been analyzed in juvenile Atlantic salmon (*Salmo salar*) (Bakhmet 2005). Whole-cell recording has been applied to study the mechanisms underlying contractile dysfunction in fish caused by cardiotoxic polycyclic aromatic hydrocarbons (Brette et al. 2017). Over the past decade, standard neuro-anatomic and immunohistochemical techniques have been used to determine the detailed characteristic organization of the nervous system. More recently, researchers have shifted their focus to functional studies, many of which center on behavioral responses and the electrophysiological characteristics of sensory systems. Electrophysiological recording includes measurements of the electrical activity of neurons and action potential activity, as well as recording of large-scale electric signals from the nervous system, such as those captured by electroencephalography.

Extracellular recording, intracellular recording, and the patch-clamp technique are common neuro-electrophysiological techniques. Extracellular recording is the most popular method in neuro-electrophysiological studies of fish and is used to study the characteristics of local field potentials and the electric activity of single or several neurons in the central nervous system while they respond to different environmental stimuli. The sublethal effects of three different pesticides on the olfactory function of juvenile coho salmon (*Oncorhynchus kisutch*) were evaluated using extracellular recording (odor-evoked field potentials) from the olfactory epithelium and the olfactory bulb (Sandahl et al. 2004). Auditory evoked potentials have been used to measure the threshold of hearing for specific frequencies after exposing fish to simulated tidal turbine noise presented continuously (Halvorsen et al. 2011). The effect of ocean acidification projected to occur by the end of this century has been observed on retinal responses in damselfish by determining the threshold of its flicker electroretinogram (Chung et al. 2014).

The extracellular recording method enables a very sensitive and rapid analysis of brain activity. However, it is difficult to assess the precise location of the recording electrode tip relative to specific brain nuclei (Baraban 2013). The availability of zebrafish and medaka, which can carry fluorescent reporters in specific nuclei or cell types, will mitigate this limitation (Zhao and Wayne 2013).

37.2 Basic Equipment for Electrophysiological Recording

Bioelectricity is generated by a variety of biological processes and generally ranges in strength from one to a few hundred millivolts. Bioelectric potentials, such as resting potentials, action potentials, and postsynaptic potentials, are weak. Bioelectric potentials can be amplified from 50 to 100,000 times during recording and then

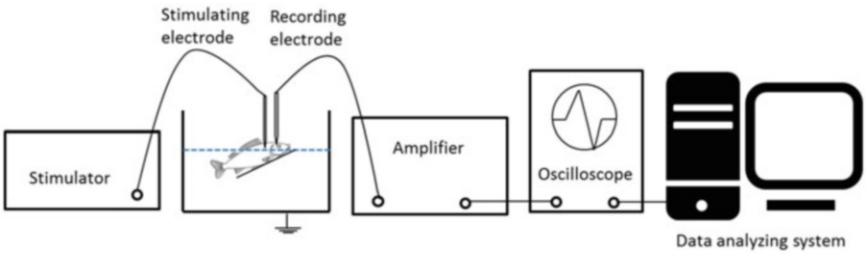

Fig. 37.1 Basic electrophysiological recording equipment

can be selected and displayed on an oscilloscope. According to their function, basic electrophysiological equipment can be divided into input units, amplifying units and output units (Fig. 37.1). In addition to the basic equipment, an anti-vibration platform, microscope, micro manipulator, glass capillary puller, and micro-electrode holder are also commonly used for electrophysiological experiments.

An input unit, such as an electrode and stimulator, is used to collect the bioelectric potentials, which are passed to an amplifier. Biological tissues produce nerve responses only under stimulatory conditions. Brief pulses of electricity are used in various physiological research applications as a stimulus to excite nerve or muscle fibers. As a source of stimulation, an electronic stimulator is convenient for control, and its electronic components produce different forms of output pulses, which stimulate the nerve tissue. Electrodes can be divided into stimulating electrodes and recording electrodes. The current or potential produced by the stimulator is passed to the tissue by a stimulating electrode. Then, the bioelectric signal is passed to the recording equipment by the recording electrode.

The amplifying unit is used to increase the power of a weak signal passed from the recording electrode. The amplifier is the main electronic part of this unit and includes a preamplifier and a power amplifier. The preamplifier precedes other signal processing stages and converts a weak electrical signal into an output signal strong enough to be noise-tolerant and strong enough for further processing. The preamplifier is placed near the recording electrode to reduce the effects of noise and interference. A power amplifier is an amplifier designed primarily to increase the power available to a load. In general, the power amplifier is the last amplifier or actual circuit in a signal chain (the output stage) and is the amplifier stage that requires power efficiency.

The output unit is a third component of electrophysiological equipment. This unit includes various oscilloscopes, recorders, analytical devices, data processing machines, and computers. Analog devices make use of continually varying voltages, whereas digital devices employ binary numbers, which correspond to voltage samples. In the case of a digital oscilloscope, an analog-to-digital converter is used to change the measured voltages into digital information. The digital storage oscilloscope can be used to store the electrical signals in digital form, and the stored data can be outputted in analog form and sent to the computer interface for recording, storage, and data analysis.

37.3 Basic Procedure of Neural Electrophysiology Recording in Fish

According to the research purpose, different electrophysiological recording methods are used to study different brain regions. The equipment setup, craniotomy, and electrophysiology recording are the basic procedures used for electrophysiological study of fish.

37.3.1 Equipment Setup

37.3.1.1 Perfusion System for Craniotomy

The fish should be anesthetized before performing the surgery. After anesthesia is induced, the fish cannot breathe actively and requires an intubation system to deliver dissolved oxygen (Fig. 37.2a). Immobilized fish are usually placed on the lower edge of a plate to facilitate anatomical operations with both hands. A piece of plastic foam is placed on the anatomical plate and with a groove cut in it according to the size and shape of the fish. The fish is placed in the groove, and some pins are placed to prevent body lean. A peristaltic pump is used to pump tank water into the mouth of the fish. After flowing out of the gill cavity, the water flows into a storage tank through an outlet on the plate. The level of the fish immersed in water to keep the fish moist can be changed by adjusting the rotating speed of the peristaltic pump and the outlet valve.

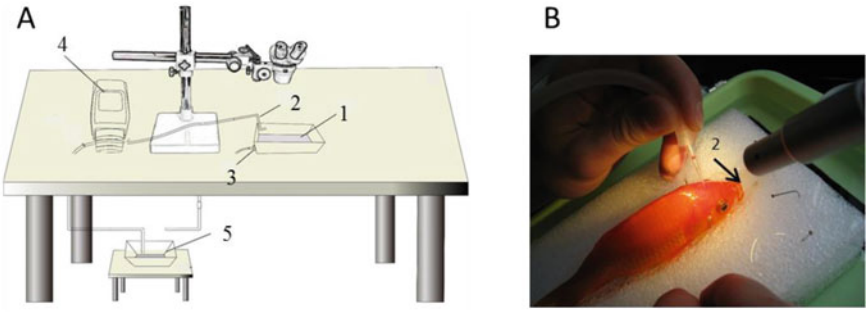

Fig. 37.2 Perfusion system for craniotomy. (**a**) Sketch of perfusion system for craniotomy; (**b**) picture of anatomical plate; (1) anatomical plate; (2) inlet; (3) outlet; (4) peristaltic pump; (5) storage tank

37.3.1.2 Perfusion System for Electrophysiological Recording

The experimental tank is usually placed on an anti-vibration platform, and other shock-producing devices are placed at the other sites to maintain the stability of the signal during electrophysiological recording. For example, the storage tank and the water pump are placed on the ground. As shown in Fig. 37.3, the water is pumped into the mouth and flows out through a movable pipe outlet capable of regulating the water height in the tank. The water flows into the storage tank on the ground by gravity. Moreover, some fixation devices are needed to keep the fish stable and keep the target brain region out of the water, such as a supporting plate under the ventral side of the fish and two fixation screws on the head (Fig. 37.3c).

37.3.1.3 Capillary Needle and Electrodes

The glass microelectrode is the most widely used electrode for cellular electrophysiological recording. It is made up of a Plexiglass tube with diameter 1–2 mm pulled with a micropipette puller. According to the recording method, the shape of the glass pipe tip is determined, and then the parameters are set on the puller. Glass microelectrodes are usually filled with a salt solution. The composition of the solution is determined by the individual experimenter and depends on the experimental protocol. Electrolyte-filled (usually with NaCl) micropipettes are used for extracellular recording of neuronal discharges, as they can also faithfully reproduce the potential wave-form down to DC levels. The NaCl solution is injected into the microelectrode tube with a syringe. After discharging the bubbles, a silver chloride wire connected to the amplifier is plugged into the solution.

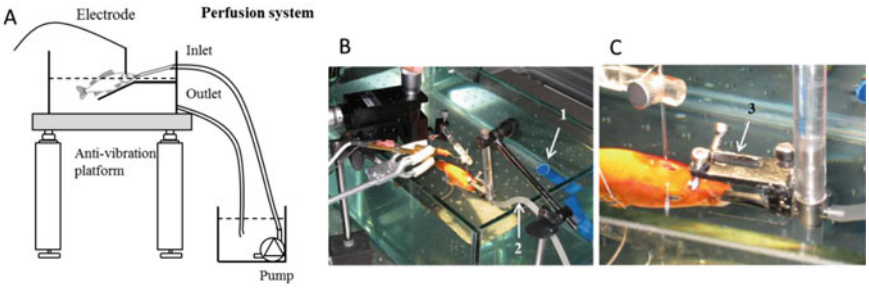

Fig. 37.3 Perfusion system for electrophysiological recording. (**a**) Sketch of perfusion system for electrophysiological recording; (**b**) picture of electrophysiological tank; (**c**) picture of fixation screws on the fish's head; (1) outlet; (2) inlet; (3) fixation screws on the fish's head

37.3.2 Craniotomy

The fish is placed in 1 L water containing 0.03–0.05% tricaine (MS 222, Sigma, St. Louis, MO, USA). The immobilized fish is placed in the anatomical plate. First, the bubbles from the perfusion system are discharged from the open pipe. The outlet pipe is placed in the fish's mouth. The speed of the peristaltic pump is adjusted to allow the water on the anatomical plate to immerse most of the body. An electric dental drill is used under an anatomical microscope to punch a hole in the cranium and expose the target brain area. The cerebrospinal fluid and blood are removed from around the brain using the sample sucking pipe. The sucking pipe can be self-made. A 10 μL pipette tip is connected with one rubber tube and the other end is in the experimenter's mouth. The experimenter sucks the liquid out of the fish brain (Fig. 37.2b). To prevent the fish from waking up during the dissection experiment, 0.003% MS222 is added to the storage tank. If the experiment take a long time, the fish should be covered with wet gauze to prevent it from losing water and drying out.

37.3.3 Electrophysiology

The fish is placed into the electrophysiological tank after the craniotomy. The perfusion system is connected with the head or body fixed in the device, and the surgical part is exposed to air. The reference electrode is inserted into the fish's nostril or under the trunk skin with a micromanipulator. The recording electrode is inserted into the target brain region with a micromanipulator under the anatomical microscope. The recording electrode should not be inserted too deep, otherwise the recorded signal may be weak. The electrical signal difference between the recording electrode and the reference electrode can be collected and analyzed, and the extracellular electrophysiological signals are obtained. It is usually necessary to record a baseline of normal physiological activity for at least 15 min and then record the change in electrical signals after the mechanical or chemical stimuli. The nervous system activity of one fish can be recorded for 2–3 h using this method. We use excessive MS222 to anesthetize the fish and killed them by decapitation.

References

Bakhmet IN (2005) Electrophysiological study of effects of environmental factors on respiration and cardiac activity in the fry of the Atlantic salmon *Salmo salar*. J Evol Biochem Physiol 41 (2):176–184

Baraban SC (2013) Forebrain electrophysiological recording in larval zebrafish. J Vis Exp 71: e50104

Brette F, Shiels HA, Galli GL, Cros C, Incardona JP, Scholz NL, Block BA (2017) A novel cardiotoxic mechanism for a pervasive global pollutant. Sci Rep 7:41476

Chung WS, Marshall NJ, Watson SA, Munday PL, Nilsson GE (2014) Ocean acidification slows retinal function in a damselfish through interference with Gabaa receptors. J Exp Biol 217 (Pt 3):323

Halvorsen MB, Carlson TJ, Copping AE (2011) Effects of tidal turbine noise on fish hearing and tissues – draft final report - environmental effects of marine and hydrokinetic energy. Office of Scientific & Technical Information Technical Reports

Piccolino M (1998) Animal electricity and the birth of electrophysiology: the legacy of luigi galvani. Brain Res Bull 46(5):381

Sandahl JF, Baldwin DH, Jenkins JJ, Scholz NL (2004) Odor-evoked field potentials as indicators of sublethal neurotoxicity. Can J Fish Aquat Sci 61(61):404–413

Spoor WA, Neiheisel TW, Drummond RA (1971) An electrode chamber for recording respiratory and other movements of free-swimming animals. Trans Am Fish Soc 100(1):22–28

Verkhratsky A, Parpura V (2014) History of electrophysiology and the patch clamp, Patch-clamp methods and protocols. Springer, New York

Zhao Y, Wayne NL (2013) Recording electrical activity from identified neurons in the intact brain of transgenic fish. J Vis Exp 864–867(74):e50312

Chapter 38
Heart Rate Measurement in Mollusks

Yunwei Dong, Guodong Han, and Xiaoxu Li

Abstract Heart rate (HR) has been proven to be an informative indicator of metabolism in mollusks. Extensive studies showed that the HR determination of mollusks under different environmental conditions can help to investigate the mechanisms how these species physiologically respond to the environmental stresses and to understand the ecological impacts of environment stresses. Recently, infrared radiation sensors have been widely used for heart rate measurement. Along with the development of related techniques, the applications of HR measurement of mollusks have been introduced in many fields, including ecology, aquaculture, and ecotoxicology. In this chapter, we briefly introduce the method of HR measurement in mollusks using infrared radiation sensors.

Keywords Heart rate · Mollusks · Physiological adaptation · Temperature · Thermal limit

38.1 Introduction

Heart rate (HR) of ectotherms is an important physiological trait that is closely related to species environmental tolerance, and the determination of HR was widely used for investigating animals' physiological responses to environmental stresses. The HR of mollusks has been determined for understanding the effects of environment factor on physiological performances for several decades. In 1967, Helm and

Y. Dong (✉)
The Key Laboratory of Mariculture, Ministry of Education, Fisheries College, Ocean University of China, Qingdao, China
e-mail: dongyw@ouc.edu.cn

G. Han
College of Life Science, Yantai University, Yantai, China

X. Li
State Key Laboratory of Marine Environmental Science, College of Ocean and Earth Science, Xiamen University, Xiamen, China

K. Gao et al. (eds.), *Research Methods of Environmental Physiology in Aquatic Sciences*, https://doi.org/10.1007/978-981-15-5354-7_38

Trueman studied the effect of air exposure on the HR of the mussel *Mytilus edulis* and found a depression of heart rate with increased duration of air exposure. These results indicated that bradycardia was caused by hypoxia during air exposure (Helm and Trueman 1967). As a widely used physiological trait, HR has its unique advantages. Firstly, thermal limit to environmental factors can be analyzed for each individual using HR. This is important for understanding the inter-individual variation of the physiological trait (Dong et al. 2017). Secondly, the physiological response curves can be continuously monitored using HR, and this is important for calculating tipping points of the physiological performance (Stillman and Somero 1996). Finally, HR can be determined noninvasively with an infrared radiation sensor. This noninvasive technique makes it possible to study the physiological adaptation of endangered species or commercial important species with a limited sample size. Because of these unique advantages, HR is widely used in eco-physiology studies of mollusks (Dong and Williams 2011; Marshall et al. 2011; Han et al. 2013), artificial breeding of species with good economic characteristics (Chen et al. 2016; Xing et al. 2016), and ecotoxicology (Curtis et al. 2000). Thermal limit calculated with HR data and environmental temperature data have been used for calculating the thermal safety margin (TSM) (Dong et al. 2015, 2017; Sinclair et al. 2016). TSM is the difference between the species thermal limit and maximum environmental temperature and is widely used for analyzing the sensitivity of species to future climate warming (Deutsch et al. 2008; Sunday et al. 2014). Here, we review the methods to measure the heartbeat of mollusks, including heartbeat determination and breakpoint temperatures calculation.

38.2 Equipment and Methods for HR Measurement

38.2.1 Brief History of HR Measurement

Heartbeat was initially measured using an invasive method (Helm and Trueman 1967; Stillman and Somero 1996). Two fine electrodes were inserted into the pericardial space, and HR was measured by the changes of electrical impedance between the electrodes. Because at least two small holes have to be drilled exterior to the pericardial space, the physiological status of the experimental animals can be altered to a certain extent by using this method. Therefore, this invasive method was gradually replaced by noninvasive methods. In recent years, two noninvasive methods have been developed based on infrared radiation (IR) technology. One is to use an IR sensor, consisting of an infrared light emitting diode and a phototransistor detector. HR signals can be detected by an IR sensor and transduced to changes in electrical current, and then the signal is amplified by an amplifier and processed by a software (Depledge and Andersen 1990; Chelazzi et al. 1999). Another method is to use infrared photoplethysmogram (IR-PPG), which measures heart rate by detecting the changes of light intensity. The limitation of this method is that activity of adductor muscles, and opening-closing of shells of bivalves may

produce artifacts and reduce the accuracy of HR measurement (Seo et al. 2016). Comparatively, the IR sensor method is more popular in heartbeat measurement of mollusks. Because of its wide applications, low cost, and noninvasive detection, the IR sensor method is introduced here.

38.2.2 Components and Assembly of the HR Measurement System

The HR measurement system consists of an IR sensor, a signal amplifier, an oscilloscope, and a computer (Fig. 38.1). To assemble the HR measurement system, an IR sensor is inserted into a signal amplifier, which is powered by two AA size batteries. The signal amplifier and an oscilloscope are connected with a Bayonet Nut Connector (BNC). The oscilloscope and personal computer are connected with a USB cable. To measure the heartbeat, the IR sensor is deployed above the animal's heart, and the changes of IR light are transduced to the changes in electrical current. Electrical signal is amplified by an amplifier, filtered, and converted to digital format by an oscilloscope. Digital signal is then plotted and recoded using a personal computer with related software. PowerLab (ADInstruments) and PicoScope (Pico Technology) are two widely used oscilloscopes. PowerLab is a multichannel oscilloscope and allows for multiple individuals to be monitored concurrently, and the matching software (LabChart 7) has rich features. PicoScope (Pico Technology) can be powered by a laptop and can be used for measuring HR in the field.

38.2.3 Deployment of the IR Sensor

The IR sensor is usually deployed above the heart of test animals. However, the shell curvature of mollusks makes it difficult to find the exact location for sensor placement. The appropriate location can be checked by the observing real-time signal quality. Based on our experience, the optimal deploying position among mollusks is highly variable. For limpets, good signals can be detected on the top of the shell; for the right-handed snails, the upper left to the aperture is a good position; for bivalves,

Fig. 38.1 Components of the HR measurement system. (**a**) IR sensor (IR-EX, Newshift, Portugal); (**b**) Signal amplifier (AMP03, Newshift, Portugal); (**c**) Oscilloscope (PowerLab 4/35, ADInstruments, Australia); (**d**) PC and matching software (LabChart 7, ADInstruments, Australia)

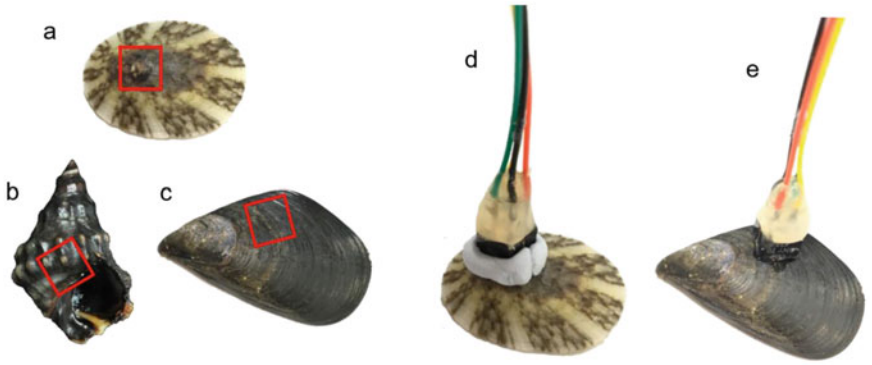

Fig. 38.2 Positions and methods for attaching IR sensors on the shells. Positions for sensor deployment of (**a**) *Cellana toreuma*, (**b**) *Echinolittorina malaccana* and (**c**) *Mytilus galloprovincialis*. The sensors were attached in *C. toreuma* using Blu-Tack (**d**) and in *M. galloprovincialis* using Super Glue (**e**)

heartbeat can be detected next to the mid-dorsal posterior hinge area of the valves (Fig. 38.2). However, the optimal deploying position may change during the process of determining, and so sensors may be possibly relocated.

According to the shell shape and the experimental medium (seawater or air), Blu-Tack (Bostik, Australia) or Super Glue (Loctite, USA) can be chosen for attaching the IR sensor on the shell. Blu-Tack is suitable for the shells with irregular shape, and it can be easily removed. The disadvantage of Blu-Tack cannot be applied underwater. Super Glue works well both in air and in water; however, it is difficult to be removed from the IR sensor (Fig. 38.2).

38.2.4 Calculation of Heartbeat

In the HR document from LabChart, *x*-axis and *y*-axis are time and electric potential, respectively (Fig. 38.3). One regular repeating waveform indicates one heartbeat. Therefore, HR can be calculated by counting the numbers of regular waveforms. Although HR can be calculated automatically using LabChart 7 software, manual calculating is usually necessary because of the signal noises. For most species, there is only one peak per heartbeat (Fig. 38.3a); however, there are two or even more peaks per heartbeat for some species, for example, *Mytilus galloprovincialis* in seawater and *Septifer virgatus* in air (Fig. 38.3b, c).

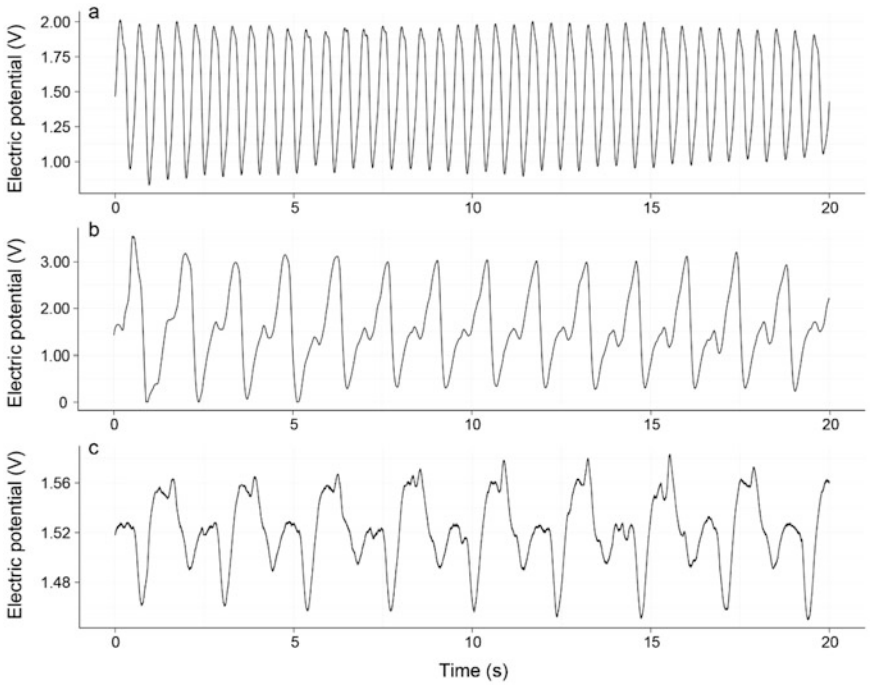

Fig. 38.3 Heartbeat waveforms of (**a**) *Cellana toreuma* in air, (**b**) *Mytilus galloprovincialis* in seawater, and (**c**) *Septifer virgatus* in air

38.3 An Example of Heart Rate Analysis: Cardiac Thermal Response

Heart rate is sensitive to temperature changes in intertidal mollusks. With increase in body temperature, HR keep increasing until the maximum value arrives (Fig. 38.4). The cardiac thermal performance curve (cTPC), which describes the relationship between body temperature and heartrate, is often left-skewed, so that small changes in body temperature above optimal levels can lead to large decreases in performance (Fig. 38.4).

Arrhenius breakpoint temperature (ABT) and flat line temperature (FLT) are two indicators for thermal limit of mollusks (Stenseng et al. 2005). ABT is the temperature at which the heart rate decreases sharply with progressive heating. It is determined using a regression analysis method that generates the best fit line on either side of a putative break point for the relationship of log-transformed HR against absolute temperature (1000/K). FLT is the temperature at which the heart rate decreases to zero. For most mollusks, ABT and FLT have explicit physiological significance (Stenseng et al. 2005; Han et al. 2013). When body temperature exceeds ABT, mollusks cannot resist thermal stress by further increasing metabolic rate, and

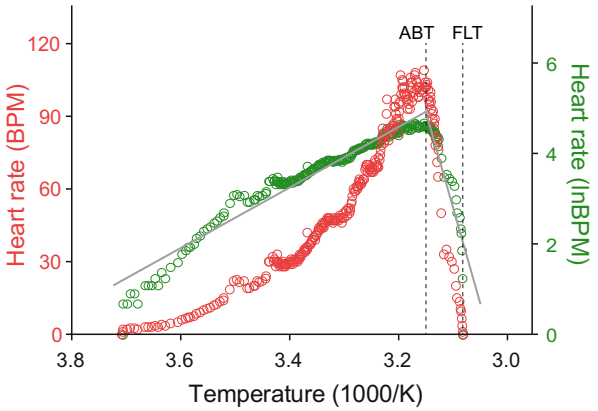

Fig. 38.4 Cardiac performance curve of mollusks. FLT is the temperature where HR decreases to zero (the red circles following the left *y*-axis). ABT is the temperature at which the HR decreases sharply with progressive heating (the green circles and grey lines following the right *y*-axis, see main text for further details)

then ABT is usually regarded as sublethal temperature for mollusks. When the body temperature exceeds FLT, mollusks cannot recover from the thermal stress. Thus, FLT is regarded as lethal temperature for mollusks.

Th procedures for determining heartbeat and calculating ABT and FLT using HR measurement system are listed as follows:

1. Assemble HR measurement system. The oscilloscope PowerLab can be identified by the software LabChart 7. Set time format as "time of day" in LabChart 7.
2. Click the start button in LabChart 7. Find the optimal position to bond the IR sensor on the shell of mollusks until clear waveforms appear in LabChart 7, and mark the position on the shell.
3. Attach the IR sensor to the marked position. Turn on the water bath and set the temperature to the starting temperature. Animals are acclimated under the starting temperature for 30 min before heating.
4. Start to heat the animals at a designed heating rate and measure the body temperature every minute using a thermocouple which is inserted into the shell. Open a new Chart View and start to record the heartbeat signal in LabChart 7.
5. Turn off the water bath and stop heating until no clear wave is observed in LabChart 7. Click the stop button in LabChart 7 and save the document. Turn off the thermometer and export the temperature data.
6. Match the HR data with the temperature data according to actual time. The temperature at which the HR decreases to zero is FLT.
7. Natural logarithmic transformation of the HR data and the body temperature is transformed to 1000/K. Calculate ABT using the "*Segmented*" package in R.

38.4 Limitations of the IR Sensor Method

The IR sensor method is a convenient and noninvasive way to measure heartbeat of mollusks. However, this method still has some limitations. Firstly, IR sensor method can be widely applied in many mollusks. But in our experience, it is difficult to measure the heartbeat for the tiny specimens, especially for the animals who are smaller than the infrared light-emitting diode. Secondly, signals from the IR sensor can be affected by body movements such as foot movement in the littorinid snails, radula movement in the gastropods, and siphon activity in the bivalves. Thirdly, this method may not work well for animals with thick shells due to the limited penetration depth of the infrared light. Finally, the signal can be disturbed by the sunlight, and then the signal-to-noise ratio becomes worse in the field.

References

Chelazzi G, Williams GA, Gray DR (1999) Field and laboratory measurement of heart rate in a tropical limpet, *Cellana grata*. J Mar Biol Assoc U K 79:749–751

Chen N, Luo X, Gu Y, Han GD, Dong YW, You WW, Ke CH (2016) Assessment of the thermal tolerance of abalone based on cardiac performance in *Haliotis discus hannai*, *H. gigantea* and their interspecific hybrid. Aquaculture 465:258–264

Curtis TM, Williamson R, Depledge MH (2000) Simultaneous, long-term monitoring of valve and cardiac activity in the blue mussel *Mytilus edulis* exposed to copper. Mar Biol 136:837–846

Depledge MH, Andersen BB (1990) A computer-aided physiological monitoring system for continuous, long-term recording of cardiac activity in selected invertebrates. Comp Biochem Physiol 96:473–477

Deutsch CA, Tewksbury JJ, Huey RB, Sheldon KS, Ghalambor CK, Haak DC, Martin PR (2008) Impacts of climate warming on terrestrial ectotherms across latitude. Proc Natl Acad Sci U S A 105:6668–6672

Dong YW, Williams GA (2011) Variations in cardiac performance and heat shock protein expression to thermal stress in two differently zoned limpets on a tropical rocky shore. Mar Biol 158:1223–1231

Dong YW, Han GD, Ganmanee M, Wang J (2015) Latitudinal variability of physiological responses to heat stress of the intertidal limpet Cellana toreuma along the Asian coast. Mar Ecol Prog Ser 529:107–119

Dong YW, Li XX, Choi F, Williams GA, Somero GN, Helmuth B (2017) Untangling the roles of microclimate, behavior and physiological polymorphism in governing vulnerability of intertidal snails to heat stress. Proc R Soc B Biol Sci 284:20162367

Han GD, Zhang S, Marshall DJ, Ke CH, Dong YW (2013) Metabolic energy sensors (AMPK and SIRT1), protein carbonylation and cardiac failure as biomarkers of thermal stress in an intertidal limpet: linking energetic allocation with environmental temperature during aerial emersion. J Exp Biol 216:3273–3282

Helm MM, Trueman ER (1967) The effect of exposure on the heart rate of the mussel, *Mytilus edulis* L. Comp Biochem Physiol 21:171–177

Marshall DJ, Dong YW, McQuaid CD, Williams GA (2011) Thermal adaptation in the intertidal snail *Echinolittorina malaccana* contradicts current theory by revealing the crucial roles of resting metabolism. J Exp Biol 214:3649–3657

Seo E, Sazi T, Togawa M, Nagata O, Murakami M, Kojima S, Seo Y (2016) A portable infrared photoplethysmograph: heartbeat of *Mytilus galloprovincialis* analyzed by MRI and application to *Bathymodiolus septemdierum*. Biol Open 5:1752–1757

Sinclair BJ, Marshall KE, Sewell MA, Levesque DL, Willett CS, Slotsbo S, Dong YW, Harley CDG, Marshall DJ, Helmuth BS, Huey RB (2016) Can we predict ectotherm responses to climate change using thermal performance curves and body temperatures? Ecol Lett 19:1372–1385

Stenseng E, Braby CE, Somero GN (2005) Evolutionary and acclimation-induced variation in the thermal limits of heart function in congeneric marine snails (genus Tegula): implications for vertical zonation. Biol Bull 208:138–144

Stillman J, Somero G (1996) Adaptation to temperature stress and aerial exposure in congeneric species of intertidal porcelain crabs (genus *Petrolisthes*): correlation of physiology, biochemistry and morphology with vertical distribution. J Exp Biol 199:1845–1855

Sunday JM, Bates AE, Kearney MR, Colwell RK, Dulvy NK, Longino JT, Huey RB (2014) Thermal-safety margins and the necessity of thermoregulatory behavior across latitude and elevation. Proc Natl Acad Sci U S A 111:5610–5615

Xing Q, Li YP, Guo HB, Yu Q, Huang XT, Wang S, Hu XL, Zhang LL, Bao ZM (2016) Cardiac performance: a thermal tolerance indicator in scallops. Mar Biol 163:244

Chapter 39
Measuring the Feeding Rate of Herbivorous Zooplankton

Wei Li and Zengling Ma

Abstract As the secondary primary producer in aquatic ecosystem, zooplankton play key roles in energy flow and biogeochemical cycles through food chain. For herbivorous zooplankton, many measurement methods can be used for the determination of feeding rate, such as the dilution technique, fluorescence analysis of zooplankton gut contents, radiotracer technique, fluorescence-labeled technique, and cell concentration subtractive method. We will brief introduce these methods in this chapter.

Keywords Herbivorous zooplankton · Feeding rate measurement · Indirect estimation · Direct estimation

39.1 Introduction

Zooplankton spread worldwidely in aquatic environments, including copepods, rotifers, cladocerans, ciliates, and flagellates. One often-used method for partition of zooplankton is based on the difference of their body size. They can be classified as megalo-plankton (>20 mm), macro-plankton (2–20 mm), meso-plankton (200–2000 μm), micro-plankton (20–200 μm), and nano-plankton (2–20 μm) (Li et al. 2001; Omori and Ikeda 1984). According to the feeding habits, zooplankton can be classified as herbivorous zooplankton, carnivorous zooplankton and omnivorous zooplankton. Ecological study of zooplankton feeding have been reported in early twentieth century, mainly in feeding mechanism, feeding habits, and feeding rate measurement (Zheng 1987).

W. Li (✉)
College of Life and Environmental Sciences, Huangshan College, Huangshan, China
e-mail: livilike@163.com

Z. Ma (✉)
Zhejiang Provincial Key Laboratory for Subtropical Water Environment and Marine Biological Resources Protection, Wenzhou University, Wenzhou, China
e-mail: mazengling@wzu.edu.cn

K. Gao et al. (eds.), *Research Methods of Environmental Physiology in Aquatic Sciences*, https://doi.org/10.1007/978-981-15-5354-7_39

The feeding process of suspension-feeding zooplankton (e.g., Calanoid copepods and cladocerans) includes using their sieve-like appendages to generate water currents and using setae and setules to sieve food organism from the currents. Different food type, size, morphology, concentration, and quality are known to have differed feeding preference by different body sized zooplankton, which may determine the grazing pressure to phytoplankton and subsequently mediate the primary production.

Studies on the feeding process of zooplankton have been extensively carried out from early 1970s (Beers and Stewart 1971). Methods for feeding measurement developed rapidly since the 1930s, both indirect methods such as estimation from the stand stock of micro-zooplankton and extrapolation methods from the experience (indoor or outdoor measurement), and direct measurement methods such as dilution method, fluorescence analysis of zooplankton gut contents, radioisotope technique, fluorescence-labeled technique, and cell concentration subtractive method. Each method has both merits and demerits. Nevertheless, these methods help to clarify the relationship between primary and secondary primary production of energy and matter flow through food chain.

39.2 Indirect Estimation of Zooplankton Feeding Rate

39.2.1 Estimation the Feeding Pressure from the Stand Stock of Micro-Plankton

The stand stock of major group of micro-zooplankton (dinoflagellate, ciliate, etc.), phytoplankton and bacteria in the studied areas can be investigated, and use the feeding rates of different group that measured from laboratory or field, multiply with its stand stock. The feeding rates obtained this way can be used to indicate the feeding pressure of that specific group (Lessard and Swift 1985). This method assumes that the acquired feeding rate (from laboratory or field study) and food organisms do not change, which means the flagellates only graze on bacteria and phytoplankton that with size below 2 μm, the ciliates and other dinoflagellates mainly feed phytoplankton with size range from 2 to 20 μm, and filtering rate of micro-zooplankton varies with temperature change.

39.2.2 Extrapolation Method

Extrapolation method mainly uses feeding rate measured indoor or in situ to extrapolate to relevant aquatic area (Beers and Stewart 1970; Takahashi and Hoskins 1978; Andersen and Sørensen 1986). The estimation of feeding rate with this method is not based on direct measurement of the studied zooplankton. Therefore, the

accuracy of applying this approach can be questioned as the biotic and abiotic conditions vary spatio temporally, and the extrapolation with certain data may not truly reflect the complicated ecological processes under in situ conditions.

39.3 Direct Estimation of Zooplankton Feeding Rate

39.3.1 Dilution Technique

The dilution technique was initially put forwarded by Landry and Hassett (1982), which used for grazing impact estimation of micro-zooplankton. The method is based on three assumptions which can be briefly described as:

1. The growth rate of phytoplankton will not be affected by the cell density change.
2. Zooplankton clearance rate will not be affected by changed cell density.
3. The growth of phytoplankton in accordance with the exponential model is as follow:

$$P_t = P_o e^{(k-g)\,t}$$

where P_o and P_t are the phytoplankton density, chlorophyll *a* or specific pigments at the initial and over a period of time t; k is a constant growth coefficient, and g is mortality coefficient due to the grazing process.

The overall process of dilution technique are as follows:

1. First, freshly collect water sample filter through a mesh (e.g., mesh size 200 μm) to remove large zooplankton, then the water sample is divide into two parts, one part is filtered through 0.22 or 0.45 μm filters to remove the particles and is indicated as "filtered water," using which to dilute with another part of water sample (unfiltered water) with dilution ratio of unfiltered to filtered water at 1:0 (100% unfiltered water), 3:1 (75% unfiltered water), 1:1 (50% unfiltered water), and 1:3 (25% unfiltered water). Normally, the dilution experiment can be carried in 2 or 3 L bottles with three or more replicates in each dilution series.
2. Grazing impact of micro-zooplankton calculation will be determined by the change of phytoplankton density or chlorophyll *a* concentration over a certain period (e.g., 24 h) of culture under experimental condition. Note that long-term culture may induce a nutrient limited condition for phytoplankton growth, thus nutrient enrichment may be needed at the initial stage of culture. As assumed the constant growth coefficient dose not change, though it may differ a lot in different dilution ratio, grazing under above dilutability are 0.25, 0.5, 0.75, 1.0 g, and the specific growth rates (μ) of phytoplankton are represented by the following equations:

$$\begin{aligned} P_t &= P_0 e^{(k-g)t} \\ P_t &= P_0 e^{(k-0.25g)t} \\ P_t &= P_0 e^{(k-0.5g)t} \\ P_t &= P_0 e^{(k-0.75g)t} \end{aligned} \Rightarrow \begin{aligned} \mu &= (1/t)\ln(P_t/P_0) = k - g \\ \mu &= (1/t)\ln(P_t/P_0) = k - 0.25g \\ \mu &= (1/t)\ln(P_t/P_0) = k - 0.5g \\ \mu &= (1/t)\ln(P_t/P_0) = k - 0.75g \end{aligned}$$

P_t and P_0 can be determined directly before and after the culture, therefore the phytoplankton constant growth coefficient k (interception), and the mortality coefficient g (negative slope) can be acquired from the liner regression of μ (apparent growth rate, Y-axis) and dilution factor (X-axis).

Nowadays dilution technique has been used widely in micro- and macro-zooplankton feeding measurement, as both phytoplankton constant growth coefficient and zooplankton feeding rate can be determined simultaneously with a relatively low interference. However, there are also some disadvantages, for example, the chlorophyll *a* that is used for indicating the biomass change may be influenced by other environmental factors, such as light intensity and nutrients (Gifford 1988); also, the proliferation rate of micro-zooplankton under different dilution ratio may differ due to the varied food density; and the nutrient enrichment may have influence on the micro-zooplankton (Zhang 1998; Zhou et al. 2013).

39.3.2 Fluorescence Analysis of Zooplankton Gut Contents

Nemoto (1968) first used fluorometric method to evaluate the chlorophyll pigments in the stomach of euphausiids, and Mackas and Bohrer (1976) described the feeding rate evaluation of herbivorous zooplankton through gut content fluorescence analysis. This method assumes that the measured fluorescence of gut contents is a balance between feeding and defecation, and feeding rate can be determined with the fluorescence of gut contents and gut clearance time using the following equation from Mackas and Bohrer (1976):

$$I = G/T(1 - A)$$

where "I" indicates feeding rate, "G" indicates pigment concentration of gut, "T" indicates gut clearance time, and "A" indicates loss of gut contents during fluorescence. Determination of the total fluorescence of both chlorophyll *a* and phaeophytin (the main degradation product of chlorophyll *a*) from gut contents is needed. The gut contents of fluorescence may degrade into non-fluorescent substance, and the content varies depending on multiple factors such as the experimental condition and the taxon of species; therefore, the loss of gut contents fluorescence (indicate as "A" in above equation) should be considered when using fluorescence analysis of zooplankton gut contents for feeding rate determination. The gut clearance time can be determined experimentally.

Briefly, gut clearance time is normally determined as follows: first transfer the well-fed zooplankton into pre-filtered natural water (filtered through pore size of 0.22 μm filter), and sample these zooplankton at a time course. For example, sampling can be taken at 15, 30, 60, 120, and 180 min after the transfer using screen and washed with distilled water for 2–3 times, then stored at −20 °C until the fluorescence measurements of gut contents. For the measurement of florescence, a certain number of individuals are needed, no specific number requirements, but should be sufficient enough to detect the fluorescence signal (e.g., 25–100 individuals may be collected at each time point). Sample extract with 90% acetone overnight, then fluorescence can be determined with fluorometer. Determination of the gut clearance time is based on the assumption that existence of food or not will not affect the gut clearance time (evacuation time is constant), the recorded fluorescence of gut contents change with time in accordance with the exponential equation (Wang and Conover 1986):

$$G_t = G_0 \mathrm{e}^{-rt}$$

where "G_t" indicates gut pigment concentration at time "t", G_0 indicates initial gut pigment concentration, and "r" indicates the evacuation rate. The evacuation time can be determined with the following equation:

$$T = 1/r$$

By directly measuring the gut pigment concentration to evaluate feeding rate, there should be no artificial interference on studied zooplankton using fluorescence analysis of gut contents. However, cautions need to be beared in mind that using this method also have some disadvantages. The degradation of pigments into non-florescence materials may affect the calculated feeding rate, and artificial interference from the experimental measurement of evacuation time may have impact on the tested zooplankton (e.g., closed environment) and the derived evacuation time; not like the herbivorous zooplankton, omnivorous zooplankton feed on not only phytoplankton but also the small zooplankton or debris; therefore, the feeding rate may be underestimated through the evaluation from gut fluorescence contents.

39.3.3 Radiotracer Technique

The feeding and grazing rates are estimated from the accumulated radioactivity of zooplankton through feeding of radiotracer (e.g., ^{14}C-biocarbonate)-labeled algae cells by using radiotracer technique. The algae cells cultured in medium with ^{14}C-biocarbonate or ^{32}P-phosphoric acid for a certain time (e.g., 48 or 72 h) to make sure completely and evenly labeling of the cells. After the radiotracer labeling,

the cells can be collected through centrifuge or membrane filter and suspended in unlabeled medium for feeding experiment. After a certain time of feeding (normally the exposure time less than the gut clearance time), zooplankton is gently removed from the medium (e.g., filter), narcotized with carbonated water to avoid potential loss of tracer, and then washed with distilled water and put into scintillation vials with Soluene 350 tissue solubilizer (United Packard) at 60 °C for 12 h to increase the tissue solubility. After the above treatment, scintillation cocktail is added in both zooplankton and phytoplankton samples, and the samples are counted with a liquid scintillation counter. The phytoplankton concentration can be represented as cell number, cell volume, dry weight, etc. For example, if the dry weight of phytoplankton is used for concentration, its relationship with concentration of phytoplankton can be predetermined using the absorbance of A720, and using which the dry weight can be indirectly acquired through the built relationship with A720 value (Adrian 1991). The feeding (I) and grazing rates (C) can be determined using the following equation (Peters 1984):

$$C\ \left(\text{ml Ind.}^{-1}\,\text{h}^{-1}\right) = A_\text{a} \times 60/A_\text{s} \times N \times t$$
$$I\ \left(\text{mg dw. Ind.}^{-1}\,h^{-1}\right) = C \times S$$

where "A_a" is the radioactivity of zooplankton, "A_s" is the radioactivity of phytoplankton, "N" is the number of zooplankton, "t" is the minutes of feeding process, "S" is the food concentration represented as dry weight (mg dw L^{-1}).

Compared with fluorescence analysis of zooplankton gut contents or cell concentration subtractive method, the experimental time for feeding test is normally lowered in radiotracer technique (10–20 min), less than the gut clearance time. Therefore, the phytoplankton concentration and community structure change due to the long period of feeding process evidenced in other methods can be avoided. However, in order to obtain completed and even labeling of cells, long-term phytoplankton culture is needed, which may have effects on the community structure when the food organism comes from the natural phytoplankton community.

39.3.4 Fluorescence-Labeled Technique

Fluorescent-labeled bacteria/algae technique (FLB/FLA) for protozoans feeding study was first reported by Sherr and Sherr (1987). This technique shows better effect with continuous improvement by other researchers. For example, Hong et al. (2001) using the improved FLB technique studied the feeding rate of *Strombidium sulcatum*, and they discussed the advantages and disadvantages of the improved method (Hong et al. 2001). The improved method uses isolated and indoor cultured ciliate instead of filter collection from natural condition, the ciliate pipette under glass slide, and then feed with fluorescent-labeled bacteria (dyed with 2 mg DTAF for 10 min, then put under 60 °C water bath for another 2 h). The feeding rate of

protozoans (more than 20 individuals) can be recorded microscopically within a certain time. The feeding rate can be determined from series of the bacteria number change at different time point.

The improved FLB/FLA technique omits the dye of DAPI process, improving the potential interference of dye of ciliate debris. This technique is much suitable for indoor application but not in field study, and experienced isolation and operation skills are required.

39.3.5 Cell Concentration Subtractive Method

This technique for feeding and grazing rate calculation are based on the concentration (cell number or chlorophyll *a*) change of food organisms before and after feeding test, which was established by Frost (1972). Briefly, the collected zooplankton are dispatched into bottles (5–10 individuals per bottle) with certain concentration of phytoplankton, and the bottles are incubated for a 12 or 24 h feeding under dark condition; bottles with phytoplankton alone (without zooplankton added) are used as control group. Feeding rate and grazing rate can be calculated according to the following equation:

$$\text{Grazing rate } \left(\text{mL ind.}^{-1}\,h^{-1}\right): \quad G = V/N * (\ln C_t - \ln C_{tf})/t$$

$$\text{Feeding rate } \left(\text{cells ind.}^{-1}\ h^{-1}\right): \quad F = V/N * (\ln C_t - \ln C_{tf})/t * (C_{tf} - C_0)/(\ln C_{tf} - \ln C_0)$$

where "G" is the grazing rate (mL ind.$^{-1}$ h^{-1}), "F" is the feeding rate (cells ind.$^{-1}$ h^{-1}), "V" is the culture volume (mL), "N" is the zooplankton number in each bottle, "t" is the feeding time, "C_0" is the initial phytoplankton concentration, "C_{tf}" is the phytoplankton concentration at the end of feeding experiment, and "C_t" is the phytoplankton concentration at the end of feeding experiment in the control bottle (without zooplankton).

The cell concentration subtractive technique is a quantitative and an easy operation, which can be taken under both indoor and outdoor conditions. As the feeding process (both feeding rate and grazing rate) of zooplankton depends on food availability (Frost 1972; Peters 1984), the experimental design should consider the food concentration level, and low or high food supplies may have different effects as shown in Ma et al. (2012) (Fig. 39.1).

39.4 Factors Influencing Zooplankton Feeding

Zooplankton feeding rate could be influenced by many factors and can be classified into internal cause and external cause. Where the internal cause mainly relates to its own features including age, development stage, and sex, which are known to differ their feeing rate significantly.

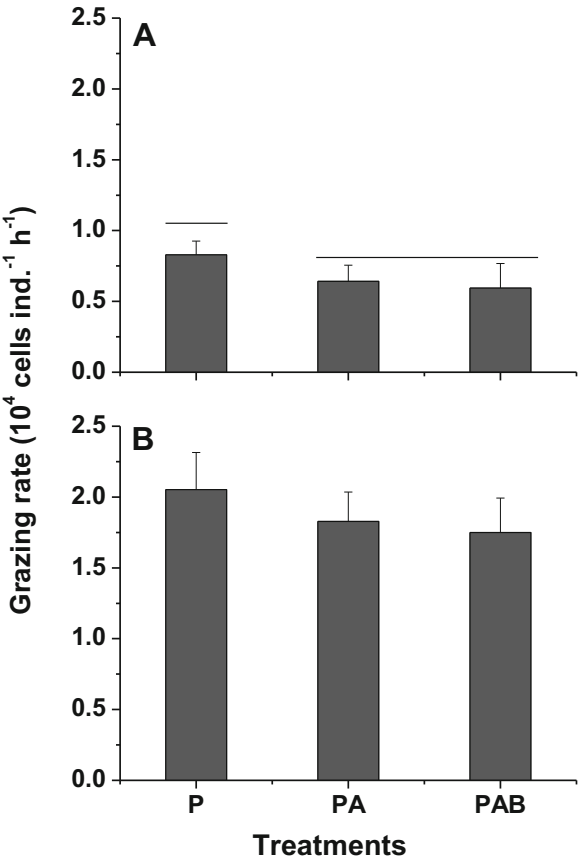

Fig. 39.1 Effects of different irradiation treatments on grazing rates of *Acartia pacifica* on *Phaeodactylum tricornutum* with the initial concentration of 2.5×10^4 cells/mL (**a**) and 2.5×10^5 cells/mL (**b**). P, PA and PAB represent different solar radiation treatments in the abscence or presence of UV radiation. The grazing rate is much higher with higher diatom concentration (Reconstructed from Ma et al. 2012)

External causes that influence zooplankton feeding generally are the surrounding environmental factors (Li and Wang 2002). Feeding rate is known to have a regression relationship with water temperature, for example (Liu and Li 1998), feeding rate of *Centropages hamatus* was significantly enhanced with increase in temperature at a range of 1–15 °C (Kiørboe et al. 1985). Feeding rate decreased with increased light intensity (Stearns 1986), and the type of food organism and its feature such as size, concentration, nutritional quality, and toxicity all have decisive effects on the zooplankton feeding (Nejstgaard et al. 1995; Sipaúba-Tavares et al. 2001; Chen et al. 2005; Zeng et al. 2006; Li et al. 2007; Ger et al. 2016; Liu et al. 2016). Therefore, the habitat environmental condition of the zooplankton being studied should be considered when carrying out the feeding test, to simulate the in situ condition, and try to avoid artificial interference.

39.5 Advantages and Disadvantages of Feeding Measurement Methods

Methods for the measurement of zooplankton feeding and grazing rate depend on the needs and the scientific questions one is going to address, as all the above-described methods have advantages and disadvantages. Indirect estimation of zooplankton feeding rate does not measure the feeding rate directly, which is mainly determined from the extrapolation, and therefore may not accurately reflect natural situations. Direct estimation of zooplankton feeding rate, however, also has limitations in reflecting the feeding process of natural environment as the feeding process may be influenced by the food type, size, concentration, and the experimental conditions. Acquired results can be underestimated (experimental condition superior to in situ water) or overestimated (existence of artificial interference or stress) in comparison with natural condition. Therefore, the following suggestions can be considered when choosing a method for the measurement of feeding rate:

1. Try to avoid potential artificial interference before the measurement; pre-adaptation to the set experimental condition may need.
2. Density of the zooplankton being tested should be controlled, and try to avoid the density effects.
3. Better to simulate the experimental condition close to the natural condition, such as the water temperature, light intensity, light/dark cycle, water turbulence, type of food organism and the concentration, and nutritional quality. Additionally, effects of water motion may be considered.
4. Conclusions from direct measurement of feeding and grazing rates need to be made carefully as acquired results are usually obtained by using single species of both zooplankton and food organism, without consideration of grazers, competitors and feeding selectivity.

References

Adrian R (1991) Filtering and feeding rates of cyclopoid copepods feeding on phytoplankton. Hydrobiologia 210:217–223

Andersen P, Sørensen H (1986) Population dynamics and trophic coupling in pelagic microorganisms in eutrophic coastal waters. Mar Ecol Prog Ser 33:99–109

Beers J, Stewart G (1970) The ecology of the plankton off La Jolla, California, in the period April through September, 1967. Bull Scripps Inst Oceanogr 17:67–87

Beers JR, Stewart GL (1971) Micro-zooplankters in the plankton communities of the upper waters of the eastern tropical Pacific. Deep-Sea Res Oceanogr Abstr 18:861–883

Chen Y, Yan T, Zhou MJ (2005) Effects of harmful algal blooms on feeding of zooplankton. Mar Sci 29(12):81–87. (in Chinese)

Frost B (1972) Effects of size and concentration of food particles on the feeding behavior of the marine planktonic copepod *Calanus pacificus*. Limnol Oceanogr 17:805–815

Ger KA, Faassen EJ, Pennino MG, Lürling M (2016) Effect of the toxin (microcystin) content of Microcystis on copepod grazing. Harmful Algae 52:34–45

Gifford DJ (1988) Impact of grazing by microzooplankton in the northwest arm of Halifax Harbour, Nova Scotia. Marine ecology progress series. Oldendorf 47(3):249–258
Hong HS, Ke L, Huang BQ, Lin XJ (2001) The grazing rate of *Strombidium sucaltum* using a modified fluorescence-labeled technique. Oceanol Limnol Sin 32(3):260–266. (in Chinese)
Kiørboe T, Møhlenberg F, Hamburger K (1985) Bioenergetics of the planktonic copepod *Acartia tonsa*: relation between feeding, egg production and respiration, and composition of specific dynamic action. Mar Ecol Prog Ser 26:85–97
Landry M, Hassett R (1982) Estimating the grazing impact of marine micro-zooplankton. Mar Biol 67:283–288
Lessard EJ, Swift E (1985) Species-specific grazing rates of heterotrophic dinoflagellates in oceanic waters, measured with a dual-label radioisotope technique. Mar Biol 87:289–296
Li CL, Wang K (2002) Feeding ecology progress of the Herbivorous copepod. Acta Ecol Sin 22 (4):593–596. (in Chinese)
Li SJ, Xu ZZ, Huang JQ, Cao WQ, Chen G, Ke CH, Chen LH (2001) Studies on biology of marine zooplankton in China. J Xiamen Univ (Nat Sci) 40(2):574–585. (in Chinese)
Li CL, Sun S, Wang R (2007) An experimental study on grazing selectivity of *Calanum sinicus* to natural food particles. Oceanol Limnol Sin 38(6):529–535. (in Chinese)
Liu GX, Li S (1998) Seasonal variations in body length and weight and ingestion rate of *Centropages tenuiremis*. Acta Oceanol Sin 20(3):104–109. (in Chinese)
Liu H, Chen M, Zhu F, Harrison PJ (2016) Effect of diatom silica content on copepod grazing, growth and reproduction. Front Mar Sci 3:89
Ma Z, Li W, Gao K (2012) Impacts of solar UV radiation on grazing, lipids oxidation and survival of *Acartia pacifica* Steuer (Copepod). Acta Oceanol Sin 31:126–134
Mackas D, Bohrer R (1976) Fluorescence analysis of zooplankton gut contents and an investigation of diel feeding patterns. J Exp Mar Biol Ecol 25:77–85
Nejstgaard JC, Båmstedt U, Bagøien E, Solberg PT (1995) Algal constraints on copepod grazing. Growth state, toxicity, cell size, and season as regulating factors. ICES J Mar Sci 52:347–357
Nemoto T (1968) Chlorophyll pigments in the stomach of euphausiids. J Oceanogr Soc Japan 24:253–260
Omori M, Ikeda T (1984) Methods in marine zooplankton ecology. John-Wiely and Sons. Inc., New York
Peters RH (1984) Methods for the study of feeding, grazing and assimilation by zooplankton. In: Downing JA, Rigler FH (eds) A manual on methods for the assessment of secondary productivity in fresh waters. Blackwell, Oxford, pp 334–411
Sherr EB, Sherr BF (1987) High rates of consumption of bacteria by pelagic ciliates. Nature 325:710–711
Sipaúba-Tavares LH, Bachion MA, Braga FMDS (2001) Effects of food quality on growth and biochemical composition of a calanoid copepod, *Argyrodiaptomus furcatus*, and its importance as a natural food source for larvae of two tropical fishes. Springer, Netherlands
Stearns DE (1986) Copepod grazing behavior in simulated natural light and its relation to nocturnal feeding. Mar Ecol Prog 30:65–76
Takahashi M, Hoskins K (1978) Winter condition of marine plankton populations in Saanich Inlet, BC, Canada. II. Micro-zooplankton. J Exp Mar Biol Ecol 32:27–37
Wang R, Conover RJ (1986) Dynamics of gut pigment in the copepod Temora longicornis and the determination of in situ grazing rates. Limnol Oceanogr 31:867–877
Zeng XB, Huang BQ, Chen JX, Hong HS (2006) Grazing impact of microzooplankton on algal bloom in the Taiwan Strait in summer. Acta Oceanol Sin 28(5):107–116. (in Chinese)
Zhang WC (1998) Methods for estimating in situ zooplankton grazing pressure. Mar Sci 5:17–19. (in Chinese)
Zheng Z (1987) Zhong Zheng anthology (continued). Ocean Press, Beijing. (in Chinese)
Zhou LB, Tan YH, Huang LM (2013) Negative phytoplankton growth rates in dilution experiments and the possible causes. J Trop Oceanogr 32(1):48–54. (in Chinese)

Chapter 40
Measurement of Virus-Induced Phytoplankton Mortality

Dapeng Xu, Yunlan Yang, and Rui Zhang

Abstract Viruses are the most abundant biological entities in global ecosystems. Viral infection and lysis are one of the major causes of phytoplankton mortality. The methods used to measure the virus-induced phytoplankton mortality include the modified dilution assay and indirect estimations based on the measurements of viral production, viral infection rate, viral contact rate, and viral decay rate. The modified dilution method is the only approach that can determine and differentiate directly the virus- and grazer-induced phytoplankton mortality and does not require the use of conversion factors, thus avoiding introducing error. However, cautions should be made when applying the modified dilution method to natural assemblages of phytoplankton because the method requires accurate measurement of the phytoplankton abundance and significant difference between virus- and grazer-induced phytoplankton mortality.

Keywords Infection · Modified dilution assay · Mortality · Phytoplankton · Viruses

40.1 Introduction

Viruses are ultramicroscopic and infectious organisms that can multiply only in living cells of animals, plants, or bacteria/archaea and do not have a cellular structure, thus considered as "organisms at the edge of life." The sizes of viruses range mostly from 20 to 350 nm, averaging 100 nm. Viruses usually consist of the

D. Xu (✉) · R. Zhang (✉)
State Key Laboratory of Marine Environmental Science, Institute of Marine Microbes and Ecospheres, College of Ocean and Earth Sciences, & Fujian Key Laboratory of Marine Carbon Sequestration, Xiamen University, Xiamen, Fujian, China
e-mail: dapengxu@xmu.edu.cn; ruizhang@xmu.edu.cn

Y. Yang
State Key Laboratory of Marine Environmental Science, Institute of Marine Microbes and Ecospheres, College of the Environment and Ecology, & Fujian Key Laboratory of Marine Carbon Sequestration, Xiamen University, Xiamen, Fujian, China

K. Gao et al. (eds.), *Research Methods of Environmental Physiology in Aquatic Sciences*, https://doi.org/10.1007/978-981-15-5354-7_40

genetic materials and a protein coat, which surrounds the genetic materials. In some cases, an outside envelope of lipids or saccharides is also found in some viruses. A virus has either a DNA (single- or double-stranded DNA) or a RNA (single- or double-stranded RNA) genome but never both. While not inside the host cell or in the process of infecting a cell, viruses exist in the form of free-living independent particles. Once getting into the host cell, viruses release their genomes and direct host cells to ultimately produce viral proteins and genetic materials, packaging new viral particles. The new viruses can be released from the host cell by lysis and start new cycles of infection. Marine viruses mainly include bacteriophage, which infects bacteria, and phycovirus, which infects eukaryotic algae. The known phycoviruses are mostly double-stranded DNA viruses, with diameter ranging from 100 to 220 nm and genome sizes from 100 to 560 kb. Recently, single-stranded DNA viruses and single- or double-stranded RNA viruses have also been reported, which indicate the hidden diversity of unknown marine viruses (Tucker et al. 2011; Steward et al. 2013).

Viruses are ubiquitous and the most abundant biological agent in aquatic environments, with a typical surface water abundance of 10^6 virus-like particles per milliliter and a total of 4×10^{30} virus-like particles in the sea. It is widely accepted that viruses play key roles in regulating biogeochemical cycles in the ocean (Fuhrman 1999; Wommack and Colwell 2000; Weinbauer 2004; Suttle 2005, 2007; Brussaard et al. 2008a). Viral lysis has been proposed as one of the major causes of phytoplankton mortality. In the microbial loop, protists that graze on phytoplankton will transfer the energy and substances to higher trophic level. However, viral lysis of phytoplankton cells converts cells into viruses and cellular debris, the latter of which consists of dissolved molecules (monomers, oligomers, and polymers), colloids, and cell fragments, which is termed as viral shunt. It has been estimated that approximately 6–26% of primary production through photosynthesis has been channeled back to dissolved organic carbon pool in the ocean (Fuhrman 1999; Wilhelm and Suttle 1999). In the coastal as well as open ocean environments, when the spring/autumn algal blooms occur, phytoplankton populations rapidly increase, followed by the accumulations of viruses. It has been reported that some phytoplankton blooms can be terminated through large-scale lytic events (Bratbak et al. 1993).

40.2 Estimation of Viral Abundance

Three methods are generally used to estimate the abundance of viruses in aquatic samples, including transmission electron microscopy (TEM), epifluorescence microscopy (EFM), and flow cytometry (FCM). Viruses from the environmental samples or lab cultures are concentrated through filtering or ultracentrifuge and deposited onto TEM grids and stained with an electron-dense material (e.g., uranyl acetate) (Børsheim et al. 1990). In addition to the abundance of viruses, TEM observation can also provide information about the key morphological characters

of the viruses, such as the size of the capsid, the length of the tails, and fibers which are important to determine the type of the viruses. Direct observations of virally infected phytoplankton cells using TEM can be used to estimate virus induced mortality rates of phytoplankton. EFM is currently the most widely used approach for estimating the abundances of viruses, which was first used for viruses in 1990 (Suttle et al. 1990). A certain volume (typically 1 mL) of seawater is vacuum-filtered onto a filter with a 0.02 mm pore size, followed by staining with the nucleic acid dyes such as SYBR Gold/Green. The filter was then mounted on a slide and observed under an epifluorescence microscope which will give the abundance but not the size and classification of viruses owing to the intrinsic limitation of resolution given by the light microscopy. More recently, FCM has been used to estimate the abundance and biomass of viruses, which is also used to quantify or even sort subpopulations of viruses that differ in their characteristics of fluorescence after stained by the nucleic acid dyes such as SYBR Gold/Green (Marie et al. 1999; Mojica et al. 2014; Brussaard et al. 2010). For example, viruses (e.g., members in Phycodnaviridae family) infecting eukaryotic algae usually have more fluorescence and scatter and thus can be differentiated from virus-infecting prokaryotes that have relatively lower nucleic acid content.

40.3 Measurement of Virus-Induced Phytoplankton Mortality

Currently, studies on the virus-induced phytoplankton mortality and its impact on the local and global carbon cycling are rather scarce, with lack of method being one of the major reasons. To determine the impact of virus on its hosts, various approaches have been developed (Proctor and Fuhrman 1990; Heldal and Bratbak 1991; Steward et al. 1992; Weinbauer et al. 1993; Noble and Fuhrman 2000; Wilhelm et al. 2002; Parada et al. 2008). However, most of these approaches have been designed for bacterioplankton and may not be applicable to phytoplankton. One of the conventional methods would be using TEM to quantify the frequency of virus-infected host cells to further estimate the number of cells lysed. In the other method, the rates of virus production are determined on the basis of the rate of ^{32}P-orthophosphate ($^{32}P_i$) or ^{3}H-thymidine (^{3}H-TdR) incorporation into the DNA of the viruses released from host cells, and the mortality rates of hosts are thus calculated (Steward et al. 1992; Weinbauer et al. 1993). To obtain the potential rates of viral infection, contact rate model of virus and host cells and decay rate of virus have been incorporated by Murray and Jackson (1992). However, the above methods all use viral abundance, production, or decay rates to estimate the virus-induced host mortality rate indirectly.

The modified dilution assay, which was adapted from the original dilution approach (Landry and Hassett 1982), is the only one at present that attempts to directly partition phytoplankton mortality into virus- versus grazing-induced

fractions (Gallegos 1989; Landry et al. 1995; Worden and Binder 2003). The original dilution method was designed for estimating the micro-zooplankton grazing impact on natural communities of marine phytoplankton. Three assumptions were made which serve as the basis of the method: (1) the growth of individual phytoplankton is not directly affected by the presence or absence of other phytoplankton within the same community; (2) the probability of a phytoplankton cell being consumed is a direct function of the rate of encounter of consumers with prey cells; and (3) change in the density of phytoplankton (P), over some time (t), can be represented appropriately by the exponential equation $P_t = P_0 e^{(k-g)t}$ (Landry and Hassett 1982). According to the protocol, half of sampled seawater was filtered to remove grazers and then combined with the remaining, unfiltered seawater in different ratios of unfiltered to filtered water to get a series of "diluted" grazer-containing incubations. After a certain period (usually 24 h) of incubation in in situ waters, instantaneous coefficients of phytoplankton growth (k) and micro-zooplankton grazing (g) could be obtained from least squares and linear regression analysis of the relationship between the rate of change of chlorophyll and the fraction of unfiltered seawater in the various bottles (Landry and Hassett 1982). In the grazer-free filtered seawater, most viruses are usually detained due to the size of filter used. In the modified dilution assay, further mixing step involving the virus-free and unfiltered seawater at certain proportions was generated. The phytoplankton mortality induced by grazer alone and grazer and virus combined was measured. The virus-induced mortality was thus obtained by deducting grazer-induced mortality from grazer and virus combined phytoplankton mortality rates.

Seawater with high primary production, undergoing a bloom event, or with agitated sediment substances needs to be prefiltered to prevent blockage during filtration. Slow filtration is expected to avoid formation of bubbles to impact the grazer, virus, and phytoplankton communities. Due to phytoplankton cell fission and potential diurnal change effects on viral infection, experiments should be set up at the same time during the same day. Filtration and setting up of experiments should be performed at the in situ temperature. The incubation is recommended to be performed in situ or under the same temperature and light conditions to simulate the in situ environment.

The success of the modified dilution method relies on the production of the dilution efficiencies of both grazing and viral lysis effects. One of the basic assumptions of the modified dilution method is that grazing and lysis impacts on phytoplankton cells vary in direct proportion to the dilution of grazers and lysis population abundances. However, phytoplankton cells may already be infected at the beginning of the experiment, and viral lysis of this group of cells cannot be serially diluted, and only new infection will be detected. Twenty-four hours of incubation period with no nutrition addition is preferred because the addition of extra nutrients can cause unnatural growth of phytoplankton cells.

Since its first application on the determination of viral lysis on a *Micromonas* spp. population (Evans et al. 2003), the modified dilution method has been successfully applied in various marine environments to directly determine virus-induced phytoplankton mortality including mesocosm (Evans et al. 2003), coastal area (Baudoux

et al. 2006; Kimmance et al. 2007), estuary (Tsai et al. 2015b), as well as oligotrophic open ocean (Baudoux et al. 2007; Brussaard et al. 2008b; Baudoux et al. 2008). It has been reported that during a mesocosm study, the virus-induced *Micromonas* spp. mortality rates ranged from 0.10 to 0.29 day^{-1}, and up to ~34% of *Micromonas* spp. production could be lysed daily by viruses. Baudoux et al. (2006) used this method to study virus-mediated mortality rates of *Phaeocystis globosa* during two consecutive spring blooms and found that during the bloom events, viral lysis was the major cause of *P. globosa* mortality (up to ~0.35 day^{-1}), which is comparable to that due to microzooplankton grazing (up to 0.4 day^{-1}). Later, Baudoux et al. (2007) studied the virus-induced mortality of picophytoplankton in the deep chlorophyll maximum layer and found that viral lysis was responsible for 50–100% of the cell losses of picoeukaryotic phytoplankton cells, with mortality rates ranging from 0.1 to 0.8 day^{-1}. In a recent study, Mojica et al. (2016) investigated virus-induced phytoplankton mortality rates along a latitudinal gradient within the North Atlantic Ocean. The study reported that virus-induced mortality was the major loss process at low and mid latitudes, whereas at higher latitudes microzooplankton grazing surpassed virus-induced mortality. Tsai et al. (2012) studied diel variations in the protozoan grazing and virus-mediated mortality of *Synechococcus* spp. in the coastal waters off Taiwan and subtropical western Pacific Ocean and found that grazing was the dominant cause of *Synechococcus* spp. mortality during daytime; however, virus-induced and nanoflagellate grazing-mediated mortalities were more balanced at night. A study performed in a subtropical estuary reported that viral lysis overran microzooplankton grazing to be the major cause of *Synechococcus* spp. losses upriver and in the estuary (Tsai et al. 2015a).

40.4 Evaluation of Techniques

The approach based on the frequency of infected cells using TEM does not need incubation and is a straightforward method to derive the virus-mediated phytoplankton mortality. However, relatively high number of viruses (at least 10^5 particles mL^{-1}) are required for TEM observation. Therefore, samples from oligotrophic environments with low microbial abundance should be concentrated before TEM observation, which will introduce bias (Weinbauer and Suttle 1997). In addition, this method relies on the knowledge of lytic cycle of host-virus system, such as the time periods when viruses are visible in cells and viral latent period. Unfortunately, these information for phytoplankton-virus system are very scarce (Proctor and Fuhrman 1990; Brussaard et al. 1996). Virus-induced mortality of the phytoplankton can also be obtained from the result of the viral production divided by the burst size. Viral decay rate can be used instead of viral production, and the assumption is that viral production and viral decay rates are balanced. This approach relies on the known burst size, as well as high-frequency sampling during incubation. It is worthy of pointing out that decay of viral particles will occur during the measurement of viral production, and this will introduce errors for the calculation of viral production

and then virus-induced mortality of the phytoplankton. The modified dilution approach is the only method that can simultaneously estimate virus- and grazing-induced phytoplankton mortality without the use of conversion factors. However, relative high abundances of phytoplankton and grazers/viruses are required to ensure a high encounter rate even at the lowest level of dilution. Accurate measurement of phytoplankton abundance is also needed. The detectable difference between the slopes of two regressions is fundamental for the calculation of virus-induced mortality rate, which is difficult in case of low virus-induced mortality, such as in oligotrophic environments (Baudoux et al. 2008; Kimmance et al. 2007; Brussaard et al. 2008b). In order to increase the utility of the modified dilution method to estimate the viral mortality of phytoplankton in natural communities, laboratory studies of virus-host systems at different density are urged to determine their encounter rates and infection dynamics.

References

Baudoux A-C, Noordeloos AAM, Veldhuis MJW et al (2006) Virally induced mortality of *Phaeocystis globosa* during two spring blooms in temperate coastal water. Aquat Microb Ecol 44:207–217

Baudoux A-C, Veldhuis MJW, Witte HJ et al (2007) Viruses as mortality agents of picophytoplankton in the deep chlorophyll maximum layer during IRONAGES III. Limnol Oceanogr 52(6):2519–2529

Baudoux A-C, Veldhuis MJW, Noordeloos AAM et al (2008) Estimates of virus- vs. grazing induced mortality of picophytoplankton in the North Sea during summer. Aquat Microb Ecol 52:69–82

Børsheim KY, Bratbak G, Heldal M (1990) Enumeration and biomass estimation of planktonic bacteria and viruses by transmission electron microscopy. Appl Environ Microbiol 56 (2):352–356

Bratbak G, Egge JK, Heldal M (1993) Viral mortality of the marine alga *Emiliania huxleyi* (Haptophyceae) and termination of algal blooms. Mar Ecol Prog Ser 93(1/2):39–48

Brussaard CPD, Kempers RS, Kop AJ et al (1996) Virus-like particles in a summer bloom of *Emiliania huxleyi* in the North Sea. Aquat Microb Ecol 10:105–113

Brussaard CPD, Wilhelm SW, Thingstad F et al (2008a) Global-scale processes with a nanoscale drive: the role of marine viruses. ISME J 2(6):575–578

Brussaard CPD, Timmermans KR, Uitz J et al (2008b) Virioplankton dynamics and virally induced phytoplankton lysis versus microzooplankton grazing southeast of the Kerguelen (Southern Ocean). Deep-Sea Res II Top Stud Oceanogr 55(5–7):752–765

Brussaard CPD, Payet JP, Winter C et al (2010) Quantification of aquatic viruses by flow cytometry. In: Manual of aquatic viral ecology, vol 11. American Society of Limnology and Oceanography, Waco, TX, pp 102–109

Evans C, Archer SD, Jacquet S et al (2003) Direct estimates of the contribution of viral lysis and microzooplankton grazing to the decline of a *Micromonas* spp. population. Aquat Microb Ecol 30:207–219

Fuhrman JA (1999) Marine viruses and their biogeochemical and ecological effects. Nature 399:541–548

Gallegos CL (1989) Microzooplankton grazing in phytoplankton in the Rhode River, Maryland: nonlinear feeding kinetics. Mar Ecol Prog Ser 57:23–33

Heldal M, Bratbak G (1991) Production and decay of viruses in aquatic environments. Mar Ecol Prog Ser 72:205–212
Kimmance SA, Wilson WH, Archer SD (2007) Modified dilution technique to estimate viral versus grazing mortality of phytoplankton: limitations associated with method sensitivity in natural waters. Aquat Microb Ecol 49:207–222
Landry MR, Hassett RP (1982) Estimating the grazing impact of marine microzooplankton. Mar Biol 67:283–288
Landry MR, Kirshtein J, Constantinou J (1995) A refined dilution technique for measuring the community grazing impact of microzooplankton, with experimental tests in the central equatorial Pacific. Mar Ecol Prog Ser 120:53–63
Marie D, Brussaard CPD, Thyrhaug R et al (1999) Enumeration of marine viruses in culture and natural samples by flow cytometry. Appl Environ Microbiol 65(1):45–52
Mojica KDA, Evans C, Brussaard CPD (2014) Flow cytometric enumeration of marine viral populations at low abundances. Aquat Microb Ecol 71(3):203–209
Mojica KD, Huisman J, Wilhelm SW et al (2016) Latitudinal variation in virus-induced mortality of phytoplankton across the North Atlantic Ocean. ISME J 10:500–513
Murray AG, Jackson GA (1992) Viral dynamics: a model of the effects of size shape, motion and abundance of single-celled planktonic organisms and other particles. Mar Ecol Prog Ser 89:103–116
Noble RT, Fuhrman JA (2000) Rapid virus production and removal as measured with fluorescently labeled viruses as tracers. Appl Environ Microbiol 66(9):3790–3797
Parada V, Baudoux AC, Sintes E et al (2008) Dynamics and diversity of newly produced virioplankton in the North Sea. ISME J 2:924–936
Proctor LM, Fuhrman JA (1990) Viral mortality of marine bacteria and cyanobacteria. Nature 343:60–62
Steward GF, Wikner J, Cochlan WP et al (1992) Estimation of virus production in the sea. Mar Microb Food Webs 6(2):79–90
Steward GF, Culley AI, Mueller JA et al (2013) Are we missing half of the viruses in the ocean? ISME J 7(3):672–679
Suttle CA (2005) Viruses in the sea. Nature 437(7057):356–361
Suttle CA (2007) Marine viruses-major players in the global ecosystem. Nat Rev Microbiol 5 (10):801–812
Suttle CA, Chan AM, Cottrell MT (1990) Infection of phytoplankton by viruses and reduction of primary productivity. Nature 347:467–469
Tsai AY, Gong G-C, Sanders RW et al (2012) Viral lysis and nanoflagellate grazing as factors controlling diel variations of *Synechococcus* spp. summer abundance in coastal waters of Taiwan. Aquat Microb Ecol 66:159–167
Tsai AY, Gong G-C, Hu SL (2015a) Virus effect on marine *Synechococcus* spp. loss in Subtropical Western Pacific Coastal waters during winter. Terr Atmos Ocean Sci 26(5):613–617
Tsai AY, Gong G-C, Huang YW et al (2015b) Estimates of bacterioplankton and *Synechococcus* spp. mortality from nanoflagellate grazing and viral lysis in the subtropical Danshui River estuary. Estuar Coast Shelf Sci 153:54–61
Tucker KP, Parsons R, Symonds EM et al (2011) Diversity and distribution of single-stranded DNA phages in the North Atlantic Ocean. ISME J 5:822–830
Weinbauer MG (2004) Ecology of prokaryotic viruses. FEMS Microbiol Rev 28(2):127–181
Weinbauer MG, Suttle CA (1997) Comparison of epifluorescence and transmission electron microscopy for counting viruses in natural marine waters. Aquat Microb Ecol 13:225–232
Weinbauer MG, Fuks D, Peduzzi P (1993) Distribution of viruses and dissolved DNA along a coastal trophic gradient in the Northern Adriatic Sea. Appl Environ Microbiol 59 (12):4074–4082
Wilhelm SW, Suttle CA (1999) Viruses and nutrient cycles in the sea: viruses play critical roles in the structure and function of aquatic food webs. Bioscience 49(10):781–788

Wilhelm SW, Brigden SM, Suttle CA (2002) A dilution technique for the direct measurement of viral production: a comparison in stratified and tidally mixed coastal waters. Microb Ecol 43:168–173

Wommack KE, Colwell RR (2000) Virioplankton: viruses in aquatic ecosystems. Microbiol Mol Biol Rev 64(1):69–114

Worden AZ, Binder BJ (2003) Application of dilution experiments for measuring growth and mortality rates among *Prochlorococcus* and *Synechococcus* populations in oligotrophic environments. Aquat Microb Ecol 30:159–174